THE UNIVERSITY
of EDINBURGH

THE UNIVERSITY
of EDINBURGH

Development of circulatory microRNAs as markers of organ injury and mediators of inter-organ signalling

Dr Emma Elisabeth Morrison

Thesis presented for the degree of Doctor of Philosophy

College of Medicine and Veterinary Medicine
University of Edinburgh

Jan 2018

Declaration

The work presented is entirely my own, with the following exceptions:

- Chapter 2 – Al Ivens was contracted to provide bioinformatics support for the second-generation sequencing data.
- Chapter 2 and 6 - Iqbal Toor performed the surgery required for the murine coronary artery ligation model.
- Chapter 3 – Marion Rook performed some of the mouse RNA processing required for validation of the miRNAs of interest.

The material contained within this thesis has not been presented, nor is currently being presented, either wholly or in part for any other degree or qualification.

Emma Elisabeth Morrison

This research was carried out at the BHF Centre for Cardiovascular Science, Queen's Medical Research Centre, University of Edinburgh, UK

Table of Contents

Abstract

Plasma contains small, non-protein coding RNA species, microRNAs (miRNAs). Circulating miRNAs originate from tissues throughout the body and circulate in the blood bound to proteins or encapsulated in extracellular vesicles (EVs). The pattern of circulating miRNAs changes in different pathological states, leading to the hypothesis that they could act as biomarkers or mediators of inter-organ signalling. Acute kidney injury (AKI) is associated with high morbidity worldwide. Recent work has highlighted a potential role for EV signalling in the delivery of functional exogenous miRNA into kidney cells, which may contribute to the pathogenesis of AKI. The studies described in this thesis investigate the effects of circulating miRNAs on renal proximal tubular (PT) cells.

Utilising next generation sequencing technology, circulating miRNA profiles were demonstrated to change significantly following myocardial injury. These findings were translated from humans into a mouse model of myocardial injury. Investigation of EV cell signalling, using flow cytometry and nanoparticle tracking analysis, demonstrated that PT cell EV uptake was not affected by known physiological agonists. By contrast, EV release from PT cells was regulated by purinergic $P2Y_1$ and dopamine D_1 receptors. Toxic cisplatin injury of PT cells resulted in increased EV release and reduced EV uptake in a dose-dependent manner. Cisplatin toxicity in PT cells was unaffected by EVs from mice with myocardial injury, but toxicity was reduced by EVs from mice with drug-induced liver injury (DILI). Circulating EVs from mice with DILI transferred the liver specific miRNA, miR-122, into PT cells in both *in vivo* and *in vitro* models. The consequence of miR-122 transfer was modulation of downstream target genes including Foxo3 which has been implicated in cell injury by apoptosis.

These findings therefore show that circulatory miRNA profiles change in different models of organ injury and suggest miRNAs can be transferred to PT cells *in vivo* and *in vitro*. The improved viability of injured PT cells following co-incubation with DILI EVs, and subsequent transcriptomic work, suggests this may be as a consequence of miRNA transfer. In conclusion, circulatory miRNAs may act as mediators of inter-organ signalling and could play a crucial role in the propagation of systemic illness.

Acknowledgements

I would like to thank the many people who have contributed to the work presented in this thesis. Special thanks must go to:

- The Medical Research Council, for affording me the opportunity of my fellowship. A debt of thanks also to Chest, Heart, Stroke Scotland and the University of Edinburgh British Heart Foundation Core for additional funding.
- The University of Edinburgh British Heart Foundation Core staff for support, especially to the technical staff for their help and advice.
- Professor David Webb, for his mentorship. Your advice has been invaluable in navigating the field of clinical pharmacology.
- Professor Matthew Bailey, my second supervisor, for not only his scientific knowledge but pastoral care and guidance.
- And finally, my supervisor, Dr James Dear, for his endless optimism, encouragement and support. You have my heartfelt gratitude.

I would like to dedicate this work to my family:

- To my parents, my cheerleaders, who never burdened me with unduly high expectations.
- To my husband Iain for enduring many lonely nights and weekends during the pursuit of this research, and who always understood.
- To my unborn child, who rather unwittingly participated in the latter stages of this work.

Publications

PUBLICATIONS:

- **Morrison EE**, MA Bailey, Dear JE. Renal exosomes: from physiology to clinical application. J Phys. 2016; doi: 10.1113/JP272182
    - Sections 1.4 to 1.7 in Chapter 1 and elements of in chapter introductions have been published in the above review
- Sandilands EA, **Morrison EE**, Bateman DN. Adverse reactions to intravenous acetylcysteine in paracetamol poisoning. Adverse Drug Reaction Bulletin. 2016; 297(1):1147–50
- Oosthuyzen W, Scullion KM, Ivy JR, **Morrison EE** et al., Vasopressin regulates the uptake of extracellular vesicles by kidney collecting duct cells. JASN 2016; 27(11):3345-55.

PRESENTATIONS:

- Dear JW, **Morrison EE**, Henriksen D, Näsström J. Calmangafodipir is a new treatment for late stage liver toxicity after acetaminophen overdose. Oral presentation at The Liver Meeting 2017, American Association for the Study of Liver Diseases
- **Morrison EE**, Webb DW, Bailey MA, Dear JW. The Effect of Circulating Extracellular Vesicles on the Response of the Kidney Proximal Tubule to Injury. Poster presentation at Kidney Week 2016, American Society of Nephrology
- **Morrison EE**, Oosthuyzen W, Webb DJ, Bailey MA, Dear JW. Extracellular vesicle signalling in the kidney. Oral abstract presentation at Extracellular vesicles, UK-Russia workshop 2016, British Council meeting
- **Morrison EE**, Webb DW, Bailey MA, Dear JW. Agonist-dependent Extracellular Vesicle Release From Proximal Tubule Cells. Oral presentation at Pharmacology 2015, British Pharmacological Society meeting
- **Morrison EE,** Oosthuyzen W, Webb DJ, Bailey MA, Dear JW. Pathological role of extracellular vesicle cell-to-cell signalling in nephrotoxic renal injury. Poster presentation at Physiology 2015, Physiological Society meeting

List of Tables

List of Figures

Abbreviations

ADP ..... Adenosine Diphosphate
Ago2 ..... Argonaute-2
AKI ..... Acute Kidney Injury
ALT ..... Alanine transaminase
AQP2 ..... Aquaporin 2
ARF6 ..... ADP-ribosylation factor 6
ATP ..... Adenosine Triphosphate
AUC ..... Area Under Curve
B ..... Baseline
BCA ..... Bicinchoninic Acid Assay
BPE ..... Bovine Pituitary Extract
CABG ..... Coronary Artery Bypass Graft
CAL ..... Coronary Artery Ligation
cAMP ..... Cyclic Adenosine Monophosphate
cDNA ..... Complementary Deoxyribonucleic Acid
CLM ..... Cell Loading Media
Ct ..... Cycle Threshold
cTnI ..... Cardiac Troponin I
CYP ..... Cytochrome P
DAPI ..... 4',6-diamidino-2-phenylindole
DILI ..... Drug Induced Liver Injury
DMSO ..... Dimethyl Sulfoxide
DPBS ..... Dulbecco's Phosphate-Buffered Saline
DTT ..... Dithiothreitol
EDTA ..... Ethylenediaminetetraacetic Acid
EGF ..... Epithelial Growth Factor
eGFR ..... Estimated Glomerular Filtration Rate
EGTA ..... ethylene glycol-bis(β-aminoethyl ether)-N,N,N',N'-tetraacetic acid
EMPIRE ..... Elafin Myocardial Protection from Ischaemia RepErfusion injury
ESCRT ..... Endosomal Sorting Complex Required for Transport
EV ..... Extracellular Vesicle
FSC/SCC ..... Forward Scatter/Side Scatter

GSH..... Glutathione
HAVRC..... Hepatitis A Virus Receptor Complex
HDL..... High Density Lipoprotein
HEPES..... 4-(2-hydroxyethyl)-1-piperazineethanesulfonic acid
HPV-16..... Human Papilloma Virus-16
HRP..... Horseradish Peroxidase
hsTnI..... High Sensitivity Troponin I
IHD..... Ischaemic Heart Disease
ILV..... Intraluminal Body
i.p..... Intraperitoneal
IRI..... Ischaemic Reperfusion Injury
KEGG..... Kyoto Encyclopedia of Genes and Genomes
KIM-1..... Kidney Injury Molecule-1
LDL..... Low Density Lipoprotein
LH..... Lithium Heparin
LOD..... Limit of Detection
MeSADP..... 2-Methylthioadenosine diphosphate trisodium salt
MI..... Myocardial Infarction
miRNA..... MicroRNA
mRNA..... Messenger RNA
MRS2500..... (1*R**,2*S**)-4-[2-Iodo-6-(methylamino)-9*H*-purin-9-yl]-2-(phosphonooxy)bicyclo[3.1.0]hexane-1-methanol dihydrogen phosphate ester tetraammonium salt
MSC..... Mesenchymal Stem Cell
MTS..... (3-(4,5-dimethylthiazol-2-yl)-5-(3-carboxymethoxyphenyl)-2-(4-sulfophenyl)- 2H-tetrazolium
MV..... Microvesicle
MVB..... Multivesicular body
NADPH..... Nicotinamide Adenine Dinucleotide Phosphate
NAPQI..... *N*-acetyl-*p*-benzoquinone imine
NHE3..... Sodium/hydrogen Antiporter 3
NTA..... Nanoparticle Tracking Analysis
OCT2..... Organic Cation Transporter 2

PBS ..... Phosphate Buffered Saline
PDVF..... Polyvinylidene Fluoride
PPT ..... Primary Proximal Tubule
Pre-miRNA ..... Precursor microRNA
Pri-miRNA..... Primary microRNA
PT..... Proximal Tubule
PTM..... Post-translational Modifications
QDot..... Quantum Dot
RIN ..... RNA integrity number
RIPA..... Radioimmunoprecipitation Assay Buffer
RISC..... RNA-induced Silencing Complex
RNAseq ..... RNA Sequencing
ROC ..... Receiver Operating Characteristic
rtPCR..... Real-time Polymerase Chain Reaction
RNA..... Ribonucleic Acid
S..... Sham
s.c..... Subcutaneous
siRNA ..... Silencing RNA
SUMO..... Small Ubiquitin-Related Modifier
TGF ..... Tissue Growth Factor
TnI ..... Troponin I
UC ..... Ultracentrifugation
URP..... Uridine Diphosphate
UTP ..... Uridine Triphosphate
VAMP3 ..... Vesicle-Associated Membrane Protein 3

Designation of Statistical Significance:

$P < 0.05$ = *

$P < 0.01$ = **

$P < 0.001$ = ***

$P < 0.0001$ = ****

Chapter 1: General Introduction

Contents

1.1. EXTRACELLULAR MIRNA

MicroRNA (miRNA) are small (~22 nucleotides), non-coding RNA species expressed in all eukaryotic cell types[1]. Since their discovery in 2001[2], they have emerged as key regulators of post-transcriptional gene expression, by base-pairing with messenger RNA. Wielding this influence over protein translation, miRNAs are critical in a wide range of physiological and pathophysiological processes, and have been implicated in a wide range of diseases.

MiRNA have been described in all biological fluids; including plasma, urine, cerebrospinal fluid, saliva, breast milk [3], yet the total miRNA concentration and relative concentration of specific miRNAs vary substantially across different fluid types. In the extracellular space, miRNAs are protected from RNase degradation by extracellular vesicles (EVs) [4] and RNA binding protein complexes [5]. While the precise mechanism of release of miRNA from cells into the extracellular environment is subject to speculation, it is clear that the extracellular miRNA signature exhibits a specific pattern in different pathological states [6-8]. This dynamic miRNA signature change has underpinned the two main threads of miRNA research; biomarker discovery and cell to cell signalling.

1.1.1. MiRNA biogenesis

In order to critically investigate extracellular miRNAs, researchers must consider miRNA biogenesis [9] (Figure 1.1).

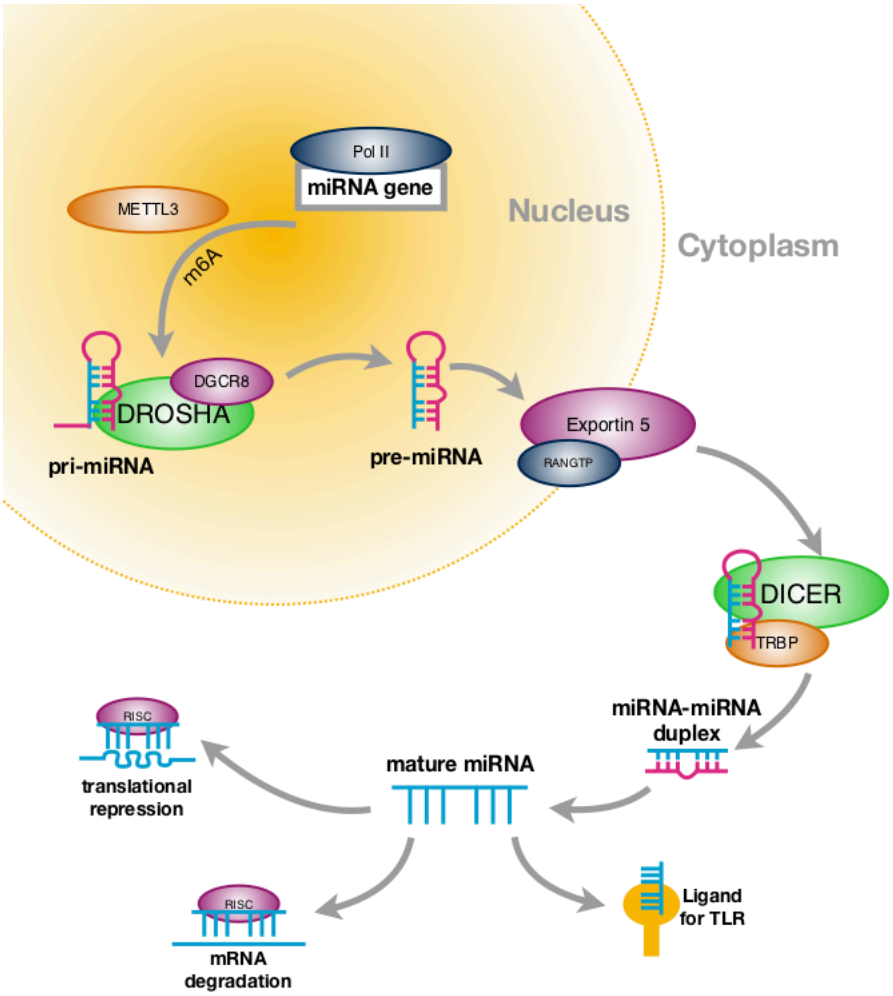

Figure 1.1: Biogenesis of microRNA. Modified from [10]

All miRNAs originate in the cell nucleus, initially as long primary 5′ capped and 3′ polyadenylated miRNA primary transcripts (pri-miRNA). This initial transcription is mainly regulated by RNA polymerase II, although RNA polymerase III may be responsible for the generation of specific transcripts[11, 12]. Pri-miRNA is then cleaved by a microprocessing complex, comprising of type III RNAse Drosha and RNA-binding protein DGCR8, to form a stem-loop structure referred to as precursor miRNA (pre-miRNA) [13]. This pre-miRNA is shuttled into the cytoplasm via an Exportin 5 complex [14], where is it further processed by the enzyme Dicer into a duplex miRNA/miRNA* (the duplex refers to a passenger strand and a mature strand, in which *denotes which is the passenger in published literature) [15]. When the duplex in unwound, the mature miRNA becomes incorporated into an RNA-induced silencing complex (RISC), ultimately targeting messenger RNA (mRNA)[16].
RISC represses protein expression either by mRNA degradation or translation repression, a process dictated by the degree of complimentary binding between the miRNA and the 3'untranslated region of the target mRNA [17]. Recently, miRNAs have been described to affect downstream signalling pathways, by directly binding with toll-like receptors (TLR) [18].

1.1.2. Cellular Release and Stability of Extracellular miRNAs

Exogenous miRNAs are quickly degraded by the high level of ribonuclease activity in plasma [19]. Endogenous extracellular miRNA is, however, relatively stable within the plasma. This is hypothesised to be due to their incorporation in RNA-binding proteins (such as argonaute-2 (Ago)2 [5]) and lipoprotein complexes [20]); or association with EVs [21].

1.1.3. MiRNAs Associated With Protein Complexes

Utilising size discrimination, Arroyo *et al.* isolated a vesicle- and non-vesicle population of circulating miRNAs, concluding the latter population existed by forming a miRNA-protein complex. More than 90% of plasma miRNAs are reported to be bound to proteins [5, 22]. Interestingly, the population of protein bound miRNAs is not the same as that of the circulating EVs [5]; suggesting these two cohorts have different mechanisms of cellular release or cell source. This research has been further extended by *in vitro* observations in which the miRNA population in the EV and non-vesicle fractions was different from that of the cell line of origin, supporting the hypothesis that the populations had different export systems [23]. Mature miRNAs are protein bound within the cell cytoplasm [9], and the picture is emerging that the majority of circulating miRNAs is associated with Ago2 [5, 22], one of the major components of RISC complex. Nucleophosmin-1 is also associated with miRNA biogenesis, shuttling the pre-miRNA from the nucleus into the cytoplasm, but at present this miRNA-protein complex has not been described in the circulation. How protein bound miRNAs are transported from a cell into the extracellular environment has yet to be elucidated. It has been hypothesised that this may be a non-specific passive process as a result of cell lysis[24]. The proposed non-selective process of protein bound miRNA release would be consistent with the close correlation in circulating miRNA and cell death reported in toxicity and cell injury studies[25-27].

1.1.4. Circulating miRNAs associated with HDL

Studies which demonstrated the transfer of small interfering RNA (siRNA) via the reconstituted functional protein of HDL[28] opened up the field to miRNA association with lipoproteins. The seminal work in the field was published 2 years later, in which both high-density lipoprotein (HDL) and low-density lipoprotein (LDL) were found to

associate with miRNA in human plasma[20], and the HDL quotient was able to affect the transcriptome of hepatocytes *in vitro.* MiRNA-HDL complexes have since been demonstrated to affect the transcriptome and function of endothelial cells, suggesting they may have wider cell-cell signalling implications[29]. In additional to their proposed functional capability, miRNA-lipoprotein complexes have also been interrogated as a biomarker reservoir. MiRNAs associated with HDL, miR-486 and miR-92a, have been proposed as biomarkers for stable coronary artery disease[30]

1.1.5. Plasma miRNAs in EVs

EVs is an umbrella term for the array of vesicles found in the extracellular space. Proteins, pre-miRNA, mature miRNA, retrotransposon RNA transcripts, single-stranded DNA (ssDNA), double-stranded DNA (dsDNA) and mitochondrial DNA have all been in identified within EVs (Figure 1.2)[31-34]. Rigorous characterisation of EVs has identified protein and RNA content specific to their cell of origin, identifying both molecules unique to the originator cell and identifying products of genes associated with multiple disease processes [35, 36]. First described as a cell signalling pathway in 2011[21], accumulating evidence suggests that EVs can function as inter-cellular transmitters to convey their contents, in particular miRNA, from one cell to another. The composition, biogenesis, targeting and physiological role of EVs will be discussed extensively from Section 1.4.

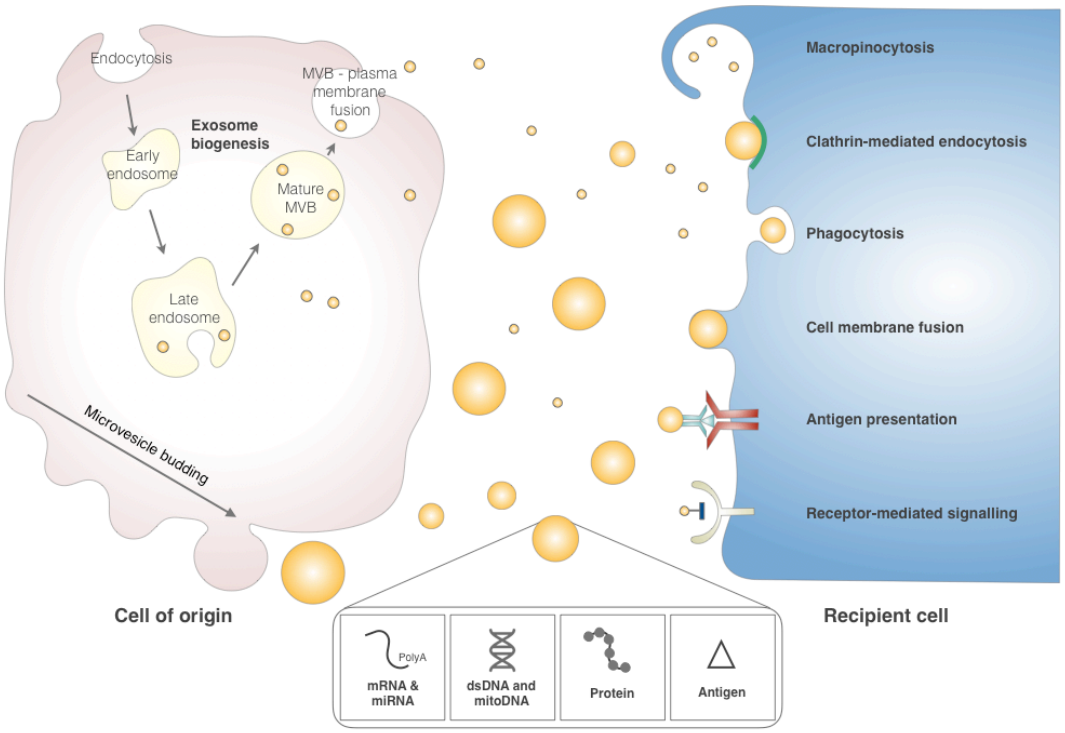

Figure 1.2: EV biogenesis and interaction with recipient cells. Published in [37].

EVs broadly consist of exosomes and microvesicles. Exosomes are generally considered a homogenous population of vesicles, derived from the endosomal pathway. This process commences with the invagination of the plasma membrane and terminates when the mature MVB fuses with the limiting aspect of the plasma membrane. The contents of the MVB are liberated into the extracellular environment, releasing exosomes. Microvesicles are formed by the budding of the plasma membrane, releasing a heterogeneous population of larger vesicles. Due to their biogenesis, EVs (yellow) act as vectors for mRNA, miRNA, protein, dsDNA, mitoDNA and antigens. This parcel of biological information can be interrogated as a biomarker reservoir or propagate a signal to a recipient cell. EV interaction with a recipient cell has been described through a number of modalities, ultimately influencing a recipient cell's proteome and function. The contents can be delivered directly to the cytosol by fusion with the recipient cell membrane or through phagocytosis, macropinocytosis or clathrin-mediated endocytosis. Alternatively, the vesicles can signal by directly activating cell surface receptors via ligands or present antigen and MHC.

1.2. CIRCULATING MIRNAS AS BIOMARKERS

As discussed, miRNAs can form intriguing expression profiles within the plasma, providing detailed feedback on the fine function of the tissue of interest. Unsurprisingly, circulating miRNAs have therefore emerged as potential biomarkers for diagnosis of illness and disease prognostication [7, 38]. The plasma biomarker reservoir has been interrogated in a broad array of fields including, but not exclusive to: cardiology[39], oncology[40], hepatology[41] and nephrology[42]. For the purposes of this thesis, an overview of miRNA biomarkers in myocardial infarction and drug-induced liver injury (DILI) will be considered.

1.2.1. Circulatory miRNAs as biomarkers of myocardial infarction

Myocardial infarction is a leading cause of morbidity and mortality in the developed world[43]. Timely intervention is critical to its clinical management[44] and consequently it is a rich area for biomarker research. To date, the gold standard biomarker is high-sensitivity troponin I (hsTnI), a highly sensitive but poorly specific marker for myocardial infarction [45]. HsTnI is used in clinical care to diagnose myocardial ischaemia, an umbrella term encompassing myocardial infarction (related to coronary artery disease) and myocardial injury. Patient outcome has improved in myocardial infarction following the introduction of lower diagnostic TnI thresholds [46], yet the number of patients with myocardial injury undergoing additional investigation has doubled with no change in patient outcome [47].Consequently, novel biomarker research within the field of myocardial ischaemia focuses upon improving the specificity of cardiac biomarkers for myocardial infarction; improving time to definitive intervention in myocardial infarction, and avoiding unnecessary additional tests for those with myocardial ischaemia.

The investigation of miRNAs as cardiac biomarkers has been extensively reviewed in the literature [39, 48], and specific patterns of miRNA have been described in both the trans-coronary and peripheral circulations correlating to the degree of myocardial injury[7]. Specifically, several miRNAs have been described as promising early biomarkers of myocardial ischaemia. Concentrations of miR-1[49, 50], miR-499[49, 51] miR-208a/b[52, 53] and miR-133a[54, 55] have been

consistently demonstrated to increase in the circulation post-myocardial insult and translate across species. Significantly, circulatory miRNA-499 has been positively correlated to cardiac infarct size[7, 56-58].

Despite these observations, head-to-head comparisons with hsTnI, have reported that measurement of these miRNAs did not improve diagnostic accuracy [59]. Furthermore, with the exception of miR-208a, all other identified cardiac miRNAs are enriched in skeletal muscle[60]; limiting specificity for the diagnosis of myocardial injury. Investigation of biomarker panels, incorporating known protein and miRNA biomarkers, has been investigated for improved positive predictive power for myocardial infarction in comparison to hsTnI alone. The combination of miR-1, miR-499 and miR-21 may improve the diagnostic accuracy of troponin for myocardial ischaemia when used in combination[25]. However, other studies investigating miRNA/TnI biomarker panels have failed to describe added diagnostic value [61].

1.2.2. Circulatory miRNAs as biomarkers of DILI

DILI is defined as the development of abnormal liver tests or liver dysfunction following the use of drugs, both prescription and over-the-counter, with the reasonable exclusion of other aetiologies[62]. DILI is implicated in negative outcomes across the spectrum of translational medicine: limiting early-phase drug development [63] and contributing to morbidity and mortality in clinical practice [64]. It is, therefore, important that DILI-biomarkers can translate across species, sensitively diagnose early liver injury and predict development of severe or life-threatening DILI. Conventional liver-injury biomarkers, such as alanine transaminase(ALT), relate to reduced hepatocyte integrity and lacks both sensitivity and specificity for liver injury when measured early in the onset of illness[65].

Within the field of DILI, management of paracetamol poisoning is of paramount importance. Paracetamol is a safe analgesic, when taken at the recommended dose. Taken in overdose, paracetamol is hepatotoxic and is the most common cause of DILI in the UK and the US. The decision to commence treatment is based

on a binary 'stop-go' approach based on ALT and the paracetamol serum concentration normogram, plotted 4 hours following overdose[66]. The clinical decision is further complicated in staggered overdose, when the normogram can no longer be applied. A stratified approach to identify patients who will develop severe DILI is therefore ideal and a growing body of evidence suggests novel biomarkers, including miRNAs could be of clinical utility[67].

MiR-122, miR-192, miR-194, miR-483 and miR-210 have been identified as liver-enriched miRNAs with potential as biomarkers in paracetamol DILI [6].
MiR-122 and miR-192, have been demonstrated to have high sensitivity for DILI and exhibit dose- and temporal-dependent changes[26], outperforming ALT in a murine model of paracetamol poisoning. These findings have been subsequently reproduced in humans[68]. MiR-122 accounts for 72% of an hepatocytes total miRNA [69], a finding translated across several species[70-72]. It plays an important role in modulation of several critical pathways including fatty acid metabolism, stress response and gluconeogenesis [73]. MiR-122 increases 100-fold in the circulation of patients with paracetamol-induced DILI and exhibits a greater sensitivity and specificity than the current biomarker ALT [74]. Recently, miR-122, in addition to other novel biomarkers, has been shown to be effective in identifying patients progressing to severe liver injury, despite current best clinical care[75].

1.3. A POSSIBLE ROLE FOR MIRNAS IN CELL COMMUNICATION

The mounting evidence of a dynamic population of transcription regulators in the circulation has given rise to the concept they may mediate paracrine signalling or even distal signalling via the blood steam. Protein bound miRNA, presumably released as a process of cell lysis[9], remains stable in the circulation for prolonged periods, providing a rich source of biomarker information regarding their cell of origin. However, there is no evidence in the literature of their selective release or subsequent uptake by recipient cells; suggesting they have no role in cell-cell communication. Conversely, since the first description by Valadi *et al.* in 2007[21], EVs have been repeatedly demonstrated to transfer miRNA to recipient cells to alter the cell's transcriptome, and ultimately modulate cellular function [76-78].

Consequently, the rest of this introduction shall be dedicated to discussion of the biogenesis and functional capability of EVs.

1.4. COMPOSITION AND BIOGENESIS OF EVS

EVs encompass a vast heterogeneous and dynamic population of membrane bound vesicles; their content and membrane composition is dictated by their cellular source and is sensitive to both cellular stress and environmental changes. Historically, naming of EVs was dependent upon their cell of origin e.g. cardiosomes (cardiomyocyte origin), prosatosomes (seminal fluid). Current nomenclature, however, largely distinguishes vesicles by their biogenesis. Criteria for EV classification have been proposed based on their origin, function or biogenesis; yet there is still no consensus about their nomenclature. Subpopulation categories range from 3-6 in number in most reviews and have been extensively discussed elsewhere [79, 80]. These categories are often difficult to use in practice, which results in confusing overlapping nomenclature. For the purposes of this review, we will consider three distinct subtypes with characteristics related to their origin, size and identifying markers.

1.4.1. Exosomes

Exosomes are derived from the endosomal pathway. Transmembrane proteins are trafficked to early endosomes by endocytosis. These early endosomes undergo sorting to late endosomes, which in turn become multivesicular bodies (MVBs). Formation of MVBs is directed by the recruitment of proteins and budding of intraluminal vesicles (ILVs), via the endosomal sorting complex required for transport (ESCRT). ILVs are released as exosomes upon fusion of MVBs with the plasma membrane (Figure 1.3). Alternatively, MVBs can fuse with lysosomes, resulting in degradation of their contents.

Intriguingly, the relative abundance of cellular RNA and protein does not closely correlate with that of the exosome, suggesting a selective process of entry into vesicles [21]. This cargo sorting may allow the cell to generate exosomes of precisely defined biochemical composition. ESCRT, tetraspanins and lipid-dependent mechanisms have all been implicated in the selective loading of proteins[81]. A specific pattern of protein post-translational modifications (PTMs)

has been noted in exosomes and a potential role in exosome sorting has been suggested [82]. The most commonly described PTM, ubiquitination, involves the addition of ubiquitin to a target protein (Figure 1.3). In MVBs, a ubiquitinated protein is sorted into ILVs by the ESCRT and the downstream fate of the MVB is dependent upon the type of ubiquitin modification on a specific substrate. Ubiquitin may be cleaved from its cargo protein during incorporation to the ILV but a recent *in vivo* study reported that 15% of proteins in EVs are ubiquitinated, suggesting a significant proportion are sequestered into ILVs without deubiquitination [83, 84]. Others PTMs that have been described include phosphorylation and glycosylation[82].

The sorting of RNA into exosomes is less well understood; specific small ubiquitin-related modifier (SUMO) proteins are hypothesized to interact with cis-acting elements within RNA, such as hnRNPA2B1, to selectively load vesicles [85]. MiRNA sorting to exosomes may be modulated by the dynamic transcriptomic changes seen in cell activation, differentially engaging miRNAs at P bodies or MVBs [86].

As a result of the above processes, exosomes represent a parcel of protein, DNA and various RNA species [78, 87]. The majority of RNA species isolated from exosomes are small RNAs including microRNAs (miRNAs) [88]. Exosomes are identified by their lipid bilayer membrane, 20–120 nm size and density of 1.15–1.19 g/ml in continuous sucrose gradient [89]. Their often cited cup-shaped morphology is likely artificial, attributed to collapse during drying [90]. An exosome's lipid bilayer outwardly displays the apical surface of the membrane from which the vesicle was formed, therefore displaying the same extracellular surface markers as the cell of origin (Figure 1.3)[79]. This membrane orientation has lead to the postulation of inward budding, from the limiting membrane of endosomes, as the mechanism of exosome biogenesis. Exosomal protein markers mainly relate to intra-cellular vesicle trafficking and exosome biogenesis i.e. ESCRT components, tetraspanins and flotillin. Although there are signature protein profiles for exosomes from defined tissue, there is no single unifying marker. Specific to the urinary exosome population, CD24 has been postulated as a suitable biomarker [91, 92].

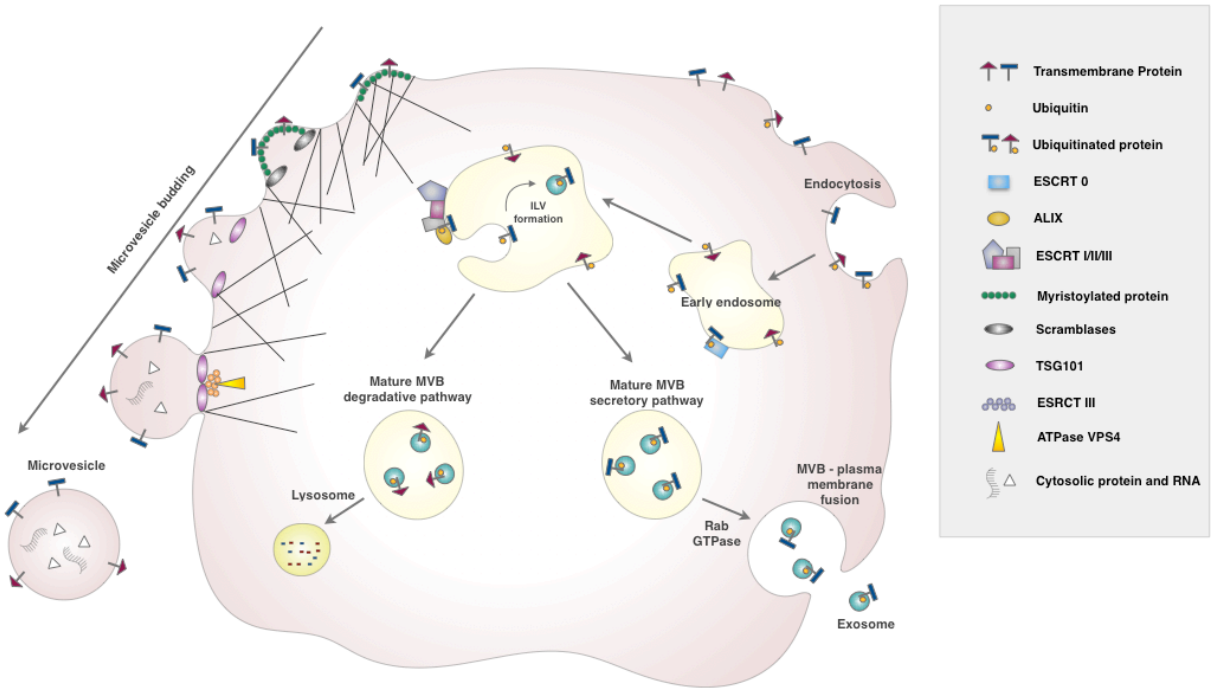

Figure 1.3: EV biogenesis and role of ubiquitination. Modified from [93]

Exosome biogenesis is depicted on the right. Transmembrane proteins are internalized from the cell surface via endocytosis and their cytosolic domains ubiquinated. ESCRT 0 recognises the ubiquitinated protein and segregates these proteins into microdomains. ESCRT I and II are subsequently recruited, by ESCRT I, and initiate the reverse budding of intraluminal vesicles (ILVs). At this stage, a same amount of cytosol, and therefore cytosolic proteins and RNA, have access to the interior of the ILV. The ILV is cleaved from the bud, following recruitment of ESCRT III, by ESCRT II and ALIX. The mature multivesicular body (MVB) formed can either follow a degradation pathway, or proceed to fusion with the plasma membrane. The pathway for each MVB is likely determined by its contents. For example, ubiquitinated LMP2A has been shown to follow the secretory pathway, while MVBs containing ubiquitinated EGFR are degraded. The degradation pathway consists of fusion of the mature MVB with a lysosome. In the secretory pathway MVBs fuse with the plasma membrane mediated by a Rab27A-dependent pathway, releasing the ILVs, now termed exosomes, into the extracellular environment. Please note, not all proteins require ubiquitination to be targeted to ILVs. Other post-translation modifications can result in recruitment to ILVs and have been reviewed in [82].

Microvesicle assembly is illustrated on the left. Transmembrane proteins cluster in membrane lipid microdomains during nucleation at the plasma membrane. Myristoylated protein contributes to membrane curvature, lipid distribution is randomized by calcium dependent scramblases and, concurrently, the cytoskeleton loosens. A member of the ESCRT-I complex, TSG101, recruits ESCRT III to the plasma membrane, which promotes the assembly of a spiral, ultimately disassembled by ATPase VPS4. This process results in cleavage of the bud and release of a heterogeneous population of microvesicles.

1.4.2. Microvesicles

Microvesicles are shed directly from the plasma membrane via detachment of small cytoplasmic protrusions[94] in response to cell stress. This process is dependent on calcium influx, calpain, and cytoskeleton reorganization (*Figure 1.3)*[95]. As a result of this outward budding, microvesicles contain a small volume of cytoplasm and are enriched with membrane markers from their cell of origin including proteins associated with membrane lipid rafts [96]. Microvesicles are characteristically 50 - 1000nm in size and specific markers proposed for their identification are ADP-ribosylation factor 6 (ARF6; implicated in endocytosis of protein) and vesicle-associated membrane protein 3 (VAMP3)[97].

Consideration can also be given to demonstrating the absence of non-EV protein markers when screening exosome and microvesicle populations. For example transferrin receptors are enriched in the exosomes but are absent in the microvesicle population from the same tissue [98].

1.4.3. Apoptotic bodies

Apoptotic bodies are blebs containing cytoplasm and densely packed organelles. They are extensively liberated from the plasma membrane in the later stages of apoptosis. Although apoptotic bodies are generally considered to be larger in size than other vesicles (500-4000nm), a smaller subpopulation has been proposed, 50-500nm [79, 99]. The translocation of phosphatidylserine onto the outer cell membrane during apoptosis has been previously described and it is unsurprising that apoptotic bodies are enriched for this phospholipid. Binding of annexin V to phosphatidylserines therefore can be used as a protein marker for apoptotic bodies. Phosphatidylserines are also exposed by microvesicles and, to a lesser extent, exosomes. Increased binding sites for thrombospondin and C3b allow these proteins to be used as markers [100]. Given the circumscribed pathophysiological role of apoptotic bodies and their efficient local clearance by phagocytosis *in vivo*, apoptotic bodies will not be discussed in further detail.

Pisitkun *et al*. first described the presence of urinary EVs, identifying these as exosomes due to their small size and biogenesis, and describing the proteome of

these vesicles [35]. Since this seminal work was published, the presence of different vesicle subtypes has also been described [101]. Over recent years, a wealth of studies have gone on to describe both the proteome and transcriptome of the urinary EV population [36, 102], culminating in the development of public access online databases (http://www.exocarta.org, https://hpcwebapps.cit.nih.gov/ESBL/Database/Exosome/).

Isolation of a pure vesicle sub-population is notoriously difficult, in part because of the size overlap between the vesicle sub-populations, and other vesicles are often co-purified along with the specific type of interest. Due to inconsistency in EV isolation protocols and often-incomplete vesicle characterization, there is an inherent difficultly in differentiating between the subpopulations in published work. For clarity, in this thesis, vesicle like structures that are not rigorously defined will be referred to as EVs unless clearly stated.

1.5. EV CONCENTRATION AND QUANTIFICATION

Technical standardisation of sample processing is an area of controversy in EV research, although the influence of varying practice on downstream outputs remains unclear. Variability exists in storage, handling and characterisation of EVs between published works; fortunately, guidance is now available through position papers of best practice and consensus statements on EV isolation and minimal experimentation requirements for EV definition [103, 104].

1.5.1. Storage and handling of EVs

Fresh serum or urine samples are preferable for isolation of EVs, although for practicality frozen samples may need to be used with like-for-like being compared (i.e. fresh-to-fresh, frozen-to-frozen). EVs are relatively insensitive to freeze/thaw cycles and may even resist bursting in a hypotonic environment [104]. Storage of samples at -80°C is appropriate and EVs have been concentrated from samples after 7 months in storage [92, 105]. Use of protease inhibitors to preserve samples has been described, but opinion remains inconsistent regarding their use [92, 105]. Calcium oxalate and amorphous calcium crystal precipitates can be present after

thawing, macroscopically forming a cloudy sample. Vigorous vortexing can re-dissolve these salts [106].

1.5.1.1. Ultracentrifugation

Differential ultracentrifugation, with or without a size exclusion technique, remains the most accepted method of exosome isolation from biological fluids [107, 108]. Following cell depletion of a biological fluid by slow speed centrifugation, 10,000 to 20,000 x *g* is used to pellet larger EVs. Subsequently, smaller EVs, including exosomes, are pelleted from this supernatant using an ultracentrifuge (100,000 to 200,000 x *g*). The limitations of this technique are that ultracentrifugation introduces variability, has a low through put, and is heavily operator and rotor dependent [109]. Importantly, not all exosomes are recovered following ultracentrifugation; 40% remain in the supernatant although it is unknown if this subpopulation contains unique features of biological/clinical relevance [110]. Size exclusion chromatography can be used in conjunction with ultracentrifugation to remove protein contaminants and is considered the gold standard for isolation of a highly purified population of morphologically intact exosomes [101, 111].

Alternatively, filtration through a nano-membrane, using slow centrifugation or gravity, can further aid size exclusion and theoretically improve purity of the vesicle subpopulation. Limitations of this technique include a lower EV recovery, vesicle fragmentation and contamination with proteins, with further protein retention on the membrane[104, 112]. Addition of a sucrose gradient can further improve purity and isolate subpopulations, but this process is lengthy and associated with a very low EV yield (<1% of the initial crude pellet)[113]. Interestingly, sucrose gradient ultracentrifugation has been used to elucidate 2 different subtypes of exosome population within melanoma cell supernatant. The populations were distinct in their proteome, transcriptome and effect on recipient cell gene expression; raising the possibility of heterogeneous exosome population capable of exerting different effects on downstream cell physiology[114].

1.5.1.2. Other concentration techniques

A number of commercial platforms support rapid EV precipitation. These proprietary polymers pellet EVs, with the aid of a slow centrifugation step, and have been used

for a wide variety of downstream applications. This approach is attractive due to the rapid aggregation, low user variability and relative simplicity [115, 116]. However, caution must be exercised as these techniques also concentrate larger vesicles and protein aggregates, forming an impure pellet [117]. Immunoaffinity precipitation has been used in a number of studies to concentrate purified subpopulations of EVs, utilising magnetic beads coated with antibody against proteins of interest [118, 119]. Similar peptide-based isolation techniques have also been described [120]. Although these techniques have the capability to achieve an adaptable, rapid platform for EV isolation, they do, inherently, introduce population bias due to targeting only vesicles that express a certain protein marker [121].

Novel microfluidic devices utilise a variety of techniques; namely, immunoaffinity, sieving (through nanoporous membranes) and trapping of vesicle structures, to identify a highly purified EV population [122-124]. Although in its infancy, this technique could be used in point-of-care rapid exosome isolation [124]. There remain a number of hurdles to employment of this technique, mainly low recovery of exosomes, sheer stress to structures, and requirement for prior sample preparation.

1.5.2. Normalisation

Total EV number can be ascertained by nanotracking analysis (NTA) without or with fluorophores to known protein targets, with the additional benefit of using unprocessed urine samples [92]. This methodology could be used to sample 2 populations (the subpopulations of interest and a control) or even dichromatous populations [125]. Alternatively, manipulation of pore size of a stretchable nanopore membrane, utilised in resistive pulse sensing, can allow for measurement size distribution and concentration but this approach is limited by the inability to provide phenotypic information[124]. The primary issue with NTA and nanopore technologies include lengthy processing and inter-assay variability. Until recently conventional flow cytometry could only phenotype EVs down to ~500nm in size, restricting its use to the study of larger vesicle populations. The advent of newer instruments has raised the exciting possibility of discriminating between particles as small as 100 nm in diameter [104]. The impact of different refractive indices

between biological, silica and polystyrene microparticles, and the resultant possibility of confounding results, remains debatable [104, 126]. This issue is further complicated in the study of urinary EVs, as calcium-phosphate microprecipitates have been shown to overlap the EV population on the flow cytometry signal[127].

Given the limitations of describing a total EV population, alternative normalisation methods across samples are needed to allow valid analysis of proteomic and transcriptomic changes. This has previously been described 'the holy grail' of EV study, with a number of well described limitations [128]. Theoretically, protein-normalization (normalizing to a target housekeeping protein) can also be used. Example proteins include: CD9, CD63, CD81, TSG-101, and ALIX[117, 129]. This approach assumes the normalising protein expression does not change in different disease states and there is no biological/clinical relevance to a change in the number of vesicles within the sample.

1.6. EVs AND THE KIDNEY

The kidney is the one of the most important regulators of the body's physiological state, manipulating filtration and reabsorption of solutes in order to maintain an optimal environment for health. The kidney is vulnerable to a plethora of injury modalities. High oxygen demand and low tissue oxygen tensions in the renal parenchyma sensitise tubular cells to hypoxia and can lead to acute and chronic kidney injury, disease processes which are associated with substantial morbidity and mortality. Furthermore, tubular cells are vulnerable to the toxic effects of drugs. Increasing intra-tubular drug concentrations as the filtrate moves along the nephron combined with reuptake mechanisms for solutes result in potentially toxic intracellular drug concentrations. As a result of the high morbidity associated with renal disease, and the limiting role of nephrotoxicity in translation of drug development to clinical practice, improving our understanding of the underlying molecular signalling would be of value to prevent toxicity and treat kidney injury [130].

Urine, the excreted filtrate of the kidney, is unique in providing a non-invasive snapshot of the kidney's function. This filtrate is composed of ions, inorganic and

organic compounds (including proteins, hormones and metabolites) suspended in water. Investigation of the protein fraction of urine has demonstrated the presence of integral membrane proteins within small EVs [131]. Rigorous characterisation of the urinary EV's protein and RNA content has been conducted, identifying molecules unique to all regions of the nephron and identifying products of genes associated with multiple disease processes [35, 36]. Several subtypes of vesicles have been identified in urine, including exosomes and microvesicles, the characteristics of which are described below [35, 101].

Inter-cellular communication depends upon an EV's ability to influence a recipient cell, either by receptor-mediated interaction, endocytosis of the EV or fusion of the vesicle membrane to the plasma membrane. This latter signalling mechanism results in delivery of an EV's contents directly into the cytoplasm; including transcription factors, miRNA, mature RNA and infective particles [21, 95, 132, 133]

1.6.1. Physiology

Along the nephron, EV-mediated intercellular signalling has been postulated to explain why proximal tubule proteins are present in downstream nephron segments [134-136], but this has not yet been conclusively demonstrated *in vivo* [135]. EVs are released into urine from all regions of the nephron and can be readily identified by transcriptomic and proteomic markers specific to the cell of origin [35, 117]. Hypothetically, via EV release and downstream reuptake, EV contents could affect the function of a downstream recipient cell [137]. Notably, the exosomal fraction of aquaporin-2 (AQP2) increases in response to desmopressin and transfer of EVs from desmopressin-treated cells to untreated cells results in an increase of functional AQP2 expression in the recipient cell [129, 138]. Cortical collecting duct cells stimulated with vasopressin take up ECVs, *in vitro* and *in vivo*. This process can be manipulated to deliver miRNA to collecting duct cells resulting in downregulation of target transcripts [139]. This study demonstrated that EV signalling is a physiologically regulated process, which can be manipulated to deliver miRNA. Interaction of EVs with recipient cells may involve specific interaction with primary cilia, as reported with polycystic disease-positive vesicles using transmission electron microscopy images [140, 141]. This observation is supported

by data from a biliary model that demonstrate exosome signalling affects ERK signalling, miRNA expression and cell proliferation, with abolishment of this signal following removal of cilia [142]. This work, in conjunction with the observation of multiple protein products of genes known to be responsible for renal and systemic diseases in normal urine, raises interesting questions about the role of EV signalling in health and disease [35].

1.6.2. Pathophysiology

EV signalling has been implicated in the pathogenesis of acute kidney injury (AKI): exosomes from injured tubular cells transfer TGF-b1 mRNA into fibroblasts, resulting in cell activation [143]. *In vitro*, vesicles appear to be important in mediating vascular smooth muscle cell calcification, a potential mechanism for accelerated vascular calcification in end stage renal disease[144]. Interestingly, the paracrine effect of liver stem cells has been shown to aid regeneration of renal tubular injury via release of EVs, highlighting the possible beneficial role of exosome signalling in systemic illness[145].

Mesenchymal stem cells (MSC) accelerate recovery and repair tissue following AKI; an effect demonstrated using diverse injury modalities [146-150]. Whether this reflects direct cell engraftment and differentiation, or is mediated through release of paracrine factors is unclear. Interestingly, MSC supernatant conferred the same effect as the cells themselves, giving rise to the hypothesis of EV signalling [151]. Several groups have since confirmed EV signalling in this circumstance, likely exerting their effect through RNA interference [152-156]. Recent work suggests EV miRNA has a significant role in this MSC effect on kidney cell injury [157]. Notably, miRNAs associated with EV endothelial progenitor cells reduced apoptosis and promoted cell regeneration in ischemia reperfusion injury [153, 158, 159]. This possible role of EV signalling in the delivery of functional miRNA and pathogenesis of AKI highlights their potential as a therapeutic intervention. Abnormal levels of miRNA could be one of the mechanisms explaining dysregulated protein expression during kidney disease progression and interference with this process represents a potential therapeutic target [160].

In addition, EVs may also act as antibacterial immune effectors within the urine, mediating the host response to urinary tract infection by inhibiting growth of pathogenic and commensal Escherichia coli and inducing bacterial lysis [161]. This highlights the multimodality capacity of EVs in therapeutics, specifically their potential as novel antibiotics for urinary tract infections, a common illness affecting 150 million patients annually[162]. Furthermore, renal brush border-derived exosomes can induce calcium oxalate crystallization in nephrolithiasis and may have a role in renal stone disease although this mechanism is yet to be demonstrated *in vivo* [163].

1.6.3. Vectors for drug delivery

The contribution of EV signalling in health and disease highlights their potential as attractive therapeutic targets and there are a number of on-going phase I and II clinical trials harnessing EV-based therapeutics. Although we remain in the early phase of such studies, theoretical clinical utility could be mediated by interfering with EV biogenesis or the manipulation of EVs as therapeutics vectors.

EVs are candidate drug delivery systems; they are stable vehicles with a wide biodistribution. At least in theory they can be selectively loaded and can deliver functional RNA into cells. The integrity of RNA isolated from vesicles is similar to that of tissue and far higher than RNA in whole urine, as the membrane protects the RNA cargo from RNase degradation [36, 88]. Interestingly, EVs have natural targeting capacity, presumably by receptor-ligand binding [164-166]. In oncology, intergrins displayed on the EV surface may direct tissue specific uptake [167], manipulation of which may reduce EV uptake and impede metastatic spread of cancer. This ability to predict the metastatic course of cancer raises the exciting possibility of prediction and redirection of tumour progression. A similar mechanism could also be responsible for EV signalling along the kidney and the *in vitro* transfer proximal tubular specific proteins in distal tubule cells[168]. EV signal manipulation *in vivo,* to target exogenous vesicles to the tissue of interest through delivery of miRNA and siRNA, has already been demonstrated, ultimately affecting downstream gene expression [169, 170]. Furthermore, bioengineered nanoparticles

can serve as exosome mimics, recreating these functions and delivering targeted chemotherapeutics [171].

1.6.4. Inhibiting EV biogenesis and uptake

The circulating concentration of exosomes has been correlated to cancer progression and overall survival, which suggests that reducing exosome numbers may be a potential therapeutic approach. Proof-of-concept using amiloride (an antihypertensive agent) to attenuate endocytic vesicle recycling increased the effect of chemotherapy agents in a murine model, speculatively as a result of reduced EV numbers in the circulation [172]. Although precise regulation of exosome release remains unclear, a number of possible therapeutic targets have been identified. Rab27b interference inhibits exosome release and can reduce tumour progression [173-175]. Other therapeutic targets of interest include P53 and GTPases, implicated in the cytoskeleton dependent mechanism underpinning exosome exocytosis [164, 176, 177]. Inhibition of EV uptake into cells is also possible by blocking surface phosphatidylserine, however due to lack of specificity this mechanism it is unlikely to translate into a therapeutic intervention. Regardless of the therapeutic strategy employed, there are a large number of limitations to targeting exosome biogenesis and uptake; in particular, currently elucidated mechanisms are not tissue-specific and affect a number of complex, core functions in diseased and healthy tissue. For a future drug, this may manifest in a large number of off-target effects, greatly affecting this approach as a therapeutic strategy.

1.7. URINARY EVS AND BIOMARKER DISCOVERY

In both acute and chronic kidney disease current biomarkers, such as creatinine, focus on the recognition of established disease rather than early detection of imminent renal dysfunction. These investigations provide little information about the underlying pathophysiology and renal biopsy is considered the gold-standard investigation. Renal biopsy is an invasive technique with a number of adverse events such as infection and haemorrhage. Also biopsy cannot be performed serially (daily) and is prone to sampling error. There is hope that harnessing the proteomic and transcriptomic changes of urinary EVs in varying disease states will present a non-invasive alternative to biopsy. As discussed, urinary EVs are released

into urine from all regions of the nephron and are readily identified by proteins specific to the cell of origin, potentially providing a non-invasive snapshot of the physiological state of nephron [35, 117]. Urinary EVs represent a remarkably stable, easily accessible, biomarker reservoir, which protects its cargo from the harsh extra vesicular environment. EVs are promising biomarker candidates, with potential to predict disease, define mechanisms and prognosticate. Intriguingly, EV biomarkers for systemic disease have been identified in the urine, adding further evidence to the debate surrounding passage of EVs across the glomerulus (Table 1.1).

Three fundamental biomarker development stages have been described; biomarker *discovery*, *validation* of the markers predictive value within the population and *implementation* of a clinically approved assay [178, 179]. In relation to urinary EVs, biomarker discovery in well-defined populations has identified a number of targets. Table 1.1 summarises the candidate EV biomarkers to date, distinguishing biomarkers of interest by disease process. In models of kidney injury, the proteins in the exosomal fraction have been reported to change prior to elevation in the 'free' fraction in urine and, importantly, prior to traditional biochemical and histological diagnostic tests [180, 181]. Lower EV recovery rates in patients with heavy proteinuria and the outlined difficulties in normalisation have led investigators to pursue qualitative targets i.e. the presence or absence of the target defines disease or health. Ultimately, quantitative measurements would be desirable, allowing the ability to track deterioration or improvement in the clinical condition. The validation phase of study, and the challenges to further progress, perhaps best reflect the current situation. Large population studies are required, outwith the population of interest, to identify both the positive and negative predictive value of the EV-based biomarker. Several studies have investigated the selectivity of EVs but few have interrogated the specificity. The practicality and cost of the necessary large-scale clinical studies limits further progress, as sample processing and quantification are not currently translatable to hundreds or thousands of samples.

	Potential urinary EV biomarker	
Disorder	**Protein**	**miRNA/mRNA**
Acute Kidney injury		
AKI	Fetuin -A*, Activating transcription factor-3*, Na+/H+ exchanger type 3*	CD2AP*†
Ischaemic reperfusion injury	Aquaporin-1*, Activating transcription factor-3*	
Glomerular injury		
Diabetic nephropathy	Dipeptidydl peptidase IV†, Podocalyxin*, Wilm's tumour-1*, Histone-lysine N-methyltransferase* Voltage-dependent anion-selective channel protein 1*, Alpha-1-microglobulin/bikunin precursor*	miR-145*, miR-130*,miR-155*, miR-424*
Focal segmental glomerular sclerosis	Wilm's tumour 1†‡, Podocalyxin*	
Autoimmune glomerulonephritis		miR-26a†
Lupus nephritis	A disintegrin and metalloprotease 10*	miR-29c*†, miR-26a*, miR-146a*
Glomerular disease (mixed population)	A disintegrin and metalloprotease 10*	
IgA nephropathy	α1 antitrypsin*, Aminopeptidase N*, Vasorin precursor*, Ceruloplasmin*,	
Glomerular fibrosis		CD2AP*†
Other disorders		
Polycystic Kidney Disease	Polycyctin-1*†, Polycyctin-2*†, Polyductin*, Transmembrane protein 2*†	
Primary aldosteronism	Phosphorlyated NCC*, Prostasin*	
Obstructive Nephropathy	Transforming growth factor β*	
Bartter syndrome	Na+, K+, Cl- cotransporter type 2*	
Gitelman syndrome	Phosphorlyated NCC*	
Renal fibrosis		miR-29c*, miR-200*
Chronic Kidney Disease	Neutrophil gelatinase-associated lipocalin*	
Transplant	Neutrophil gelatinase-associated lipocalin†,	mRNA Il-18†

Cancer		
Prostate cancer	Integrin β1*, Integrin α3*, Prostate specific antigen*‡, Prostate specific membrane antigen*	miR-34a‡
Bladder cancer	EGF-Like Repeats And Discoidin I-Like Domains 3*, Tumor-associated calcium-signal transducer 2*, Mucin 4, Epidermal Growth Factor Receptor Pathway Substrate 8-Related Protein 2*	LASS2*, GALNT1*
Renal Cell carcinoma	Matrix metalloproteinase 9*, Ceruloplasmin*, Podocalyxin*, Dickkopf related protein 4*, Carbonic Anhydrase IX*, Aquaporin-1*, Extracellular Matrix Metalloproteinase Inducer*, Neprilysin*, Dipeptidase 1*, Syntenin-1*	
Systemic illness		
Acute myocardial infarction		miR-1*, miR-208*
Parkinsons Disease	Protein deglycase DJ-1†	
Ovarian serous adenocarcinoma		miR-30a-59*
Lupus erythematosus		miR-146a*
Autoimmune encephalomyelitis		miR-155-5p*‡
Type 2 diabetes		miR-143*
NSCLC	Leucine-rich α-2-glycoprotein*	

Table 1.1: Examples of urinary EV biomarkers and proposed clinical usage

*diagnostic †prognostic ‡response to treatment

1.8. HYPOTHESIS

Functional, circulatory miRNAs are transferred from injured distant organs to the renal proximal tubule (PT) via EVs.

1.9. RESEARCH AIMS

- Describe the circulatory miRNA concentration changes following myocardial injury in human and mouse models of illness.
- Develop a PT model of EV uptake and release, and identify physiological and pathophysiological regulators.
- In the PT model, compare the effect of circulating EVs containing miRNA from injured heart and liver.

Chapter 2: Circulatory miRNA concentration changes in a human model of myocardial ischaemia

Contents

2.1. INTRODUCTION

2.1.1. Background

Circulating miRNAs represent a potentially rich reservoir of biological information as they provide insights into the fine regulatory function of the tissue of origin[1]. MiRNA's negative interference with post-transcriptional gene expression, and their subsequent role in cellular function, provide potential for these molecules to be both biomarkers of illness and therapeutic agents.

Despite recent advances, coronary artery disease is a major contributor to worldwide morbidity and mortality[182, 183]. Post-infarct miRNA expression changes are an active area of research and several miRNAs have been described as early biomarkers of myocardial ischaemia, potentially reducing time from start of symptoms to diagnosis (or exclusion of cardiac injury) [53]. Concentrations of miR-208a/b[52, 53] and miR-133a[54, 55] have been demonstrated to increase significantly in the circulation post-myocardial insult, and circulatory miRNA-499 has been positively correlated to cardiac infarct size[7, 56-58]. However, head-to-head comparisons with established biomarkers, such as high-sensitivity troponins, have reported that measurement of these miRNAs did not improve diagnostic accuracy [59]. Furthermore, with the exception of miR-208a, all other previously described cardiac miRNAs are enriched in skeletal muscle[60]; limiting specificity for the diagnosis of myocardial injury. Measurement of circulating high-sensitive troponin concentration at presentation to hospital can accurately identify patients at low risk of myocardial infarction [184]. At present, it remains unclear if and how miRNAs as biomarkers can contribute to this clinical scenario.

Research into the potential role of miRNA in cell signalling within the myocardium is still in its infancy. MiRNAs have been implicated in multiple disease processes, including; heart failure[185], myocardial infarction[7], cardiac remodelling[186], arrhythmias[187] and ischaemic heart disease[188]. Exosomal miRNA transfer between cells has been implicated as a paracrine signalling process within the myocardium. For example, cross-talk between cardiac fibroblasts and cardiac myocytes may be underpinned by exosomal transport of miR-21. This microRNA

transfer significantly impacts upon cardiac function via repression of the SH3 domain containing 2 (*SORB2*) and PDZ and LIM domain 5 (*PDLIM5*) target genes[189]. Exosomes from cardiac progenitor cells may aid in cardiac remodelling after myocardial infarction by inhibiting apoptosis in cardiac myocytes[190]. Although these results are promising, the relevance of miRNA signalling within the myocardium is not fully understood, much less the potential biological role changing circulatory miRNA patterns may exert on a distant organ.

The experiments described in this chapter aimed to define the change in circulatory miRNA expression following myocardial injury in humans, with a line of sight on determining the impact of these changes on the kidney in subsequent chapters.

To elucidate circulating miRNA expression changes small RNA sequencing was conducted on plasma samples from patients prior to and following myocardial injury. The study design focused on interrogating the changing miRNA signature at early time points. Elective coronary artery bypass graft (CABG) is a predictable model of ischaemic myocardial injury[191], ideal for miRNA biomarker discovery and was therefore selected as our group of interest. Patients undergoing elective hip arthroplasty were recruited as a control group because they experienced bone and skeletal muscle injury without cardiac damage.

2.1.2. Objectives

To describe the changes in circulatory miRNA expression associated with myocardial ischaemia at 2 and 6 hours following start of cardiac injury in humans.

2.2. METHODS

2.2.1. Study design

2.2.1.1. Research governance and ethics

Studies were approved by a local Research Ethics Committee and were performed in accordance with the Declaration of Helsinki of the World Medical Association and approved by the Medical Ethics Committee of NHS Lothian. Written informed consent was obtained from all subjects.

CABG patient blood sampling was conducted during the Elafin Myocardial Protection from Ischaemia RepErfusion injury (EMPIRE; EudraCT number: 2010-019527-58) trial. This trial was conducted between September 2011 and August 2013. Age- and sex-matched blood samples required for the control group were collected in the Stratification of heart disease using miRNA biomarker discovery study (EMPIRE miRNA study; REC reference number 15/LO/0727) between July and September 2015. Both studies had comparable protocols which are described as follows.

2.2.1.2. Subjects

Potentially suitable subjects were identified from patients awaiting elective coronary artery bypass graft surgery (EMPIRE study) or elective hip arthroplasty (EMPIRE miRNA study), attending clinics in the Royal Infirmary of Edinburgh.

2.2.1.2.1. Inclusion criteria

- Male.
- Adults (aged 16-75 inclusive).
- Patients undergoing elective CABG or hip arthroplasty involving general anaesthetic.
- Adults within the CABG group administered placebo

2.2.1.2.2. Exclusion criteria

- Female.
- Adults unable to provide informed consent.

- Recent troponin positive event (a recorded troponin higher than the normal range indicated for the assay < 1 month of surgery).
- Severe left ventricular dysfunction (ejection fraction less than 30%).
- Chronic renal failure (preoperative estimated glomerular filtration rate (eGFR) <60 ml/minute/1.73m^3)
- Adults undergoing emergency surgery.
- Adults undergoing re-intervention surgery.
- Adults within the CABG group administered Elafin (the elastase-specific protease inhibitor used as the pharmacological intervention within the EMPIRE study)

2.2.1.3. Study protocol

Blood samples were taken at baseline (defined as up to 4 hours before the first skin incision, T0) and at 2-(T2), 6-(T6) and 24- (T24) hours after first skin incision (CABG or hip arthroplasty). These blood samples were taken on the ward by either the named researcher or clinical research nurse. Blood samples required to be taken intra-operatively, were obtained by the theatre staff and collected by the clinical research nurse or named researcher. Samples taken at T0, T2 and T6 represented additional blood sampling to the routine care of the patient.

2.2.1.3.1. Sample handling

Blood samples were taken from patients for measurement of serum urea, creatinine, sodium, potassium and troponin I. A sensitive cardiac troponin I assay (ARCHITECT$_{stat}$ troponin I assay; Abbott Laboratories, IL, USA) was used because it was the highest standard of care at the time of blood sampling. These samples were analysed by the clinical laboratories at the Royal Infirmary of Edinburgh, ensuring robust analysis. Notably, the limit of detection for the troponin assay was 10 ng/L and the upper reference limit (99th centile) of a normal reference population was 28 ng/L [46]. The inter-assay coefficient of variation was less than 10 % at 50 ng/L under local laboratory conditions and this concentration was used as the diagnostic threshold.

Concomitant blood samples were taken for isolation of RNA. After blood collection, 1 serum gel (S-Monovette® Z-Gel, Sarstedt, Nümbrecht, Germany) and 2

ethylenediaminetetraacetic acid (EDTA; S-Monovette® 1.6 ml K3EDTA, Sarstedt, Nümbrecht, Germany) were centrifuged at 1000 x *g* for 10 minutes, and the subsequent supernatant isolated and stored as 500μL aliquots. Samples were immediately stored at -80°C until RNA extraction.

2.2.1.3.2. Patient followup

The following adverse event information was collected up to 24 hours post procedure. Patients encountering any of these events were excluded from downstream analysis.

- Any cardiac arrhythmia, including atrial fibrillation (sustained for more than 5 minutes).
- Deterioration in renal function as defined by a serum creatinine rise from baseline by ≥ 26*μ*mol/L within 24 hours (AKI Stage 1 for acute kidney injury).
- Low cardiac output syndrome and inotrope requirement.
- Red blood cell transfusion.
- Re-operation for bleeding.
- Orthopaedic group only: Increase in Troponin I from baseline (T0) concentration (defined as >10% troponin rise at any time point in comparison to T0)

2.2.2. Second generation sequencing

2.2.2.1. Study design

132 plasma samples were transported to BGITech, Hong Kong, for small RNAseq analysis. This represented 22 patients in the CABG and control group, respectively, with bloods samples corresponding to T0, T2 and T6 time points.

Total RNA was extracted from 200μL of each sample using the miRNeasy Serum/Plasma kit and Qiazol (Qiagen, MD, United States) according to the manufacturer's instructions. Small RNA sequencing libraries were prepared using the TruSeq Small RNA Library Prep Kit (Illumina, CA, United States). RNA quality and quantity was assessed using the Agilent 2100 (Agilent technologies, CA, United States) and 106 samples were confirmed to contain >4ngμL and and RNA integrity number (RIN) >2. These 106 samples contained complete temporal profiles (T0, T2

and T6) of 14 patients in CABG group and 14 in the orthopaedic group and were subsequently taken forward to sequencing.

8 samples were pooled by lane and underwent single-end sequencing using the HiSeq4000 (Illumina, CA, United States). Sequence data (raw fastq format) for the 84 samples was transferred by hard disk for bioinformatics analysis.

2.2.2.2. Analyses performed

Raw sequences, provided as 18-44 base long single-end reads in gzipped fastq format were quality assessed using FASTQC (Babraham Institute, Cambridge, United Kingdom). Based on the output of the FASTQC analysis, the raw fastq sequences required further pre-processing to remove contaminating primers. This was done using Cutadapt software (Massachusetts Institute of Technology, MA, United States). Cleaned sequences were collapsed within each sample to generate a non-redundant set of fasta sequences. Singletons were excluded.

Using miRDEEP2 software[192], the hg19 human genome (obtained from NCBI, chromosomes and unmapped sequences, 68 in total) was the reference sequence used to identify miRNAs. Alignments (end-to-end, -very-sensitive settings) to the reference were performed using Bowtie (John Hopkins University, MD, United States). No mismatches were allowed. Raw "tag counts" (i.e. sequences aligning) per sample were normalised, within each of the two groups, to the sample with the lowest number of miRNA alignments, and counts converted to log2.

Pairwise comparisons of sample groups (e.g. T2 relative to T0, T6 relative to T0, T6 relative to T2) were performed within groups. Analyses were also conducted between groups but given the group-group variation in number of reads obtained, these data were largely uninterpretable and were not pursued further. Only patients that had all three time points were included (84 of the 106 initial samples). A series of 6 group-wise comparisons was undertaken to identify differences (fold changes) between the normalised tag counts, using linear modelling including vertical P value

adjustment (Bioconductor *limma* package)[193]. All data are presented as a log2 fold change, a log2 fold change of 1.5 represents a fold change of 2.8.

2.2.3. PCR validation of sequencing results

2.2.3.1. RNA extraction

Total RNA was extracted from 200μL of each sample using the miRNeasy Serum/Plasma kit (Qiagen, MD, United States) according to the manufacturer's instructions. *Caenorhabditis elegans* miRNA mimic (cel-miR-39; Qiagen, MD, United States) was used for the spiked-in control.

2.2.3.2. Heparinase treatment

Patients undergoing CABG receive intravenous heparin intraoperatively. To remove possible heparin contamination of the plasma samples, 6 μl of heparin RNA was added to a master mix consisting of 2 μl of 10x reaction buffer (New England Biolabs, Ipswich, United Kingdom), 10.75 μl of RNA free H_2O, 0.25 μl of Heparinase I (New England Biolabs, Ipswich, United Kingdom) and 1 μl of RNase inhibitor (Promega, WI, United States). Samples were incubated for 1 hour at 30°C followed by 1 minute at 99°C. Samples were stored at -80°C.

To validate our heparin decontamination methodology, paired blood samples were taken from healthy volunteers; 1 serum gel collection tube (S-Monovette® Z-Gel, Sarstedt, Nümbrecht, Germany) and 1 lithium-heparin collection tube (S-Monovette® LH, Sarstedt, Nümbrecht, Germany). Samples were centrifuged at 1000 x *g* for 10 minutes, and the subsequent supernatant isolated and stored as 500μL aliquots. Samples were immediately stored at -80°C until RNA extraction. In this study miR-122 was chosen as a high abundance miRNA target to assess DNA polymerase inhibition.

2.2.3.3. Reverse transcription reaction setup

To generate cDNA the miScript II Reverse Transcription Kit (Qiagen, MD, United States) was used according to manufacturer instructions. 6 μl of treated RNA was added to a master mix consisting of 4 μl of 5x HiSpec buffer, 2 μl of 10x Nucleics mix, 6 μl RNA free H_2O and 2 μl of reverse transcriptase mix. Samples were

incubated for 1 hour at 37 °C followed by 5 minutes at 95 °C. All cDNA syntheses were diluted 10-fold and stored at -80°C.

2.2.3.4. Quantitative real time analysis

Real-time quantification to measure miRNAs was performed by using the SYBR green miRNA kit (Qiagen, MD, United States) with Lightcycler 480 (Roche Diagnostics, IN, United States). For quantification, 1μl of cDNA was added to a master mix consisting of 5 μl SYBR green PCR mix, 1 μl of miScript universal primer, miScript primer assay and 2 μl of RNA free H_2O. MiRNA-specific miScript primer sets were obtained from Qiagen. Melting curve analyses showed specific amplification with no primer dimer or non-specific products. The data were analysed with automatic setting for assigning baseline; the Ct is defined as the fractional cycle number at which the fluorescence exceeds the given threshold. The Ct values from real-time PCR assays greater than 40 were treated as 40. All samples were processed in triplicate and Ct values were normalized by using the mean Ct obtained from the spiked-in or internal controls. The data obtained by real-time PCR were translated by the $2^{\Delta Ct}$ method [194].

2.2.3.5. Primer details

The following pre-designed MiScript Primer Assays were purchased from Qiagen (MD, United States):

Primer name	Mature miRNA target	Catalogue Number	Sequence
Hs_let-7e_3	hsa-let-7e-5p	MS00031227	5'UGAGGUAGGAGGUUGUAUAGUU
Hs_miR-125b-2*_1	hsa-miR-125b-2-3p	MS00008568	5'UCACAAGUCAGGCUCUUGGGAC
Hs_miR-133a_2	hsa-miR-133a-3p	MS00031423	5'UUUGGUCCCCUUCAACCAGCUG
Hs_miR-140-3p_1	hsa-miR-140-3p	MS00008673	5'UACCACAGGGUAGAACCACGG
Hs_miR-145_1	hsa-miR-145-5p	MS00003528	5'GUCCAGUUUUCCCAGGAAUCCCU
Hs_miR-199a-3p_1	hsa-miR-199a-3p	MS00007602	5'ACAGUAGUCUGCACAUUGGUUA
Hs_miR-208_1	hsa-miR-208a-3p	MS00003794	5'AUAAGACGAGCAAAAAGCUUGU
Hs_miR-23a_2	hsa-miR-23a-3p	MS00031633	5'AUCACAUUGCCAGGGAUUUCC
Hs_miR-378g_1	hsa-miR-378g-5p	MS00037618	5'ACUGGGCUUGGAGUCAGAAG
Hs_miR-769-5p_1	hsa-miR-769-5p	MS00007210	5'UGAGACCUCUGGGUUCUGAGCU
Hs_miR-99a_2	hsa-miR-99a-5p	MS00032158	5'AACCCGUAGAUCCGAUCUUGUG
Hs_miR-22_1	hsa-miR-22-3p	MS00003220	5'AAGCUGCCAGUUGAAGAACUGU
Hs_miR-1_2	hsa-miR-1-3p	MS00008358	5'UGGAAUGUAAAGAAGUAUGUAU
Hs_miR-499_1	hsa-miR-499a-5p	MS00004375	5'UUAAGACUUGCAGUGAUGUUU
Hs_miR-30a-5p_1	hsa-miR-30a-5p	MS00007350	5'UGUAAACAUCCUCGACUGGAAG
Hs_miR-30d_2	hsa-miR-30d-5p	MS00009387	5'UGUAAACAUCCCCGACUGGAAG
Hs_miR-99b_2	hsa-miR-99b-5p	MS00032165	5'CACCCGUAGAACCGACCUUGCG
Hs_miR-100_2	hsa-miR-100-5p	MS00031234	5'AACCCGUAGAUCCGAACUUGUG
Hs_miR-486_1	hsa-miR-486-5p	MS00004284	5'UCCUGUACUGAGCUGCCCCGAG
Ce_miR-39_1	cel-miR-39-3p	MS00019789	5'UCACCGGGUGUAAAUCAGCUUG

Table 2.1: MiScript Primer Assays used during real-time PCR validation of miRNA expression changes in human model of myocardial injury

2.2.3.6. Data evaluation and statistical analysis of PCR data

Where possible data were presented as Tukey box plots. Tukey box plots consist of 4 parameters; box ends at the quartiles Q1 and Q3, median as a horizontal line in the box, 'whiskers' to the farthest points that are not outliers (i.e. within 3/2 times the interquartile range of Q1 and Q3) and dot plot of outliers. Data were analysed using a one-way ANOVA with Dunnett's post-hoc test. The software used was GraphPad PRISM (version 6.03 for Windows, GraphPad Software, San Diego, USA). A P-value < 0.05 was considered statistically significant.

2.3. RESULTS

2.3.1. Subjects

Male subjects were recruited to the CABG group (n=22) and the orthopaedic control (n=22). There was no difference in the mean age or BMI between the 2 groups but significant differences were seen in baseline co-morbidity and medications (Table 2.2). Increased incidence of hypertension and hyperlipidaemia, and subsequent statin prescription, was present in the CABG cohort.

Characteristics		CABG Group	Orthopaedic Group	P value
Age (mean±SD)		62.45 ± 7.92	67.82 ± 10.72	0.070
BMI		29.67±3.86	29.18±5.42	0.755
Smoker, *n* (%)		7 (31.8)	2 (9.1)	0.132
6 hour troponin (mean±SD)		7.924 ± 9.326	below LOD	n/a
Comorbidities	IHD	22 (100)	3 (13.6)	<0.001
n (%)	Hypertension	16 (72.7)	6 (27.3)	0.006
	Hyperlipidaemia	13 (59.1)	3 (13.6)	0.004
	Diabetes	3 (13.6)	1 (4.5)	0.607
Medication	Aspirin	22 (100)	3 (13.6)	<0.001
n (%)	Clopidogrel	9 (40.9)	2 (9.1)	0.034
	Statin	21 (95.5)	2 (9.1)	<0.001

Table 2.2: Baseline characteristics of the subjects

Significance of numerical data between groups was ascertained using 2-tailed t-test. Analysis of nominal data was calculated using 2-tailed Fishers exact test.

2.3.2. Second generation sequencing results

2.3.2.1. Summary of raw data

333 mature miRNAs were identified within the CABG group. Circulatory miRNAs within the CABG group showed reduced variance in their temporal fold change following myocardial injury (Figure 2.1, Group 1, panels A-C) in comparison to the orthopaedic control group (Figure 2.1, Group 2, panels D-F). This likely was as a consequence of the difference in storage times between the 2 cohorts. The study was technically challenging in that the input samples were generally small, leading, in some cases, to poor RNA yields for sequencing purposes. CABG blood samples were stored for 4-6 years at -80°C, while the orthopaedic control group were stored at the same temperature for 2-3 months. Consequently, there was significantly reduced variance in the miRNA temporal fold change following myocardial injury (Figure 2.3, Group 1, panels A-C) in comparison to the orthopaedic control group (Group 2, panels D-F)(Table 2.3).

	CABG (Group 1)	Orthopaedic (Group 2)	F test	P value
	Mean± SD	Mean± SD		
T2-T0	0.0881 ± 0.4634	0.1006 ± 1.1080	5.721	< 0.0001
T6-T0	0.0403 ± 0.4597	0.1577 ± 0.7486	2.651	< 0.0001
T6-T2	-0.0479 ± 0.3769	0.0577 ± 0.9331	6.128	< 0.0001

Table 2.3: Comparison of variance between groups of miRNA concentration mean log fold change

Comparison of mean log fold change of circulating miRNAs in CABG and orthopaedic cohorts. F test conducted to ascertain variance between log fold changes between group 1 and group 2 (group 2 exhibited the largest variance and was consequently used in the numerator).

2.3.2.2. Temporal expression of miRNA within groups

The following comparisons were undertaken: CABG group, T2 relative to T0, T6 relative to T0 and T6 relative to T0, and; orthopaedic group T2 relative to T0, T6 relative to T0 and T6 relative to T0.

The 10 miRNAs exhibiting the largest differential temporal expression changes in the CABG group and orthopaedic group are shown in Table 2.5. Within the CABG cohort, several miRNAs have previous been identified as biomarkers of myocardial injury, significantly more than in the orthopaedic group (8 and 2 miRNAs respectively, 2-tailed Fishers exact test, $P < 0.05$; Table 2.4 and Table 2.5).

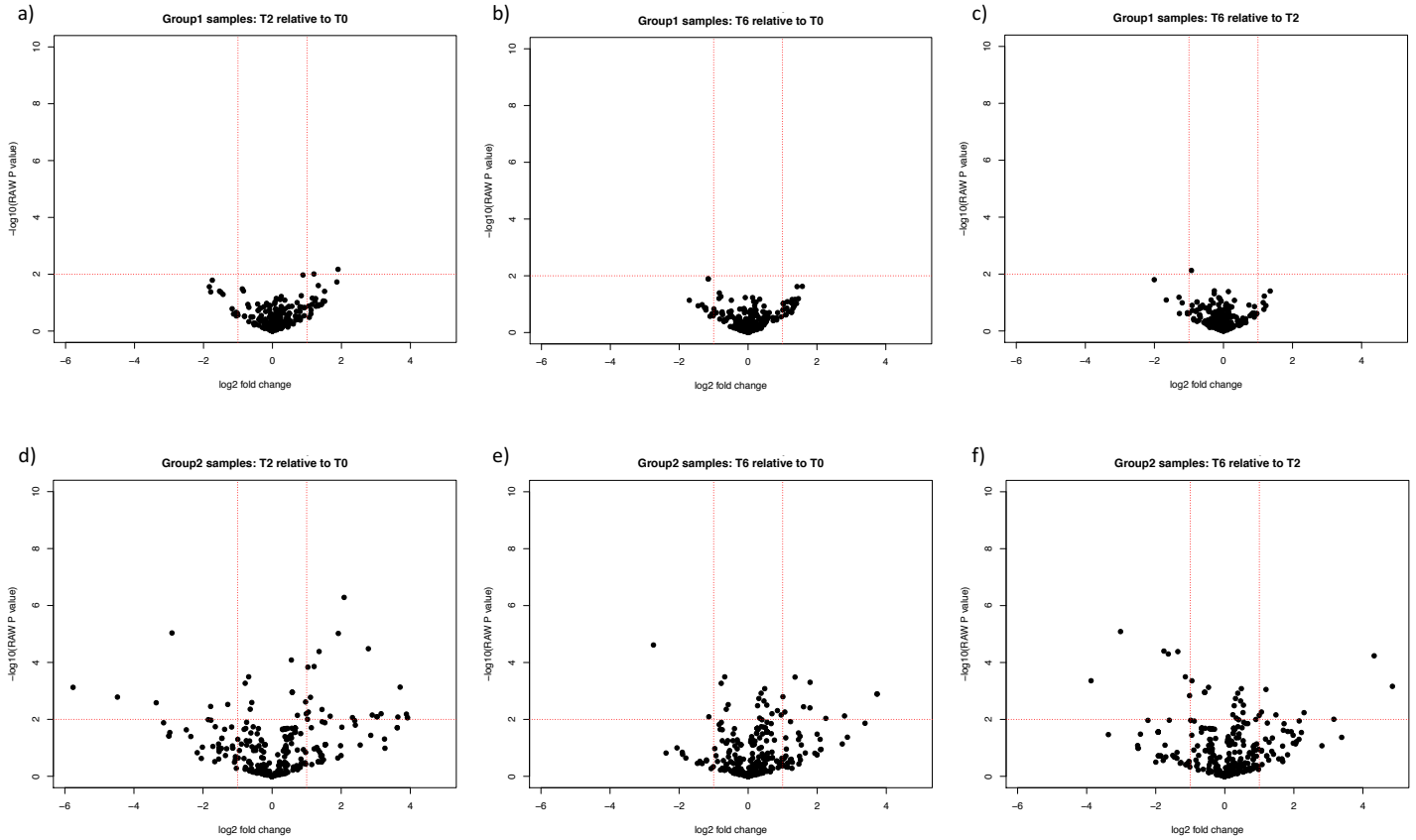

Figure 2.1: Volcano plots of group comparisons

Panels A-F show volcano plots (-log(10) raw P value versus log(2) fold change) for all comparisons. Red lines transecting x- and y-axis' demonstrate ± 1 fold change and P-value 0.05 respectively. CABG group mature miRNA (Group 1; panels A-C) demonstrate reduced variance in respect to fold change and statistical significance, in comparison to control orthopaedic group (Group 2, panels D-F).

2.3.2.3. 66 miRNAs exhibited a 1.5 fold log change within the CABG cohort

Across all 3 time-point comparisons, 66 miRNAs were found to be up-or down-regulated 1.5 log2 fold within the CABG group (Table 2.6). Of these 66, 42 have previously been identified in the myocardium. 12 out of the 66 miRNA species identified to have changed in the CABG have previously been described as potential cardiac biomarkers.

15 miRNAs of interest were selected for further study. Selection criteria were based on their previous identification in the myocardium, degree of expression change and stability in comparison to control (Figure 2.2). The 15 miRNAs were: hsa-let-7e-5p, hsa-miR-100-5p, hsa-mir-125b-2-3p, hsa-miR-133a-3p, hsa-miR-140-3p, hsa-miR-145-5p, hsa-miR-199a-3p, hsa-miR-22-3p, hsa-miR-23a-3p, hsa-miR-30a-5p, hsa-miR-30d-5p, hsa-miR-378g, hsa-miR-769-5p, hsa-miR-99a-5p and hsa-miR-99b-5p.

2.3.2.4. miR-486-5p is a potential internal normaliser

Within the CABG cohort, expression levels were considered for each miRNA for each time point. Mir-486-5p varied the least across the 3 considered time points (19.2957 $\pm$ 0.0001729; mean normalised read count $\pm$ SD) and therefore taken forward as a potential internal normalizer in this experimental design.

2.3.3. rtPCR validation of miRNAs of interest

The process of miRNA validation was undertaken using rtPCR. The 15 miRNAs of interest identified from the second generation sequencing document study were interrogated, as were 3 additional miRNAs proposed in the literature as biomarkers of myocardial injury (miR-1, miR-208 and miR-499). Plasma samples interrogated in the rtPCR verification phase were collected from patients using the same EMPIRE and EMPIRE miRNA study protocol as the second generation sequencing biomarker discovery phase. Notably, the scarcity of samples resulted in the same study patients not being available for both experiments. Plasma samples from T0, T2 and T6 time points were analysed from both CABG (n=10) and Orthopaedic cohorts (n=10). T24 samples were included for the CABG cohort alone, as samples were not collected for this time point in the orthopaedic control group.

Time point comparison	Mature miRNA	Log fold change	Raw P value
T2-T0	**hsa-miR-22-3p**	**1.9**	**0.006**
	hsa-miR-451a	**1.87**	**0.018**
	hsa-miR-99a-5p	**1.51**	**0.089**
	hsa-miR-769-5p	**1.51**	**0.039**
	hsa-miR-30a-5p*	**1.47**	**0.087**
	hsa-let-7f-5p	**-1.83**	**0.027**
	hsa-let-7f-5p	**-1.79**	**0.041**
	hsa-let-7e-5p*	**-1.74**	**0.016**
	hsa-let-7a-5p	**-1.53**	**0.039**
	hsa-let-7a-5p	**-1.49**	**0.043**
T6-T0	**hsa-miR-22-3p**	**1.58**	**0.023**
	hsa-miR-451a*	**1.46**	**0.064**
	hsa-miR-145-5p*	**1.42**	**0.024**
	hsa-miR-186-5p	**1.41**	**0.094**
	hsa-miR-27b-3p*	**1.36**	**0.068**
	hsa-miR-150-5p	-1.71	0.073
	hsa-miR-21-5p*	**-1.45**	**0.14**
	hsa-miR-146b-5p*	**-1.34**	**0.14**
	hsa-miR-148a-3p	**-1.26**	**0.13**
	hsa-let-7f-5p	**-1.23**	**0.13**
T6-T2	hsa-miR-203a-3p	1.35	0.039
	hsa-miR-26b-5p*	**1.23**	**0.128**
	hsa-miR-145-5p	**1.18**	**0.059**
	hsa-miR-92b-3p	1.17	0.174
	hsa-miR-181a-3p*	**1.15**	**0.100**
	hsa-miR-146b-5p	-2	0.016
	hsa-miR-150-5p	-1.66	0.081
	hsa-miR-140-3p	**-1.29**	**0.065**
	hsa-miR-320a	-1.28	0.243
	hsa-miR-769-5p	**-1.2**	**0.102**

Table 2.4: Circulatory miRNAs exhibiting the largest differential expression (fold change) in the CABG cohort

The 10 miRNAs demonstrating the greatest differential expression (five up-regulated, five down-regulated) for each comparison are shown with accompanying statistical significance details. Fold change data shown at Log2.*Previously described as biomarker of cardiac injury. MiRNAs highlighted in bold have previously been described in the myocardium

Time point comparison	Mature miRNA	Log fold change	Raw P value
T2-T0	**hsa-miR-101-3p**	**3.92**	**0.008**
	hsa-miR-101-3p	**3.92**	**0.008**
	hsa-miR-99a-5p	**3.89**	**0.006**
	hsa-miR-19a-3p	3.71	<0.001
	hsa-miR-30a-5p*	**3.64**	**0.008**
	hsa-miR-423-5p*	**-5.76**	**<0.001**
	hsa-miR-423-3p	**-4.48**	**0.002**
	hsa-miR-22-3p	**-3.36**	**0.003**
	hsa-miR-409-3p	**-3.14**	**0.013**
	hsa-miR-320b	-2.99	0.028
T6-T0	**hsa-miR-24-3p**	**3.73**	**0.001**
	hsa-miR-24-3p	**3.73**	**0.001**
	hsa-miR-125a-5p	**3.38**	**0.013**
	hsa-miR-99a-5p	**2.87**	**0.042**
	hsa-miR-21-3p	**2.79**	**0.007**
	hsa-miR-877-5p	**-2.74**	**<0.001**
	hsa-miR-423-5p*	**-2.38**	**0.152**
	hsa-miR-409-3p	**-2.06**	**0.100**
	hsa-let-7f-5p	**-1.91**	**0.143**
	hsa-let-7f-5p	**-1.9**	**0.169**
T6-T2	**hsa-miR-24-3p**	**4.85**	**<0.001**
	hsa-miR-24-3p	**4.33**	**<0.001**
	hsa-miR-125a-5p	**3.38**	**0.0427**
	hsa-miR-99a-5p	**3.16**	**0.010**
	hsa-miR-21-3p	**2.81**	**0.084**
	hsa-miR-877-5p	**-3.87**	**<0.001**
	hsa-miR-423-5p*	**-3.37**	**0.034**
	hsa-miR-409-3p	**-3.02**	**<0.001**
	hsa-let-7f-5p	**-2.52**	**0.083**
	hsa-let-7f-5p	**-2.51**	**0.103**

Table 2.5: Circulatory miRNAs exhibiting the largest differential expression (fold change) in the orthopaedic cohort

The 10 miRNAs demonstrating the greatest differential expression (five up-regulated, five down-regulated) for each comparison are shown with accompanying statistical significance details. Fold change data shown at Log2. *Previously described as biomarker of cardiac injury. MiRNAs highlighted in bold have previously been described in the myocardium

	T2-T0		T6-T0		T6-T2	
Mature miRNA	Log fold change	P value	Log fold change	P value	Log fold change	P value
hsa-let-7a-5p*	-1.5	0.039	-0.68	0.35	0.85	0.25
hsa-let-7b-5p	0.92	0.29	-0.12	0.89	-1	0.23
hsa-let-7c-5p	-0.3	0.74	-1	0.26	-0.72	0.42
hsa-let-7e-5p*†	**-1.7**	**0.016**	**-0.92**	**0.2**	**0.83**	**0.25**
hsa-let-7f-5p*	-1.8	0.028	-1.2	0.13	0.6	0.46
hsa-let-7g-5p	-1.1	0.25	-0.48	0.62	0.65	0.51
hsa-miR-100-5p*	**0.25**	**0.81**	**-0.52**	**0.62**	**-0.76**	**0.46**
hsa-miR-101-3p*	0.8	0.41	1.3	0.19	0.63	0.49
hsa-miR-103a-3p*†	0.39	0.59	1.3	0.087	0.87	0.24
hsa-miR-106b-3p	1.3	0.12	1.3	0.12	0.0007	1
hsa-miR-107	0.5	0.5	1.1	0.14	0.62	0.41
hsa-miR-125b-5p*	0.37	0.5	-0.073	0.89	-0.44	0.42
hsa-mir-125b-2-3p*	**0.88**	**0.011**	**-0.073**	**0.89**	**-0.93**	**0.007**
hsa-miR-127-3p	-0.34	0.42	-0.55	0.19	-0.21	0.61
hsa-miR-133a-3p*	**0.44**	**0.32**	**0.4**	**0.36**	**-0.036**	**0.93**
hsa-miR-140-3p*	**1.1**	**0.13**	**-0.24**	**0.73**	**-1.3**	**0.065**
hsa-miR-142-3p	0.12	0.84	1	0.093	0.9	0.14
hsa-miR-143-3p*	0.69	0.2	0.4	0.6	-1.3	0.065
hsa-miR-144-5p	0.38	0.58	-0.29	0.68	-0.29	0.59
hsa-miR-145-5p*	**0.24**	**0.7**	**1.4**	**0.024**	**1.2**	**0.06**
hsa-miR-146a-5p	1.1	0.25	0.25	0.79	-0.86	0.37
hsa-miR-146b-5p	0.67	0.41	-1.3	0.1	-2	0.016
hsa-miR-148a-3p*	-1.2	0.16	-1.3	0.13	-0.094	0.91
hsa-miR-150-5p	-0.24	0.78	-1.7	0.073	-1.7	0.082
hsa-miR-151a-5p*†	0.46	0.45	1	0.097	0.56	0.36
hsa-miR-151a-3p*	1.3	0.13	0.27	0.75	-0.99	0.24
hsa-miR-155-5p	-0.62	0.32	-0.74	0.23	-0.12	0.85
hsa-miR-16-5p	-0.22	0.69	0.73	0.38	0.96	0.24

hsa-miR-181a-3p*†	0.13	0.85	1.3	0.069	1.2	0.1
hsa-miR-181a-2-3p*†	0.31	0.6	-0.6	0.31	-0.77	0.13
hsa-miR-181c-5p*	0.45	0.35	-0.23	0.64	-0.68	0.16
hsa-miR-182-5p	0.77	0.31	0.46	0.54	-0.3	0.69
hsa-miR-186-5p*†	1.1	0.18	1.4	0.095	0.29	0.79
hsa-miR-191-5p	-0.093	0.69	-0.99	0.15	-0.9	0.19
hsa-miR-192-5p	0.37	0.61	1	0.16	0.64	0.68
hsa-miR-199a-3p*†	**0.8**	**0.14**	**0.58**	**0.29**	**-0.23**	**0.68**
hsa-miR-19b-3p*	1.4	0.11	0.38	0.37	-1	0.25
hsa-miR-203a-3p	-0.21	0.74	1.1	0.082	1.4	0.039
hsa-miR-21-5p*†	-1	0.27	-1.5	0.11	-0.69	0.62
hsa-miR-215-5p	-0.68	0.15	-0.52	0.26	0.16	0.73
hsa-miR-22-3p*	**1.9**	**0.006**	**1.6**	**0.024**	**-0.33**	**0.63**
hsa-miR-223-3p	-0.68	0.46	-0.17	0.85	0.51	0.58
hsa-miR-23a-3p*	**0.84**	**0.057**	**0.21**	**0.63**	**-0.63**	**0.15**
hsa-miR-25-3p	0.77	0.39	0.96	0.28	0.19	0.83
hsa-miR-26a-5p*†	-0.81	0.31	-0.98	0.21	-0.17	0.83
hsa-miR-26b-5p*†	-0.4	0.62	0.83	0.3	1.2	0.13
hsa-miR-27a-3p	-1.1	0.22	-0.82	0.34	0.23	0.69
hsa-miR-27b-3p*†	0.76	0.31	1.4	0.068	0.6	0.41
hsa-miR-28-3p*	-0.48	0.57	-1	0.22	-0.57	0.5
hsa-miR-30a-5p*	**1.5**	**0.087**	**1.3**	**0.12**	**-0.15**	**0.86**
hsa-miR-30d-5p*	**0.35**	**0.6**	**0.86**	**0.2**	**0.51**	**0.44**
hsa-miR-30e-3p*	1.3	0.072	0.72	0.3	-0.53	0.44
hsa-miR-32-5p*	-0.59	0.32	-0.76	0.21	-0.16	0.79
hsa-miR-320a	1.1	0.33	-0.21	0.5	-1.3	0.24
hsa-miR-340-5p	-1	0.29	-1.1	0.27	-0.057	0.95
hsa-miR-342-3p*	0.9	0.46	-0.31	0.43	-0.61	0.12
hsa-miR-3615	0.71	0.099	0.46	0.28	-0.25	0.56
hsa-miR-363-3p	0.93	0.15	0.53	0.41	-0.41	0.53
hsa-miR-378c*	-0.57	0.32	-0.75	0.19	-0.18	0.75
hsa-miR-378d*	-0.71	0.12	-0.84	0.063	-0.13	0.77

hsa-miR-378f*	-0.87	0.033	-0.79	0.054	0.086	0.83
hsa-miR-378g*	**-0.84**	**0.039**	**-0.83**	**0.04**	**0.0071**	**0.99**
hsa-miR-421	-0.55	0.53	-1	0.24	-0.49	0.58
hsa-miR-423-3p*	1.3	0.13	1.2	0.18	-0.15	0.86
hsa-miR-425-5p*	1.2	0.069	0.35	0.57	-0.8	0.21
hsa-miR-451a*†‡	1.9	0.019	1.5	0.064	-0.41	0.6
hsa-miR-501-3p	0.9	0.15	0.21	0.73	-0.69	0.27
hsa-miR-532-5p	1.1	0.12	1.3	0.086	0.1	0.88
hsa-miR-660-5p	-0.12	0.79	0.61	0.2	0.74	0.12
hsa-miR-769-5p*	**1.5**	**0.04**	**0.31**	**0.66**	**-1.2**	**0.1**
hsa-miR-9-5p	-0.24	0.78	-0.7	0.4	-0.46	0.58
hsa-miR-92b-3p	-1	0.24	0.15	0.86	1.2	0.17
hsa-miR-93-5p	1.2	0.087	1	0.15	-0.2	0.78
hsa-miR-99a-5p*†	**1.5**	**0.09**	**1.3**	**0.14**	**-0.22**	**0.81**
hsa-miR-99b-5p*	**0.45**	**0.72**	**0.05**	**0.97**	**-0.4**	**0.75**

Table 2.6: Temporal miRNA changes within the CABG cohort.

miRNAs exhibiting a greater than 1.5 fold change in expression in any time point comparison are shown above.
*Previously identified in the myocardium, †Previous described as a biomarker of myocardial injury, ‡Haemolysis marker, miRNAs highlighted in bold were taken forward for further study

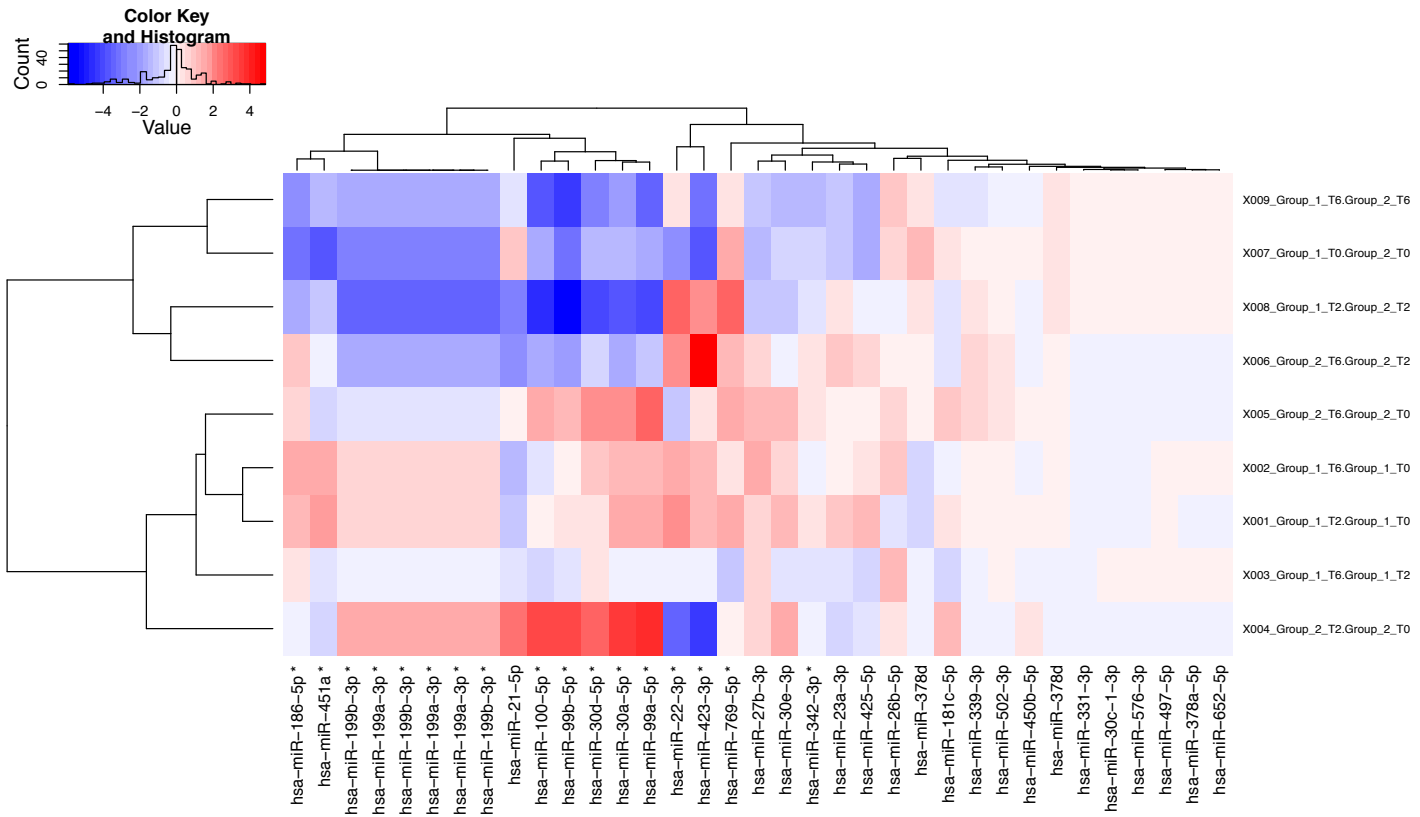

Figure 2.2: Temporal expression changes of miRNAs of interest

X axis represents the 42 miRNAs identified in the CABG cohort, which demonstrated a >1.5 log2 fold change from baseline and have been previously identified in the myocardium. Y-axis represents temporal and cohort comparison between the CABG cohort (group1) and the orthopaedic cohort (control, group 2).

2.3.3.1. Heparinase treatment prior to reverse transcription effectively removes heparin

Before PCR replication of the sequencing data, it was essential to remove the inhibitory effect of heparin. Within our healthy volunteer cohort (n=5), it was evident contamination with heparin significantly reduced the absolute Ct levels of detectable miR-122 in comparison to serum control; with similar results seen with spike in *C.elegans* miR-39 (LH only vs serum only; Figure 2.3 a & b respectively). Interestingly, when miR-122 was normalised to the external control miR-39, relative expression of miR-122 appeared to be higher in the LH contaminated samples in comparison to serum only (LH only vs serum only; Figure 2.3 c).

Following treatment with heparinase, samples contaminated with LH had significantly lower absolute miR-122 and miR-39 content in comparison to serum control (LH+heparinase vs serum only; Figure 2.3 a & b). When miR-122 is normalised to the external control miR-39, there was no significant difference in the relative miR-122 content of LH samples treated with heparinase when compared to either serum or serum treated with heparinase (LH+heparinase vs serum only and serum+heparinase, respectively; Figure 2.3 c).

2.3.3.2. miR-486-5p is not an approriate internal normaliser within the CABG cohort

Initial analysis of the raw Ct miR-486-5p values demonstrated that this varied significantly by time within the CABG group at T2 in comparison to T0 (T0 28.867 $\pm$ 2.022, T2 27.721 $\pm$ 1.973; mean expression level $\pm$ SD; 2-tailed paired t-test, $p = 0.0341$). Consequently, this miRNA was not used as the internal control and the external control *C. elegans* miR-39 was used for all further analyses.

2.3.3.3. Temporal expression profile of miRNA within groups

The temporal miRNA expression changes within the CABG cohort are described in Appendix 1. Plasma expression of miR-30a significantly increased at T2 in comparison to baseline. MiR-499a, miR-1 and miR-30a significantly increased at 6

hours in comparison to baseline. In the control group (hip arthroplasty), none of the selected miRNAs showed a significant change from baseline 2- or 6-h after myocardial injury (Appendix 2). The data from Appendix 1 and Appendix 2 has been converted using the $2^{\Delta\Delta}$Ct method and demonstrated in Figure 2.4 to allow for easier visual comparison. In light of variation in mean miRNA expression in the second generation sequencing biomarker study phase (Table 2.3), no direct comparison was made between the CABG and Orthopaedic cohort.

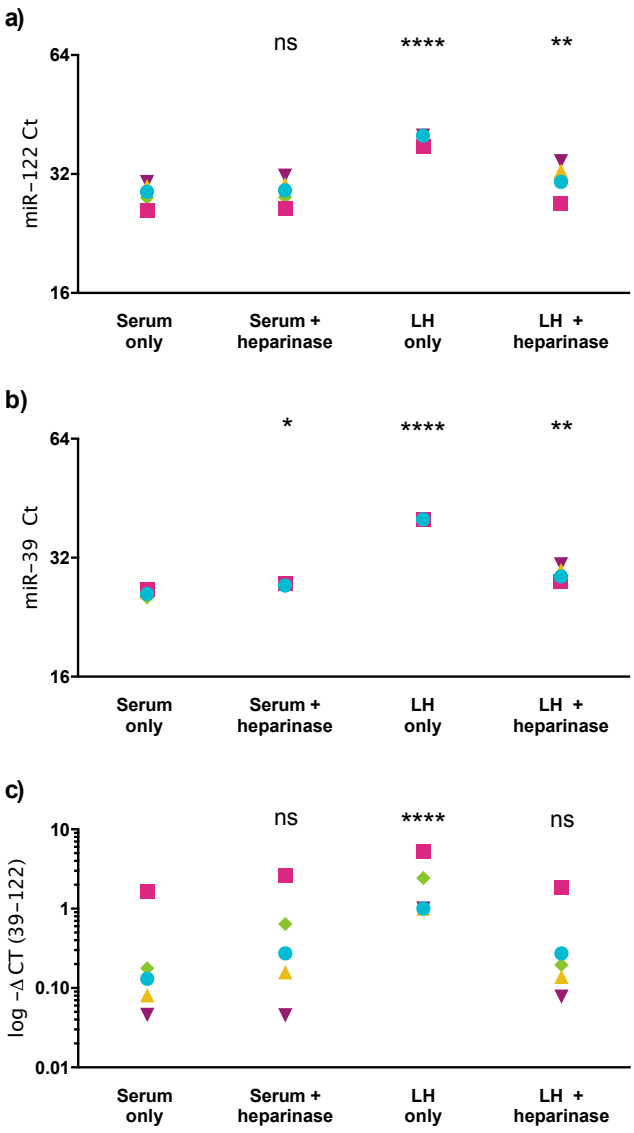

Figure 2.3: rtPCR analysis of heparinised serum samples.

Matched lithium-heparin (LH) and serum blood samples from healthy volunteers were treated with heparinise and the miRNA content quantified using rtPCR (n=5). Figure 2.3 a & b demonstrate absolute Ct value of miRNA of interest, miR-122 and miR-39 respectively and Figure 2.3 c shows miR-122 normalised to external control miR-39. Statistically significant differences were established using 1-way ANOVA and Tukey's multiple comparison test between serum only and group of interest.

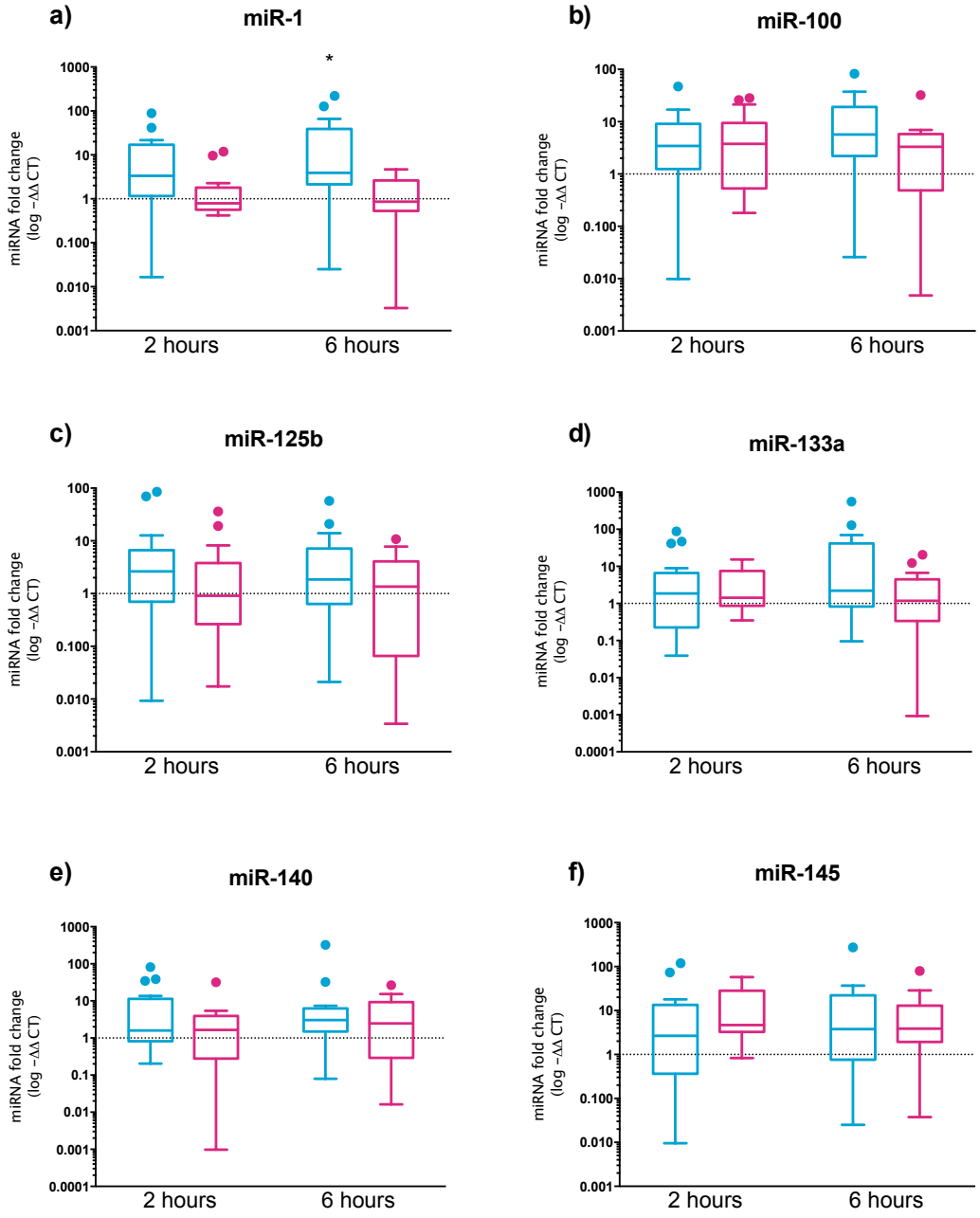

Figure 2.4: Plasma rtPCR results of miRNA expression changes from baseline.

Tukey boxplot analyses of miRNA expression changes in comparison to baseline using $2^{\Delta\Delta Ct}$ method (normalising miRNA of interest to first to miR-39 and subsequently to baseline expression). Blue boxplot corresponds to CABG cohort for indicated time point; red corresponds to orthopaedic cohort. Comparison to baseline expression was conducted using paired 1-way ANOVA and Dunnet's multiple comparison; statistically significant differences from baseline are indicated by symbol ascribed to each group.

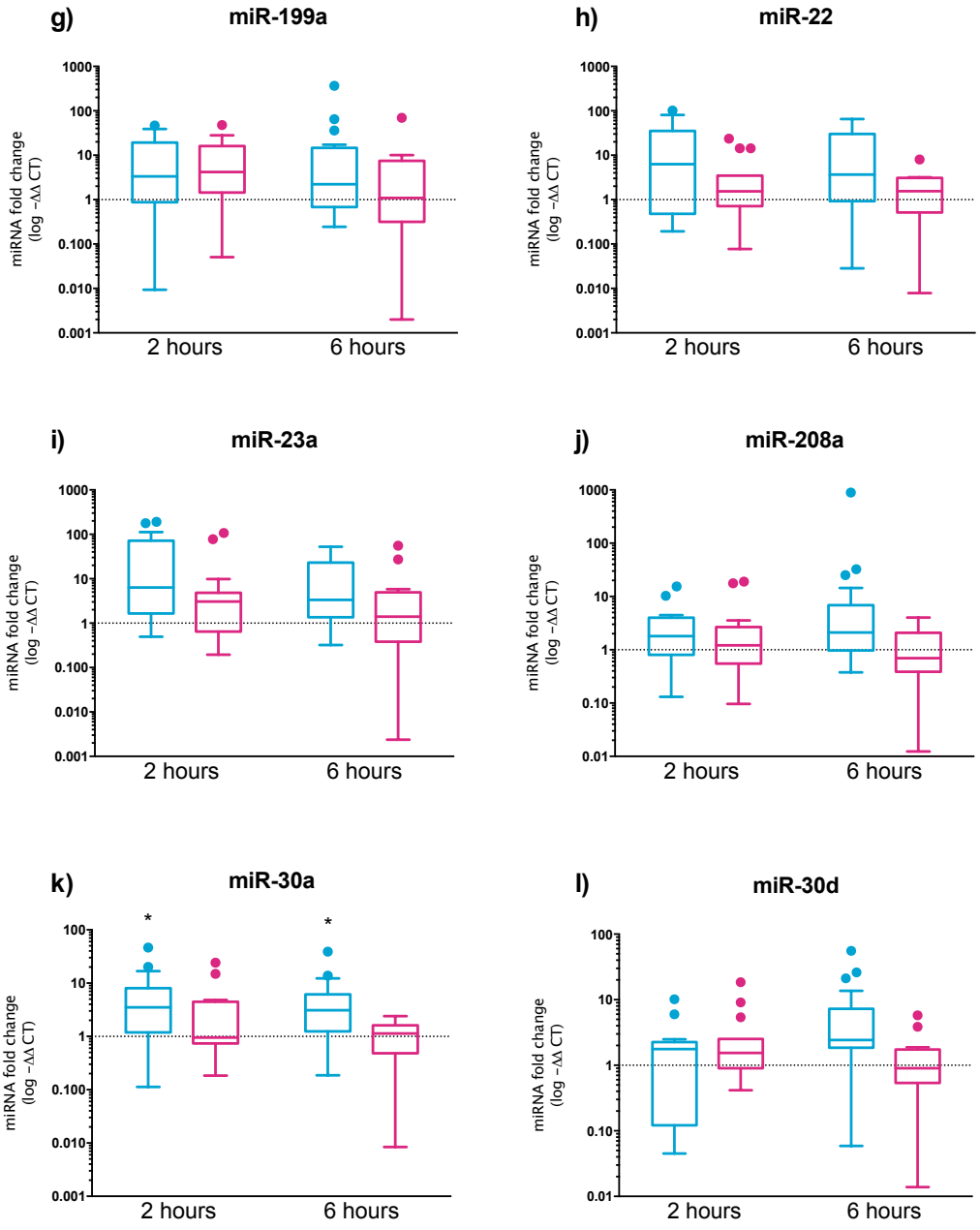

Figure 2.4 (cont.)

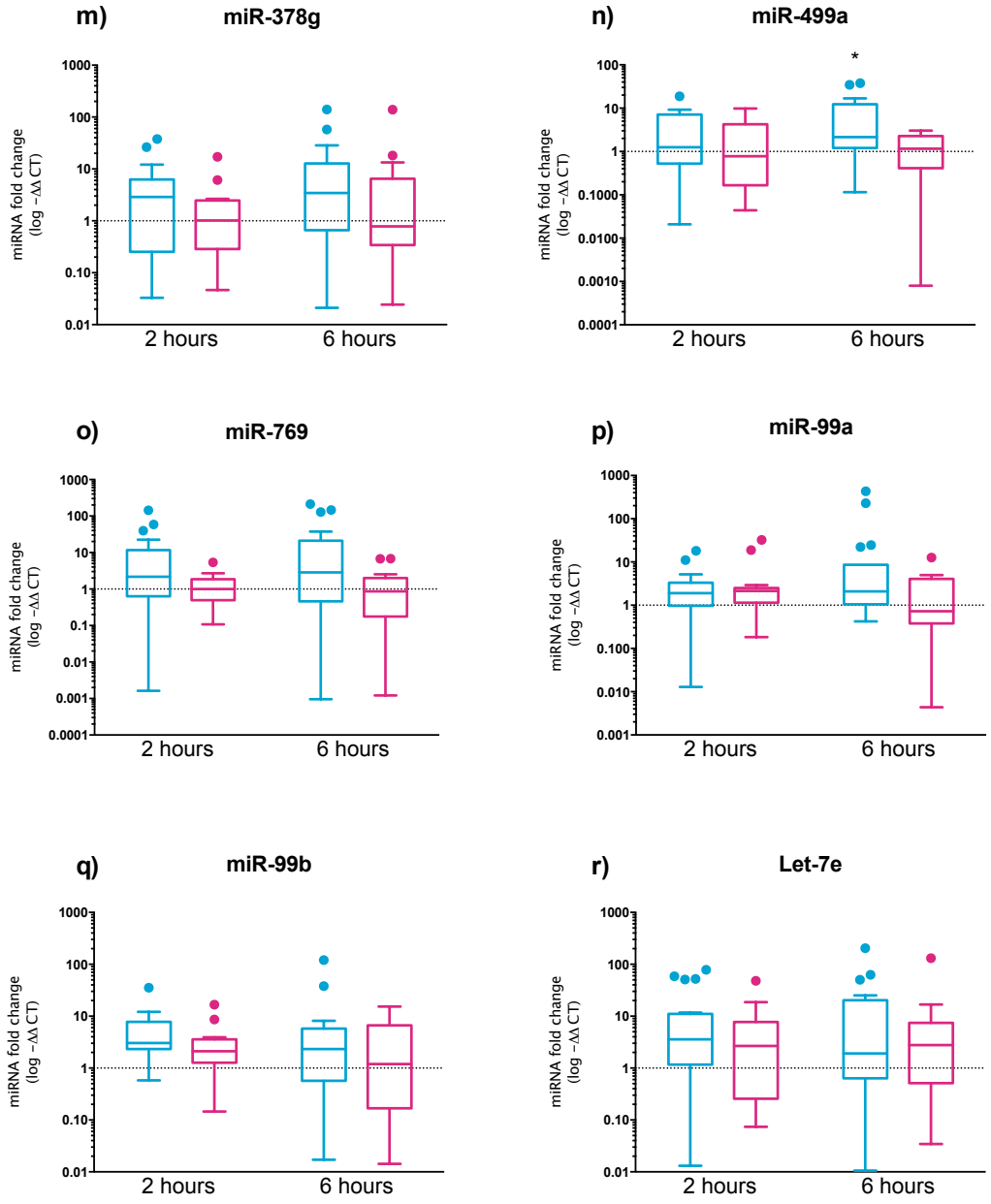

Figure 2.4 (cont.)

2.3.3.4. Comparison of second generation sequencing and rtPCR methodology

Consistency of fold change of miRNA of interest across the 2 platforms; second generation sequencing and rtPCR was interrogated. Comparison between methodologies was done across time points (i.e. T2-T0, T6-T0) for both the CABG and orthopaedic cohorts (Figure 2.5)

a) CABG cohort - 2 hours

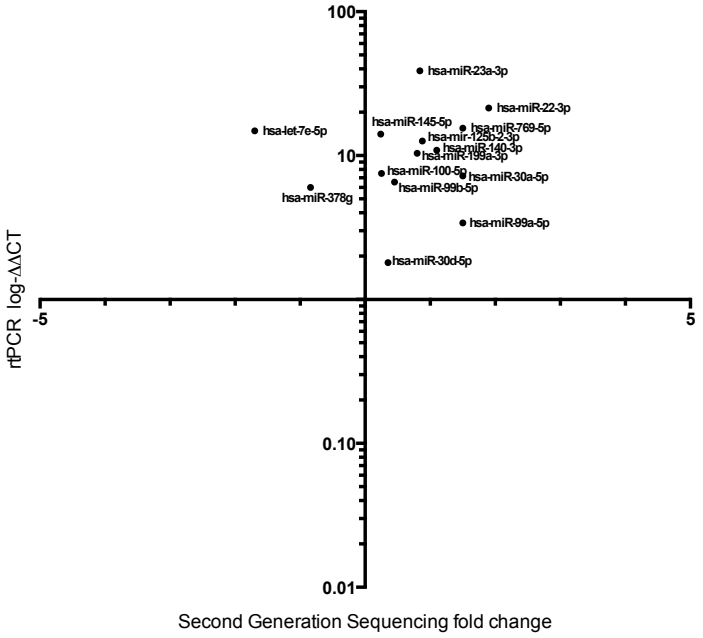

b) CABG cohort - 6 hours

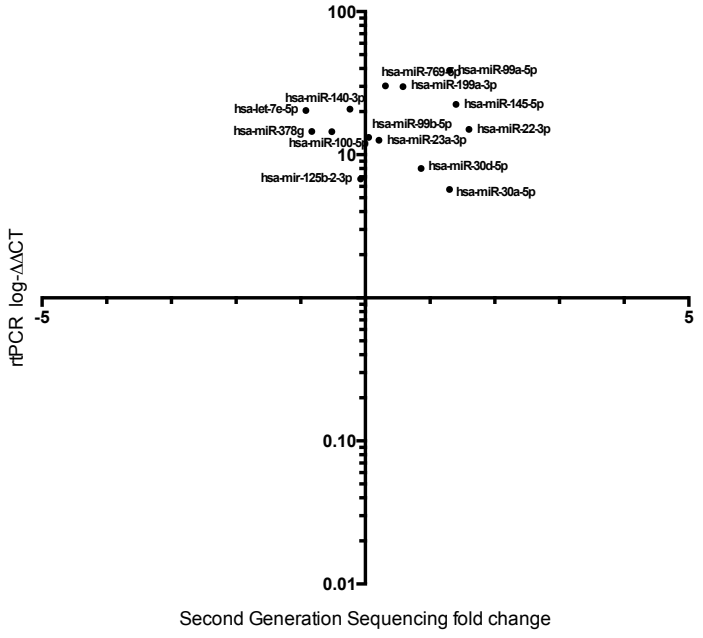

Figure 2.5: Comparison of miRNA temporal expression changes using rtPCR and second-generation sequencing.

Mean fold change in miRNA of interest using second-generation sequencing (x-axis) was compared to mean expression change using rtPCR methodology (y-axis).

c) Ortho cohort - 2 hours

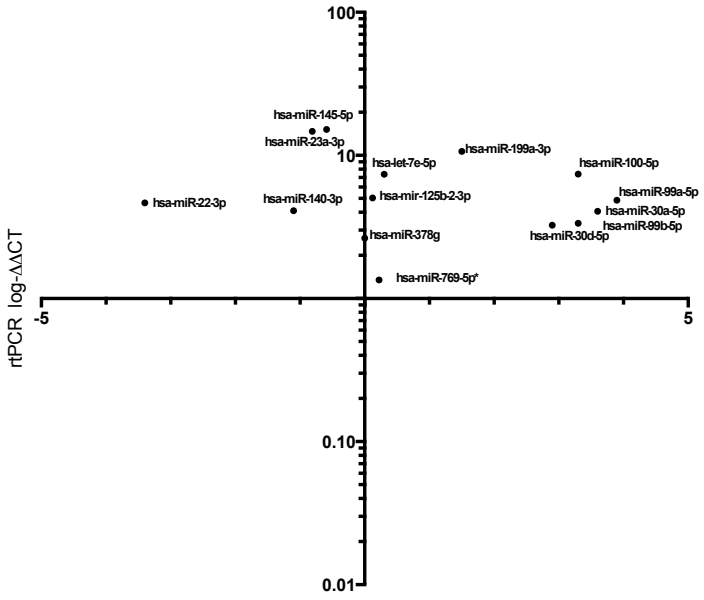

Second Generation Sequencing fold change

d) Ortho cohort - 6 hours

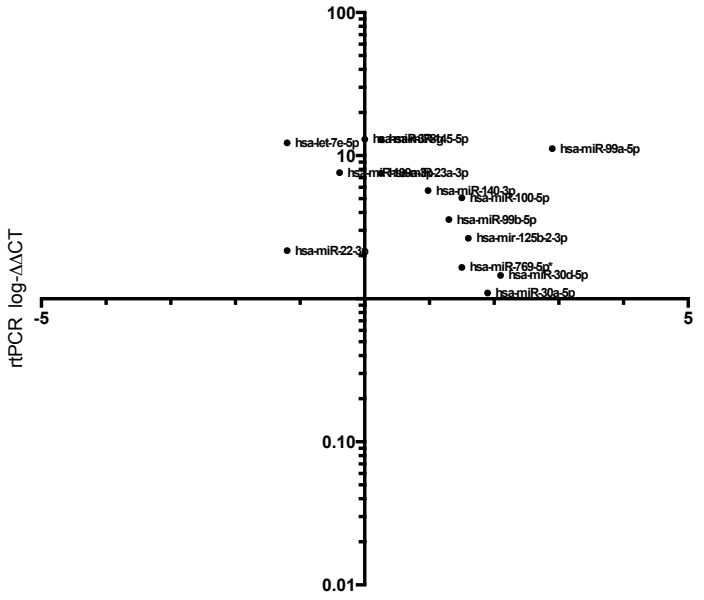

Second Generation Sequencing fold change

Figure 2.5 (cont.)

2.4. DISCUSSION

2.4.1. Main findings

The main findings of this chapter were:

- Circulating miR-30a significantly increases 2 hours following myocardial injury in humans.
- 6 hours following myocardial injury, miR-499a, miR-1 and miR-30a significantly increased within human serum.
- Heparinase effectively removes heparin contamination from serum samples.

2.4.2. CABG affects the circulating miRNA signature in humans

The main objective of the present study was to identify miRNAs that change with cardiac injury within a human model of cardiac injury. Figure 2.3 and Table 2.6 reveal the breadth of the changing miRNA signature in both the cardiac and control cohort.

In comparison to published literature, the presented study design is novel, particularly with regard to control cohort. Previous studies using cardiac surgery as a model of myocardial injury typically include healthy volunteers as the control cohort [195], if a control cohort is used at all [57, 196, 197]. In the presented study, it was felt to be vital to control for injury unrelated to the myocardium. While miRNA profile changes following CABG have been correlated to changes seen in IRI injury [197], circulating miRNA expression changes have been described as a consequence on anaesthesia , bone injury [198] and muscle turnover [199]. Critically, miR-1 and -133a, typically cited as cardiac biomarkers, have both been described as biomarkers of skeletal muscle injury [199]. Consequently, both miRNA species have been described to be upregulated in the circulation following sham cardiac procedures in mice [53]. Negating for these predictable insults was critical in the present study and consequently, orthopaedic patients undergoing an elective procedure were included as an appropriate control population. Using second generation sequencing, the circulating miRNA signature was shown to vary following myocardial injury. Significantly more of the fluctuating miRNAs identified within the CABG cohort have been previously described as biomarkers of myocardial injury in comparison to the orthopaedic cohort, adding credence to our

study design. Notably, many of the miRNAs in both groups have been previously identified in human myocardial tissue, likely reflecting the ubiquitous nature of the majority of miRNAs.

Validation of sequencing data is required by many journals for publication and remains the gold standard for second generation technologies [200]; yet the requirements for technical validation are controversial. The correlation between sequencing results and rt-PCR is reassuring and has cast doubt on the utility of the time-and resource- consuming technical validation process; fold changes estimated from RNA-seq have been shown to have a high correlation with that from the qRT-PCR [201]. Current best practice guides recommend validation and have clear guidelines on methodology [202]. This study used different biological replicates from the same population, validating both the sequencing technology but also the biological conclusion of the second-generation sequencing experiment. PCR validation of sequencing data using the same RNA samples only validates the sequencing methodology.

Of the miRNAs taken forward to rtPCR validation, the only significant temporal relationships identified were miR-30a increasing at T2 in comparison to baseline, and miR-499a, miR-1 and miR-30a significantly increasing at 6 hours in comparison to baseline (Figure 2.4). There were no significant temporal changes noted in the orthopaedic group. All three of these miRNAs have been described as biomarkers of myocardial injury in humans previously [7, 57, 203] but miR-30a has not been noted significantly increase at a 2h time point, suggesting it has potential as an early biomarker of myocardial injury.

Mir-499-5p is an intronic miRNA encoded within MyH7p, a myosin gene and subsequently enriched within the myocardium [7, 204]. Its expression is regulated by other myosin genes, as well as miR-208a. miR-499 kinetics have previously been described, with peak circulation concentration at 12 hours post-injury, returning to baseline 72 hours following injury onset [205]. Other groups have concluded it may remain elevated within the serum up to 7 days post-injury [206]. It has been noted to accurately predict myocardial damage within 6 hours of onset of symptoms [25].

With regard to its performance against the current gold standard biomarker, it is likely to have similar diagnostic accuracy an TnI and may outperform miR-208a [207], despite close biological association.

MiR-1-1/133a-2 and miR-1-2/133a-1 are two bicistronic miRNA clusters identified in both myocardial and skeletal muscle [208, 209], explaining the necessity to exclude or negate for skeletal muscle injury and avoid confounding cardiac biomarker data [53, 210]. MiR-1 has been proposed to be an earlier biomarker of cardiac damage in comparison to miR-499, becoming significantly elevated in the circulation 2 hours following injury [49]. Similarly, miR-1 has also been proposed to correlated to plasma TnI and predict degree of myocardial damage [59]. MiR-30a is enriched in many more tissues and has been reported to be an effective biomarker of cardiac injury [7], predicting myocardial damage as early as 4 hours following myocardial ischaemia [203].

Despite promising studies, no biomarker study has concluded that a cardiac miRNA biomarker is more effective than TnI. What may be of clinical utility is a panel of dynamic proteomic and transcriptomic biomarkers, to provide detailed information regarding the temporal course of, and extent of, myocardial injury. Elevated high sensitivity TnI, in a clinical setting, predominantly reflects myocardial injury rather myocardial infarction [45] and a panel of candidate biomarkers may improve the positive predictive value for myocardial infarction. The combination of miR-1, miR-499 and miR-21 may improve the diagnostic accuracy of troponin when used in combination [25]. However, other studies investigating miRNA/TnI biomarker panels have failed to describe added diagnostic value when combined with cTnT [61].

2.4.3. Heparin can be effectively removed from RNA extract

All the miRNAs taken forward to the rtPCR validation phase were identified within the circulating serum of both the CABG and orthopaedic cohorts. Removal of contaminating heparin from samples was necessary due to the inhibition of DNA polymerase by heparin, an enzyme critical in the synthesis of complementary DNA. Heparin is an anticoagulant, commonly administered to hospital patients to prevent thrombosis and has been previously shown to reduce the perceived concentration of

circulating miRNA due to interference in reverse transcription [211, 212]. Chemical digestion was not necessary for second generation sequencing as the gel electrophoresis stage of small RNA sequencing preparation effectively removes contaminants. These data suggest that heparin can be effectively removed by heparinise, but only when the miRNA of interest is normalised using the ΔCt method (Figure 2.3). This highlights a potential difficulty in absolute miRNA quantification of heparin-contaminated samples, an observation not previously reported [213].

2.4.4. Limitations

There was variation in sample storage times across both groups; orthopaedic serum samples were stored for 2-3 months and CABG samples were stored for 4-6 years. This probably affected the number of samples that were passed through quality control for the sequencing study. Of the original 132 samples, 106 passed on dual measures of RNA quantity and quality (RIN). To ensure balanced patient numbers across cohorts 84 samples were ultimately sequenced, lowering the power of the study. The prolonged storage of the CABG samples likely caused the reduced variance seen in RNA fold changes in the CABG cohort in comparison to the orthopaedic cohort (Figure 2.1 and Table 2.3). This difference complicated head-to-head comparison between the CABG and orthopaedic groups and limited the ability to demonstrate a statistically significant effect of temporal miRNA profile change within the CABG cohort. Consequently, raw P values were reported to ascertain statistical significance and all identified miRNAs were taken forward to verification in another species (Chapter 3). Current opinion regarding the recommended storage time for miRNAs appears to vary. Analysis of frozen serum samples in long-term storage (>10years) suggests it is possible to isolate enough RNA for analysis [214], but how expression changes over time has yet to be fully understood. RNA quantity has been demonstrated to drop by >50% following 4 years in storage[215] and each circulating miRNA may not affected at a similar rate, leading to possible confounding over time [216].

Another source of potential confounding could be the difference in concomitant medications across cohorts. Cell-free circulating miRNAs have huge potential as

biomarkers of illness yet a number of studies have recently highlighted the effect of medication alone on the miRNA pool. In the present study, greater use of statin and antiplatelet agents was noted within the CABG cohort (Table 2.2). This is unsurprising, given these medications are recommended for secondary prevention of IHD, but both drug categories have been implicated in changing the miRNA signature and represent possible confounding factors [217, 218]. Of the miRNAs identified, only miR-140-3p has previously been implicated in statin-induced changes to the circulating miRNA profiles [218], and longstanding drug therapy would not account for acute changes in the miRNA profile described in the present study. Despite this, differences in baseline medication must be considered in case-control studies relating plasma miRNAs to cardiovascular disease.

2.4.5. Summary

The circulating miRNA profile significantly changes in human subjects following myocardial injury. Some of the identified miRNA biomarkers may have potential as early biomarkers of myocardial injury. In the next chapter these microRNA biomarkers are back translated into a mouse model with a view to subsequently investigating whether changes in circulating microRNA may have an impact on distant organs.

Chapter 3: Validation of circulatory miRNA changes in a murine model of ischaemic injury

Contents

3.1. INTRODUCTION

3.1.1. Background

Circulating miRNAs are a rich source of clinical biomarkers and have therapeutic potential in identifying severity of myocardial injury and prognostication at point of clinical care. Three fundamental biomarker development stages have previously been described; biomarker *discovery*, *validation* of a markers predictive value within the population and *implementation* of a clinically approved assay [178, 179]. Within the discovery phase, candidate biomarkers are identified within a well-defined human study clinical population and these finding are translated across species. Ensuring effective translation across species remains an ideal characteristic of clinical biomarkers for 2 main reasons. Firstly, the connection of a certain biomarker signature with a disease usually emerges from experimental studies using small sets of patient samples. Even with optimal study design and analysis, confounding issues inherent to the population of interest, for example with concomitant illness or medication use, may limit the discovery process and therefore require verification in an alternative model [217, 218]. Secondly, pre-clinical studies are dependent on non-human experimental modelling and an ideal biomarker should translate across species; facilitating appropriate interpretation of biological experiments which model human disease and informing pre-clinical safety evaluations [219].

This chapter aims to provide vital information to correlate with the human myocardial injury studies described in Chapter 2. The temporal changes in miRNA profiles of the human samples were investigated using RNAseq and verified using rtPCR. miR-1, miR-100, miR-133a, miR-140, miR-145, miR-22, miR-23a, miR-30a, miR-30d, miR-499, miR-99b were interrogated based on their validation using rtPCR against the control cohort (Figure 2.4). In the present chapter, these targets were translated into a murine model of myocardial injury and described in both tissue and serum.

3.1.2. Objectives

- To describe the changes in circulatory miRNA associated with myocardial ischaemia at 2 and 6 hours following cardiac injury in mice.
- To ascertain the presence of miRNA of interest within mouse myocardial tissue.

- To correlate circulating miRNA concentration to TnI, the gold-standard cardiac biomarker in current clinical care.

3.2. METHODS

3.2.1. Animals

3.2.1.1. Breeding and maintenance of mice

Mouse studies were in accordance with the Animals (Scientific Procedures) Act 1986 and approved by the local Animal Ethics Committee. A total of 25 male, 10-14 week old C57BL/6NCrl mice were used for this study (purchased from Charles River Laboratory, Wilmington, MA). Animals were housed in standard sterile conditions with free access to chow and water. No adverse effects were encountered.

3.2.2. Study protocol

3.2.2.1. Surgical technique

Mice were randomly assigned to 3 groups: baseline (B, n=5) coronary artery ligation (CAL, n=10) or sham (S, n=10). All mice underwent tail blood sampling at baseline. Mice in group B were culled using cervical dislocation following baseline blood sampling. Ten mice underwent coronary artery ligation for induction of myocardial infarction. A further 10 mice underwent sham surgery without coronary artery ligation (S).

CAL was performed as described previously [220, 221]. The CAL and S mice were weighed, given fluid and subcutaneous analgesia just prior to surgery. Analgesia was 0.05 mg/kg of s.c. vetergesic (buprenorphine) in a 50 µl volume of saline and 0.5-1 ml sterile saline (0.9%, s.c.) to aid recovery. Mice were intubated via the mouth for mechanical ventilation (120 strokes/minute, 200µl stroke volume). An incision was made in the lower thorax and the chest opened at the fourth intercostal space and held open using retractors. The left anterior descending coronary artery was ligated in mice randomised to the CAL group, at the level below the left atrium using an 8-0 Ethilon suture. After ligation, the chest was closed using a 5-0 silk suture. The skin was closed using 9mm stainless steel autoclips. For mice undergoing sham surgery (S), thoracotomy alone was performed; ligation of the left anterior descending coronary artery was not conducted. Following surgery, mice are returned to their cages, and observed until they had fully recovered. The cages were

left on a 37 °C heat pad. Mice were observed post-operatively until moving about their cage.

Five mice from both the CAL and S groups had blood taken 2 hours (T2) following surgery and were then culled for tissue. The remaining 5 mice from each group had blood taken 6 hours following surgery (T6) and were then culled for tissue.

3.2.2.2. Blood and tissue sampling

Blood sampling at T2 and T6 was conducted by mandibular bleed. Blood was mixed at 1:6 ratio with 0.109 mM buffered sodium citrate before isolation of plasma. Samples were centrifuged at 1000 x *g* for 10 minutes, and the subsequent supernatant isolated and stored at –80 °C. The mice then underwent a schedule 1 procedure (cervical dislocation) and tissue was collected for further sample processing. Tissue samples for RNA interrogation were immediately placed in RNAlater (Sigma Aldrich, Dorset, UK) and stored at –80 °C.

3.2.3. Troponin quantification

An ultra-sensitive mouse cardiac troponin-I ELISA (Life Diagnostics, Stoke on Trent, UK) was used as per the manufacturer's instructions. As sample volume was limited all samples were diluted to a volume of 100 μl with cardiac troponin-I (cTnI) diluent.

3.2.4. PCR validation

3.2.4.1. RNA extraction

3.2.4.1.1. Blood

Total RNA was extracted from 20μL of each plasma sample using the miRNeasy Serum/Plasma kit (Qiagen, MD, United States) according to the manufacturer's instructions. *Caenorhabditis elegans* miRNA mimic (cel-miR-39; Qiagen, MD, United States) was used for the spiked-in control.

3.2.4.1.2. Tissues

Murine tissue was macroscopically dissected, as necessary, using anatomical landmarks. Total RNA from tissue samples was isolated by using the miRNeasy mini kit (Qiagen, Germantown, MD) according to the instructions from the manufacturer. No more than 25 mg of tissue was used.

Following extraction, RNA quantity was measured with the Nanodrop instrument (Thermo Scientific, Perth, UK). Samples were further diluted to an RNA concentration of 250 ng/μl with a total volume of 6 μl.

3.2.4.2. Reverse transcription reaction setup and quantitative real time analysis.

Reverse transcription and rtPCR analysis was conducted as previous described (section 2.2.3.3 & 2.2.3.4). Ct values were normalized in plasma samples by using the mean Ct obtained from the spiked-in external control (cel-miR-39). U6 was used as the internal control for tissue samples and validated in our cohorts (data not shown).

3.2.4.3. Primer details

The following pre-designed MiScript Primer Assays were purchased from Qiagen (MD, United States)(Table 3.1). Where relevant, the human primer sequence was clarified to function in the corresponding murine target.

3.2.5. MiRNA target prediction and function annotation

To predict miRNA targets in tissues, miRDB was used as the online open source database for miRNA target prediction and functional annotations in human tissue [222]. MiRDB predicts targets using a bioinformatics tool, MirTarget, which catalogues miRNA-target interactions from high-throughput sequencing experiments. Additionally, miRDB includes a prediction program based on support vector machines (SVMs; machine learning procedures based on statistical learning theory) and high-throughput training datasets. High predicted target scores (reported between 50-100) have increased confidence in prediction. As per the developer's guidelines, scores below 60 should have supporting evidence presented and consequently have not been reported in this work. Additionally, functional prediction of miRNA effect was ascertained using miRpath v.3[223]. miRPath can utilize predicted miRNA targets provided by the DIANA-microT-CDS algorithm and/or experimentally validated miRNA interactions derived from DIANA-TarBase v6.0; p-value selected as <0.05 and micro-T threshold 0.8 for prediction of affect Kyoto Encyclopedia of Genes and Genomes (KEGG) pathways.

3.2.6. Data evaluation and statistical analysis

Where possible data were presented as Tukey box plots. Tukey box plots consist of 4 parameters; box ends at the quartiles Q1 and Q3, median as a horizontal line in the box, 'whiskers' to the farthest points that are not outliers (i.e. within 3/2 times the interquartile range of Q1 and Q3) and dot plot of outliers. Data were analysed using GraphPad PRISM (version 6.03 for Windows, GraphPad Software, San Diego, USA) and a P-value < 0.05 was considered statistically significant. Statistical significance was ascertained as follows: t-tests to test for difference in means between two datasets (temporal miRNA /troponin concentration changes); Pearson's correlation coefficients to correlate TnI and miRNA of interest, and receiver operator characteristic (ROC) was calculated to illustrate the diagnostic ability of the miRNAs of interest.

Primer name	Mature miRNA target	Catalogue Number	Sequence
Hs_miR-1_2	mmu-miR-1a-3p	MS00008358	5'UGGAAUGUAAAGAAGUAUGUAU
Hs_miR-100_2	mmu-miR-100-5p	MS00031234	5'AACCCGUAGAUCCGAACUUGUG
Hs_miR-133a_2	mmu-miR-133a-3p	MS00031423	5'UUUGGUCCCCUUCAACCAGCUG
Hs_miR-140-3p_1	mmu-miR-140-3p	MS00008673	5'UACCACAGGGUAGAACCACGG
Hs_miR-145_1	mmu-miR-145a-5p	MS00003528	5'GUCCAGUUUUCCCAGGAAUCCCU
Hs_miR-22_1	mmu-miR-22-3p	MS00003220	5'AAGCUGCCAGUUGAAGAACUGU
Hs_miR-23a_2	mmu-miR-23a-3p	MS00031633	5'AUCACAUUGCCAGGGAUUUCC
Hs_miR-30a-5p_1	mmu-miR-30a-5p	MS00007350	5'UGUAAACAUCCUCGACUGGAAG
Hs_miR-30d_2	mmu-miR-30d-5p	MS00009387	5'UGUAAACAUCCCCGACUGGAAG
Hs_miR-499_1	mmu-miR-499-5p	MS00004375	5'UUAAGACUUGCAGUGAUGUUU
Hs_miR-99b_2	mmu-miR-99b-5p	MS00032165	5'CACCCGUAGAACCGACCUUGCG
Ce_miR-39_1	cel-miR-39-3p	MS00019789	5'UCACCGGGUGUAAAUCAGCUUG
Hs_miR-22_1	mmu-miR -22-3p	MS00003220	5'AAGCUGCCAGUUGAAGAACUGU
Hs_RNU6-2_1	RNU6-6P	MS00033740	5'CGCAAGGAUGACACGCAAAUUCG UGAAGCGUUCCAUAUUUUU

Table 3.1: MiScript Primer Assays used during real-time PCR validation of miRNA expression changes in murine model of myocardial injury

3.3. RESULTS

3.3.1. Circulating MiRNA profile changes following ischemic injury in mice

Plasma samples from mice undergoing CAL were interrogated for the 11 miRNAs exhibiting the largest fold changes in the human myocardial injury study (Chapter 2). Baseline and 'time point of interest' samples were taken from the same animal and miRNA profile changes were investigated using paired two-tailed t-test (n=5). Table 3.2 describes the temporal miRNA profile changes within the CAL group. MiR-11, -100, -133a, -145, -22, -30a, -499 and -99b all significantly increased from their baseline circulating concentration, 2 hours following CAL. 6 hours following injury, significant increases from baseline remained for miR-1, -133a, -145, -30a, -499 and -99b and changes in expression of miR-23a and -30d could now be detected.

MiRNA profile changes within the circulation of mice undergoing the sham procedure are described in Table 3.3. Increased expression of miR-1, -133a, -145, -23a, -30d, and -99b were all seen 2 hours following sham procedure; at 6 hours only miR-1, -100, -23a, -499 and -99b were significantly altered from baseline.

Head-to-head comparison of temporal miRNA fold changes was undertaken between groups (Table 3.4). 2 hours following procedure, miR-499 was significantly increased in the CAL cohort compared to the sham group. Of the miRNAs interrogated, only miR-1, -30d and -499 significantly increased in comparison to the sham procedure 6 hours post-operation. These fold change data have been visually represented with corresponding significance to baseline miRNA expression in Figure 3.1. As miR-499, miR-1 and miR-30d all demonstrated significant changes within the circulation, their downstream targets were predicted and demonstrated in Appendix 3-5, respectively.

MiRNA of interest	Time point	log ΔCt		Comparison	Mean difference	95% CI of diff.	P-value
		Mean	SD				
miR-1	T0 (T2 Baseline)	0.0117	0.0031				
	T2	8.4100	3.7340	T2 baseline vs. T2	8.399 ± 1.670	4.548 to 12.25	0.001
	T0 (T6 baseline)	0.0098	0.0074				
	T6	14.340	13.570	T6 baseline vs. T6	14.330 ± 6.070	0.331 to 28.330	<0.05
miR-100	T0 (T2 Baseline)	0.0725	0.0254				
	T2	0.1263	0.09151	T2 baseline vs. T2	0.054 ± 0.042	-0.0440 to 0.152	ns
	T0 (T6 baseline)	0.1289	0.0792				
	T6	0.2829	0.1263	T6 baseline vs. T6	0.154 ± 0.067	0.0002 to 0.308	<0.05
miR-133a	T0 (T2 Baseline)	0.0032	0.0013				
	T2	0.1936	0.1105	T2 baseline vs. T2	0.190 ± 0.049	0.076 to 0.304	<0.01
	T0 (T6 baseline)	0.0024	0.0023				
	T6	0.4366	0.3311	T6 baseline vs. T6	0.434 ± 0.148	0.093 to 0.776	<0.05
miR-140	T0 (T2 Baseline)	0.4319	0.1533				
	T2	0.4591	0.1651	T2 baseline vs. T2	0.027 ± 0.101	-0.205 to 0.259	ns

	T0 (T6 baseline)	0.3093	0.1080				
	T6	0.5605	0.4020	T6 baseline vs. T6	0.251 ± 0.186	-0.178 to 0.681	ns
miR-145	T0 (T2 Baseline)	0.2969	0.2533				
	T2	1.8940	2.6870	T2 baseline vs. T2	1.598 ± 0.421	0.627 to 2.568	<0.01
	T0 (T6 baseline)	0.1957	0.2152				
	T6	1.3800	0.6649	T6 baseline vs. T6	1.184 ± 0.476	0.087 to 2.281	<0.05
miR-22	T0 (T2 Baseline)	0.6969	0.4282				
	T2	7.9260	4.9650	T2 baseline vs. T2	7.229 ± 2.229	2.090 to 12.370	<0.05
	T0 (T6 baseline)	0.5449	0.1464				
	T6	3.9210	3.7450	T6 baseline vs. T6	3.376 ± 1.676	-0.489 to 7.241	ns
miR-23a	T0 (T2 Baseline)	4.1500	1.6410				
	T2	9.1040	5.1350	T2 baseline vs. T2	4.954 ± 2.411	-0.606 to 10.510	ns
	T0 (T6 baseline)	4.1640	1.5530				
	T6	12.3600	7.7700	T6 baseline vs. T6	8.193 ± 3.543	0.022 to 16.360	<0.05
miR-30a	T0 (T2 Baseline)	1.4630	0.6537				
	T2	6.2050	3.5270	T2 baseline vs. T2	4.741 ± 1.604	1.042 to 8.441	<0.05
	T0 (T6 baseline)	1.1170	0.3007				

	T6	2.5820	1.2140	T6 baseline vs. T6	1.465 ± 0.559	0.175 to 2.755	<0.05
miR-30d	T0 (T2 Baseline)	0.0809	0.0427				
	T2	0.2943	0.2100	T2 baseline vs. T2	0.213 ± 0.096	-0.008 to 0.434	ns
	T0 (T6 baseline)	0.0959	0.0298				
	T6	0.5825	0.2397	T6 baseline vs. T6	0.487± 0.108	0.237 to 0.736	<0.01
miR-499	T0 (T2 Baseline)	0.0009	0.0002				
	T2	0.0961	0.0784	T2 baseline vs. T2	0.095 ± 0.035	0.014 to 0.176	<0.05
	T0 (T6 baseline)	0.0012	0.0015				
	T6	0.2421	0.1682	T6 baseline vs. T6	0.241 ± 0.075	0.067 to 0.414	<0.05
miR-99b	T0 (T2 Baseline)	0.0076	0.0028				
	T2	0.0223	0.0133	T2 baseline vs. T2	0.015 ± 0.006	0.001 to 0.029	<0.05
	T0 (T6 baseline)	0.0065	0.0009				
	T6	0.0420	0.0168	T6 baseline vs. T6	0.035 ± 0.008	0.018 to 0.053	<0.01

Table 3.2: Temporal circulatory miRNA changes following murine coronary artery ligation (CAL) procedure.

Mice randomised to the CAL underwent blood sampling at baseline and either 2- or 6-hours post-procedure (n=5 in both cohorts). Plasma samples were analysed for miRNA of interest and normalised to external control ce-miR-39 using the ΔCt method. Statistical significance was ascertained using paired 2 tailed t-test.

MiRNA of interest	Time point	log ΔCt		Comparison	Mean difference	95% CI of diff.	P-value
		Mean	SD				
miR-1	T0 (T2 Baseline)	0.0207	0.0144				
	T2	9.2500	4.6370	T2 baseline vs. T2	9.229 ± 2.074	4.447 to 14.010	<0.01
	T0 (T6 baseline)	0.0101	0.0073				
	T6	1.576	0.8848	T6 baseline vs. T6	1.566 ± 0.396	0.653 to 2.480	<0.01
miR-100	T0 (T2 Baseline)	0.1302	0.0724				
	T2	0.3202	0.1887	T2 baseline vs. T2	0.190 ± 0.090	-0.0189 to 0.398	ns
	T0 (T6 baseline)	0.1097	0.0166				
	T6	0.2297	0.1039	T6 baseline vs. T6	0.120 ± 0.047	0.012 to 0.229	<0.01
miR-133a	T0 (T2 Baseline)	0.0012	0.0007				
	T2	0.3156	0.1706	T2 baseline vs. T2	0.314 ± 0.076	0.138 to 0.490	<0.01
	T0 (T6 baseline)	0.0010	0.0007				
	T6	0.1233	0.1289	T6 baseline vs. T6	0.122 ± 0.058	-0.012 to 0.255	ns
miR-140	T0 (T2 Baseline)	0.4471	0.1089				
	T2	0.6123	0.4573	T2 baseline vs. T2	0.165 ± 0.210	-0.320 to 0.650	ns
	T0 (T6 baseline)	0.3306	0.0855				

	T6	0.2734	0.1599	T6 baseline vs. T6	-0.057 ± 0.081	-0.244 to 0.130	ns
miR-145	T0 (T2 Baseline)	0.2533	0.0844				
	T2	2.6870	1.4650	T2 baseline vs. T2	2.433 ± 0.656	0.920 to 3.946	<0.01
	T0 (T6 baseline)	0.2152	0.0458				
	T6	0.6649	0.4809	T6 baseline vs. T6	0.450 ± 0.216	-0.048 to 0.948	ns
miR-22	T0 (T2 Baseline)	0.8825	0.3731				
	T2	10.9900	13.0500	T2 baseline vs. T2	10.110 ± 5.840	-3.355 to 23.580	ns
	T0 (T6 baseline)	0.6236	0.0895				
	T6	1.8440	1.9540	T6 baseline vs. T6	1.221 ± 0.875	-0.797 to 3.238	ns
miR-23a	T0 (T2 Baseline)	5.9900	2.6460				
	T2	14.1100	7.11300	T2 baseline vs. T2	8.123 ± 3.394	0.296 to 15.950	<0.05
	T0 (T6 baseline)	4.5050	1.4550				
	T6	7.3190	2.1780	T6 baseline vs. T6	2.814 ± 1.171	0.112 to 5.515	<0.05
miR-30a	T0 (T2 Baseline)	2.0610	1.1660				
	T2	6.2509	4.7270	T2 baseline vs. T2	4.199 ± 2.177	-0.822 to 9.219	ns
	T0 (T6 baseline)	1.0700	0.1590				

	T6	1.6370	0.8536	T6 baseline vs. T6	0.568 ± 0.388	-0.328 to 1.463	ns
miR-30d	T0 (T2 Baseline)	0.1200	0.0644				
	T2	0.6228	0.2902	T2 baseline vs. T2	0.503 ± 0.133	0.196 to 0.809	<0.01
	T0 (T6 baseline)	0.0999	0.0165				
	T6	0.3688	0.2808	T6 baseline vs. T6	0.269 ± 0.126	-0.021 to 0.559	ns
miR-499	T0 (T2 Baseline)	0.0010	0.0004				
	T2	0.0061	0.0059	T2 baseline vs. T2	0.005 ± 0.003	-0.001 to 0.011	ns
	T0 (T6 baseline)	0.0006	0.0002				
	T6	0.0019	0.0009	T6 baseline vs. T6	0.001 ± 0.0004	0.0003 to 0.002	<0.05
miR-99b	T0 (T2 Baseline)	0.0111	0.0075				
	T2	0.0588	0.0357	T2 baseline vs. T2	0.048 ± 0.016	0.010 to 0.085	<0.05
	T0 (T6 baseline)	0.0071	0.0011				
	T6	0.0360	0.0216	T6 baseline vs. T6	0.029 ± 0.009	0.007 to 0.051	<0.05

Table 3.3: Temporal circulatory miRNA changes following murine sham (S) procedure.

Mice randomised to the sham cohort underwent blood sampling at baseline and either 2- or 6-hours post-procedure (n=5 in both cohorts). Plasma samples were analysed for miRNA of interest and normalised to external control ce-miR-39 using the ΔCt method. Statistical significance was ascertained using paired 2 tailed t-test.

MiRNA of interest	Time point	log ΔΔCt		Comparison	Mean difference	95% CI of diff.	P-value
		Mean	SD				
miR-1	T2 sham	506.3	207.2				
	T2 CAL	715.5	190.6	T2 sham vs. T2 CAL	209.2 ± 125.9	-81.11 to 499.5	ns
	T6 sham	274.6	348.6				
	T6 CAL	2730.0	3132.0	T6 sham vs. T6 CAL	2456 ± 1409	-793.8 to 5706.0	<0.05
miR-100	T2 sham	3.5	3.6				
	T2 CAL	1.7	1.1	T2 sham vs. T2 CAL	-1.9 ± 1.7	-5.7 to 1.9	ns
	T6 sham	2.1	0.8				
	T6 CAL	2.4	0.7	T6 sham vs. T6 CAL	0.3 ± 0.5	-0.8to 1.4	ns
miR-133a	T2 sham	399.6	451.4				
	T2 CAL	86.8	81.3	T2 sham vs. T2 CAL	-312.8 ± 205.1	-785.8 to 160.2	ns
	T6 sham	185.9	155.0				
	T6 CAL	368.7	528.1	T6 sham vs. T6 CAL	182.7 ± 246.1	-384.8 to 750.3	ns
miR-140	T2 sham	1.6	1.4				
	T2 CAL	1.2	0.6	T2 sham vs. T2 CAL	-0.4 ± 0.7	-2.0 to 1.2	ns
	T6 sham	0.9	0.6				
	T6 CAL	2.5	2.4	T6 sham vs. T6 CAL	1.6 ± 1.1	-0.9 to 4.1	ns
miR-145	T2 sham	11.8	7.2				
	T2 CAL	6.5	2.1	T2 sham vs. T2 CAL	-5.3 ± 3.3	-13.0 to 2.4	ns

	T6 sham	3.0	1.9				
	T6 CAL	8.7	8.1	T6 sham vs. T6 CAL	5.7 ± 3.7	-2.9 to 14.4	ns
miR-22	T2 sham	11.8	10.9				
	T2 CAL	15.3	9.5	T2 sham vs. T2 CAL	3.6 ± 6.5	-11.3 to 18.5	ns
	T6 sham	3.2	3.6				
	T6 CAL	7.8	9.0	T6 sham vs. T6 CAL	4.6 ± 4.3	-5.4 to 14.6	ns
miR-23a	T2 sham	2.7	1.5				
	T2 CAL	2.1	0.8	T2 sham vs. T2 CAL	-0.6 ± 0.8	-2.3 to 1.2	ns
	T6 sham	2.0	1.4				
	T6 CAL	3.8	3.3	T6 sham vs. T6 CAL	1.9 ± 1.6	-1.8to 5.6	ns
miR-30a	T2 sham	3.3	2.3				
	T2 CAL	4.1	0.9	T2 sham vs. T2 CAL	0.7 ± 1.2	-2.0 to 3.5	ns
	T6 sham	1.6	1.4				
	T6 CAL	2.7	2.0	T6 sham vs. T6 CAL	1.2 ± 1.0	-1.1 to 3.4	ns
miR-30d	T2 sham	6.8	4.9				
	T2 CAL	4.4	3.4	T2 sham vs. T2 CAL	-2.4 ± 2.7	-8.6 to 3.7	ns
	T6 sham	3.6	2.1				
	T6 CAL	5.9	2.1	T6 sham vs. T6 CAL	2.4 ± 1.3	-0.7 to 5.4	<0.05
miR-499	T2 sham	6.8	5.3				
	T2 CAL	102.1	70.2	T2 sham vs. T2 CAL	95.3 ± 31.5	22.8 to 167.9	<0.01

	T6 sham	3.3	1.3				
	T6 CAL	403.9	455.1	T6 sham vs. T6 CAL	400.6 ± 203.5	-68.68 to 870.0	<0.05
miR-99b	T2 sham	9.3	10.5				
	T2 CAL	3.3	3.0	T2 sham vs. T2 CAL	-5.9 ± 4.9	-17.2 to 5.4	ns
	T6 sham	5.2	3.0				
	T6 CAL	6.3	2.5	T6 sham vs. T6 CAL	1.2 ± 1.7	-2.8 to 5.2	ns

Table 3.4: Comparison of miRNA fold changes following coronary artery ligation and sham procedure.

Mice were randomised to CAL or sham procedure (n=10 each cohort). They underwent blood sampling at baseline and either 2- or 6-hours post-procedure (n=5 each time point). Plasma samples were analysed for miRNA of interest, normalised to external control ce-miR-39 and transformed to fold change from baseline using the ΔΔCt method. Statistical significance was ascertained using unpaired 2 tailed t-test

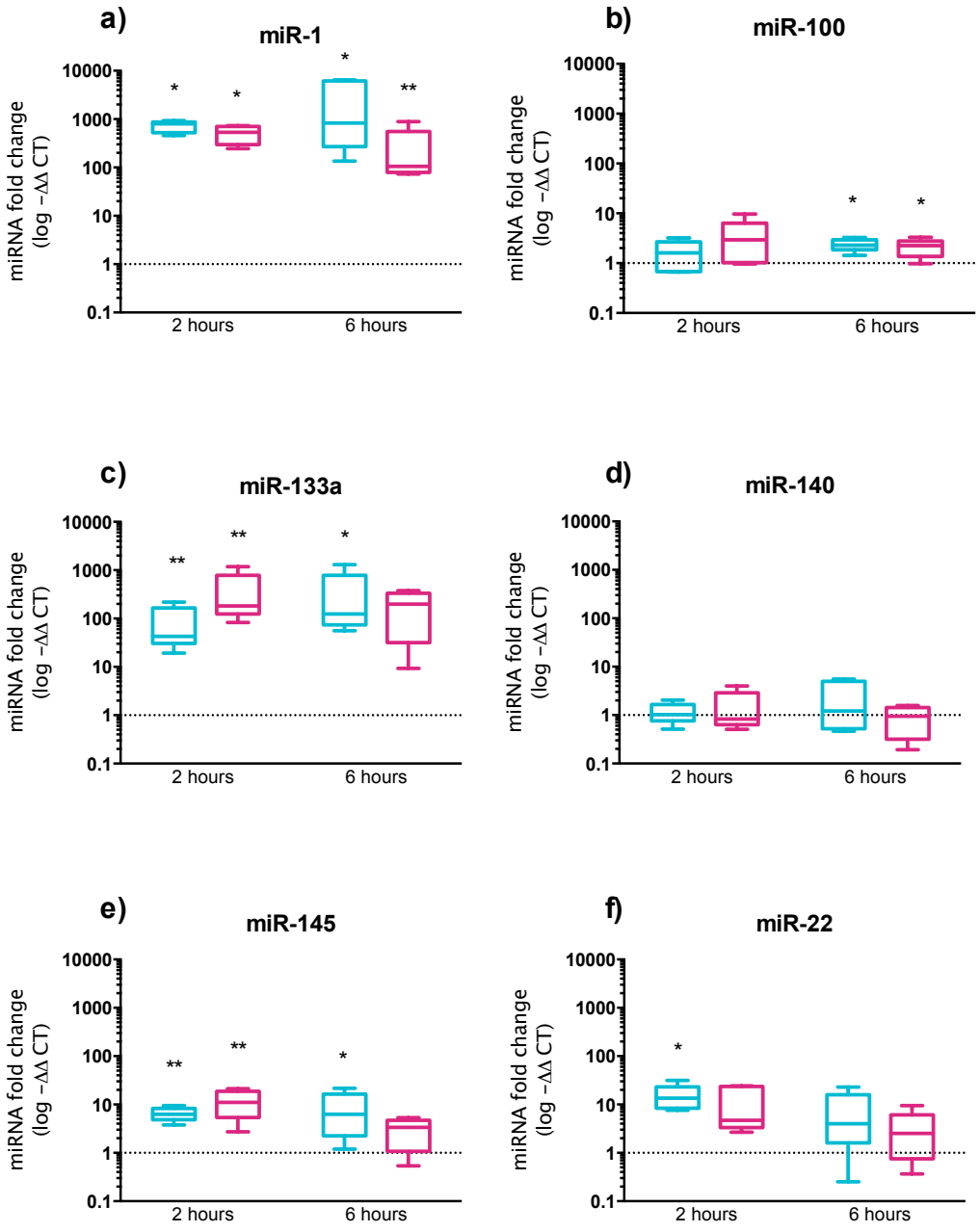

Figure 3.1: MiRNA of interest fold changes following coronary artery ligation (CAL) and sham (S) procedure

Mice were randomised to CAL (blue) or sham (pink) procedure, undergoing blood sampling at baseline and either 2- or 6-hours post-procedure (n=5 each group). Plasma samples were analysed for miRNA of interest, normalised to external control ce-miR-39 and transformed to fold change from baseline using the ΔΔCt method. Data shown as Tukey boxplot (n=5 each group). Statistical significance was ascertained using paired 2 tailed t-test comparing time point of interest to baseline.

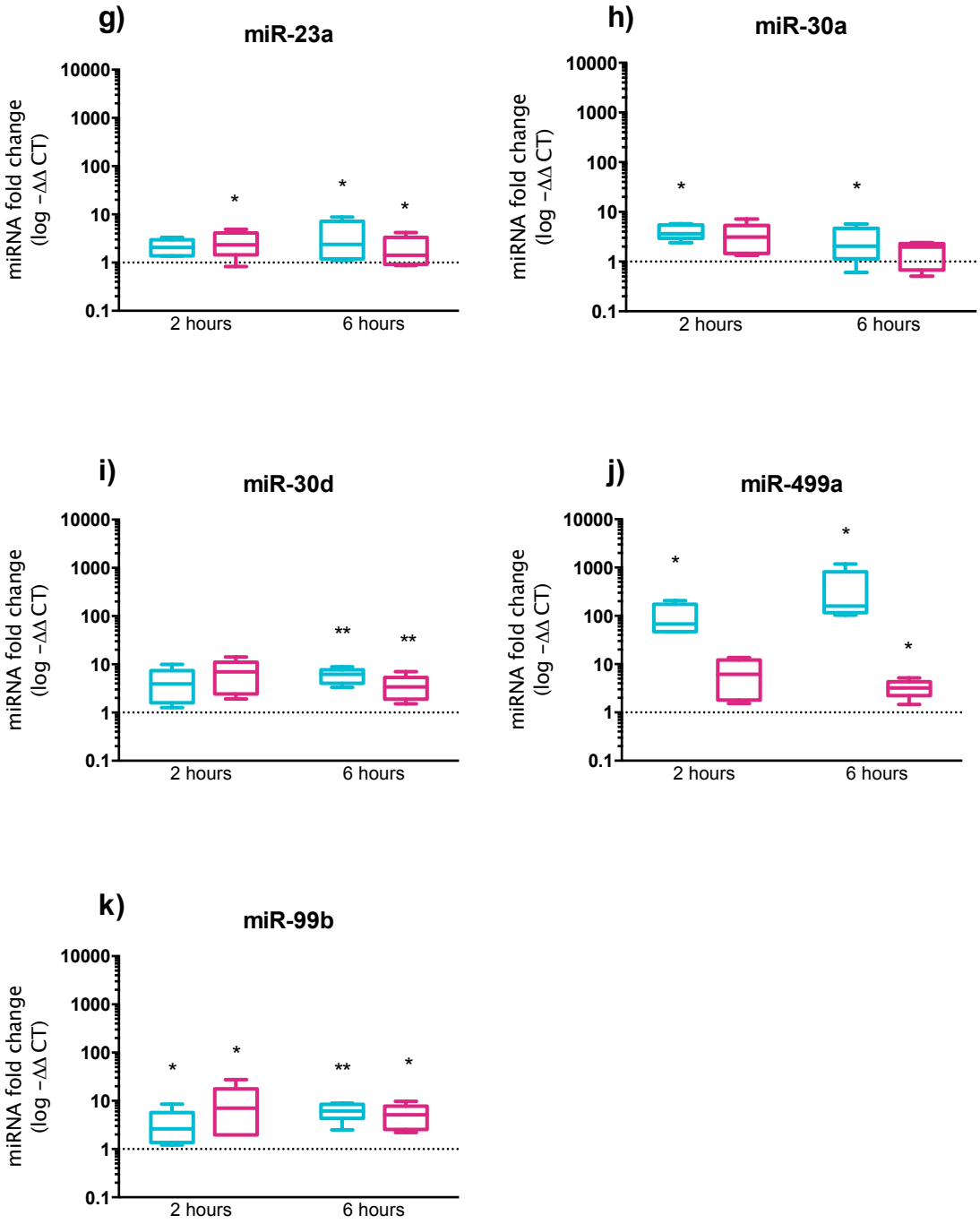

Figure 3.1(cont.)

3.3.2. Circulating miRNAs correlate to troponin in a mouse model of myocardial injury

Firstly, the temporal changes of TnI were investigated following both the CAL and sham procedure. As predicted, TnI significantly increased 2- and 6-hours post-CAL but TnI also increased in the sham cohort 6 hours post procedure (Figure 3.2). Despite this increase within the control population, a significant difference in TnI concentration was seen between both cohorts at both time points of interest.

To ascertain the utility of miRNA targets as biomarkers of myocardial injury, miRNAs of interest were correlated to circulating TnI concentration (Figure 3.3). Of the 11 interrogated miRNA biomarkers, only miR-499 correlated to TnI levels 2 hours post procedure (Figure 3.3a). At 6 hours, both miR-499, -1, -133a all correlated to TnI concentration at that time (Figure 3.3b).

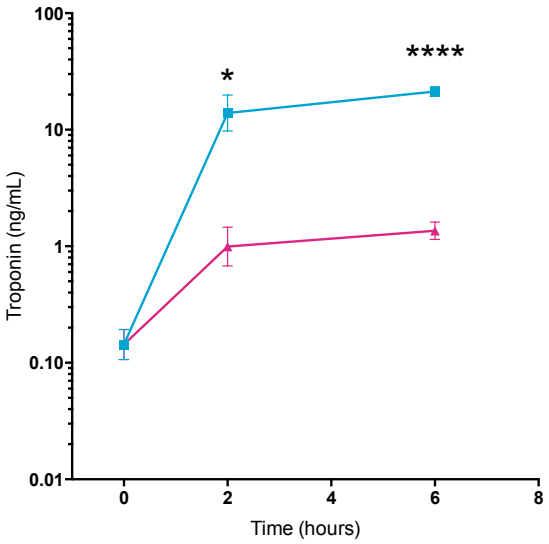

Figure 3.2: Circulating troponin concentration increases following sham and CAL procedure.

Statistically significant differences were seen between CAL (blue) and S (red) group 2- and 6- hours (P = 0.04 and <0.00001 respectively). Notably within the sham group, troponin concentration at 6- hours was statistically higher than baseline (P=0.0014), but at 2- hours it was not (p>0.05). Both 2- and 6- hour values in the CAL group were statistically higher than baseline (p = 0.034 and p<0.00001, respectively). The plotted values represent mean troponin concentration and SEM for each group, statistically significance was ascertained using unpaired t-tests (n=5)

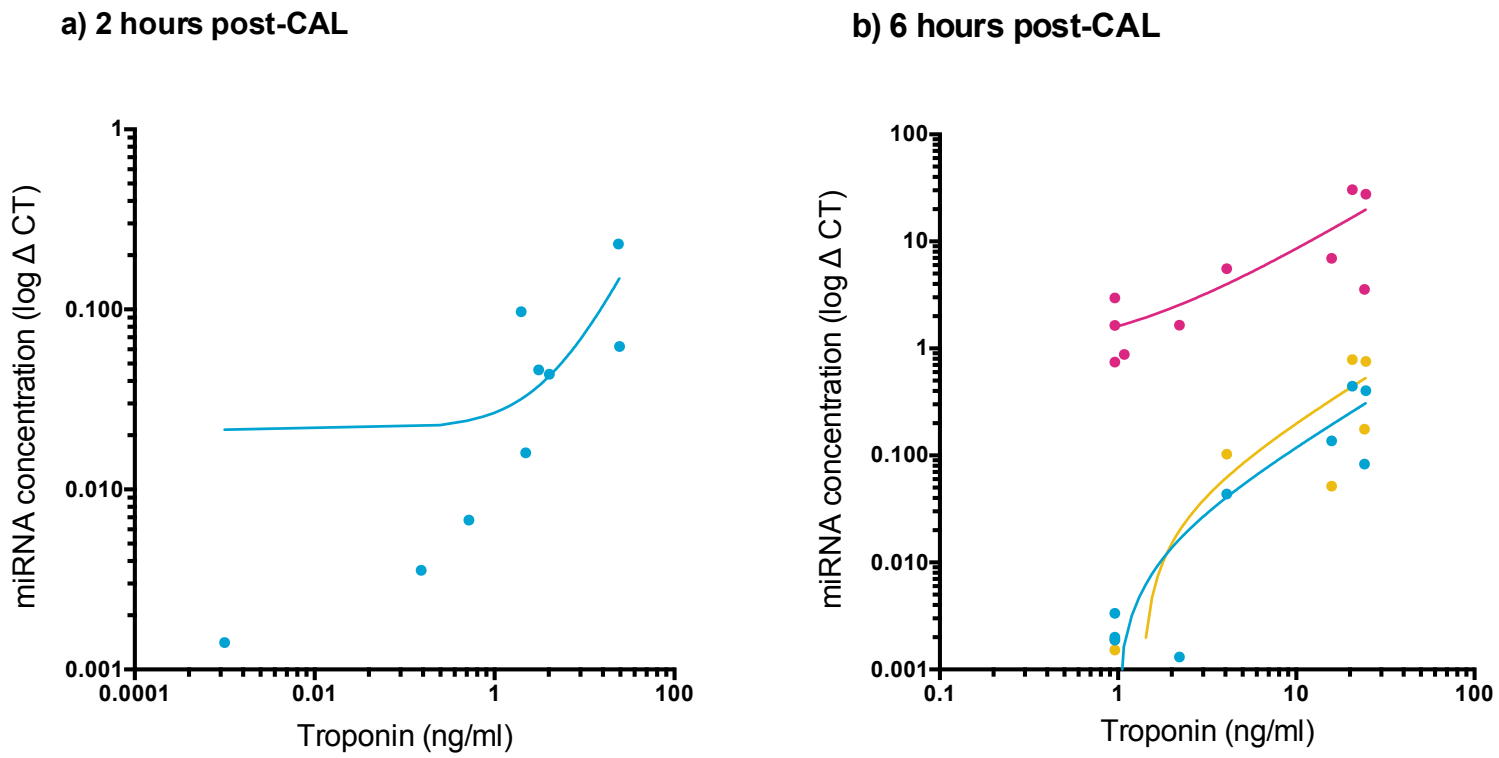

Figure 3.3: Expression of circulating miRNA correlates to plasma troponin.

Mice were randomised to CAL or sham procedure and underwent blood samples at either 2- or 6-hours post-procedure (n=5 each group). Plasma samples were analysed for TnI and miRNA of interest (normalised to external control ce-miR-39 using the ΔCt method) and correlated. Figure 3.3a shows miR-499 (blue) correlates with TnI 2 hours following procedure (r=0.7157, p=0.0302). Figure 3.3b demonstrates miR-499 (blue), miR-1 (red), miR-133a (yellow) all significantly correlated with plasma TnI (r = 0.80, p<0.01; r = 0.72, p<0.05; r = 0.76 p <0.01 respectively). Only miRNA/troponin correlations with a P value of <0.05 have been shown.

3.3.3. Cardiac miRNAs have potential as biomarkers of myocardial injury

miRNAs identified in the human cohort and described in the murine model of myocardial injury were interrogated for the diagnostic accuracy. The troponin rise in the sham procedure group compromised the validity of this control. Therefore, miRNA results from the baseline cohort were used as the control population. MiR-1, -133a, -145, -22, 30d, 30a and -499 significantly diagnose myocardial injury 2 hours after onset, with an ROC-AUC greater than 0.8 (Table 3.5). 6 hours following injury, miR-100, -133a, -145, -23a, -30d, -499 and -99b similarly diagnose myocardial ischaemia. Notably, miR-1, -133a, -145, -30a and -499 all performed well 2 hours following injury but at 6 hours miR-133a, 23a, 30d, and -499 had the greatest diagnostic accuracy (ROC-AUC >0.95).

3.3.4. MiRNA profile changes in tissue following ischaemic injury

The miRNAs of interest were quantified in tissue using the same experimental model of myocardial injury. The miRNA content of the left ventricle, right ventricle, renal cortex and liver were investigated at baseline and 2- and 6-hours following myocardial injury (n=5 in each group). Kidney and liver were studied as control organs but also with reference to future chapters that explore miRNA signalling.

In the left ventricle, expression of miR-499 significantly decreased 6 hours following myocardial injury but there was no significant change at the 2 hour post-injury time point (Figure 3.4b). There were no significant changes noted in the miR-499 content of the right ventricle or in expression of the other miRNAs of interest (data not shown). Downstream from the myocardium, miR-499 expression was noted to increase in the renal cortex 6 hours following CAL (Figure 3.4a). No other significant changes were noted in the other miRNAs interrogated. No change was noted in the miRNA content of the liver, with regard to our miRNAs of interest. Functional prediction of miR-499 was ascertained using miRpath v.3 and predicted pathways are demonstrated in Table 3.6.

	2-hour time point		6-hour time point	
MiRNA	ROC-AUC (95% CI)	P- Value	ROC-AUC (95% CI)	P- Value
miR-1	0.96 (0.84 to 1.077)	0.02	0.84 (0.58 to 1.101)	ns
miR-100	0.84 (0.58 to 1.101)	ns	0.92 (0.74 to 1.102)	0.03
miR-133a	1.00(1.00 to 1.000)	0.02	0.96 (0.84 to 1.077)	0.02
miR-140	0.80 (0.51 to 1.089)	ns	0.64 (0.26 to 1.016)	ns
miR-145	0.96 (0.84 to 1.077)	0.02	0.8 (0.662 to 1.098)	0.05
miR-22	1.00(1.00 to 1.000)	0.0090	0.80 (0.45 to 1.151)	ns
miR-23a	0.800 (0.49 to 1.106)	ns	1.00(1.00 to 1.000)	0.01
miR-30d	0.92 (0.74 to 1.102)	0.03	1.00(1.00 to 1.000)	0.01
miR-30a	0.96 (0.84 to 1.077)	0.02	0.76 (0.41 to 1.113)	ns
miR-499	1.00(1.00 to 1.000)	0.01	1.00(1.00 to 1.000)	0.01
miR-99b	0.840 (0.58 to 1.101)	ns	0.920 (0.74 to 1.102)	0.03

Table 3.5: ROC curves analyses of circulating miRNAs of interest.

Blood samples taken from mice, and mice 2- or 6-hours post-CAL (n=5 each group). Plasma samples were analysed miRNA of interest (normalised to external control ce-miR-39 using the ΔCt method) and compared using the ROC curve.

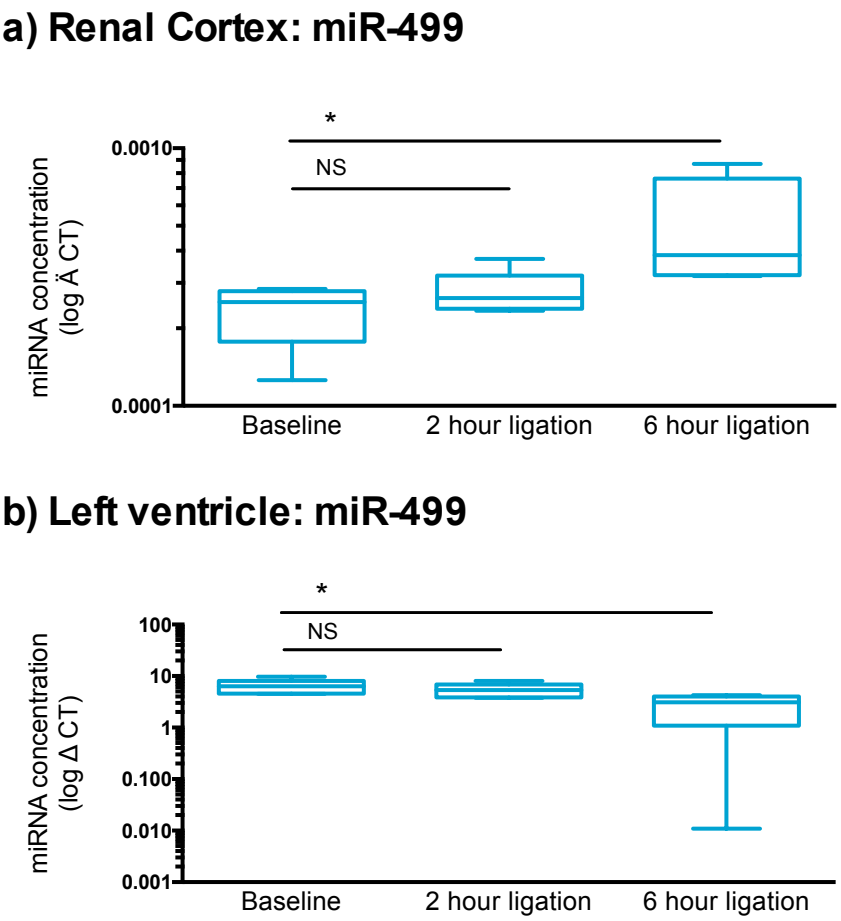

Figure 3.4: Tissue expression of miRNAs of interest change following myocardial injury.

Tissue samples taken from healthy mice (baseline), and mice 2- or 6-hours post-CAL (n=5 each group). Samples were analysed for miRNA of interest (normalised to internal control U6 using the ΔCt method). Data are shown as Tukey boxplot. Statistical significance was determined by unpaired 2-tailed t-test. Figure 3.4a: MiR-499: within the renal cortex increase 6 hours following myocardial injury (p=0.03). Figure 3.4b: Conversely, levels of miR-499 fall in the left ventricle following myocardial injury (p=0.01). Data for other miRNAs and tissues are not shown as no significant difference was noted.

KEGG Pathway Number	p-value	Gene Symbol	Gene description
Cell cycle (hsa04110)	0.001	YWHAG	Tyrosine 3-Monooxygenase/Tryptophan 5-Monooxygenase Activation Protein Gamma
		E2F5	E2F Transcription Factor 5
		SKP2	S-Phase Kinase Associated Protein 2
		MYC	MYC Proto-Oncogene, BHLH Transcription Factor
		CDC27	Cell Division Cycle 27
		PRKDC	Protein Kinase, DNA-Activated, Catalytic Polypeptide
		MDM2	MDM2 Proto-Oncogene
Fatty acid degradation (hsa00071)	0.023	ACOX1	Acyl-CoA Oxidase 1
FoxO signalling pathway (hsa04068)	0.035	FOXO4	Forkhead Box O4
		SKP2	S-Phase Kinase Associated Protein 2
		PRKAA1	Protein Kinase AMP-Activated Catalytic Subunit Alpha 1
		MDM2	MDM2 Proto-Oncogene
		BCL2L11	BCL2 Like 11
p53 signalling pathway (hsa04115)	0.035	APAF1	Apoptotic Peptidase Activating Factor 1
		PMAIP1	Phorbol-12-Myristate-13-Acetate-Induced Protein 1
		TNFRSF10B	TNF Receptor Superfamily Member 10b
		MDM2	MDM2 Proto-Oncogene

Table 3.6: MiR-499 KEGG pathway targets

3.4. DISCUSSION

3.4.1. Main findings

The main findings of chapter 3 were:

- Circulating miR-499 significantly increases 2 hours following myocardial injury in mice in comparison to control. 6 hours following myocardial injury, miR-499a, miR-1 and miR-30d significantly increased in mice in comparison to control
- 2 hours following murine myocardial injury, circulating miR-499 correlates to TnI. 6 hours following injury, miR-499, miR-1, miR-133a all correlate to TnI.
- In a mouse model of myocardial injury, TnI significantly increases in sham procedure 6 hours following intervention.
- MiR-499 expression levels decrease within the LV 6 hours following murine myocardial injury. MiR-499 increases within the renal cortex at this time point.

3.4.2. Circulatory miRNAs are biomarkers of myocardial injury that can translate across species

The main objectives of this chapter were to translate the changes in circulatory miRNA expression described in Chapter 2 into a mouse model of myocardial injury. Furthermore, circulatory miRNA changes were to be compared with miR-expression changes in murine tissue.

Chapter 3 confirms that some cardiac miRNA translate across species and can predict cardiac injury. In the animal model of myocardial injury, circulating miR-499 was significantly higher than in the sham cohort 2 hours following intervention (Table 3.4). 6 hours following CAL, miR-1, miR-30d and miR-499 were all significantly higher within the circulation, suggesting miRNAs are released into the circulation as a result of myocardial injury (Table 3.4). These results are similar that that of previously published work, using a rat model of CAL [53]. ROC analysis suggested that all of these miRNAs could be useful biomarkers of myocardial injury versus healthy controls (Table 3.5). The present study adds to the published literature by correlating circulating miR-499 and TnI, 2 hours following myocardial

injury, suggesting miR-499 may be a suitable biomarker to predict degree of myocardial damage. MiR-499 concentration has previously been correlated to TnI 6 hours following onset on injury[25], but no published work has investigated this at an earlier time point.

3.4.3. Myocardial injury affects the miRNA content of the myocardium and renal cortex

Reduced expression of miR-499 was demonstrated 6 hours following myocardial ischaemia (Figure 3.4) This instinctively seems correct, if the hypothesis of tissue miRNAs released into the circulation following injury is true. Reduced expression of miR-499 in the injured myocardium would correspond to increased concentration in circulation. Reduced miR-499 in the myocardium has previous been noted in a myocardial IRI canine model, in which miR-499 was significantly lower 2.5 hours following injury onset [224], but this observation has not been investigated in murine or human models. MiR-499-5p is an intronic miRNA encoded within MyH7p, a myosin gene, and therefore it is enriched within the cardiomyocytes and skeletal muscle [7, 204].The decrease in myocardial miR-499 expression could be as a consequence of tissue necrosis and loss of viable tissue but it has been hypothesised that it may be a therapeutic target for myocardial protection[224]. Predicted KEGG pathway targets implicate miR-499 in several pathways implicated in cell cycle regulation and apoptosis (FoxO pathway and p53; Table 3.6). Experimentally, miR-499 has been shown to inhibit cardiomyocyte apoptosis through its suppression of calcineurin-mediated dephosphorylation of dynamin-related protein-1 (Drp1), reducing myocardial infarction size induced by ischaemia[225]. Furthermore, loss of myocardial miR-499 inhibits ischaemic post-conditioning via the programmed cell death 4 (PDCD4)[226] and elevated levels have conversely been shown to protect cardiomyocytes from ischaemia via the same pathway[227]. MiR-499 has also been implicated in the pathogenesis of myocardial hypertrophy and cardiomyopathy[228]. These findings raise the intriguing possibility that loss of miR-499 may have a deleterious effect post infarction and, if it is subsequently taken up by surrounding viable cardiac myocytes, it may have a beneficial effect on the ischaemic penumbra. This hypothesis has

already been taken forward experimentally, showing miR-499 plays a role in the maturation of cardiac fibroblasts to cardiomyocytes *in vivo* and *in vitro* *[229].*

Interestingly, the observation of increased concentration of miR-499 in renal tissue in a model of myocardial injury has not previously been described (Figure 3.4). Cell-free circulating miRNAs have been reported to be biologically stable, referring to their resilience to breakdown in an RNase rich environment, a function attributed to their association with protein complexes and EVs [5]. This led to the hypothesis that paracrine miRNA cell-cell signalling could be mediated by EVs [21], an observation now reported in a large variety of tissues and disease processes [76-78]. At the time of writing, there are no indications that miRNA-protein complexes are implicated in miRNA cell-cell signalling. No group has described miRNA cell transfer to distal organs in a model of single organ injury. With regard to the role miR-499 may play in the kidney, it is possible miR-499 may play a role in cell viability. Predicted miR-499 KEGG pathway targets include cell cycle regulation and apoptosis (FoxO pathway and p53; Table 3.6); potentially affecting cell viability as demonstrated in cardiomyocytes. While no experimental work has been conducted at the proximal tubule with regard to miR-499, calcineurin inhibitors are widely used in the treatment of minimal change disease, a renal disease process driven by podocytes. MiR-499 overexpression has been shown to ameliorate podocyte injury by targeting Calcineurin Aα and Calcineurin Aβ in a minimal change disease mouse model [230],

Whether the observed increase in miR-499 in renal tissue is due to downstream miRNA transfer from heart to kidney or endogenous transcription in the renal tissue is yet to be elucidated. Correct interpretation of miRNA source is challenging, since the majority of miRNAs are not tissue specific and there are scarce reports of prevalence in diseased tissue. Further work regarding, EV uptake /release mechanisms affecting the renal tubule and the transcriptomic consequences of miRNA transfer will be further investigated in Chapters 4-6.

3.4.4. Limitations

The current gold-standard biomarker of myocardial injury, troponin I, is known to correlate to both degree of myocardial injury and predict mortality [231, 232]. This study therefore compares biomarker performance to a surrogate endpoint and does not provide information on prognosis. Myocardial infarction has been noted to cause a significant rise in TnI 4-6 hours following injury[233]. Following advent of high sensitivity TnI, this biomarker can now diagnose myocardial infarction with 1 hour of symptom onset[234]. The observation that TnI levels were elevated 2 hours following CAL was therefore unsurprising and the significant TnI rise in the sham cohort represented a unique challenge in this study (Figure 3.2). A rise in cardiac miRNAs has previously been described in the sham rat model of coronary ligation (thoracotomy only)[53], raising concerns regarding the sham cohort as the control population. Unfortunately, the presence of miR-133a and miR-1 in skeletal muscle ensures muscle injury cannot be accounted if using healthy controls[208], thus limiting the use of this CAL model for biomarker kinetic studies. Alternative models of myocyte injury have been described in the literature, for example genetically manipulating myocardial tissue via vectors to induce targeted myocyte injury. Such models include adeno-associated virus serotypes AAV-1, -6 and -8[235]. While these models are effective at specifically targeting myocytes, gene expression becomes affected 1 week post-transduction, limiting the use of this model for biomarker of early myocardial injury[236]. The work presented in Chapter 2 and 3 confirm the normalisation of the circulating miRNA signature 24 hours after injury and therefore a model requiring several days to establish injury is unlikely to be suitable.

3.4.5. Summary

Circulating miRNAs can predict myocardial injury, translate across human and mouse experimental models and may have utility as early diagnostic biomarkers. These early diagnostic biomarkers may help to improve specificity of the current gold standard biomarker TnI for myocardial infarction, through the development of a biomarker panel manipulating the different kinetics affecting these biomarkers of interest. MiRNA profiles change in organs distal to the single-organ injury but it is

not clear if this is as a result of cell-cell miRNA signalling or of endogenous origin. This will be investigated in subsequent chapters.

Chapter 4: EV uptake and release from the proximal tubule

Contents

4.1. INTRODUCTION

4.1.1. Background

Urine, the excreted filtrate of the kidney, is unique in providing a non-invasive snapshot of the kidney's function. This filtrate is composed of ions, inorganic and organic compounds (including proteins, hormones and metabolites) suspended in water. Investigation of the protein fraction of urine has demonstrated the presence of integral membrane proteins within EVs [131]. Several subtypes of vesicles have been identified in urine, including exosomes and microvesicles [35, 101], containing both proteins [102, 135]and nucleic acids [237].

EVs can be identified by transcriptomic and proteomic markers specific to the cell of origin [35, 117]. Rigorous characterisation of the EVs protein and RNA content has identified molecules unique to all regions of the nephron and products of genes associated with renal disease processes and systemic illness [35, 36]. A number of studies have demonstrated circulatory EV uptake by tubular epithelial kidney cells [238, 239] and identified EVs in urine [139, 240]. The ability of circulatory EVs to cross the glomerulus and enter the nephron is not fully understood, raising the possibility of repackaging of EV contents as EVs transit across membranes. Within the kidney, evidence suggests that EVs may be able to transit intact between cells, and through the basement membrane, until the intracellular release of its contents [241].

Inter-cellular communication depends upon the ability of EVs to influence a recipient cell, either by receptor-mediated interaction, endocytosis of the EV, or fusion of the vesicle membrane to the plasma membrane (Figure 1.2). This latter signalling mechanism results in delivery of an EV's contents directly into the cellular cytoplasm; including transfer of transcription factors, miRNA, mature RNA and infective particles [21, 95, 132, 133]. EV mediated inter-cellular signalling has been postulated to explain why PT proteins are present in downstream nephron segments [134-136], but this has not yet been conclusively demonstrated *in vivo* [135]. Hypothetically, EVs native to the kidney or derived from the circulation could affect the proteome, and therefore function, of a downstream recipient cell within the

nephron [137]. Therefore, understanding the signalling processes which drive EV release and uptake along the nephron is crucial to the translation of EVs as therapeutic targets in renal disease. Several mechanisms have been proposed to increase EV release from non-renal cells, all largely driven by cellular activation. Pro-inflammatory stimuli [242-244], toxins[245], viruses, [241, 246], low sheer stress[247], hypoxia[248] and senescence[249] have all been implicated in stimulating EV release. Interestingly, purinergic receptor activation has also been implicated[95, 250, 251]. While these drivers may affect EV release, it has yet to be elucidated what affects EV release by tubular cells.

Factors affecting EV uptake within the nephron are slightly better understood. Notably, the exosomal fraction of AQP2 increases in response to desmopressin and transfer of EVs from desmopressin-treated cells to untreated cells results in an increase of functional AQP2 expression in the recipient cell [129, 138]. Cortical collecting duct cells stimulated with vasopressin take up ECVs, *in vitro* and *in vivo*, a process which can be manipulated to deliver miRNA to collecting duct cells, resulting in downregulation of target transcripts [139]. This study demonstrated that EV signalling is a physiologically regulated process, which can be manipulated to deliver miRNA downstream along the nephron, thus affecting physiological tubular function[135, 252]. Interaction of EVs with recipient cells may involve specific interaction with primary cilia, as reported with polycystic disease-positive vesicles using transmission electron microscopy images [140, 141]. This observation is supported by data from a biliary model that demonstrate exosome signalling affects ERK signalling, miRNA expression and cell proliferation, with abolishment of this signal following removal of cilia [142]. Furthermore, EVs may be transported within uromodulin polymers , modulating the interaction between EVs and their target cells along renal tubular lumen [135].

As suggested by Chapter 3, miRNAs may transfer from the circulation to the renal tubule. An understanding of the regulatory aspects of EV uptake and release by the PT in health is a critical first step in investigating this novel signalling pathway, which can be built on to explore the effect of circulating EVs on kidney cells. Several physiological agonists of the PT were chosen for this study. These agonists were

selected as they have well-defined physiological activity at the proximal tubule and targeting pathways that may be related to EV uptake and release. Notably, EV release has been noted as a consequence of purinergic stimulation in platelets [95], dendritic cells [250], and glial cells [251]. EV release at the PT as a consequence of purinergic stimulation has not been described.

4.1.2. Objectives

- Establish an appropriate PT cell model for the study of EV release and uptake
- Identify factors which affect EV release from the PT
- Identify factors which affect EV uptake by the PT

4.2. METHODS

4.2.1. Cell culture

4.2.1.1. Previously established cell lines

Two PT cell lines were used in the following experiments; the HK2 cell line, a HPV-16 transformed human PT cell line, and the LLC-PK1, a porcine PT cell.

The HK2 cell line was a kind gift from Dr Kenneth Simpson (University of Edinburgh, United Kingdom) and grown following previously published methods [253]. Briefly, cells were grown in culture medium containing K-SFM (Gibco, CA, USA) supplemented with 0.05 mg/ml bovine pituitary extract (BPE) and 5 ng/ml human recombinant epidermal growth factor (EGF). The cells were incubated at 37°C and maintained in a humidified 5% CO_2 atmosphere. The media was changed every 48-72 hours.

The LLC-PK1 cell line was a kind gift from Dr Karen Chapman (University of Edinburgh, United Kingdom) and grown following previously published methods.[254] Briefly, cells were grown in culture medium containing Medium 199 (Gibco, CA, USA) containing 1.5 g/L to 2.2 g/L sodium bicarbonate and 3% exosome depleted foetal bovine serum (FBS; System Biosciences, CA, USA). The cells were incubated at 37°C and maintained in a humidified 5% CO_2 atmosphere. The media was changed every 48-72 hours.

Subcultivation processing was similar for both cell lines. Cells were passaged at 80% confluency, at a subcultivation ratio of 1:4. Passaging was achieved by two x 5 minute washes with 1 mM EDTA in Dulbecco's phosphate-buffered saline (DPBS) followed by incubation in 0.05% (w/v) Trypsin- 0.53 mM EDTA solution (Lonza, Basel, Switzerland). Complete growth medium was added, to terminate the reaction, and cells were pelleted at 150 x *g* for 5 minutes. Subsequently, the supernatant was removed and cells were resuspended in complete growth medium. Aliquots containing 95% culture medium and 5% DMSO were stored in liquid nitrogen.

4.2.1.2. Primary cell culture

Primary cell culture method was modified from Richardson *et al.*[255] [256-258]. Briefly, male rats were euthanised using cervical dislocation. Their kidneys were removed immediately under aseptic conditions and placed in DMEM/Ham's F12 medium with Glutamax (Gibco, CA, US) containing 10% wt/vol FBS (Gibco, CA, US), 100 U/ml penicillin and 100 µg/ml streptomycin (Gibco, CA, US) (hereafter referred to as isolation medium). After the peri-renal fat was removed, the kidneys were decapsulated and the cortex macroscopically dissected. The cortex was minced and incubated in serum-free isolation medium containing 1mg/ml collagenase I and IV (Sigma Aldrich, Dorset, UK) for 45 minutes in a shaking waterbath at 37 °C. The reaction was terminated by washing 3 times in isolation medium. The resultant solution was ground in Wheaton mortar and pestle and serially sieved to a final filter size of 40μm. The filtered solution was centrifuged at 27 000 x *g* through a 48% Percoll gradient (Sigma Aldrich, Dorset, UK) and each of the 4 distinct bands (F1-F4; top-bottom) were carefully removed.

Cells contained within the lowermost band (F4) were washed in isolation medium to remove residual Percoll and passed through a 40 μm sieve. The cells were resuspended in DMEM/Hams's F12 media with glutamax containing: 5 µg/ml insulin, 50 nM hydrocortisone, 10 ng/ml EGF, 5 µg/ml transferrin, 50 nM sodium selenite, 10 nM triiodothyronine, 100 U/ml penicillin, 100 µg/ml streptomycin and 1% (wt/vol) exosome depleted FBS (System Biosciences, CA, US) (hereafter referred to as culture medium). The suspension was plated onto collagen-coated 35-mm tissue culture dishes (Corning, NY, US) and maintained in an incubator under humidified 5% CO_2 atmosphere at 37 °C. The culture media was replaced after 48 hours and every 48 hours thereafter.

4.2.2. Validation of primary cell culture

4.2.2.1. Alkaline phosphatase activity

After the Percoll gradient stage of the primary cell culture method, cells from each of the 4 bands were washed in isolation medium and cultured in culture medium for 48 hours. Cells were subsequently washed 3 times in DPBS, lysed in 500 µL assay buffer (Abcam, Cambridge, UK) and incubated at 4 °C for 10 minutes. The

solubilised sample was subsequently centrifuged at 12,000 x *g* at 4 °C for 3 minutes to remove any insoluble material. A small aliquot of each sample was taken for protein quantification, using bicinchoninic acid assay (BCA) protein assay kit as per the manufacturer's instructions (Thermo Scientific, Perth, UK). Samples were subsequently normalised to protein concentration and immediately processed using an alkaline phosphatase colorimetric assay kit (Abcam, Cambridge, UK), as per the manufacturer's instructions.

4.2.2.2. Western blotting

4.2.2.2.1. Protein extraction from cells

Cells from each band were resuspended in ice-cold Radioimmunoprecipitation assay (RIPA) buffer (Sigma Aldrich, Dorset, UK) containing protease inhibitor (Roche, 1 tablet per 10ml). Cells were lysed by repeated passage through a 21 G needle and then incubated on ice for 15 minutes. Lysates were centrifuged at 16,000 x *g* for 15 minutes at 4 °C and then the supernatant was stored at -80 °C. The protein concentration of each sample was determined in duplicate using the BCA Protein Assay Kit (Thermo Scientific, Perth, UK).

4.2.2.2.2. Gel electrophoresis and electrophoretic transfer

Protein samples were mixed 1:1 with 2 × Laemmli buffer (giving the following final concentrations: 62.5 mM Tris-Cl pH 6.8, 2 % sodium dodecyl sulfate (SDS), 10 % vol / vol glycerol, 0.1 mg/ml bromophenol blue, 100 mM dithiothreitol (DTT)), heated to 100 °C for 2 - 10 minutes and then loaded immediately into the wells of the 12% Tris-HEPES gel (Precise, ThermoScientific, Perth, UK). Samples were electrophoresed at 100 V for 45 minutes. After equilibrating the gel and an Amersham Hybond polyvinylidene difluoride (PDVF) membrane (GE Healthcare, Buckinghamshire, UK) in Towbin transfer buffer (25 mM Tris, 192 mM glycine, 0.1 % SDS and 20 % v/v methanol), samples were transferred to the membrane using a BioRad Trans-Blot semi-dry electrophoretic transfer cell (at 10 V for 30 minutes).

4.2.2.2.3. Western Blotting

Membranes were incubated with blocking buffer (5 % w/v non-fat dry milk powder / 0.2 % v/v Tween-20 in PBS) on a rolling shaker at room temperature for 1 hour and

then incubated with primary antibody overnight at 4 °C. After three five-minute washes with wash buffer (0.2 % v/v Tween-20 in PBS) the membrane was incubated with an HRP-conjugated secondary antibody for 1 – 2 hours at room temperature and then washed again (three x ten minute washes). Peroxidase activity was revealed using SuperSignal ® West Pico Chemiluminescent Substrate (Thermo Scientific, Perth, UK) as per the manufacturer's instructions and membranes were exposed to photographic film for 1 – 30 minutes.

Gels and films were placed on a light-box and photographed using a digital SLR camera (Nikon D40), with the exposure set to maximize dynamic range without significant pixel saturation. Antibodies used are demonstrated in Table 4.1.

Target (immunogen)	Host & conjugate	Source (cat nº)	Stock (mg/mL)	Dilution for western blot
Primary Antibodies				
NHE3	Rabbit	Abcam AB95299	1000 mg/ml	1:1000
Secondary Antibodies				
rabbit IgG	goat HRP	Santa-Cruz (sc-2030)		1:2000

Table 4.1: Primary and secondary antibodies used for Western blotting.
All antibodies were polyclonal.

4.2.2.2.4. Coomassie blue staining

Gels were incubated on an orbital shaker with Coomassie blue staining solution (250 mg/L Coomassie Brilliant blue R in de-staining solution I; Bio-Rad, CA, US) for 4 hours. The bulk of the stain was removed by incubating with de-staining solution I (40 % methanol / 7 % acetic acid) for 30 minutes. The gel was then placed in de-staining solution II (5 % methanol / 7 % acetic acid), which was changed every 12 hours until a clear background was obtained (typically after 24 hours).

4.2.2.3. Confocal microscopy

Primary proximal tubule (PPT) cells were grown on a cover slip. Cells were fixed with 4% PFA for 15 minutes at room temperature, washed in PBS, and subsequently permeabilised with 0.3% triton for 10 minutes. Cells were incubated with 20% goat serum for 1 hour then co-incubated with 15μg/ml KIM-1 goat-antibody (AF3689, R&D Systems, MN, USA) for 16 hours at 4 °C. The following day, the cells were co-incubated with the 0.2% v/v donkey anti-goat antibody conjugated with Alexa 488 (A11055, Thermo Fisher, UK) and/or 0.1% v/v phalloidin conjugated to Alexa 594 (A12381, Thermo Fisher, UK) at room temperature for 20 minutes. Immediately prior to imaging, cells were stained with 0.1% v/v 4',6-diamidino-2-phenylindole (DAPI) for 10 minutes and washed with PBS.

Images were captured using a confocal laser scanning microscope (LSM 710, Zeiss, Cambridge, UK). Images were collected with a 60x oil immersion objective lens and acquired using ZenPro Software (Zeiss, Cambridge, UK). Image analysis was performed using Image J software. Each picture was acquired with laser intensities and amplifier gains adjusted to avoid pixel saturation and analysed using Image J 2016 (National Institutes of Health, Maryland, US).

4.2.3. PT cell stimulation with physiological agonists

Agonists were added to fresh cell media for up to 48 hours (as specified for each experiment). For EV uptake experimentation, agonists and QDot loaded EVs were added simultaneously to the cell media. Methodology for QDot loading described in Section 4.2.6.1. The doses used were informed by previously published PT cell studies investigating signalling provoked by MeSADP [259], angiotensin II [260], fenoldopam[261] and forskolin[262].

	Source (cat nº)	Target	Second messenger	Final Concentration.
Agonist				
MeSADP	Tocris No 1624	Purinergic receptors $P2Y_1$, $P2Y_{12}$ and $P2Y_{13}$	Ca^{2+}	100 µM
Angiotensin II	Sigma A9525	AT1 receptor	Ca^{2+}	50 nM
Ionomycin	Sigma I3909	Ionophore (positive control)	Ca^{2+}	1 µM
Fenoldopam	Sigma SML0198	Dopamine receptor D1	cAMP	1 µM
Forskolin	Sigma F6886	Directly activates eukaryotic adenylyl cyclase (positive control)	cAMP	10 µM
Antagonist				
MRS 2500 tetraammonium salt	Tocris No 2159	Purinergic receptor $P2Y_1$		1 nM

Table 4.2: Agonists and antagonist used in cell culture

4.2.4. Assessing response of proximal tubule cells to physiological agonists

4.2.4.1. cAMP concentration

Cells were grown to 70% confluency, washed twice in PBS and replaced with fresh culture media (warmed to 37°C). Cells were stimulated with agonists for 10 minutes and immediately washed in ice-cold PBS. Samples were processed according to manufacturer's instructions using Parameter™ cAMP colorimetric assay (R&D Systems, MN, USA). All biological samples were processed in triplicate.

4.2.4.2. Calcium flux

Cells were washed twice in room temperature DPBS followed by incubation in 0.05% (w/v) Trypsin- 0.53 mM EDTA solution (Lonza, Basel, Switzerland). Complete growth medium was added, to terminate the reaction, and cells were pelleted at 150 x *g* for 5 minutes. Subsequently, the supernatant was removed and cells were resuspended in cell loading media (CLM; 1 mM calcium chloride, 1 mM KCl, 1 mM MgSO4 and 0.5% v/v BSA; pH 7.35). Cells were incubated with 2 μM Indo-1 AM (Invitrogen, CA, US) for 30 minutes at 37°C. Cells were then pelleted at 400 x *g* for 5 minutes and resuspended in CLM. Total cell fluorescence was measured by flow cytometry on a 5LSR Fortessa cytometer (BD Biosciences, Oxford, UK). Cells were excited with a violet laser (405 nm) and their emission was detected using 530/30 (Indo-1 blue) and 440/40 (Indo-1 violet) band pass filters, respectively. Gates were set using unstained cells, 1,000,000 events were recorded for each sample and flow rate was set at 200 events/second. For each experiment, 10,000 events were recorded prior to introduction of agonist. 2 mM ethylene glycol-bis(β-aminoethyl ether)-N,N,N',N'-tetraacetic acid (EGTA) and 1μM ionomycin (Sigma Aldrich, Dorset, UK) were used as negative and positive controls, respectively.

Flow cytometry data were analysed with FlowJo LLC software version 8 (FlowJo LLC, Oregon, USA). The population of interest identified using FSC/SSC parameter and samples analysed as time vs mean fluorescence (Indo 1 (violet)/Indo-1 (blue)). The results are presented as the percentage of total fluorescent cells. Results are demonstrated as percentage change in peak fluorescence from baseline.

4.2.5. EV release in response to physiological agonists

4.2.5.1. Particle size and concentration distribution measurement with NTA

At the appropriate time point, media was removed from the cells and centrifuged at 300 x *g* for 5 minutes to remove cell debris. The supernatant was isolated and stored at -80°C, if not processed immediately. Nanoparticles within the supernatant were analysed using the NanoSight LM 10 instrument (NanoSight Ltd, Amesbury, UK) allowing simultaneous estimation of size, size distribution and concentration of dilute suspensions of nanoparticles. Using a 532 nm (green) diode laser beam a 60 second video was taken with a frame rate of 30 frames/second and particle movements were analysed by NTA software. Each experiment was carried out in triplicate. All experiments were carried out at a 1:100 dilution, yielding particle concentrations in the region of $1x10^8$ particles/ml in accordance with the manufacturer's recommendations. All samples were analysed in triplicate. In each run, fresh samples were injected three times and measurements were performed following each injection. Standard deviations were determined from concentrations obtained from replicate runs.

NTA software provides the number of particles of each size between 10-1000 nm. The AUC for the size range of interest was calculated using the trapezoidal rule, with values increasing incrementally on the x-axis, and expressed as the sum of the individual trapezoids.

4.2.6. EV uptake in response to physiological agonists

4.2.6.1. Isolation and dye loading of EVs

As described previously[129], culture media from PPT cells was vigorously vortexed then centrifuged at 15,000 x *g* for 10 minutes to pellet any cells, large membrane fragments and other debris. The supernatant was then centrifuged at 200,000 x *g* for 60 minutes to pellet the EV fraction. The pellet was washed with PBS and then re- centrifuged at 200,000 x *g* for 60 minutes before final resuspension in PBS. Pelleted EVs were conjugated with Cell Tracker 655 (Invitrogen, CA, US) following

the manufacturer's protocol. Briefly, pelleted EVs were incubated with the Cell Tracker 655 conjugate in 200µl fresh culture media for 1 hour at 37°C. The EV pellet suspension was washed twice with fresh media before being put back on confluent cells.

EV size distribution was confirmed by NTA of a 1:1000 dilution of Cell Tracker 655 conjugate. Dye loaded EVs were co-incubated with cells at a concentration of 250 x 10^8/ml media.

4.2.6.2. Flow cytometry for total cell fluorescence

Following trypsinisation, cells were resuspended in PBS and briefly stained with 1µM DAPI nucleus stain (Sigma Aldrich, Dorset, UK). Total cell fluorescence was measured by flow cytometry on a 5LSR Fortessa cytometer (BD Biosciences, Oxford, UK). Particles were excited with a violet laser (405 nm) and emission detected using 450/50 and 630/70 band pass filters, respectively. Gates were set using unstained cells and cells stained with DAPI alone. Flow cytometry data were analysed with FlowJo LLC software version 8 (FlowJo LLC, Oregon, USA) and the results are presented as the percentage of total fluorescent cells and mean cell fluorescence.

4.2.7. Data evaluation and statistical analysis

Where possible data were presented as Tukey box plots. Tukey box plots consist of 4 parameters; box ends at the quartiles Q1 and Q3, median as a horizontal line in the box, 'whiskers' to the farthest points that are not outliers (i.e. within 3/2 times the interquartile range of Q1 and Q3) and dot plot of outliers. Data were analysed using GraphPad PRISM (version 6.03 for Windows, GraphPad Software, San Diego, USA) and a P-value < 0.05 was considered statistically significant. When testing for a difference in the means of more than two datasets (e.g. EV release in response to physiological agonists) a one-way ANOVA and post-hoc comparison using Tukey's multiple comparison test was used. When datasets were influenced by more than one factor (i.e. EV uptake as affected by time and agonist) a two-way ANOVA with Tukey's multiple comparison test was utilised.

4.3. RESULTS

4.3.1. Validation of primary proximal tubule cells

In order to investigate the PPT cells, cell monolayers from each Percoll fraction were investigated for archetypal morphological, enzymatic and proteomic features. After 48 hours in culture, cultured cells from F4 exhibited the cobblestone-like phenotype characteristic of epithelial cells (Figure 4.1d) more prominently than cell monolayers from the other fractions (Figure 4.1a-c). The enzymatic activity associated with each fraction is depicted in Figure 4.2. Cells cultured from the F4 Percoll fraction demonstrated significantly higher alkaline phosphatase activity in comparison to cells from the 3 other Percoll fractions (alkaline phosphatase activity within cell lysate was normalized to total protein to take into account differences in total cell number). Furthermore, NHE3 was associated with cells isolated from Percoll bands F3–F4 (Figure 4.3), a protein marker specific to the PT and thick ascending limb[263]. Due to animal numbers needed for each experiment, this experiment was run once, inhibiting quantitative statistical analysis.

Cells cultured from F4 retained morphological, enzymatic and proteomic features of PT cells and were therefore taken forward as representative of PPT cells. To conclude cell validation, confocal microscopy was conducted on the PPT cells. Figure 4.4 depicts cobble-stoned cells, articulating with actin, containing KIM-1 (another archetypal proteomic marker of the PT).

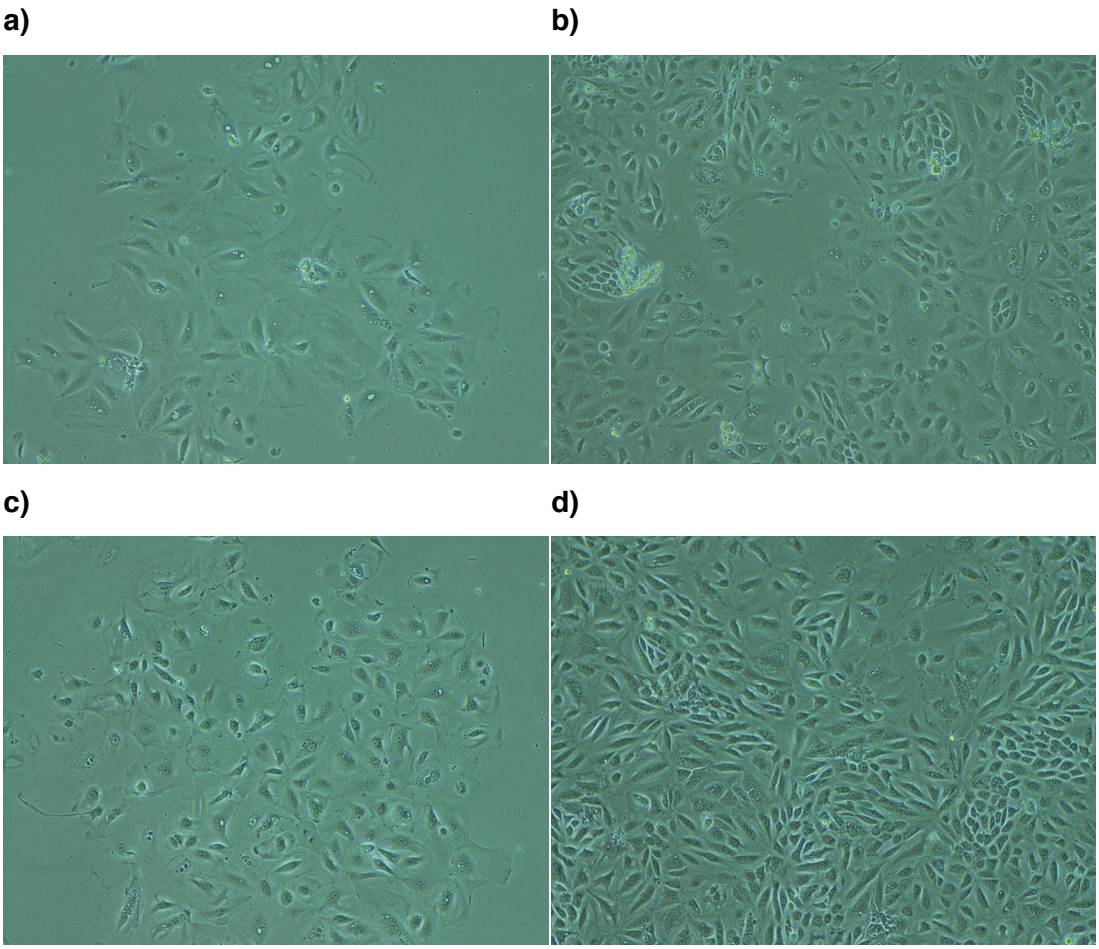

Figure 4.1: Bright-field micrograph of primary renal cell preparations in culture.

Cells isolated from Percoll fractions were grown in culture medium for 48 hours. Bright-field microscopy of cell monolayers from F1 (a), F2 (b), F3 (c) and F4 (d). Each image is representative of 3 samples from each fraction.

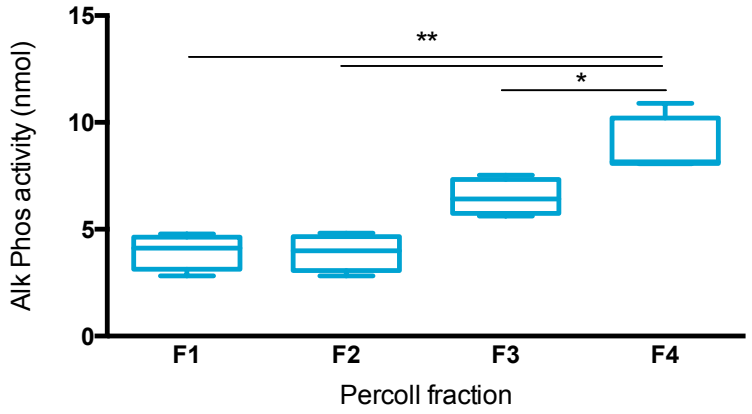

Figure 4.2: Cultured primary renal cells retain alkaline phosphatase activity.

Alkaline phosphatase activity was retained in cultured cells, isolated from Percoll bands F1-4. Cultured cells within F4 had significantly higher alkaline phosphatase activity than the 3 other bands, when normalized to total protein. Data are shown as Tukey boxplots, n=4. Statistical significance was determined by one- way AVOVA with Tukey's multiple comparison test**.**

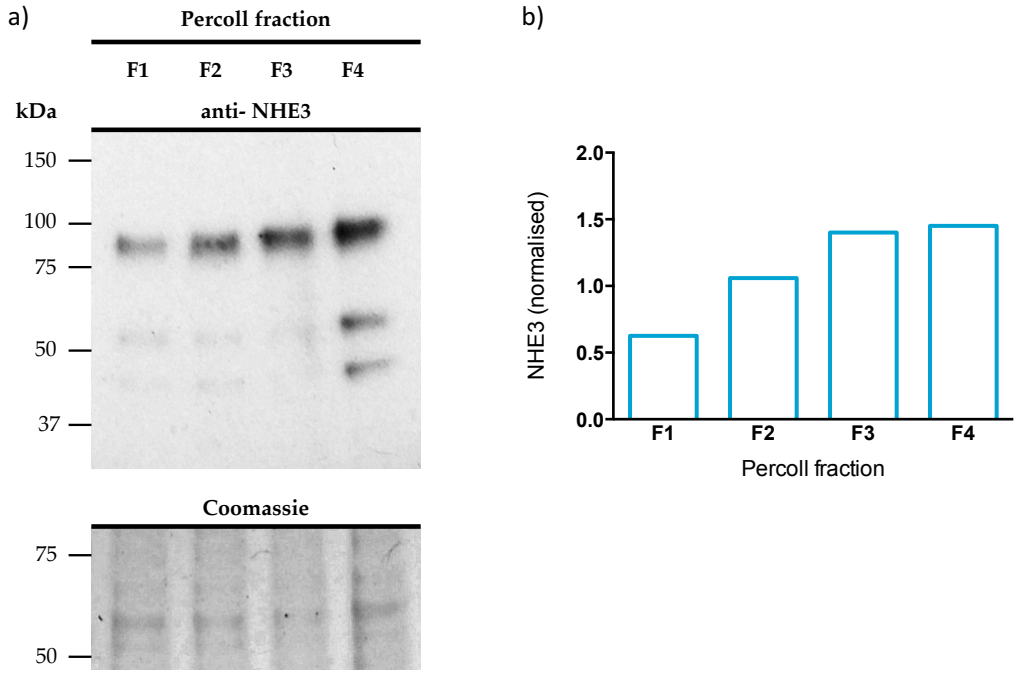

Figure 4.3: Western blots to estimate the abundance of NHE3 in primary renal cells.

Cells were isolated from each Percoll fraction and homogenized. 12 μg of protein was loaded per lane. Gels were in duplicate allowing for a Coomassie blot to provide loading controls. A) Western blot to detect total NHE3 (NHE3 band detected at ~84 kDa) B) Densitometry analysis of blots displayed in (a)

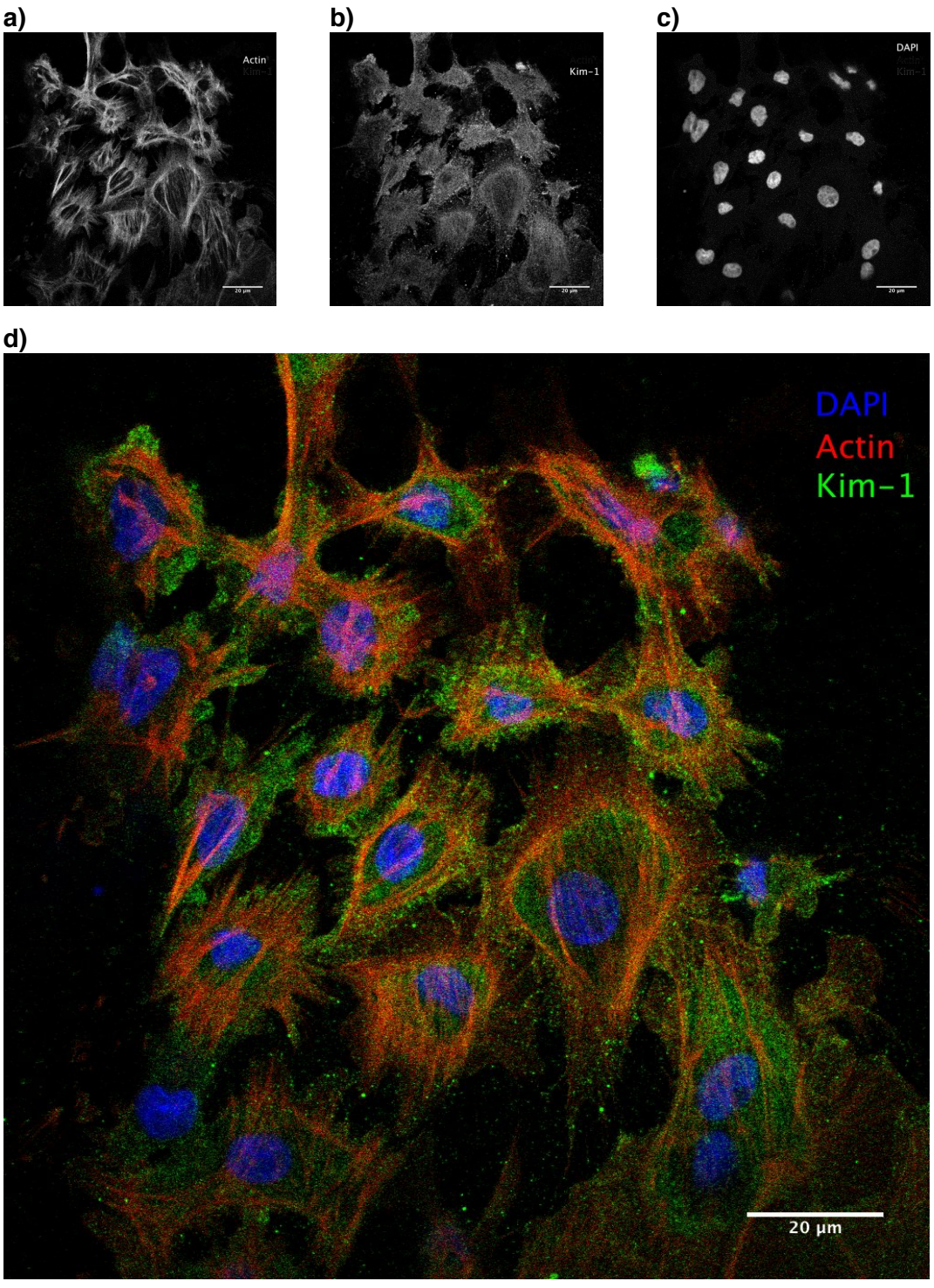

Figure 4.4: Confocal image of F4 cell monolayer confirms expression of archetypal proximal tubule proteins.

Images a-c indicates actin, KIM-1 and nuclear (DAPI) staining, respectively. Amalgamated image (d) shows KIM-1 (green), nuclei stained with DAPI (blue) and actin within the cell membrane (red). Images are representative of 3 samples. Scale bars are 20 µm.

4.3.2. Cultured cell response to physiological agonists

Firstly, HK2, LLC-PK1 and PPT cells were interrogated for an appropriate response to known physiological agonists of the PT by assessment of their secondary messengers. Data pertaining to the effect of fenoldopam on cAMP concentration are presented in Figure 4.5a. The intracellular Ca^{2+} responses to MeSADP and angiotensin II (∆mean fluorescence) are presented in Figure 4.5b.

No difference in cAMP concentration within HK2 cells could be detected following stimulation with fenoldopam or vehicle (Figure 4.5a). Likewise, HK2 intracellular Ca^{2+} concentrations remained unchanged when stimulated with MeSADP and angiotensin II (Figure 4.5b). In both experimental designs, cAMP and Ca^{2+} intracellular concentrations significantly increased in response to the relevant positive controls, forskolin and ionomycin, respectively.

By contrast, the cAMP concentration within LLC-PK1 and PPT cells in the fenoldopam treated group significantly increased, in comparison to vehicle (Figure 4.5a). Similarly, MeSADP and angiotensin II elicited an increase in intracellular Ca^{2+} in both the LLC-PK1 and PPT cell lines (Figure 4.5b).

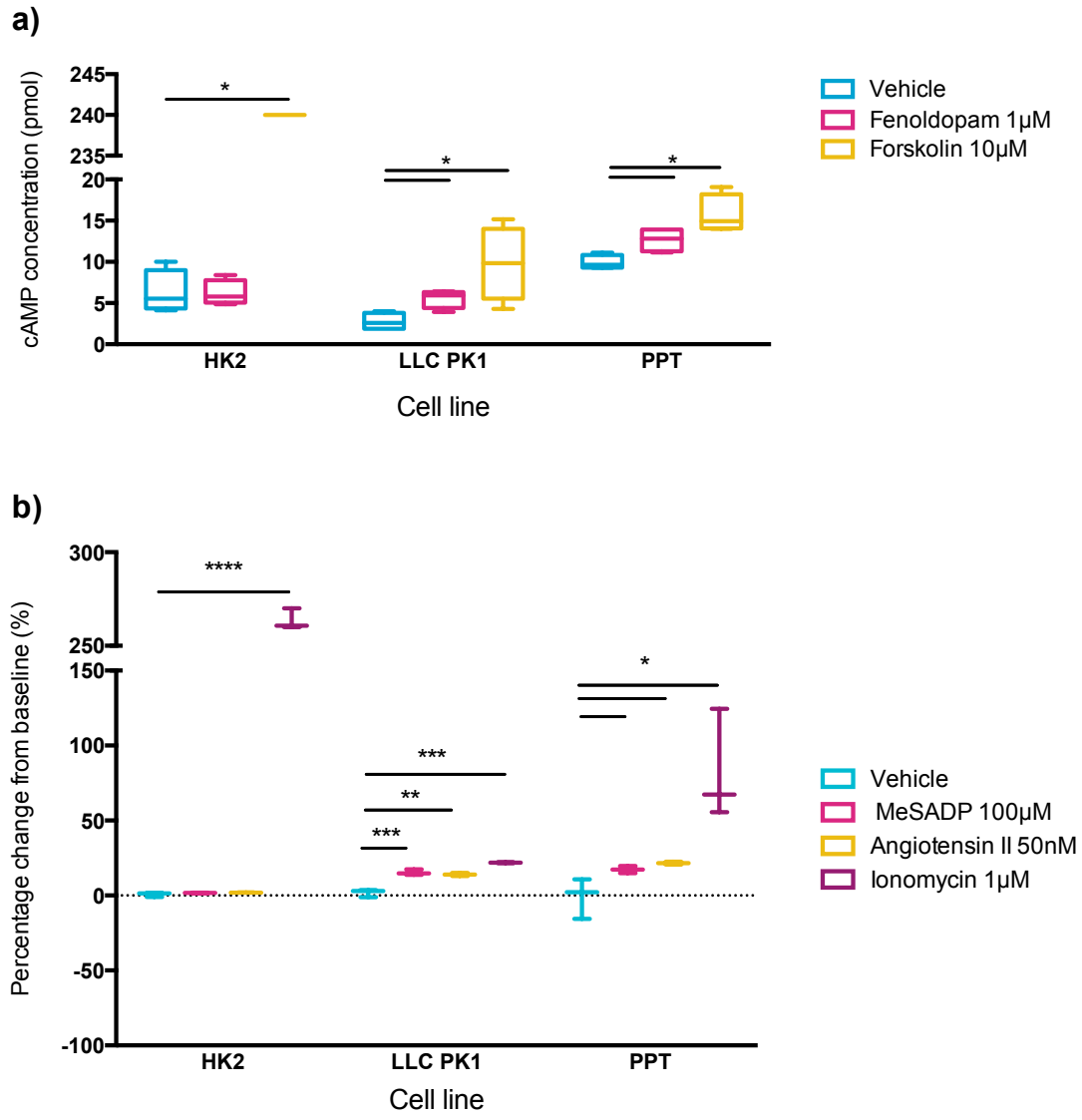

Figure 4.5: Effect of physiological agonists on cultured proximal tubule cells.

Assessment of cellular secondary messenger response to known physiological agonists of the PT. Cultured cells were challenged with vehicle (PBS; blue), fenoldopam (1 μM; pink) or forskolin (10 μM; yellow) for 10 minutes, prior to assessment of cAMP concentration (Figure a; n=4, data expressed as absolute value (pmol)). Total cell calcium concentration was viewed in real time following introduction of vehicle (PBS; blue), MeADP (100 μM; pink), angiotensin II (50 nM; yellow) or ionomycin (1 μM; purple) (Figure b; Δmean fluorescence) (Tukey box plot). Statistical significance was determined by 1 way ANOVA with Tukey multiple comparison to vehicle within the same cell line (n=3).

4.3.3. Effect on EV release by physiological agonists

EVs were considered in 3 cohorts: total EV population (20-1000 nm diameter), exosome population (20-100 nm diameter) and microvesicle population (100-500 nm), corresponding to i, ii and iii in the following figures. Example EV particle size range in cell culture supernatant is shown in Figure 4.6. EV release in response to agonist stimulation was examined in all 3 cell lines (Figure 4.7a-d) and the following findings observed:

- Angiotensin II stimulation resulted in significantly fewer EVs to be released from LLC-PK1 and PPT cells 24 hours after stimulation (Figure 4.7a-i). This corresponded to changes seen in the exosome cohort (Figure 4.7a-ii). Notably, there was not a consistent temporal response, as no significant changes were seen 48 hours following stimulation.
- MeSADP stimulation resulted in significant increase in EV release from LLC-PK1 cells after 48 hours, and from PPT cells 24 and 48 hours following stimulation (Figure 4.7b-i). These changes were all described in the exosome cohort (Figure 4.7b-ii) and an increase in the microvesicle population was also observed in the LLC-PK1 group (Figure 4.7b-iii).
- Significant changes were noted within the LLC-PK1 and PPT cell lines following stimulation with fenoldopam (Figure 4.7c). These changes were not consistent across cell lines, nor was there a temporal response.
- Direct activation of adenylyl cyclase with forskolin, with corresponding intracellular cAMP increase, did not result in any significant change in EV release within HK2 and LLC-PK1 cell lines (Figure 4.7d).
- No significant changes were noted in HK2 cell EV release within any of the cohorts in response to the physiological agonists(Figure 4.7a-d).
- Interestingly, fewer microvesicle particles were released from PPT cells in comparison to HK2 and LLC-PK1 cell lines. This effect was seen across the experimental groups as defined by agonist (Figure 4.7a-c).

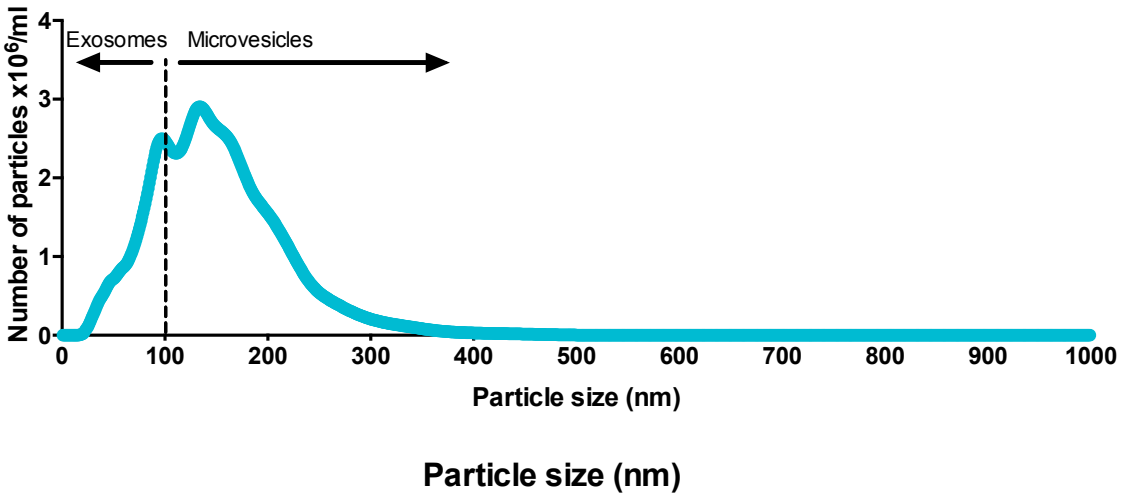

Particle size (nm)

Figure 4.6: Size distribution of EVs released from primary proximal tubule cells in culture

Mean particle size range (nm) of EVs in cell culture supernatant following 48 hours in culture. N = 12

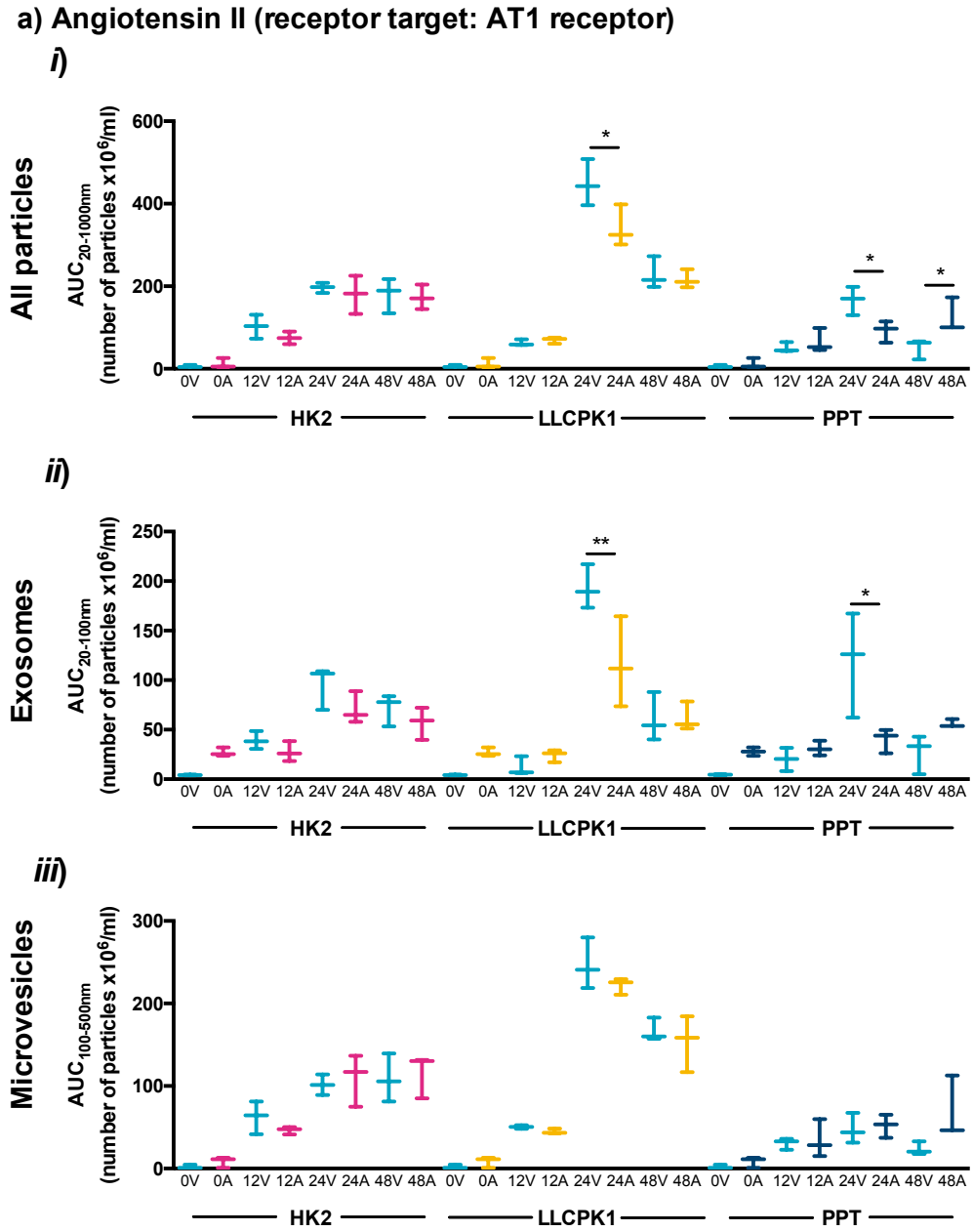

Figure 4.7: EV release is under physiological control

Cell culture media was collected at predefined time points following cell stimulation. 0, 12, 24. 48 corresponds to number of hours following stimulation with vehicle (v) or agonist (A). Cultured cells were challenged with angiotensin II (50 nM; Figure 4.7a), MeADP (100 μM; Figure 4.7b), fenoldopam (1 μM; Figure 4.7c), or forskolin (10 μM; Figure 4.7d) (mean±SD). EVs were considered in 3 cohorts: total EV population (20-1000 nm diameter), exosome population (20-100 nm diameter) and microvesicle population (100-500 nm), corresponding to i, ii and iii. The vehicle control for each time point is shown in light blue, red corresponds to HK2 cells, yellow to LLCPK1 and dark blue to primary proximal tubule. Statistical significance was determined by 1-way ANOVA with Tukey's multiple comparisons test within each cell line (n=3).

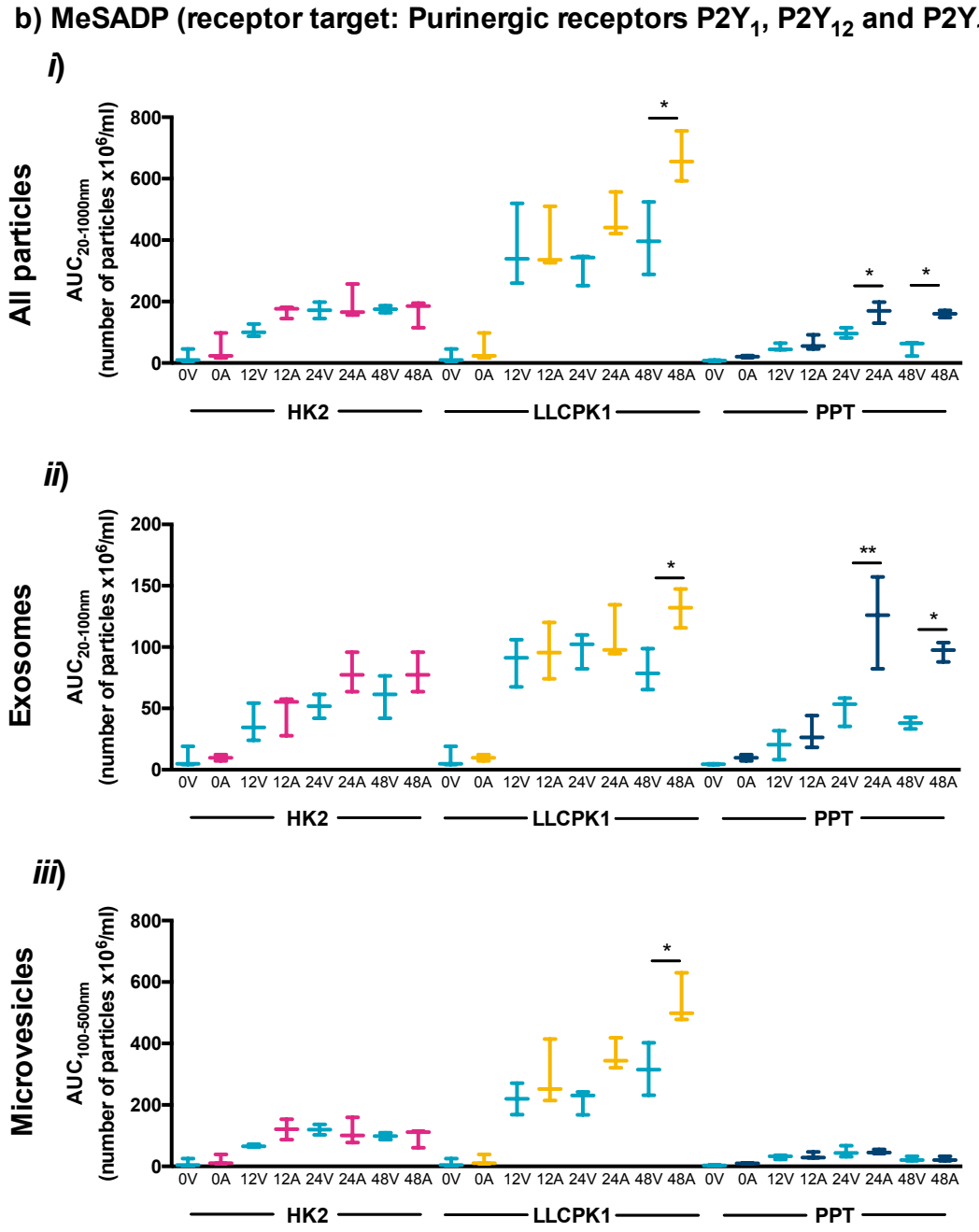

Figure 4.7 (cont.)

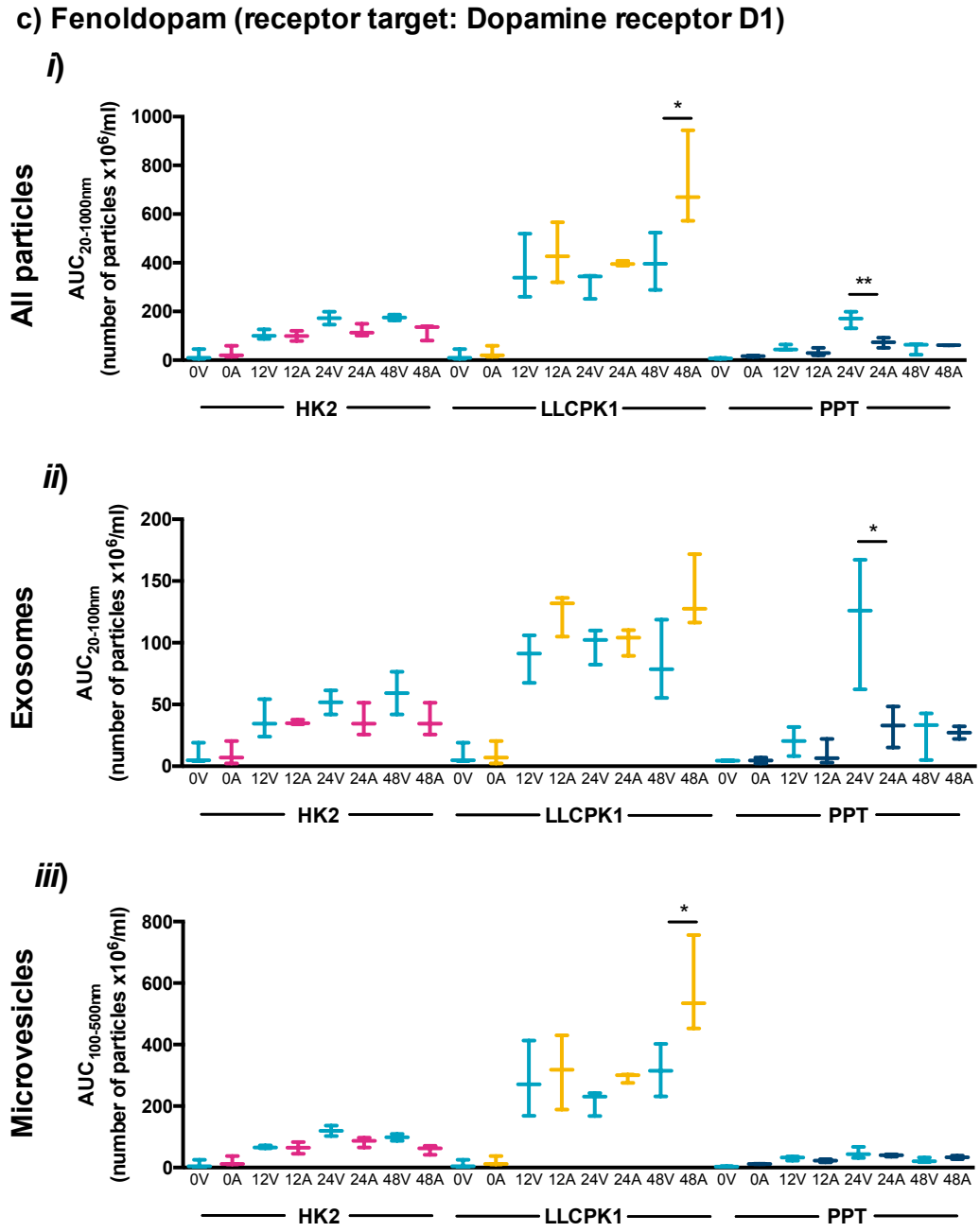

Figure 4.7 (cont.)

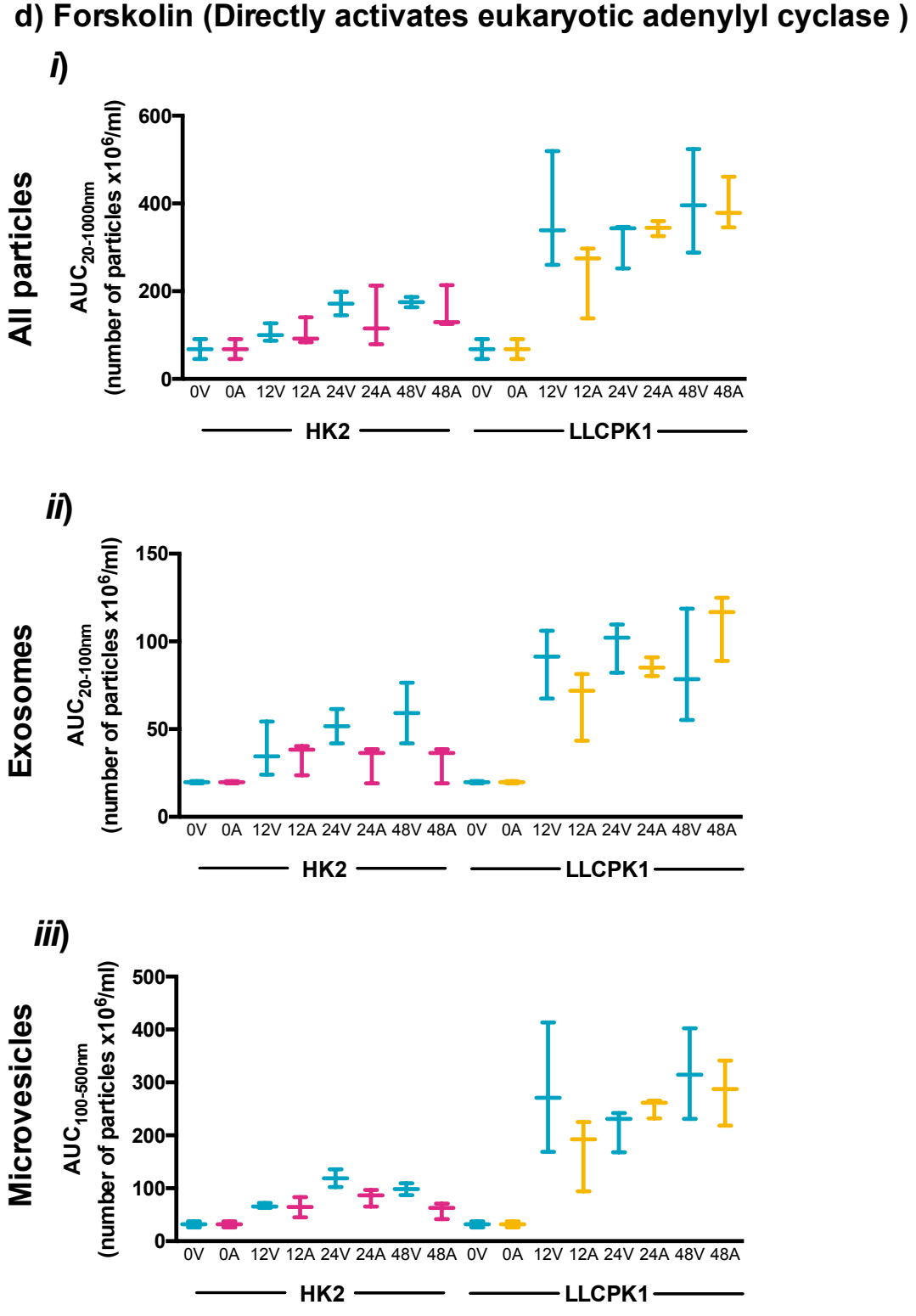

Figure 4.7 (cont.)

The EV release in response to MeSADP was further examined in the presence of the purinergic receptor $P2Y_1$ antagonist, MRS. As expected, stimulation with MeSADP alone resulted in an increase in vesicles within the exosome cohort, an increase abolished in the presence of $P2Y_1$ antagonist (Figure 4.8). Notably, stimulation with MRS alone did not have any effect on EV release within any of the cohort.

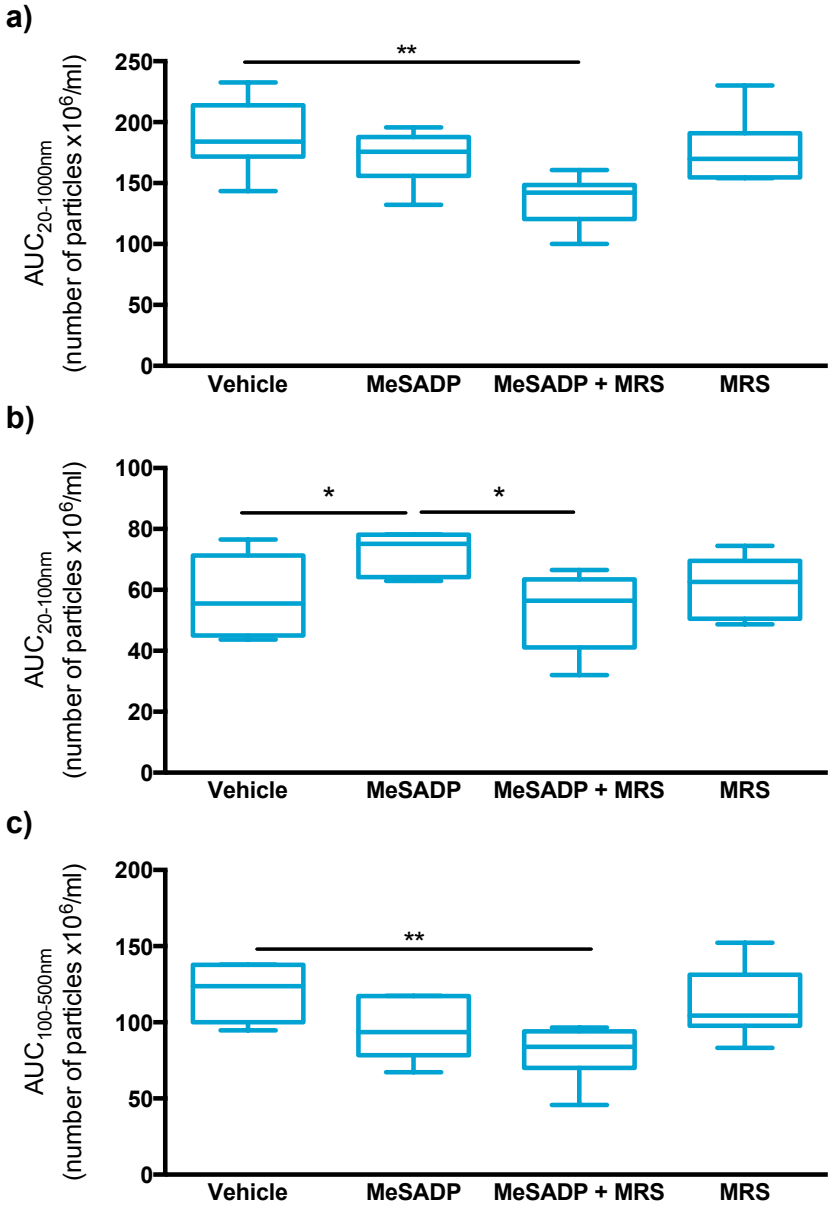

Figure 4.8: P2Y$_1$ antagonism inhibits purinergic driven EV release

LLC-PK1 cells were stimulated with MeSADP and/or MRS for 48 hours, prior to isolation of the cell medium. EVs were considered in 3 cohorts: total EV population (20-1000 nm diameter), exosome population (20-100 nm diameter) and microvesicle population (100-500 nm), corresponding to i, ii and iii. Statistical analysis was conducted using 1-way ANOVA with Tukey's multiple comparisons test (n=6).

4.3.4. Effect on EV uptake by physiological agonists

Using confocal microscopy, PPT cells uptake dye-loaded EVs when co-cultured for 48 hours (Figure 4.9). The mean particle size range of isolated EVs is demonstrated in Figure 4.10.

To quantify temporal EV uptake, flow cytometry was utilised to describe EV uptake by PPT cells (Figure 4.11a&b; percentage cell uptake and mean cell fluorescence, respectively). Using the same methodology, EV uptake in response to PT agonists was also studied.

Significantly more PPT cells take up EVs over time (12 hours vs 48 hours co-incubation; mean percentage fluorescent cells of total 4.67 vs 14.25; 1 way ANOVA with Tukey multiple comparison $p<0.01$; Figure 4.11a), correspondingly affecting the average fluorescence of the PTT cells (12 hours vs 48 hours; mean fluorescence intensity 2393 vs 3604; 1 way ANOVA with Tukey multiple comparison $p<0.05$; Figure 4.11b).

There were no significant differences in cell uptake of EVs by PTT cells between the experimental groups (i.e. vehicle vs angiotensin II vs MeSADP vs fenoldopam) as defined by percentage cell uptake or mean fluorescence intensity (Figure 4.11a&b).

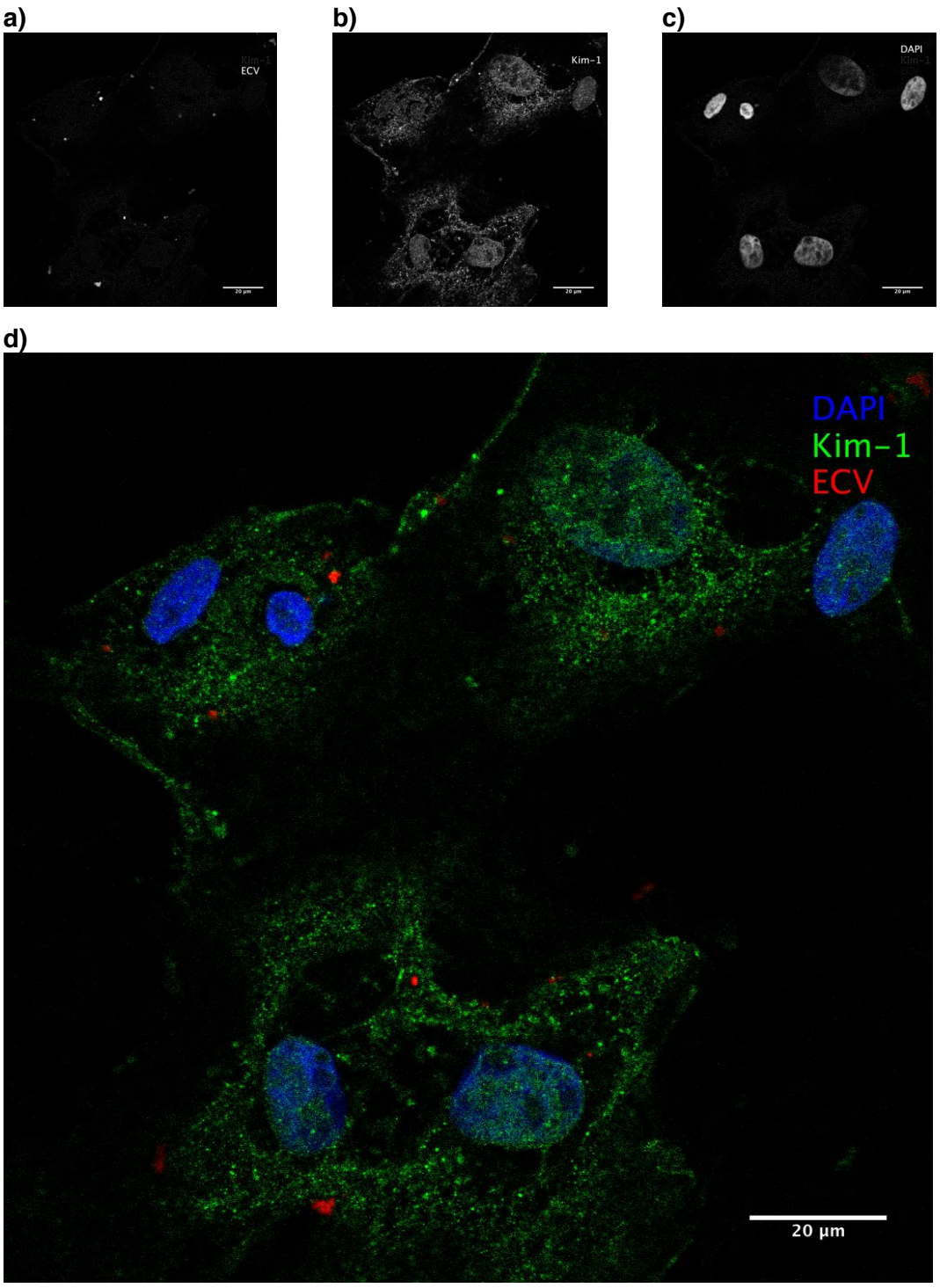

Figure 4.9: Confocal image of PPT cells confirm EV uptake.

PPT cells were co-cultured with dye-loaded EVs for 48 hours prior to analysis. Images a-c indicates EV, KIM-1 and nuclear (DAPI) staining, respectively. Amalgamated image (d) shows ECV (red), nuclei stained with DAPI (blue) and KIM-1 (green). Images are representative of 3 samples. Scale bars are 20 µm.

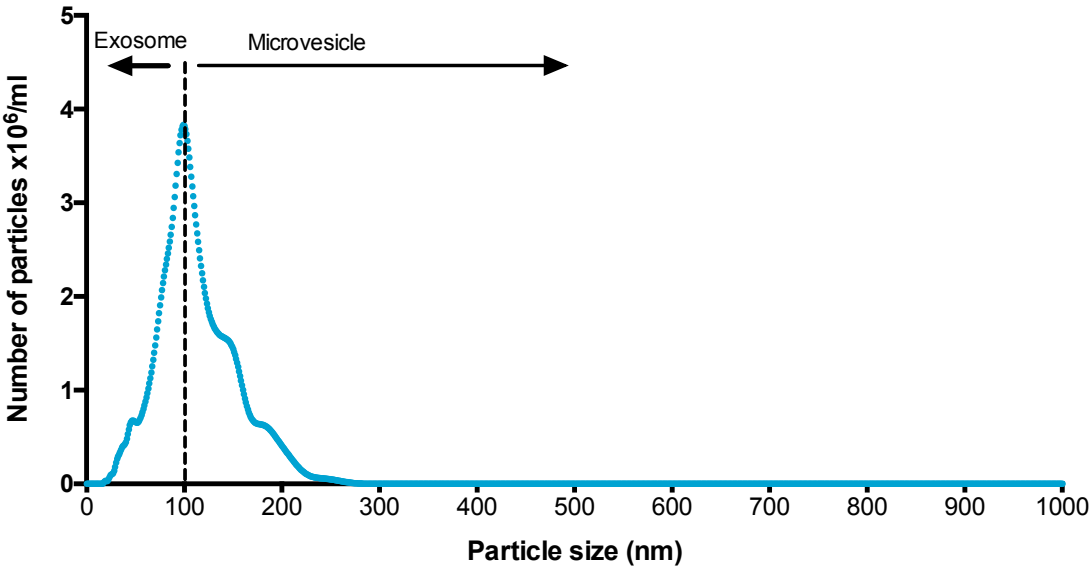

Figure 4.10: Size distribution of primary proximal tubule EVs following ultracentrifugation

Mean particle size range (nm) of EVs isolated from cell culture supernatant following ultracentrifugation protocol. N = 3

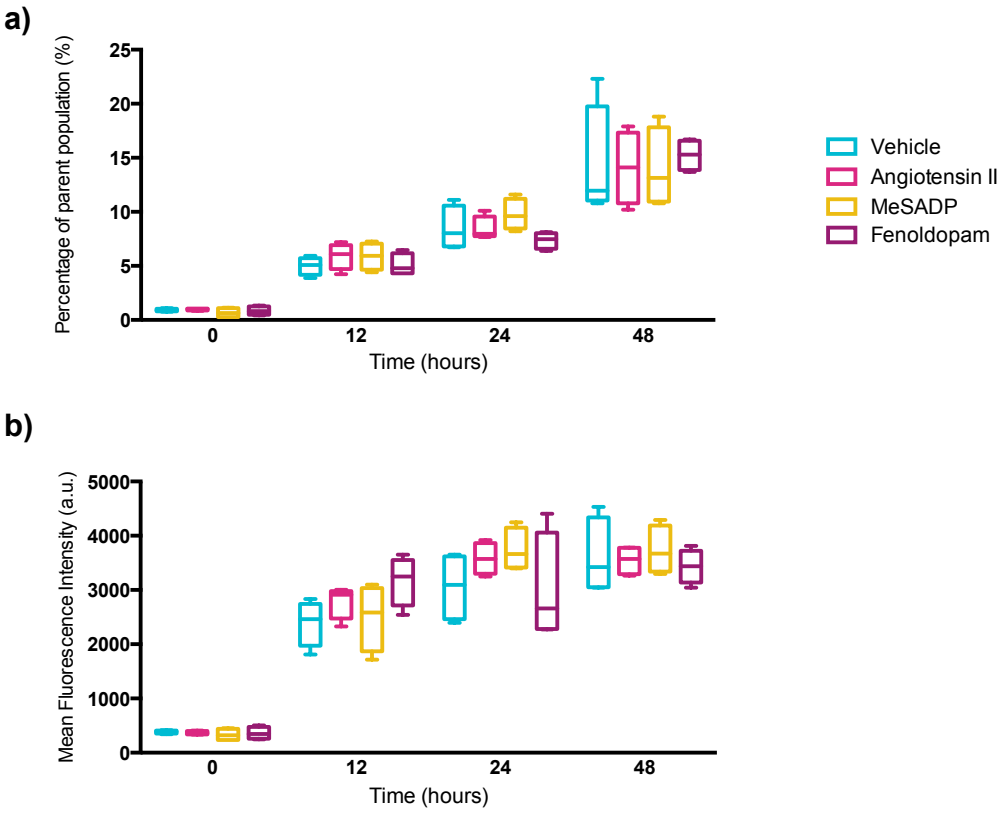

Figure 4.11: EV uptake is not under physiological control

Cells were incubated with dye-loaded EVs and stimulated with the appropriate agonist for a predefined time period (angiotensin II, pink, 50 nM; MeSADP, yellow, 100 μM; Fenoldopam, purple, 1 μM; and vehicle, PBS, blue). The raw data is presented above as %fluorescent cells of total population (Figure a) and mean fluorescent intensity (Figure b) (Tukey box plot). There are no significant differences between groups at each time point; 2-way ANOVA with Bonferroni's multiple comparisons test (n=5).

4.4. DISCUSSION

4.4.1. Main findings

The main findings of Chapter 4 were:

- Cultured PPT cells retain morphological, enzymatic, proteomic and physiological features consistent with PT cells.
- Our HK2 cell line did not reliably model PT cells.
- $P2Y_1$ stimulation increases EV release from PT cells.
- PT cells uptake more EVs over time, a process unaffected by physiological agonists.

4.4.2. Established immortalised proximal tubule cell lines do not reliably model primary cells with regard to EV biology

Improvement of our understanding of the drug transport mechanisms affecting the PT has been impaired by challenges in establishing reliable *in vitro* models. An immortalised PT cell line would be the ideal model; ensuring reproducibility, decreasing variance and reduce the number of animals required for primary cell culture. This issue is further complicated by species differences in expression levels of key PT receptors [264] and the drive towards establishing an immortalised human PT cell line is therefore understandable. The HK2 cell line has been extensively used since 1994 [253]. In this original paper, HK2 cells demonstrated a secondary messenger (protein kinase C) response to fenoldopam and angiotensin II, although similar results could not be reproduced in this chapter (Figure 4.5). Since their introduction, HK2 cells have been recommended and used extensively in cytotoxicity research [265], despite scarcity in receptor transport studies. Critically, with regard to future work in later chapters, PT cells do not express OCT2 mRNA, the receptor required for transport of cisplatin into the PT [266]. This published work, taken together with the findings in this chapter, would suggest that the HK2 cell line is of limited value in cytotoxicity studies. This may explain why LLC-PK1 cells continue to be used for research in drug transport studies. Established in 1976 [267], the LLC-PK1 cells have been used extensively in PT drug transport investigation and have crucially been shown to retain functional OCT2 [268]. In addition to their appropriate secondary messenger response to known PT agonists (Figure 4.5). They also retain function of the endocytic-receptor megalin [269]. This

is of particular interest, given the hypothesis of miRNA cell-cell transport is dependent upon the endocytosis of EVs.

Despite the favourable findings with regard to the LLC-PK1 cell line, establishing a methodology to isolate PPT was critical for 2 reasons. Firstly, the mechanisms underpinning EV signalling at the PT have yet to be elucidated. It is therefore paramount the chosen model reflects a native PT cell as closely as possible. Secondly, the ultimate goal of investigating circulating EV uptake would derive EVs from mice models of single-organ injury. Using a murine PT model would be preferable, to overcome any potential species variation in EV targeting and uptake. Consequently, the demonstration that PPT cells retain morphological (Figure 4.1), enzymatic (Figure 4.2), proteomic (Figure 4.3) and physiological features (Figure 4.5) consistent with PT cells would suggest they are a suitable model for EV signalling.

4.4.3. $P2Y_1$ stimulation affects EV release

MeSADP purinergic receptor stimulation increased EV release from both the LLC-PK1 cell line and the PPT cells (Figure 4.7bi). This increase was in the exosome size range of vesicles in both cells lines when stimulated with MeSADP (Figure 4.7ii). This finding is consistent with other work describing purinergic stimulation resulting in exosomes release from other tissues [95, 250, 251]. This is the first description of PT EV release being driven by purinergic stimulation, specifically $P2Y_1$ activation (Figure 4.8).

ATP-sensitive P2 receptors have been described in all mammalian nephron segments [270], specifically $P2Y_1$ receptors have been described in the PT[271]. P2Y receptors are G-protein-coupled and are activated by adenosine and urodine nucleotides (ATP, UTP, ADP, UDP). Renal cells have been proposed to physiologically release ATP and UTP into the extracellular space via exocytosis [272] and pathologically, when released by lytic dying or injured cells. Purinergic stimulation of the PT has been implicated in inhibition of sodium transporters PT [273, 274]. How purinergic driven exosome-release contributes to PT physiology, as yet, remains unclear. None of the other agonists investigated consistently affected the rate of EV release by PT cells (Figure 4.7).

Despite not being the focus of the investigation, fewer microvesicle particles were released from PPT cells in comparison to HK2 and LLC-PK1 cell lines. This effect was seen across all the experimental groups as defined by agonist (Figure 4.7a-c). Increased cell activation as a result of viruses has previously been described to increase EV release [241, 246]. Together with the work described in this chapter, these findings raise concerns about the validity of immortalised cell lines in the investigation of EV signalling.

4.4.4. Limitations

Isolation and identification of a pure exosome or microvesicle sub-population is notoriously challenging, largely because sub-populations are defined by their biogenesis and not an identifiable, physical characteristic. Using size discrimination methodologies, for example NTA, will result in some misclassification of vesicle origin, in part because of the size overlap between the vesicle sub-populations. This problem is a challenge in EV research and due to lack in consistency in isolation and identification techniques, there is often great difficulty in discerning which vesicle subpopulation is being discussed in published work. The International Society of Extracellular Vesicles has proposed the minimal experimental requirements required to define a exosome subpopulation [103] The requirements state that firstly, exosomes must be purified from extracellular fluid in manner limiting disruption to cells; secondly, at least three proteins expected and not expected of exosomes should be identified; and thirdly, indication of heterogeneity using 2 different methodologies must be used e.g. EM and NTA. Our previous validation of NTA provides confidence that the vesicles are exosomes but further validation would be required for certainty.

4.4.5. Summary

PPT cells retain features consistent with PT cells and are a valid study model for EV signalling. Conversely, the HK2 cell line is not an appropriate model for this context. In health, purinergic stimulation of PT cells via $P2Y_1$ results in release of small vesicles, consistent with exosomes. No tested stimulant affected EV uptake by PT cells. Having investigated EV release in health, the next chapter investigated the response to injury.

Chapter 5: Effect of proximal tubule cell injury on EV uptake and release

Contents

5.1. INTRODUCTION

5.1.1. Background

Despite decades of research, the prevalence of AKI remains high and this disease has no effective therapy [275]. The kidney is vulnerable to a plethora of injury modalities. High oxygen demand and low tissue oxygen tension in the renal parenchyma sensitise tubular cells to hypoxia and this can lead to acute and chronic kidney injury. Furthermore, tubular cells are vulnerable to the toxic effects of drugs because of the kidney's role within the body. High intracellular drug concentrations are attributed to increasing intra-tubular concentrations as the filtrate moves along the nephron and the reuptake mechanisms for solutes (which are often renal segment specific). The presence of toxic metabolites is also implicated in the pathogenesis of AKI. Cisplatin is a chemotherapeutic agent used for the treatment of solid-organ tumours [276]. Despite its high success rate, its use is limited by the incidence of AKI [276]. In PT cells, low dose cisplatin causes mitochondrial dysfunction and activation of the extrinsic and intrinsic apoptotic pathway; at higher doses this mechanism is overwhelmed and necrosis becomes the principal cell death pathway[277]. Understanding of the underlying molecular signalling is important for prevention of toxicity and treating established kidney injury [130].

EV signalling between renal cells has been implicated in the pathogenesis of acute kidney injury (AKI). For example, EVs from injured tubular cells transfer TGF-b1 mRNA into fibroblasts, resulting in cell activation [143]. *In vitro*, vesicles appear to be important in mediating vascular smooth muscle cell calcification, a potential mechanism for accelerated vascular calcification in end stage renal disease [144]. Dominguez, et.al have recently described the potential for renal tubule-derived EVs to protect against ischaemic PT injury *in vivo.* [239]. EVs administered intravenously after the onset of renal ischemia improved multiple parameters of renal structure, function, and the cellular transcriptome profile. This effect was more pronounced with EVs derived from ischaemic-preconditioned cells, in comparison to control EVs from healthy cells.

EVs have been implicated in other pathophysiological processes affecting the kidney. Renal brush border-derived exosomes can induce calcium oxalate crystallization in nephrolithiasis and may have a role in renal stone disease, a mechanism yet to be demonstrated *in vivo* [163]. EVs may also act as antibacterial immune effectors, mediating the host response to urinary tract infection by inhibiting growth of pathogenic and commensal Escherichia coli and inducing bacterial lysis [161]. This highlights the multimodality capacity of EVs in therapeutics, specifically their potential as novel antibiotics for urinary tract infections, a common illness affecting 150 million patients annually [162].

Despite the observation that EVs propagate pathophysiological processes, mechanisms underpinning EV-cell interaction and EV internalisation remain unclear. Interestingly, EVs may have natural targeting capacity, presumably by receptor-ligand binding [164-166]. Recent work, conducted by Hoshino *et al.* [167] demonstrated that tissue-specific uptake of EVs is mediated by distinct integrins via their interaction with the extracellular matrix of the target tissue. Manipulation of this mechanism, through therapeutic targeting of these integrins, reduced EV uptake and impeded metastatic spread of cancer. This ability to predict the metastatic course of cancer raises the exciting possibility of prediction and redirection of tumour progression. EV signal manipulation *in vivo,* to target exogenous vesicles to the tissue of interest through delivery of miRNA and siRNA, has already been demonstrated, ultimately affecting downstream gene expression [169, 170]. A similar mechanism could also be responsible for EV signalling along the nephron and the observation of proximal tubular specific proteins in distal segments raises the possibility this process occurs *in vivo*. Following EV-cell interaction, there are several proposed mechanisms for EV internalisation, including: direct delivery of the EV cargo to the cellular cytosol by fusion with the recipient cell membrane or through phagocytosis, macropinocytosis or clathrin-mediated endocytosis [278-281] (Figure 1.2). Notably, EV phagocytosis has been described as dependent upon the actin cytoskeleton and phosphatidylinositol 3-kinase [279]. KIM-1 is a phosphadylserine receptor, expressed on the apical surface of the PT, and is robustly induced in injury [282] . This receptor confers a phagocytic phenotype to PT

cells [283] and may responsible for the engulfment of apoptotic cells [284] and albumin [285], consequently posing an attractive target for EV internalisation.

5.1.2. Objectives

- Identify effect of nephrotoxic injury on EV release from the PT
- Identify effect of nephrotoxic injury on EV uptake by the PT
- Investigate the role of KIM-1 on PT EV uptake

5.2. METHODS

5.2.1. Cell culture

Murine PPT cells were isolated and cultured as detailed in section 4.2.1.2.

5.2.2. Cell viability, necrosis and apoptosis analysis

Cells were seeded on a 96-well plate at a cell density of $5x10^3$ cells/well in 100 µL serum-free medium for 48 hours. These cells were washed 3 times in PBS and the 100 µL serum-free medium was replaced. Temporal- and dose-response evaluation of cisplatin (Cambridge Bioscience, Cambridge, UK) to PPT cells was performed at 37 °C. Cisplatin was re-constituted from powder using PBS and stored at -20 °C for a maximum of 1 week. The following protocols were used to ascertain cell viability, necrosis and apoptosis.

5.2.2.1. Luciferase cell viability assay

The plate and its contents were equilibrated at room temperature for ~30 minutes. 100 µL of the CellTiter-Glo® Reagent (Promega, Wisconsen, USA) was added to each well, mixed on an orbital shaker for 2 minutes and then allowed to incubate at room temperature for 10 minutes. Luminescence was recorded with an integration time of 0.5 seconds per well using the Infinite® M1000 PRO (Tecan, Männedorf, Switzerland) microplate reader.

5.2.2.2. MTS cell viability assay

CellTiter 96® Aqueous Assay Reagents solution (20µL)(Promega, Wisconsen, USA) was added to each well and incubated for 60 minutes at 37 °C. The absorbance at 490 nm was recorded using a colorimetric plate reader.

5.2.2.3. Caspase 3/7 apoptosis assay

Apo-ONE® Homogeneous Caspase-3/7 Reagent (100 µL) (Promega, Wisconsen, USA) was added to each well. The contents were gently mixed using a plate shaker for 30 seconds and the content incubated for 60 minutes at room temperature. Using the T Infinite® M1000 PRO (Tecan, Männedorf, Switzerland) microplate reader, fluorescence was measured in each well (499±10 nm_{Ex}/521±10 nm_{Em}).

5.2.3. EV release in response to cisplatin

5.2.3.1. Particle size and concentration distribution measurement

Particle size and EV concentration of media was ascertained using NTA technology as defined in Section 4.2.5.1.

5.2.4. EV uptake in reponse to cisplatin

5.2.4.1. EV isolation and dye loading of EVs

EV isolation and dye loading of PPT EVs was conducted as described in Section 4.2.6.1.

5.2.4.2. Flow cytometry for total cell fluorescence

Section 4.2.6.2 describes the methodology employed for quantifying total cell fluorescence using flow cytometry.

5.2.5. KIM-1 inhibition and effect on EV uptake

5.2.5.1. KIM-1 expression analysis

Following co-incubation with cisplatin, cell culture supernatant was centrifuged at 300 x *g* at 4 °C for 3 minutes to remove any cell debris. Samples were immediately processed using an KIM-1/HAVCR Quantikine ELISA Kit (R&D Systems, MN, USA) as per the manufacturer's instructions. KIM-1 expression was normalised to total protein, as quantified from cell lysate, using the BCA Protein Assay Kit (Thermo Scientific, Perth, UK).

5.2.5.2. Inhibition of KIM-1

KIM-1 inhibition was undertaken as previously described [285]. Briefly, experiments were performed at 37 °C in a humidified atmosphere of 5% CO_2 in air. PPT cells were grown in 35-mm dishes and cultured to 90% confluence in culture medium. For inhibition experiments, the incubation medium also included anti-mKIM-1 antibody (AF3689, goat IgG, 10 μg/ml; R&D Systems, MN, USA) for 60 minutes before the addition of dye loaded EVs. EV uptake was quantified using flow cytometry (as described above).

5.2.6. Data evaluation and statistical analysis

Where possible data were presented as Tukey box plots. Tukey box plots consist of 4 parameters; box ends at the quartiles Q1 and Q3, median as a horizontal line in the box, 'whiskers' to the farthest points that are not outliers (i.e. within 3/2 times the interquartile range of Q1 and Q3) and dot plot of outliers. Data were analysed using GraphPad PRISM (version 6.03 for Windows, GraphPad Software, San Diego, USA) and a P-value < 0.05 was considered statistically significant. When testing for a difference in the means of more than two datasets (e.g. EV release in response to cisplatin injury) a one-way ANOVA and post-hoc comparison using Tukey's multiple comparison test was used. When datasets were influenced by more than one factor (i.e. EV uptake as affected by time and cisplatin injury) a two-way ANOVA with Bonferroni's multiple comparison test was utilised. Unpaired t-test were used to compare the mean difference in EV uptake following KIM-1 inhibition.

5.3. RESULTS

5.3.1. Validation of cell viability assays

The reliability of the cell assays was confirmed by seeding PPT cells to 96 well plates in multiple 1:2 serial dilutions. Readouts were conducted as detailed and linear regression analysis of the data indicated the R^2 values were as follows: MTS cell viability assay, 0.967; and, luciferase cell viability assay, 0.972.

5.3.2. Cellular effect of PT cells to cisplatin

The model confirmed a temporal- and dose-dependent change in PPT viability (Figure 5.1a & b). At 48 hours, the ED50 for ATP concentration and NADPH activity were 8.64 and 9.36 μM, respectively (Figure 5.1a & b). The dose response graphs for 1, 12 and 24 hours did not reach maximal effect and therefore ED50 cannot be calculated. However, there was a temporal effect as evidenced in Figure 5.1a & b. A concentration of 10 μM was selected for further experimental study as representative of the ED50 on cell viability

With regard to caspase 3/7 activity, the maximal apoptotic activity was present with 5 μM cisplatin after 48 hours incubation. Notably at our selected ED50 dose at 48 hours, 10 μM, there was maximum variability in the result (Coefficient of variation: 5 μM, 10 μM and 25 μM; 7.55%, 17.08% and 5.66%, respectively; Figure 5.1c).

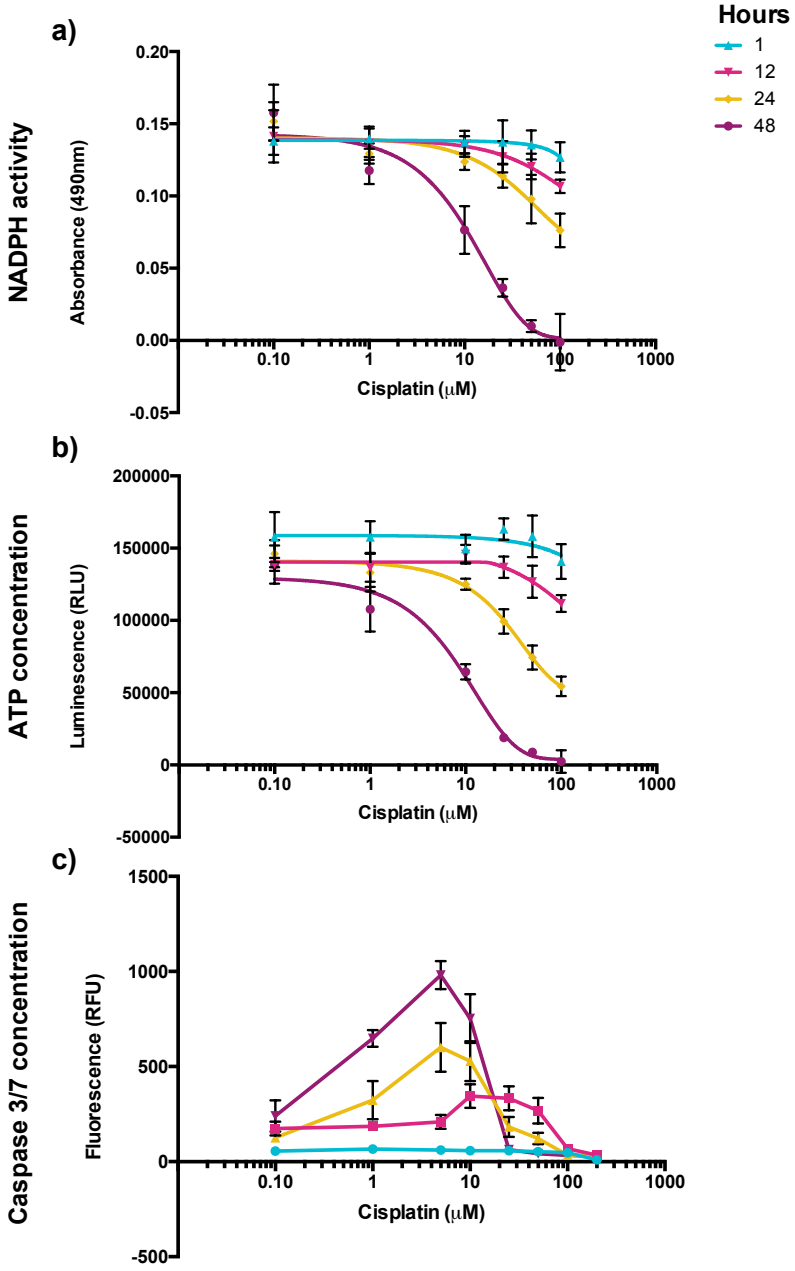

Figure 5.1: In vitro dose-response relationship of PPT cells to cisplatin exposure

PPT cells were exposed to cisplatin for 1 hour (blue), 12 hours (pink), 24 hours (yellow) or 48 hours (purple) prior to assessment of cell viability. NADPH activity (Figure a) and cellular ATP concentration (Figure b) decreased with increasing cisplatin concentration and exposure time. Caspase 3/7 concentration is affected by cisplatin concentration in a negatively skewed distribution (Figure c). Each point represents the mean±SD (n = 4)

5.3.3. Effect of cisplatin on EV release from proximal tubule cells

As in section 4.3.3, EVs were considered in 3 cohorts: total EV population (20-1000 nm diameter), exosome population (20-100 nm diameter) and microvesicle population (100-500 nm). The effect of cisplatin on EV release is presented in Figure 5.2. The following patterns of EV release were noted:

- Across all time points, total EV concentration correlated to increasing cisplatin concentration in a negatively skewed distribution, with maximal EV release corresponding to 75 μM cisplatin (Figure 5.2).
- Changes in the MV population reflected changes noted in the total EV population, with maximal release corresponding to 75 μM cisplatin (Figure 5.2).
- Greater variation was seen in the exosome population than MV population. 1- and 12- hours following injury, exosome release corresponded to increased cisplatin concentration in a negatively skewed distribution, with maximal release seen at 25 and 50 μM cisplatin, respectively (Figure 5.2). 24- and 48 hours following nephrotoxic injury, there was a positive correlation between exosome release and cisplatin concentration with maximal exosome release being noted at 100 μM (Figure 5.2).

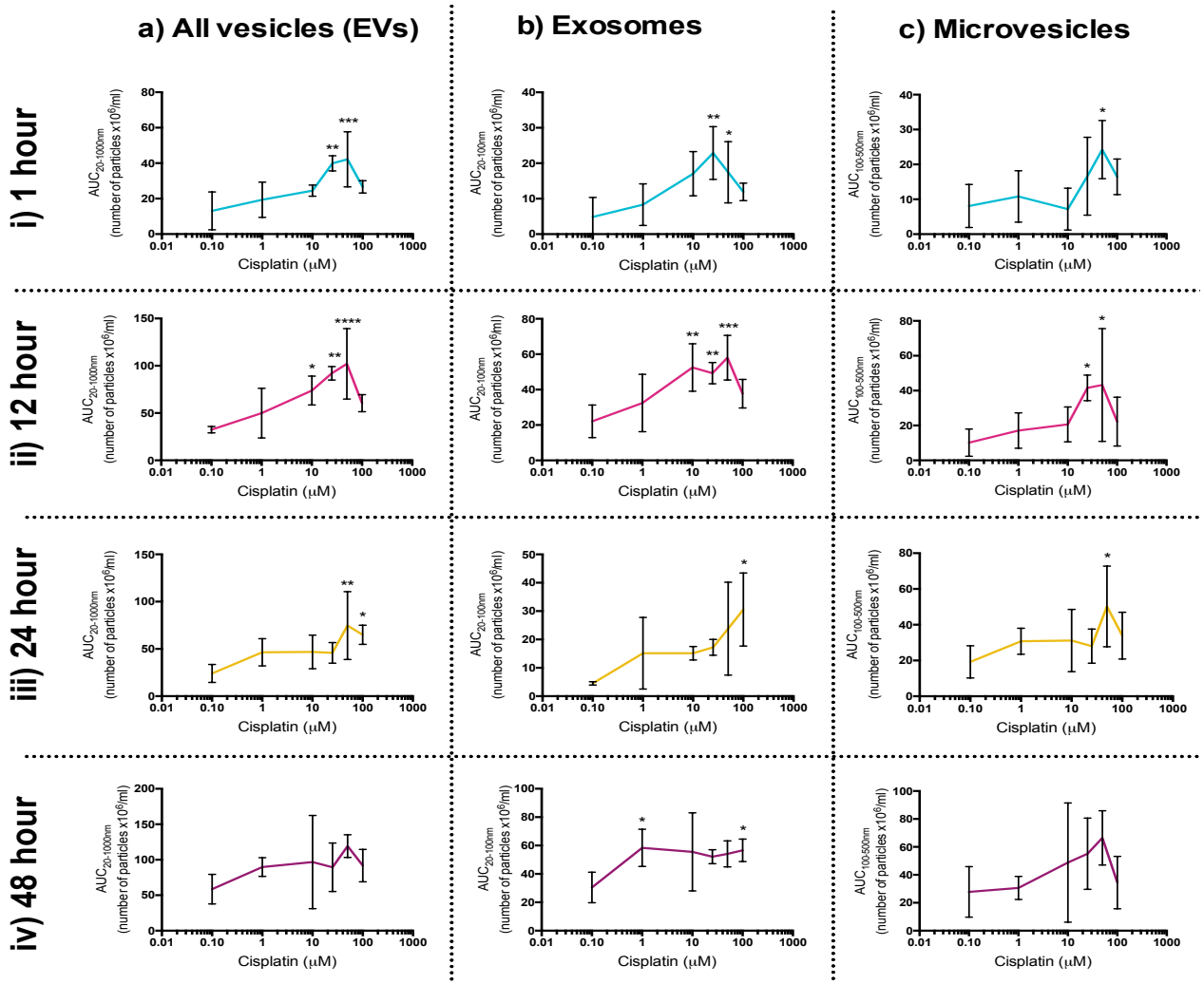

Figure 5.2: EV release increases following nephrotoxic injury

Cell culture media was collected at predefined time points following nephrotoxic injury with cisplatin Cultured cells were exposed to cisplatin for 1 hour (i; blue),12 hours (pink; ii), 24 hours (yellow; iii), or 48 hours (purple; iv). EVs were considered in 3 cohorts: total EV population (20-1000nm diameter; Figure a), exosome population (20-100nm diameter; Figure b) and microvesicle population (100-500nm; Figure c). Each point on the graphs represent the mean±SD. Statistical significance was determined by 1-way ANOVA with Tukey's multiple comparisons to vehicle population (n=3).

5.3.4. Effect of cisplatin on EV uptake by proximal tubule cells

To quantify EV uptake, flow cytometry was utilised to describe EV uptake by PPT cells following injury with cisplatin (Figure 5.3a&b; percentage cell uptake and mean cell fluorescence, respectively). Significantly fewer PPT cells take up EVs after exposure to increasing cisplatin concentrations (Figure 5.3a). A similar trend correspondingly affected the average fluorescence of the PTT cells - 48 hours following cisplatin exposure mean cell fluorescence was lower in cells treated with 10μM cisplatin in comparison to vehicle (Figure 5.3b).

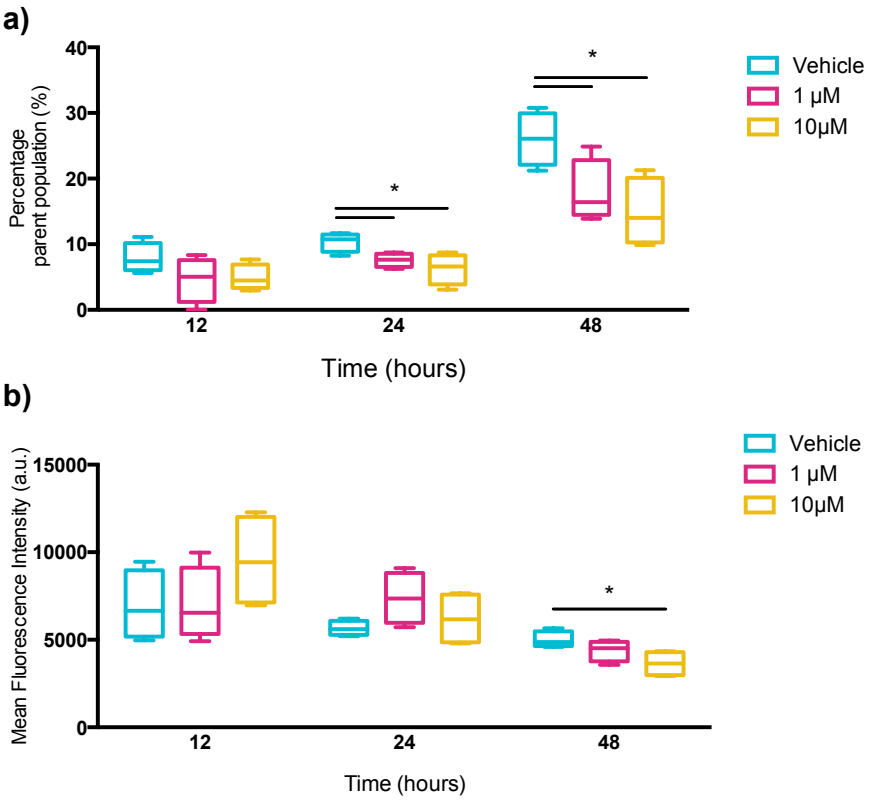

Figure 5.3: EV uptake by PPT cells negatively correlates to cisplatin injury

Cells were incubated with dye-loaded EVs and concurrently exposed to cisplatin cisplatin (vehicle (PBS), blue, 1 μM, pink; 10 μM, yellow) The raw data are presented above as %fluorescent cells of total population (Figure a) and mean fluorescent intensity (Figure b) (Tukey box plot). Significance was ascertained by 2-way ANOVA with Tukey's multiple comparison to vehicle (n=5).

5.3.5. Effect of cisplatin on proximal tubule cell KIM-1 expression

KIM-1 protein expression within cell supernatant was quantified following PPT exposure to cisplatin. This experiment was conducted to confirm the archetypal proteomic injury response exhibited by PT cells. In PPT cell media, KIM-1 concentration significantly increased at all time points following injury with 25- and 50- μM cisplatin (Figure 5.4).

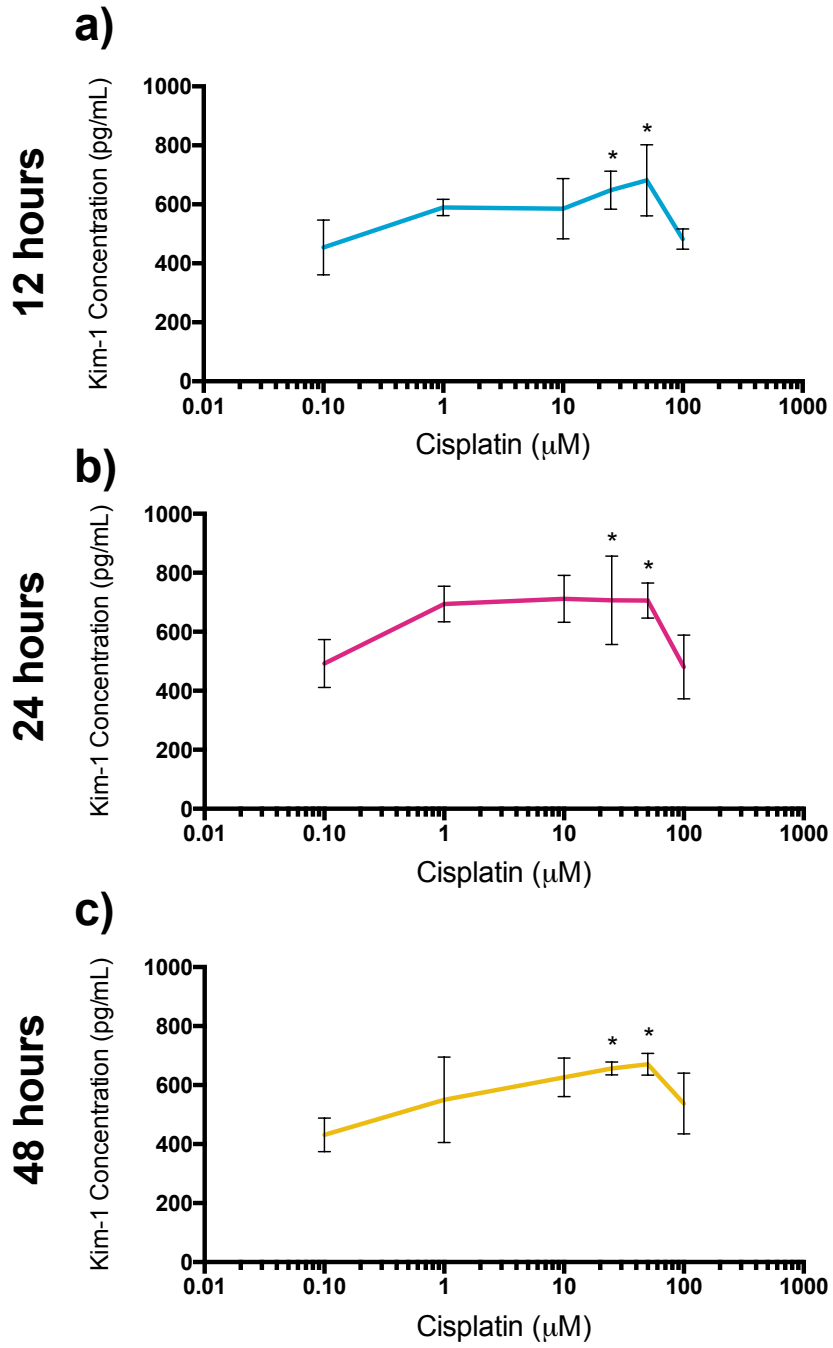

Figure 5.4: KIM-1 expression increases following nephrotoxic injury

Cell culture media was isolated following cisplatin injury of PPT cells after a pre-defined time point. KIM-1 expression follows a negatively skewed distribution to increasing cisplatin concentrations at 12-, 24- and 48-hours following injury (graphs a), b), and c), respectively; mean±SD). Significance ascertained using 1-way ANOVA and Tukey multiple comparison to vehicle (n=3).

5.3.6. Effect of KIM-1 inhibition on proximal tubule cells EV uptake

In order to ascertain if KIM-1 mediated endocytosis was implicated in PT EV uptake, PT cells were incubated with anti-KIM1 antibody for 1 hour prior to co-incubation with dye-loaded EVs. PT cells were analysed 48 hours later using flow cytometry to describe changes in PT cell fluorescence. No significant differences were observed between percentage PT cell uptake or mean cell fluorescence (Figure 5.5a&b, respectively).

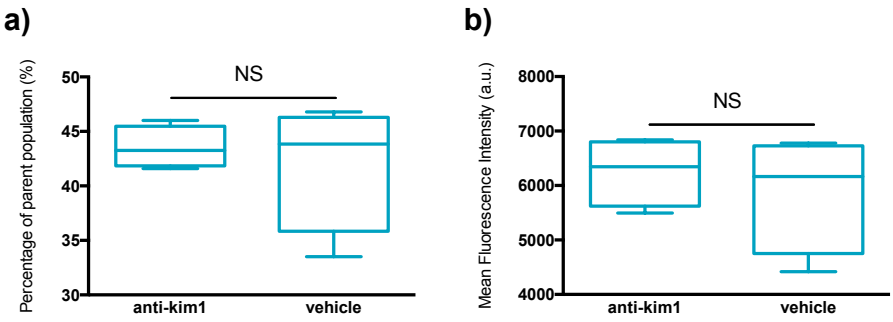

Figure 5.5: KIM-1 inhibition does not affect EV uptake by PPT cells

Incubation medium also included anti-mKIM-1 antibody for 1 hour prior to the addition of dye loaded EVs. The raw data is presented above as %fluorescent cells of total population (Figure a) and mean fluorescent intensity (Figure b) (Tukey box plot). Significance was ascertained by unpaired, 2-tailed t-test (n=4).

5.4. DISCUSSION

5.4.1. Main findings

The main findings of Chapter 5 were:

- Cisplatin causes PT cell death in a temporal- and dose-dependent manner.
- Cisplatin at low dose results in EV release but causes no significant. difference at higher doses. This is consistent with changes in the microvesicle sub-population.
- Cisplatin inhibits EV uptake by PT cells in a dose-dependent manner.
- PPT cells release KIM-1 into the cell supernatant with increasing cisplatin-induced injury.
- KIM-1 inhibition does not affect EV uptake by PT cells.

5.4.2. Cisplatin affects EV release by proximal tubule cells

As previously discussed, mechanisms driven by cell activation have been implicated in increasing EV release in non-renal cells; namely, toxins [245], hypoxia [248] and senescence [249]. *In vivo* PT cells have been described to release EVs in response to pro-inflammatory stimuli and hypoxia. These EVs contain miRNA and protein specific signatures that have known CKD association [286]. The studies presented in Chapter 5 add to this body of work, by demonstrating EV release in a dose-dependent manner in response to low dose cisplatin injury. Interestingly, EV release does not seem to be affected by high dose cisplatin, presumably because at higher doses necrosis becomes the principal cell death pathway (Figure 5.1) [277].

This pattern of EV release corresponds to changes noted in the microvesicle subpopulation, as differentiated by size. Given the pattern of MV release closely follows that of caspase 3/7 activity, this pattern of release may be related to apoptosis, as well as cell stress. Microvesicles are characteristically 100 - 1000nm in size)[97] and are shed directly from the plasma membrane in response to cell stress [94]. Apoptotic bodies are extensively liberated from the plasma membrane in the later stages of apoptosis. Although apoptotic bodies are generally considered to be larger in size than other vesicles (500-4000nm), a smaller subpopulation has been proposed, 50-500nm [79, 99]. Without further investigation and validation,

these 2 vesicle subpopulations cannot be differentiated and either could be responsible for the noted EV release pattern.

5.4.3. Cisplatin reduces EV uptake and KIM-1 expression is not correlated to EV uptake by proximal tubule cells

EV uptake by PT cells reduces in a dose-response manner with cisplatin injury (Figure 5.3). The reduction in the passive process of uptake (as demonstrated in Chapter 4) likely reflects reduced cell viability (Figure 5.1). The hypothesis that EV uptake may be dependent upon KIM-1 medicated endocytosis could not be proven. KIM-1 inhibition had no demonstrable effect on EV uptake (Figure 5.5). KIM-1 has previously been implicated in engulfment of apoptotic cells[284] and albumin[285], and is one of a number of cells which confer a phagocytic phenotype to PT cells[283]. It is worth considering a possible flaw in the study methodology; there is no positive control to KIM-1 has been effectively inhibited. Although this methodology was informed by a previous study[285], it is the only published research that utilises commercially available antibodies to inhibit the phagocytic effect of KIM-1. Other studies largely rely upon transfected cell lines[287] suggesting antibody inhibition may not be a reliable model.

5.4.4. Limitations

KIM-1 is highly expressed within the cell media of PPT cells (Figure 5.4). While KIM-1 concentration increased as expected in a dose dependent manner in response to cisplatin injury, the high levels of KIM-1 at baseline do not reflect KIM-1 expression *in vitro*. KIM-1 is not detectable in either healthy human or murine tissue but is increased more than other proteins in renal injury[288]. Elevated KIM-1 concentration has also been described in dedifferentiated epithelial cells in a model of renal carcinoma[289], and therefore may represent a marker of dedifferentiation in PT cells. Elevated KIM-1 concentration in PPT cell lysate and cell media has previously been described [290], but whether this is as a result of cell injury or dedifferentiation has yet to be elucidated.

5.4.5. Summary

In a cytotoxic model of PT injury, low dose cisplatin injury causes EV release from PT cells, an effect lost at higher doses of the nephrotoxin. This may reflect the

change from apoptotic to necrotic cell death, seen at higher dose of cisplatin. EV uptake is inhibited by increasing cisplatin and unaffected by the inhibition of the KIM-1. The following chapter will integrate the experimental work described thus far and determine whether EVs (and their miRNA cargo) released from the injured heart have an effect on our PPT cell model.

Chapter 6: Effect of EVs from injured distant organs on proximal tubule cells

Contents

6.1. INTRODUCTION

6.1.1. Background

The proposed role for EV signalling in health and disease highlights their potential as vectors to deliver therapeutic interventions. There are a number of on-going phase I and II clinical trials harnessing EV-based therapeutics (registered at https://clinicaltrials.gov). Although we remain in the early phase of such studies, theoretical clinical utility could be mediated by the manipulation of EVs as targeted therapeutic vectors.

EVs are candidate drug delivery systems because they are stable within the circulation, have a wide biodistribution and previous work has suggested EV signalling is likely related to RNA interference [152-156]. EVs can be selectively loaded and can deliver functional RNA into cells [139, 170]. The integrity of RNA isolated from vesicles is similar to that of tissue, as the membrane protects the RNA cargo from RNase degradation [36, 88]. As discussed previously, EVs have natural targeting capacity, presumably by receptor-ligand binding [164-166]. Recent work, conducted by Hoshino *et al.* [167] demonstrated tissue-specific uptake of EVs is mediated by distinct integrins via their interaction with the extracellular matrix of the target tissue. Manipulation of this mechanism, through therapeutic targeting of these integrins, reduced EV uptake and impeded metastatic spread of cancer. This ability to modify the metastatic course of cancer raises the exciting possibility of prediction and redirection of tumour progression.

Similar mechanisms could also be responsible for EV signalling along the nephron with the potential for EV to come from either an exogenous or proximal endogenous source. Initial observations of this potential were first reported in the field of mesenchymal stem cell (MSC) research. MSCs have been described to accelerate recovery and repair tissue following AKI; an effect demonstrated using diverse injury modalities [146-150]. Interestingly, the observation that the MSC supernatant conferred a beneficial effect, equal to that of MSCs themselves, opened the field to EV research [151]. Seminal work by Bruno *et al.* supported the claim that this positive result was largely due to EV transfer, likely related to RNA interference

[152-156], with further work suggesting EV miRNA has a significant role in this MSC effect on kidney cell injury [157].

This possible role of EV signalling in the delivery of functional miRNA and pathogenesis of AKI highlights their potential as a therapeutic intervention. Abnormal levels of miRNA could be one of the mechanisms explaining dysregulated protein expression during kidney disease progression and interference with this process represents a potential therapeutic target [160]. MiRNAs have been implicated in propagating inflammation, apoptosis and fibrosis within the kidney, while others have been described to have a beneficial effect on these pathological processes [291]. The first evidence of miRNAs having pathological roles in AKI was reported by Wei *et al.* who described resistance to injury in an ischemia reperfusion injury (IRI) model of AKI in DICER knockout mice [292]. These mice exhibit a global down-regulation of microRNAs in the renal cortex, demonstrating significantly better renal function, less tissue damage, and better survival than their wild-type counterparts [291, 292]. Within the field of EV research, miRNAs associated with EV endothelial progenitor cells have been noted to reduce apoptosis and promote cell regeneration in IRI, an effect lost with depletion of RNA, notably, miR-126 and miR-296 [153, 158, 159]. Similarly, EV mediated horizontal transfer of IGF-1R mRNA from bone marrow MSC to tubular cells potentiates cell proliferation in cisplatin injury and may play a significant role in renoprotection [293].

Cisplatin injury of the PT has been associated with several networks of transcriptomic changes. Cisplatin injury facilitates binding of FOXO3 and p53, critical for induction of the apoptosis pathway [130]. MiR-122 and miR-34a have been implicated as important regulatory factors in this process. MiR-122 has been reported to reduce cisplatin-induced tubular injury through inhibition of FOXO3, [130] and miR-34a antagonism had been implicated in increased cell death, although the latter finding has not been consistently described [130, 294]. In similar studies, miR-125b has also been implicated in inhibiting p53 activation, thus protecting the kidney from acute injury [295]. Together with the emerging evidence of miRNA cellular communication via ECV shuttling, this work highlights the

potential for miRNA, delivered via EVs, to confer protective properties to PT cells in nephrotoxic injury.

The role miR-122 may play in cisplatin induced nephrotoxic injury is of particular interest. MiR-122 is enriched in the liver of humans [74, 296] - a finding translated across several species [70-72] - accounting for 72% of a hepatocytes total miRNA [69]. It plays an important role in modulation of several critical pathways including fatty acid metabolism, stress response and gluconeogenesis [73]. Emerging reports have suggest that miR-122 may also have the ability to be trafficked between cells by EVs, lending to the theory of EV dependent cell-to-cell communication [23]. MiR-122 has gained prominence in recent years a biomarker at the point of implementation into routine clinical care. MiR-122 accurately predicts DILI [297], demonstrating a 100-fold increase in the circulation of patients with paracetamol-induced DILI and exhibits a greater sensitivity and specificity than the current biomarker ALT [74]. At the time of writing, little work has been conducted investigating the role of miR-122 signalling at the PT though. In support of the hypothesis of miR-122 interference at the PT, the paracrine effect of liver stem cells has been shown to aid regeneration of renal tubular injury via release of EVs [145], a process which may be related to EV transfer of miR-122.

6.1.2. Objectives

This chapter integrates the preceding experimental chapters.

- Establish if EVs isolated from the circulation can be taken up by PT cells *in vitro*
- Describe the role the circulatory EVs from cardiac injury mice may play in PT cell viability
- Ascertain if EVs from mice with liver injury transfer miR-122 to PT cells *in vitro* and describe the downstream targets which may be affected
- Describe *in vivo* miR-122 changes in the renal tissue during DILI

6.2. METHODS

6.2.1. Animals

6.2.1.1. Breeding and maintenance of mice

Mouse studies were in accordance with the Animals (Scientific Procedures) Act 1986 and approved by the local Animal Ethics Committee. 10-14 week old C57BL/6NCrl mice were used for this study (purchased from Charles River Laboratory, Wilmington, MA). Animals were housed in standard sterile conditions with free access to chow and water. No adverse effects were encountered.

6.2.1.2. Cardiac ischaemia model

CAL was performed as described previously [220, 221] and detailed in Section 3.2.2.1

6.2.1.3. Paracetamol toxicity model

The mouse model of DILI was conducted as described previously[298]. Briefly, animals were fasted for 14 hours prior to paracetamol dosing. Groups of randomly selected animals were administered 300 mg/kg of paracetamol (DILI; Sigma Aldrich, Dorset, UK) or 0.9% saline (control) with a single i.p. injection. Paracetamol was dissolved in sterile 0.9% saline, warmed to 42 °C and allowed to cool prior to administration. Injection volumes ranged from 0.6-1 ml. Animals received normal diet and water thereafter.

6.2.2. Study protocol

6.2.2.1. Blood and tissue sampling sampling

6 hours following onset of organ injury, blood was collected by cardiac puncture, under terminal inhaled anaesthesia (isoflurane). Immediately following this, the mice were humanely culled using a Schedule 1 method. This time point was selected from previous work investigating the temporal expression changes of circulatory miRNAs following onset of hepatotoxicity [298]. This demonstrated that the maximal miRNA increase was 6 hours following paracetamol dosing. Blood samples were centrifuged twice at 4000 x *g* for 5 minutes, and the subsequent supernatant isolated and stored at –80 °C.

After cervical dislocation, tissue was collected for further sample processing. Prior to tissue removal the descending aorta was isolated (proximal to the distal bifurcation, and flushed with PBS for 30 seconds). Murine tissue was then macroscopically dissected, as necessary, using anatomical landmarks. Tissue samples for RNA interrogation were placed in RNAlater (Qiagen, MD, United States) and stored at –80 °C.

6.2.3. Isolation and dye loading of EVs

As described previously [5], mouse serum was vigorously vortexed then centrifuged at 12,500 x *g* for 30 minutes to pellet any large membrane fragments and other debris. The supernatant was then centrifuged at 120,000 x *g* for 70 minutes to pellet the EV fraction. The pellet was washed with PBS and then re- centrifuged at 120,000 x *g* for 70 minutes before final resuspension in PBS.

Pelleted EVs were conjugated with Cell Tracker 655 (Invitrogen, CA, US) following the manufacturer's protocol. Briefly, pelleted EVs were incubated with the Cell Tracker 655 conjugate in 200 µl fresh culture media for 1 hour at 37 °C. The EV pellet suspension was ultracentrifuged twice with fresh media before being put back on confluent cells. EV size distribution was confirmed by NTA of a 1:1000 dilution of Cell Tracker 655 conjugate. Dye loaded EVs were co-incubated with cells at a concentration of 250 $x10^8$/ml media.

6.2.4. Particle size and concentration distribution measurement with NTA

Particle size and EV concentration of serum was ascertained using NTA technology as defined in Section 4.2.5.1.

6.2.5. Cell culture

6.2.5.1. Primary PT cell culture

PPT cells were grown and cultured as per described method in section 4.2.1.2. PPT cells were seeded on a 96-well plate at a cell density of $5x10^3$ cells/well in 100 µL serum-free medium for 48 hours. The circulatory EV uptake experiments were conducted as per Figure 6.1. Cells were washed 3 times in PBS and the 100 µL serum-free medium was replaced. Circulatory EVs were co-incubated with cells at a

concentration of 250 x10^8/ml media, 48 hours prior to induction of injury. PPT cells were again washed 3 times in PBS and the 100 μL serum-free medium was replaced. Nephrotoxic injury was induced by the addition of 10 μM cisplatin (Cambridge Bioscience) to PPT cells for 48 hours. Cisplatin was re-constituted from powder using PBS and stored at -20°C for a maximum of 1 week. Experiments were conducted in technical triplicate (3 wells) and biological quintuplicate (EVs isolated from 5 animals per group

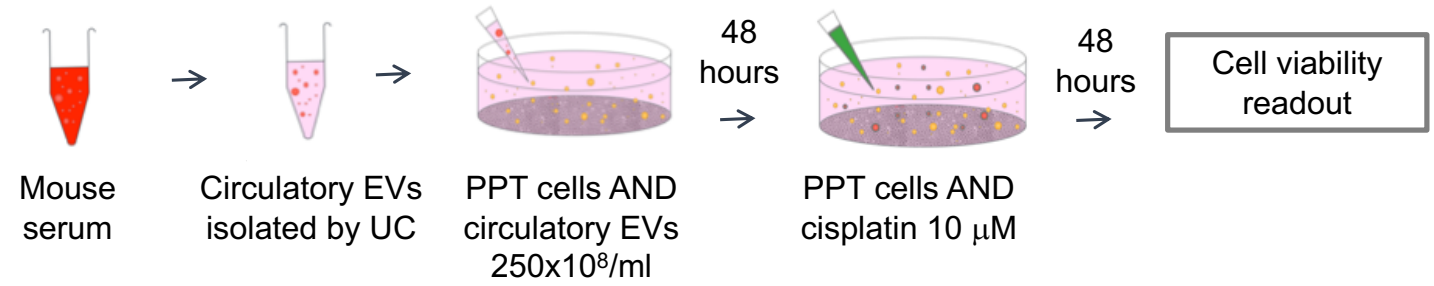

Figure 6.1: Methodology for circulatory EV loading of PPT cells

6.2.6. Cell viability, necrosis and apoptosis analysis

The following protocols were used to ascertain cell viability:

6.2.6.1. Luciferase cell viability assay

Luciferase cell viability assay was conducted as detailed in section 5.2.2.1.

6.2.6.2. MTS cell viability assay

MTS cell viability was conducted as detailed in section 5.2.2.2.

6.2.7. Flow cytometry for total cell fluorescence

Section 4.2.6.2 describes the methodology employed for quantifying total cell fluorescence using flow cytometry.

6.2.8. PCR validation

6.2.8.1. RNA extraction

RNA extraction from serum and tissue (including cells) was conducted as described in section 3.2.4.1.

6.2.8.2. Quantitative real time analysis

Reverse transcription of miRNAs was conducted as previous described (section 2.2.3.3). To generate cDNA the miScript II Reverse Transcription Kit (Qiagen, MD, United States) was used according to manufacturer instructions. 6 μl of treated RNA was added to a master mix consisting of 4 μl of 5x HiFlex buffer, 2 μl of 10x Nucleics mix, 6 μl RNA free H_2O and 2 μl of reverse transcriptase mix. Samples were incubated for 1 hour at 37 °C followed by 5 minutes at 95°C. All cDNA syntheses were diluted 10-fold and stored at -80 °C.

Quantitative real time analysis was conducted as described in section 2.2.3.4. MiRNA Ct values were normalized in serum samples by using the mean Ct obtained from the spiked-in external control (cel-miR-39). U6 was used as the internal control for tissue samples and was validated in our sample cohort. For normalisation of precursor miRNA, 18s ribosomal RNA was ultimately used based on pilot data (data not shown).

6.2.8.3. Primer details

Primer name	Mature miRNA target	Tissue	Catalogue Number	Sequence
Hs_miR-122a_1	mmu-miR-122-5p	Blood and tissue	MS00003416	5'UGGAGUGUGACAAUGGUGUUUG
Ce_miR-39_1	cel-miR-39-3p	External normaliser	MS00019789	5'UCACCGGGUGUAAAUCAGCUUG
Hs_RNU6-2_1	RNU6-6P	Internal normaliser	MS00033740	5’CGCAAGGAUGACACGCAAAUUCG UGAAGCGUUCCAUAUUUUU

Table 6.1: MiScript Primer Assays used during real-time PCR validation of miRNA expression changes in murine model of hepatotoxicity

6.2.9. Data evaluation and statistical analysis

Where possible data were presented as Tukey box plots. Tukey box plots consist of 4 parameters; box ends at the quartiles Q1 and Q3, median as a horizontal line in the box, 'whiskers' to the farthest points that are not outliers (i.e. within 3/2 times the interquartile range of Q1 and Q3) and dot plot of outliers. Data were analysed using GraphPad PRISM (version 6.03 for Windows, GraphPad Software, San Diego, USA) and a P-value < 0.05 was considered statistically significant. When testing for a difference in the means of more than two datasets (e.g. circulatory EV uptake by PPT cells, miR-122 concentration in mouse plasma in different models on injury) a one-way ANOVA and post-hoc comparison using Tukey's multiple comparison test was used. When only 2 groups were being considered, unpaired t-tests were used to compare the difference between means.

6.3. RESULTS

6.3.1. Uptake of circulatory derived EVs by PT cells

To confirm that PPT cells take up EVs, PPT cells were co-incubated for 48 hours with dye-loaded circulatory EVs isolated from serum from mice undergoing DILI (liver EV), myocardial injury (cardiac EV) or healthy mice (control EV) (Figure 6.3). The distribution of vesicle size isolated from murine plasma is demonstrated in Figure 6.2. To quantify EV uptake, flow cytometry was utilised to quantify circulatory EV uptake by PPT cells. Circulatory EV uptake was unaffected by the injury model of origin, as defined by the percentage of PPT cells and mean cell fluorescence, (Figure 6.3a&b)

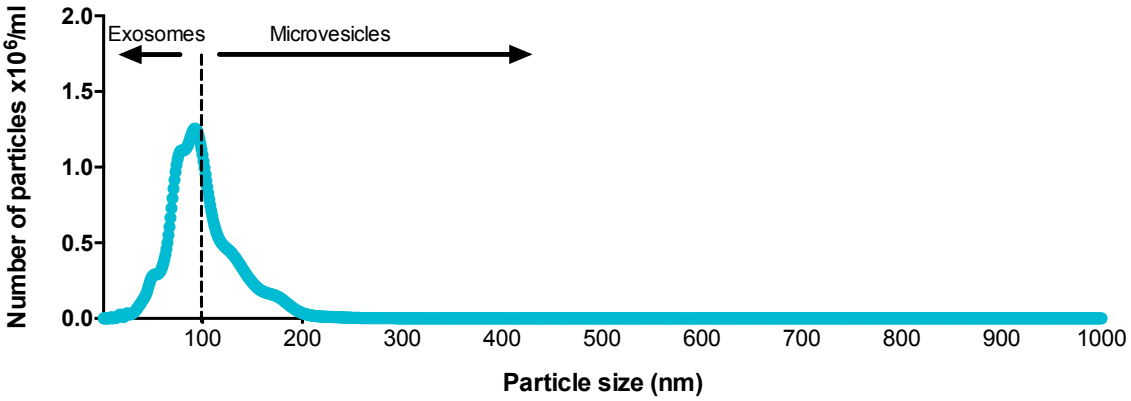

Figure 6.2: Size distribution

Mean particle size range (nm) of EVs in cell culture supernatant following 48 hours in culture. N = 12

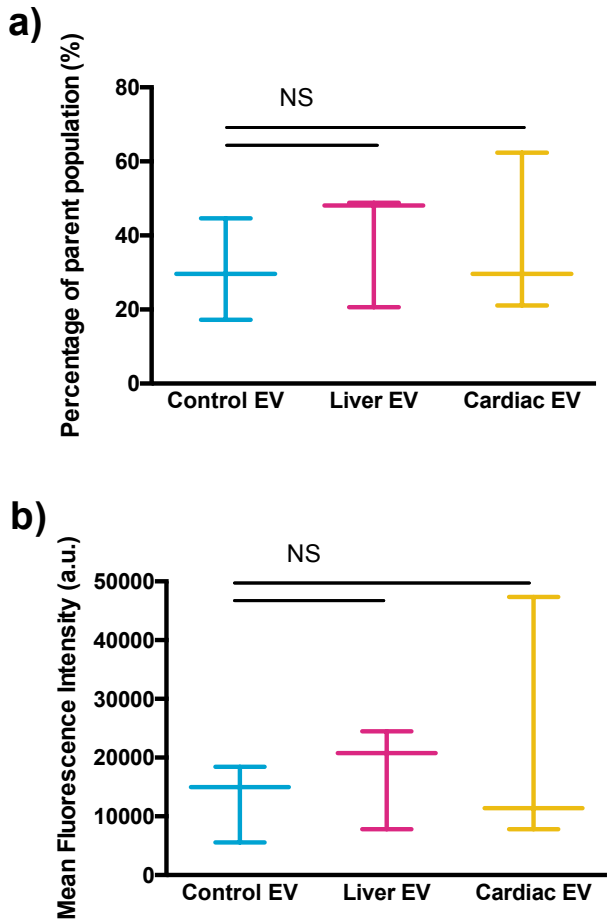

Figure 6.3: Circulatory EV uptake by PPT cells is unaffected by EV injury model

Cells were incubated with dye-loaded circulatory EVs isolated from healthy mice (control; blue) or mice 6 hours following DILI (300mg/kg paracetamol; Liver EV; pink) or myocardial injury (CAL; Cardiac EV, yellow). Flow cytometry was used to describe uptake of EVs. The raw data are presented above as %fluorescent cells of total population (Figure a) and mean fluorescent intensity (Figure b) (Tukey box plot). Significance was ascertained by 1-way ANOVA with Tukey's multiple comparison to vehicle (n=3).

6.3.2. Circulating vesicles prevent in vitro PT cell injury

Informed by the EV uptake study and PT cell dose response described in Chapter 4 and 5, respectively, PPT cells were co-incubated with circulatory EVs for 48 hours, washed with PBS and subsequently injured with 10 μM cisplatin (as described in Figure 6.1). 48 hours following cisplatin injury, readouts of cell viability were obtained (Figure 6.4). PPT cells that were co-incubated with DILI circulatory EVs (liver EV) had more NADPH activity following cisplatin injury when compared with cells co-incubated with EVs from a healthy control (control EV) (Figure 6.4a). EVs isolated from mice post-myocardial injury do not affect NADPH activity in comparison to the control population. The same pattern of cell viability was present when ATP concentration was measured (Figure 6.4b).

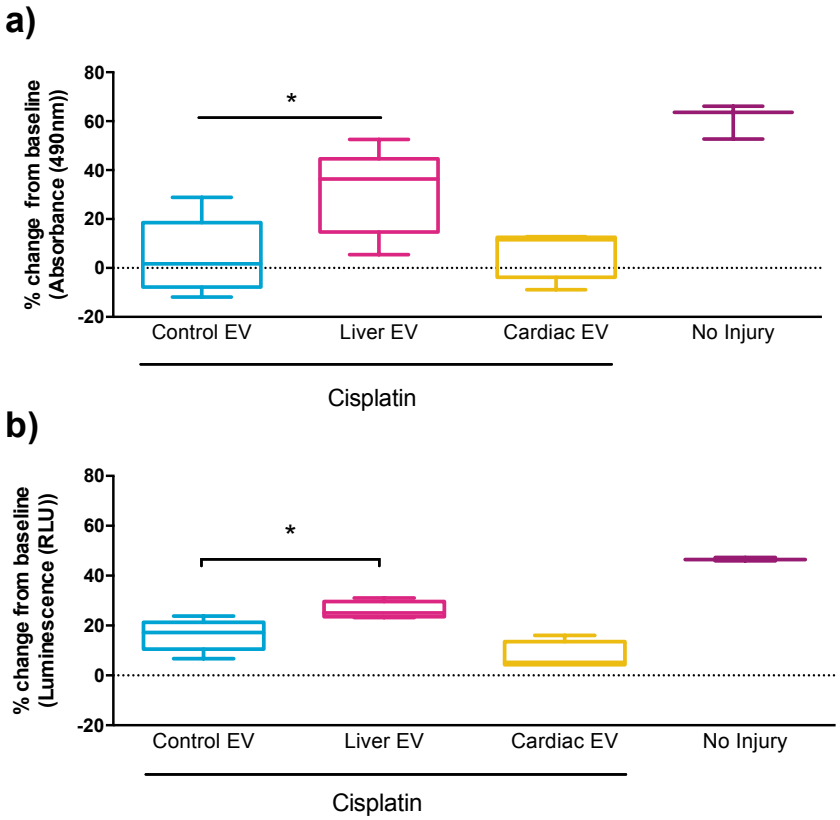

Figure 6.4: DILI EVs protect PTT cells from subsequent nephrotoxic injury.

PTT cells were co-incubated with circulatory EVs for 48 hours and subsequently injured with 10 μM cisplatin. Circulatory EVs were derived from healthy mice (control EV; blue), DILI mice (300mg/kg paracetamol IP; liver EV; pink) or myocardial injury (CAL; cardiac EV; yellow). Cells that were not injured with cisplatin and had no additional EVs added as represented by no injury (purple). All results were normalised to results from PTT cells injured with 10 μM cisplatin with no additional EVs (baseline). Data represents NADPH activity (Figure a) and ATP concentration (Figure b) as percentage change from injured cells without additional EVs. Statistical significance was ascertained using 1-way ANOVA with Tukey's multiple comparison to control EV (n=5).

6.3.3. Transcriptomic differences in plasma and circulating EVs

Previous work has suggested EV signalling is likely related to RNA interference [152-156]. Some miRNAs have organ enrichment[68]. Notably, miR- 122, is enriched in the liver of humans [38], a finding translated across several species (including: mice [38], zebrafish [299]), and accounts for >70% of the liver transcriptome[300]. Consequently, murine serum and EVs were interrogated for miR-122. Figure 6.5 demonstrates miR-122 concentration within whole serum and EVs, as defined by injury cohort. Serum and circulating EVs isolated from mice 6 hours post-DILI (liver group) had significantly higher miR-122 levels than both CAL- (cardiac) and vehicle cohorts.

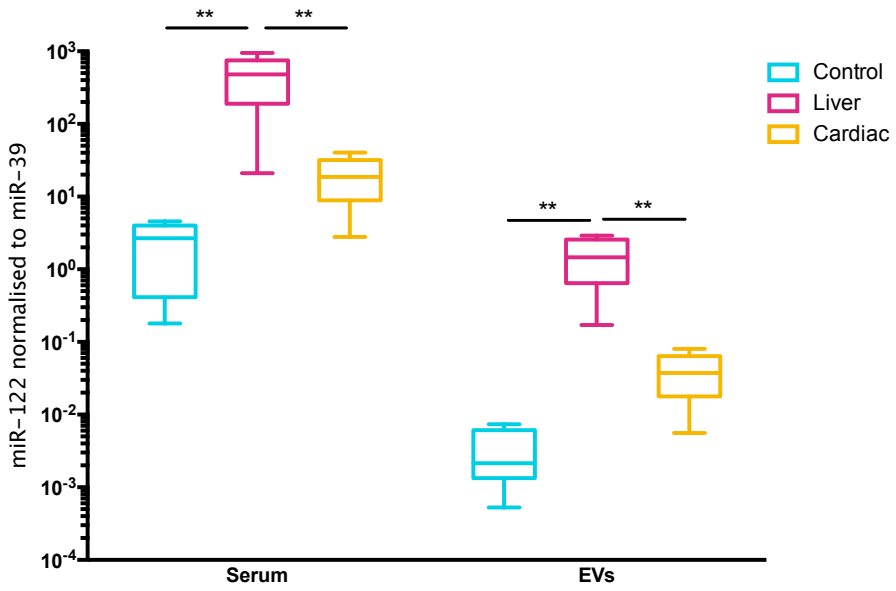

Figure 6.5: miR-122 concentration is increased in murine serum and circulating EVs following DILI

Serum and circulating EV miR-122 in healthy (control; blue), DILI (liver; pink) and myocardial injury (cardiac; yellow) mice. Values represent $2^{-\Delta Ct}$ normalised by miR-39. Statistical significance was ascertained using 1-way ANOVA with Tukey's multiple comparison to control EV (n=5).

6.3.4. *In vitro* transcriptomic differences in PPT cells coincubated with circulatory EVs

To investigate the premise of EV delivery of miRNA, PPT cell expression of miR-122 were investigated following co-incubation with DILI- and healthy circulatory EVs. PPT cells co-incubated with circulatory EVs from the DILI cohort had increased expression of miR-122, in comparison to PPT cells incubated with EVs from healthy controls (Figure 6.6). When PPT cells were injured with cisplatin for 48 hours, this significant difference in miR-122 expression remained. Notably, the trend in reduced miR-122 following cisplatin injury was not seen in the PTT cells co-incubated with DILI EVs.

To complement the miR-122 uptake data and confirm functional delivery of miRNA, cellular target mRNA suppression was investigated as a read out of functional EV uptake. Target genes influenced by miR-122 were identified: mRNA expression of ALDOA, ADAM10 and FOXO3 were measured. In the absence of cisplatin injury there was no significant difference in any of the 3 target mRNAs (Figure 6.7a-c). However, following cisplatin injury, FOXO3 was significantly lower in the PTT cell population co-incubated with DILI EV in comparison to control EVs (Figure 6.7c)

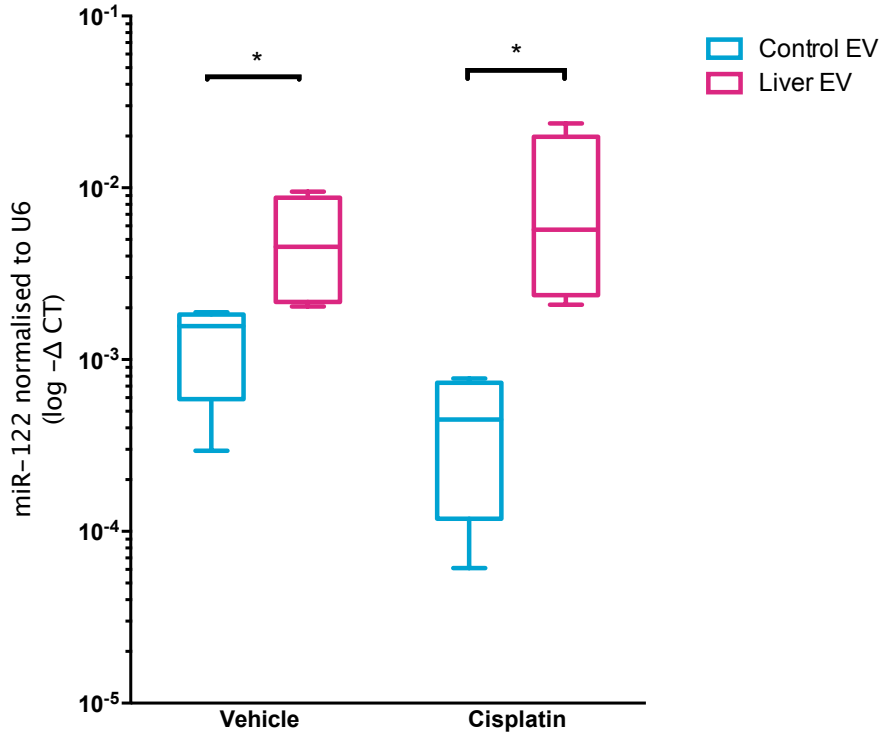

Figure 6.6: miR-122 expression levels are increased in PPT cells co-incubated with DILI EVs

miR-122 concentration in PPT cells exposed to circulating EVs from healthy (control; blue) and DILI (liver; pink) mice. The figure represents miR-122 expression with cisplatin injury (cisplatin) and in healthy control (vehicle). Values represent $2^{-\Delta Ct}$ normalised by U6. Statistical significance was ascertained using unpaired, 2-tailed t-test (n=5).

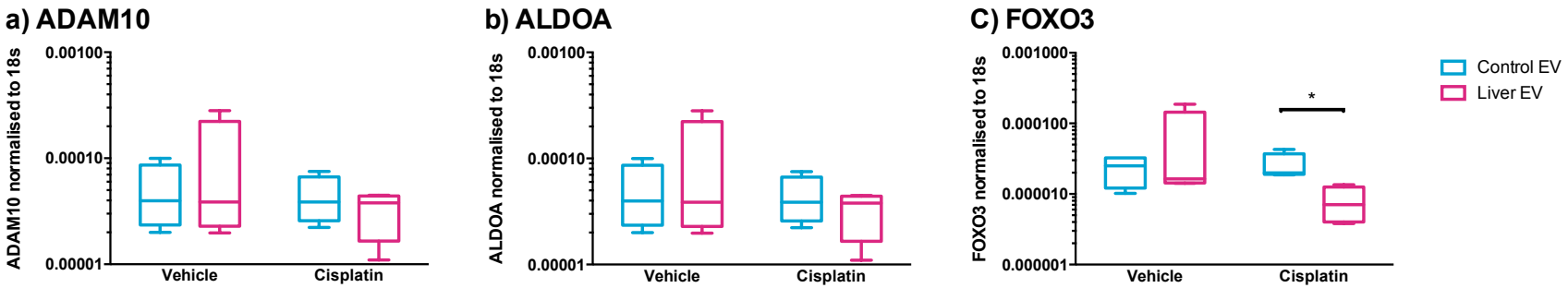

Figure 6.7: Downstream gene targets of miR-122 within PPT cells were affected by co-incubation with DILI EV

mRNA expression in PPT cells exposed to circulating EVs from healthy (control EV; blue) and DILI (liver EV; pink) mice. Each igure presents mRNA expression following cell exposure to vehicle or cisplatin A) ADAM10 B) ALDOA and C) FOXO3 expression as $2^{-\Delta Ct}$ normalised by 18s. Statistical significance was ascertained using unpaired, 2-tailed t-test (n=5).

6.3.5. *In vivo* transcriptomic changes in tissue following DILI

To investigate the role of miR-122 signalling from the liver to the kidney *in vivo*, mice were injected with 300mg/kg paracetamol i.p. An age-matched cohort was injected with PBS to act as the control group. 6 hours following i.p. injection, renal and liver tissue was perfused post-mortem and the collected tissue was subsequently interrogated for miR-122. Mice in the DILI cohort had significantly higher miR-122 in the renal medulla and cortex, in comparison to the vehicle population (Figure 6.8a). There was a non-significant downwards trend in miR-122 expression in liver tissue following DILI.

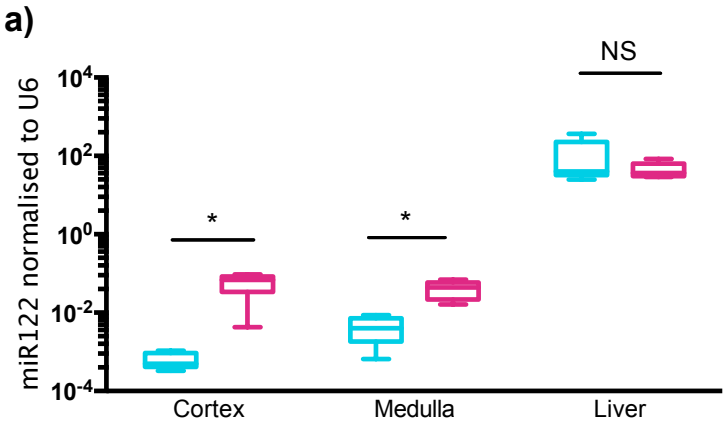

Figure 6.8: miR-122 expression was increased in renal tissue following DILI

MiR-122 expression in murine tissues following i.p injection of saline (control; blue) or 300mg/kg paracetamol (paracetamol; pink). Data are presented as a Tukey plot. Values represent $2^{-\Delta Ct}$ normalised by U6. Statistical significance was ascertained using unpaired, 2-tailed t-test (n=5).

6.4. DISCUSSION

6.4.1. Main findings

The main findings in Chapter 6 were:

- Circulating EVs from mice with injury to different organs are taken by PPT cells *in vitro.*
- Circulatory EVs in DILI reduce subsequent nephrotoxic PT injury *in vitro.*
- In DILI, miR-122 concentration increases in both the serum and circulatory EVs.
- EVs transfer miR-122 to PT cells *in vitro*, subsequently affecting FOXO3, a downstream target of miR-122.
- *In vivo* miR-122 expression increases within the renal cortex and medulla in murine DILI.

6.4.2. Circulatory EVs isolated in DILI protect the PT from nephrotoxic injury *in vitro*

Dynamic changes in the miRNA signature of PT cells have been implicated to have both a positive and negative effects in AKI [291]. As previously discussed, circulating miRNAs are stabilised in the circulation by forming miRNA-protein complexes or associating with EVs; to date there is no evidence of miRNA-protein complex uptake by recipient cells in mammals. There have, however, been multiple descriptions of functional delivery of miRNAs via EVs. A number of *in vivo* studies have demonstrated exogenous EV uptake from the circulation by PT cells and delivery of mRNA transcripts [238, 239]. In Chapter 3, miR-499 was released from the myocardium and pick up in the renal cortex, which may represent inter-organ signalling. While the ability of circulatory EVs to cross the glomerulus is poorly understood, evidence suggests that EVs may be able to transit across the basement membrane, until the intracellular release of their contents [241] or excretion in urine [139, 240]. There remains the possibility of basolateral vesicle transit, from the peritubular capillaries and interstitium to the proximal tubule, but as yet there is no evidence to support this hypothesis *in vivo*. *In vitro*, our group has demonstrated that EVs can enter polarised collecting duct cells both apically and basolaterally under the regulation of vasopressin. In principle this demonstrates basolateral uptake is possible but *in vivo* evidence is lacking. This chapter contains the first description of endogenous circulatory EVs being taken up by

PT cells *in vitro* (Figure 6.3) and subsequent delivery of their miRNA cargo (Figure 6.5 & Figure 6.6a).

The cellular consequence of circulatory EV delivery was demonstrated in a proof-of-concept *in vitro* study; DILI circulatory EVs protected PT cells from subsequent nephrotoxic injury (Figure 6.4). Increased cell viability (NADPH activity and ATP concentration) was higher in cells primed with DILI EVs comparison to EVs from both healthy mice and those with myocardial injury. The proposal that this may be as a consequence of miR-122 delivery is supported by the following observations. Firstly, EVs and serum isolated from DILI mice have significantly higher miR-122 concentration than both the 2 control cohorts, healthy and CAL mice (Figure 6.5). Secondly, miR-122 is a liver enriched miRNA and accounts for 72% of the liver miRNA transcriptome [69] and is the most likely candidate miRNA to be responsible functional changes secondary to miRNA in DILI. Thirdly, miR-122 has been shown to be trafficked between cells by EVs [23]. And lastly, manipulation of miR-122 has been reported to reduce cisplatin-induced PT injury through inhibition of FOXO3 [130], a transcriptomic response reproduced in this chapter (Figure 6.6 & Figure 6.7).

6.4.3. Limitations

No transcriptomic response to increased miR-122 was demonstrated in healthy PT cells and the only significant consequence noted in cisplatin injury was reduction in FOXO3. At the time of writing, no work has been conducted investigating the role of miR-122 signalling in healthy PT cells, and consequently the downstream mRNAs investigated were chosen from targets in other tissues or disease models of the PT injury. We reproduced the only published work pertaining to the PT, in which miR-122 reduced FOXO3 in nephrotoxic injury [130]. In order to investigate this further, network analysis of the all miRNA and mRNA consequences of DILI EV signalling would have to be conducted.

The presented work focuses on NADPH and ATP activity, both established models of cell viability[301, 302]. Further *in vitro* work should ascertain which cell death pathways are affected by EVs containing miR-122. In addition to the proposed network analysis, models should attempt to differentiate between apoptosis, necrosis and autophagy.

Apoptosis assays could include quantification of caspases and analysis of mitochondrial membrane depolarisation, in addition to investigation of leakage of mitochondrial proteins into the cell cytosol i.e. cytochrome c. Investigation of autophagy could include electron microscopy to quantify autophagosomes and necrosis could be investigated by quantifying leakage of cyclophilin A and high-mobility group box 1. These proposed assays could be further complemented by annexin V/propodium iodide cell staining evaluated by flow cytometry or fluorescent microscopy to grossly evaluate apoptosis and necrosis, respectively.

The hypothesis that miR-122 signals to the PT via EV-cell signalling is novel and would change our view on circulating miRNA changes in illness. At present, this chapter includes proof of concept studies cementing this hypothesis *in vitro*. The *in vivo* observation of miR-122 increasing in the renal medulla and cortex may be as a consequence of native PT expression in DILI rather than EV delivery of the miRNA transcript. Several *in vivo* studies would be required to demonstrate miR-122 signalling to the PT from the injured liver. If manipulation of the changing miRNA signature can be shown to be of biological relevance, clearly manipulation of circulatory miRNAs may be of interest as a potential therapeutic. Caution must be exercised, however, as miRNA's ubiquitous expression makes undesirable systemic effects unpredictable.

6.4.4. Summary

EVs isolated from DILI mice protect PT cells from subsequent nephrotoxic damage. Circulating EVs in DILI can delivery miR-122 to PT cells *in vitro* and affect downstream mRNA implicated in a key apoptotic pathway.

Chapter 7: Concluding remarks

7.1. GENERAL CONCLUSIONS

The studies presented in this thesis aimed to better understand the role miRNAs may play as markers of organ injury and mediators of inter-organ signalling. The original hypothesis proposed that miRNAs that are released into the circulation, as a consequence of organ injury, can be taken up by the renal tubule via EV mediated transfer. The key research aims identified to address this hypothesis included: description of the miRNA concentration changes in the circulation following myocardial injury in human and mouse models of illness, development of a PT model of EV uptake and release in order to identify physiological and pathophysiological regulators, and comparison of the effect of circulating EVs from injured heart and liver *in vitro*. Consequently, the findings within this thesis confirm that miRNAs are released into the circulation as a result of myocardial injury and can be taken up by renal PTT cells. EV uptake by PT cells is not under physiological regulation, at least in vitro, but can affect the PT transcriptome and function in a model of cytotoxic injury, a mechanism proposed to be underpinned by miRNA transfer. Table 7.1 summarises the key objectives and findings contained within this thesis.

To date, circulatory miRNAs have not been demonstrated to have significant consequences at distal organs in systemic illness, and the work in this thesis represents a novel signalling pathway amenable to therapeutic intervention. The transfer of miR-122 via EVs to distal organs is the ideal model for investigation of this concept. MiR-122 is unique in the miRNA population for its tissue specificity; miR-122 is a liver enriched miRNA and accounts for 72% of the liver miRNA transcriptome [69]. It has not been described in healthy tissue elsewhere in the body. Other miRNAs are ubiquitous in their expression and therefore identification of their tissue of origin is severely limited [6]. Furthermore, investigation of hepato-renal signalling is of critical clinical importance. AKI commonly complicates a spectrum of clinical illnesses and remains an important independent predictor of morbidity and mortality [303]. Specifically, AKI is of prognostic importance in patients with liver injury [304, 305], including DILI. AKI has been described as a complication resulting in prolonged hospital admission in paracetamol poisoning [306] and has been reported to occur in the absence of significant liver dysfunction [307]. Investigation of hepato-renal miRNA signalling therefore has potential as a research model and is of clinical importance.

There is great potential for EV bound miRNAs as therapeutic interventions, yet we remain some way from realising this potential and improving patient outcomes. If manipulation of the changing miRNA signature can be shown to be of biological relevance, clearly manipulation of circulatory miRNAs may be of interest as a potential therapeutic. Caution must be exercised, however, as the ubiquitous expression of most miRNA species makes undesirable systemic effects unpredictable.

Chapter	Objectives	Key observations
2	To describe the changes in circulatory miRNA expression associated with myocardial ischaemia at 2 and 6 hours following start of cardiac injury in humans.	Circulating miR-30a significantly increases 2 hours following myocardial injury in humans. 6 hours following myocardial injury, miR-499a, miR-1 and miR-30a significantly increased within human serum. Heparinase effectively removes heparin contamination from serum samples.
3	To describe the changes in circulatory miRNA associated with myocardial ischaemia at 2 and 6 hours following cardiac injury in mice. To ascertain the presence of miRNA of interest within mouse myocardial tissue. To correlate circulating miRNA concentration to TnI, the gold-standard cardiac biomarker in current clinical care.	Circulating miR-499 significantly increases 2 hours following myocardial injury in mice in comparison to control. 6 hours following myocardial injury, miR-499a, miR-1 and miR-30d significantly increased in mice in comparison to control 2 hours following murine myocardial injury, circulating miR-499 correlates to TnI. 6 hours following injury, miR-499, miR-1, miR-133a all correlate to TnI. In a mouse model of myocardial injury, TnI significantly increases in sham procedure 6 hours following intervention. MiR-499 expression levels decrease within the LV 6 hours following murine myocardial injury. MiR-499 increases within the renal cortex at this time point.
4	Establish an appropriate PT cell model for the study of EV release and uptake Identify factors which affect EV release from the PT Identify factors which affect EV uptake by the PT	Cultured PPT cells retain morphological, enzymatic, proteomic and physiological features consistent with PT cells. Our HK2 cell line did not reliably model PT cells. $P2Y_1$ stimulation increases EV release from PT cells. PT cells uptake more EVs over time, a process unaffected by physiological agonists.

5	Identify effect of nephrotoxic injury on EV release from the PT Identify effect of nephrotoxic injury on EV uptake by the PT Investigate the role of KIM-1 on PT EV uptake	Cisplatin causes PT cell death in a temporal- and dose-dependent manner. Cisplatin at low dose results in EV release but causes no significant. difference at higher doses. This is consistent with changes in the microvesicle sub-population. Cisplatin inhibits EV uptake by PT cells in a dose-dependent manner. PPT cells release KIM-1 into the cell supernatant with increasing cisplatin-induced injury. KIM-1 inhibition does not affect EV uptake by PT cells.
6	Establish if EVs isolated from the circulation can be taken up by PT cells *in vitro* Describe the role the circulatory EVs from cardiac injury mice may play in PT cell viability Ascertain if EVs from mice with liver injury transfer miR-122 to PT cells *in vitro* and describe the downstream targets which may be affected Describe *in vivo* miR-122 changes in the renal tissue during DILI	Circulating EVs from mice with injury to different organs are taken by PPT cells *in vitro.* Circulatory EVs in DILI reduce subsequent nephrotoxic PT injury *in vitro.* In DILI, miR-122 concentration increases in both the serum and circulatory EVs. EVs transfer miR-122 to PT cells *in vitro*, subsequently affecting FOXO3, a downstream target of miR-122. *In vivo* miR-122 expression increases within the renal cortex and medulla in murine DILI.

Table 7.1: Summary table of key observations by chapter

7.2. Summary of key findings

7.2.1. The circulating miRNA signature changes as a consequence of myocardial injury

The studies in chapters 2 and 3 showed the investigation and validation of the dynamic circulatory miRNA expression changes following myocardial ischemia. Circulatory miRNA changes following CABG were investigated using second generation sequencing and compared to a control cohort. Candidate miRNAs, showing the largest temporal fold change, were validated using PCR methodology and subsequently translated into a mouse model of myocardial injury. The work highlighted the expression changes in circulating miRNA following organ injury and their translation across species. Several miRNAs were identified as potential biomarkers of myocardial injury, at an earlier time point than previous described. Furthermore, expression changes of the candidate miRNAs were investigated in murine tissue, demonstrating reduced expression in damaged myocardial tissue and increased expression in downstream renal tissue. To date, cell-cell miRNA signalling has been shown to be as a consequence of EV transfer, thus lending credence to the hypothesis of EVs facilitating miRNA transfer in inter-organ signalling.

7.2.2. Physiological and pathophysiological states affect EV signalling at the PT

The studies included in chapters 4 and 5 interrogated factors that may underpin EV release and uptake at the PT – key experiments built on in Chapter 6. Purinergic stimulation via $P2Y_1$ was shown for the first time to be a regulator of EV release from the PT. Known agonists of the PT did not affect EV uptake. In a nephrotoxic model of PT injury, EV release was affected in a dose-dependent manner by cisplatin. This novel observation adds to the growing body of literature describing EV release as a consequence of cell activation and injury. Conversely, cisplatin injury reduced EV uptake in a dose dependent manner, presumably as a consequence of reduced cell viability.

7.2.3. In DILI, circulatory EV uptake by the PT can reduce subsequent nephrotoxic injury

Chapter 6 united the findings in the subsequent chapters through the investigation of the role circulatory miRNAs may play at the PT. This work includes the first description of endogenous circulatory EVs being taken up by PT cells *in vitro* and subsequent delivery of their miRNA cargo. Consequently, the functional implications of EV-PT signalling were investigated using an *in vitro* cisplatin model of nephrotoxic injury.

Cell viability reduction as a consequence of cisplatin injury was affected by prior EV uptake and varied in accordance with the circulatory EV disease model. DILI circulatory EVs protect PT cells from subsequent nephrotoxic injury, in comparison to CAL and healthy control. Further studies investigated the hypothesis that the reno-protective effect was as a consequence of the liver-enriched miRNA, miR-122. EV-PT signalling transferred miR-122 and affected known downstream mRNA targets in the PT. Thus far, proof of this concept has been largely restricted to *in vitro* modelling. Transcriptomic analysis of the renal tissue in a murine model of DILI demonstrated increased expression of miR-122 within renal tissue, but whether this is as a consequence of renal tissue transcription or EV signalling as yet remains unclear.

7.3. FUTURE EXPERIMENTS

7.3.1. Development of cardiac miRNAs as biomarkers of myocardial injury

To allow specific determination of the source of the proposed cardiac miRNAs, alternative murine models could be interrogated for trans-coronary and circulatory miRNA changes following induction of injury. Non-inducible models of DICER knockout in myocytes (inhibiting production of mature miRNAs within the cell) are lethal post-natally as a consequence of dilated cardiomyopathy and heart failure [308]. However, an inducible mouse model system could be developed to allow deletion of DICER in selectively in cardiac myocytes. For example, cre recombinase could be driven under a heart specific promoter such as Troponin T or myosin 6 inducible by tamoxifen. When crossed with a DICER floxed mice this would allow researchers to ‘turn off’ mature microRNA production in the heart and explore the effect on distant organs. In Chapter 3 it was demonstrated that miR-499 increased in the renal cortex following myocardial

injury. A mouse model with inducible deletion of DICER (or miR-499 specifically) would allow researchers to determine whether the origin of renal miR-499 was the heart. It should be noted that the success of this approach could be limited if the extent of cardiac injury is significantly changed following microRNA deletion, for example, if the injury phenotype is more severe and mice dies prematurely following CAL.

The biomarker development process has been described as 3 distant stages; biomarker *discovery*, *validation* of a markers predictive value within the context of use and *implementation* of a clinically approved assay [178, 179]. Within the discovery phase, candidate biomarkers are identified within a well-defined human study clinical population and subsequently translated across species – exemplified by the work conducted in chapters 2 and 3. The latter 2 stages therefore remain to be explored. The next step would be to move our candidate miRNAs into the validation phase, namely to determine the specificity and selectivity using a large, clinically well-defined, patient cohort. This would allow assessment of the potential for biomarkers to stratify patients presenting with chest pain by their final clinical diagnosis. Patients would be classified as having type 1 or type 2 myocardial infarction, or having myocardial injury according to the universal definition of myocardial infarction, or non-cardiac chest pain as per previous published work [45]. A panel of biomarkers: including candidate miRNAs described in this thesis and hsTnI would be measured in all patients and their positive and negative predictive values for the above conditions would be assessed.

7.3.2. Vesicle release and uptake regulation at the PT

In the proposed hypothesis of hepato-renal miRNA signalling it is crucial to investigate the mechanisms governing EV release and uptake by the PT - to ensure targeted therapeutics deliver content specifically to the renal tubule. We were able to show purinergic regulation of exosome release in the PT *in vitro.* While none of the factors investigated in chapter 4 or 5 affected EV uptake; previous studies have reported exosome uptake to be dependent on the protein signature of the vesicle coupled with the signalling status of receptors on the recipient cell [309]. Indeed, EV uptake by the renal collecting duct is driven by vasopressin *in vitro* and *in vivo* [139], a portion of the renal epithelium downstream from the proximal tubule. Hormonal- or integrin-mediated EV uptake, discussed in Section 1.6, would suggest a segment or tissue specific uptake mechanism, KIM-1 confers a phagocytic phenotype to PT cells [283] and may

be responsible for the engulfment of apoptotic cells [284] and albumin [285], consequently posing an attractive target for EV internalisation at the proximal tubule. KIM-1 inhibition had no demonstrable effect on EV uptake in Chapter 5. Further investigation could include KIM-1 transfection of LLC-PK1 cells. LLC-PK1 cells expressing KIM-1 and cells expressing empty vector could be co-incubated with dye-loaded EVs and EV uptake quantified using flow cytometry, as per methodology in Chapter 4.

7.3.3. *In vivo* study of miR-122 hepatorenal signalling

The question as to whether *in vivo* renal miR-122 expression in DILI is transcribed within the tissue or transferred by circulatory EVs remains unresolved. To further clarify this issue, homozygous DICER-floxed mice could be challenged with AAV8-Cre recombinase to induce DICER knockdown within the hepatocyte only, as previously described [310]. In the proposed murine model, cleavage of all precursor miRNAs within liver tissue would be inhibited upon induction, including miR-122; miRNA biogenesis should be unaffected in other tissues. The use of a DICER knockdown model is preferential to the pre-existing liver specific miR-122 knockout model, MiR-122 LKO, for 3 reasons. MiR-122 LKO, is a germline knockout mouse. Consequently, it is not inducible and carries an endogenous genetic aberration in which it is likely there are a variety of transcriptomic and proteomic compensatory changes in comparison to both wildtype and inducible animals [311]. Secondly, the hypothesis that the protective mediator is miR-122 is thus far speculative and using the DICER-floxed mouse would allow investigation for all liver-mediated changes to the circulating miRNA population. Finally, DICER deletion will leave the pre-miRs intact so provide specificity for testing whether the mature form is transferred between organs.

The DICER KO model could be manipulated to explore whether circulatory EVs shuttle liver specific miRNA to the PT. If the hypothesis of EV trafficking of circulatory EVs holds true, DILI using this model should result in absent miR-122 within the circulation. If miR-122 is not elevated in renal tissue, it would confirm that miR-122 has been trafficked from the circulation trafficked via circulatory EVs in the wild-type experiment in Chapter 6.

Unfortunately, further investigation of mortality, tissue injury/function would be difficult to interpret in this model. Previous studies have noted that mortality rates of liver-specific miR-122 knockout mice were significantly higher than control mice when injected a paracetamol dose, not lethal to the wild-type control [312]. MiR-122 is a regulator of cytochrome P450 (CYP) enzymes, known to metabolise paracetamol into its toxic substrate N-acetyl-p-benzoquinone imine (NAPQI) [312]. In the absence of miR-122, CYP enzymes rapidly oxidize paracetamol to NAPQI, deplete glutathione, and causing oxidative stress; culminating hepatocyte death and liver toxicity. This increased hepatotoxicity will be difficult to control, given that depletion of miR-122 in the liver is the desired intervention. Therefore, any change in mortality or renal function could not be attributed to miR-122 concentration in the renal tissue.

If miR-122 hepatorenal signalling was demonstrated in the DICER-floxed mice, EVs with high and low miR-122 cargo will be systemically injected into wildtype mice and downstream gene target expression measured in the kidney. MiRNA and mRNA expression changes will also be described following induction of DILI using paracetamol. In both models, the degree of kidney injury will be quantified using read-outs of kidney injury, including: urinary neutrophil gelatinase-associated lipocalin (NGAL), KIM-1 and sodium excretion, blood urea, creatinine and kidney histology.

7.3.4. Investigation of the mechanism underpinning the reno-protective effect of DILI circulatory EVs

The model described above could be further utilised to investigate if the *in vitro* renoprotective effect of DILI EVs is as a consequence of miRNA transfer. Circulatory EV isolated from AAV8-Cre recombinase DICER-floxed mice (and EVs from their littermate controls) could be incubated with PPT cells. PPT cells would be subsequently injured with cisplatin and readouts of cell viability would be conducted, as previous described. If the renoprotective effect is lost as a consequence of DICER knockdown it could be concluded that this effect was as a result of miRNA transfer. Further *in vitro* studies could be conducted to investigate miR-122 as the specific signal in the proposed mechanism. LLC-PK1 cells could be transfected with miR-122 and injured with cisplatin as described in Chapter 5. Dose dependent changes in cell

viability would be compared to several control cohorts including, LLC-PK1 cells loaded with negative control siRNA, mock transfected cells and un-transfected cells.

7.4. Final conclusion

This thesis interrogated the hypothesis of functional, circulatory miRNA signalling from injured distant organs to the renal PT via EVs. Circulatory EVs were shown to affect PT cell transcriptome and function *in vitro,* an effect dependent upon site of distal organ injury. If translated into an *in vivo* model, this would represent a novel signalling mechanism amenable to therapeutic intervention. The work presented in this thesis has highlighted the limitations and challenges related to EV research and should support future research within the field of EV signalling.

Bibliography

1. Bartel, D.P., *MicroRNAs: genomics, biogenesis, mechanism, and function.* Cell, 2004. **116**(2): p. 281-97.
2. Lee, R.C. and V. Ambros, *An extensive class of small RNAs in Caenorhabditis elegans.* Science, 2001. **294**(5543): p. 862-4.
3. Weber, J.A., et al., *The microRNA spectrum in 12 body fluids.* Clin Chem, 2010. **56**(11): p. 1733-41.
4. Hunter, M.P., et al., *Detection of microRNA expression in human peripheral blood microvesicles.* PLoS.One., 2008. **3**(11): p. e3694.
5. Arroyo, J.D., et al., *Argonaute2 complexes carry a population of circulating microRNAs independent of vesicles in human plasma.* Proc Natl Acad Sci U S A, 2011. **108**(12): p. 5003-8.
6. Krauskopf, J., et al., *Application of high-throughput sequencing to circulating microRNAs reveals novel biomarkers for drug-induced liver injury.* Toxicol Sci, 2015. **143**(2): p. 268-76.
7. De Rosa, S., et al., *Transcoronary concentration gradients of circulating microRNAs.* Circulation, 2011. **124**(18): p. 1936-44.
8. Mar-Aguilar, F., et al., *Serum circulating microRNA profiling for identification of potential breast cancer biomarkers.* Dis Markers, 2013. **34**(3): p. 163-9.
9. Turchinovich, A., et al., *Circulating miRNAs: cell-cell communication function?* Front Genet, 2013. **4**: p. 119.
10. Peng, Y. and C.M. Croce, *The role of MicroRNAs in human cancer.* Signal Transduct Target Ther, 2016. **1**: p. 15004.
11. Lee, Y., et al., *MicroRNA genes are transcribed by RNA polymerase II.* EMBO J, 2004. **23**(20): p. 4051-60.
12. Borchert, G.M., W. Lanier, and B.L. Davidson, *RNA polymerase III transcribes human microRNAs.* Nat Struct Mol Biol, 2006. **13**(12): p. 1097-101.
13. Lee, Y., et al., *The nuclear RNase III Drosha initiates microRNA processing.* Nature, 2003. **425**(6956): p. 415-9.
14. Yi, R., et al., *Exportin-5 mediates the nuclear export of pre-microRNAs and short hairpin RNAs.* Genes Dev, 2003. **17**(24): p. 3011-6.
15. Zhang, H., et al., *Human Dicer preferentially cleaves dsRNAs at their termini without a requirement for ATP.* EMBO J, 2002. **21**(21): p. 5875-85.
16. Okamura, K., et al., *Distinct roles for Argonaute proteins in small RNA-directed RNA cleavage pathways.* Genes Dev, 2004. **18**(14): p. 1655-66.
17. Ameres, S.L. and P.D. Zamore, *Diversifying microRNA sequence and function.* Nat Rev Mol Cell Biol, 2013. **14**(8): p. 475-88.
18. Fabbri, M., et al., *MicroRNAs bind to Toll-like receptors to induce prometastatic inflammatory response.* Proc Natl Acad Sci U S A, 2012. **109**(31): p. E2110-6.
19. Mitchell, P.S., et al., *Circulating microRNAs as stable blood-based markers for cancer detection.* Proc Natl Acad Sci U S A, 2008. **105**(30): p. 10513-8.
20. Vickers, K.C., et al., *MicroRNAs are transported in plasma and delivered to recipient cells by high-density lipoproteins.* Nat Cell Biol, 2011. **13**(4): p. 423-33.
21. Valadi, H., et al., *Exosome-mediated transfer of mRNAs and microRNAs is a novel mechanism of genetic exchange between cells.* Nat.Cell Biol., 2007. **9**(6): p. 654-659.
22. Turchinovich, A., et al., *Characterization of extracellular circulating microRNA.* Nucleic Acids Res, 2011. **39**(16): p. 7223-33.
23. Wang, K., et al., *Export of microRNAs and microRNA-protective protein by mammalian cells.* Nucleic acids research, 2010: p. gkq601.
24. Turchinovich, A., L. Weiz, and B. Burwinkel, *Extracellular miRNAs: the mystery of their origin and function.* Trends Biochem Sci, 2012. **37**(11): p. 460-5.

25. Corsten, M.F., et al., *Circulating MicroRNA-208b and MicroRNA-499 reflect myocardial damage in cardiovascular disease.* Circ Cardiovasc Genet, 2010. **3**(6): p. 499-506.
26. Wang, K., et al., *Circulating microRNAs, potential biomarkers for drug-induced liver injury.* Proc Natl Acad Sci U S A, 2009. **106**(11): p. 4402-7.
27. Laterza, O.F., et al., *Plasma MicroRNAs as sensitive and specific biomarkers of tissue injury.* Clin Chem, 2009. **55**(11): p. 1977-83.
28. Lee, H., et al., *Hepatic siRNA delivery using recombinant human apolipoprotein A-I in mice.* Biochem Biophys Res Commun, 2009. **378**(2): p. 192-6.
29. Tabet, F., et al., *HDL-transferred microRNA-223 regulates ICAM-1 expression in endothelial cells.* Nat Commun, 2014. **5**: p. 3292.
30. Niculescu, L.S., et al., *MiR-486 and miR-92a Identified in Circulating HDL Discriminate between Stable and Vulnerable Coronary Artery Disease Patients.* PLoS One, 2015. **10**(10): p. e0140958.
31. Balaj, L., et al., *Tumour microvesicles contain retrotransposon elements and amplified oncogene sequences.* Nat Commun, 2011. **2**: p. 180.
32. Guescini, M., et al., *Astrocytes and Glioblastoma cells release exosomes carrying mtDNA.* J Neural Transm, 2010. **117**(1): p. 1-4.
33. Thakur, B.K., et al., *Double-stranded DNA in exosomes: a novel biomarker in cancer detection.* Cell Res, 2014. **24**(6): p. 766-9.
34. Chen, T.S. and S.K. Lim, *Measurement of precursor miRNA in exosomes from human ESC-derived mesenchymal stem cells.* Methods Mol Biol, 2013. **1024**: p. 69-86.
35. Pisitkun, T., R.F. Shen, and M.A. Knepper, *Identification and proteomic profiling of exosomes in human urine.* Proc.Natl.Acad.Sci.U.S.A, 2004. **101**(36): p. 13368-13373.
36. Miranda, K.C., et al., *Nucleic acids within urinary exosomes/microvesicles are potential biomarkers for renal disease.* Kidney Int, 2010. **78**(2): p. 191-9.
37. Morrison, E.E., M.A. Bailey, and J.W. Dear, *Renal extracellular vesicles: from physiology to clinical application.* J Physiol, 2016. **594**(20): p. 5735-5748.
38. Antoine, D.J., et al., *Mechanistic biomarkers provide early and sensitive detection of acetaminophen-induced acute liver injury at first presentation to hospital.* Hepatology, 2013. **58**(2): p. 777-87.
39. De Rosa, S., A. Curcio, and C. Indolfi, *Emerging role of microRNAs in cardiovascular diseases.* Circ J, 2014. **78**(3): p. 567-75.
40. Hayes, J., P.P. Peruzzi, and S. Lawler, *MicroRNAs in cancer: biomarkers, functions and therapy.* Trends Mol Med, 2014. **20**(8): p. 460-9.
41. Shen, S., et al., *Biomarker MicroRNAs for Diagnosis, Prognosis and Treatment of Hepatocellular Carcinoma: A Functional Survey and Comparison.* Sci Rep, 2016. **6**: p. 38311.
42. Trionfini, P., A. Benigni, and G. Remuzzi, *MicroRNAs in kidney physiology and disease.* Nat Rev Nephrol, 2015. **11**(1): p. 23-33.
43. *G. B. D. Disease and Injury Incidence Prevalence Collaborators. Global, regional, and national incidence, prevalence, and years lived with disability for 328 diseases and injuries for 195 countries, 1990-2016: a systematic analysis for the Global Burden of Disease Study 2016.* Lancet, 2017. **390**(10100): p. 1211-1259.
44. O'Gara, P.T., et al., *2013 ACCF/AHA guideline for the management of ST-elevation myocardial infarction: a report of the American College of Cardiology Foundation/American Heart Association Task Force on Practice Guidelines.* Circulation, 2013. **127**(4): p. e362-425.
45. Shah, A.S.V., et al., *Patient selection for high sensitivity cardiac troponin testing and diagnosis of myocardial infarction: prospective cohort study.* BMJ, 2017. **359**: p. j4788.
46. Mills, N.L., et al., *Implementation of a sensitive troponin I assay and risk of recurrent myocardial infarction and death in patients with suspected acute coronary syndrome.* JAMA, 2011. **305**(12): p. 1210-6.

47. Shah, A.S., et al., *Sensitive troponin assay and the classification of myocardial infarction.* Am J Med, 2015. **128**(5): p. 493-501 e3.
48. Deddens, J.C., et al., *Circulating microRNAs as novel biomarkers for the early diagnosis of acute coronary syndrome.* J Cardiovasc Transl Res, 2013. **6**(6): p. 884-98.
49. D'Alessandra, Y., et al., *Circulating microRNAs are new and sensitive biomarkers of myocardial infarction.* Eur Heart J, 2010. **31**(22): p. 2765-73.
50. Cheng, Y., et al., *A translational study of urine miRNAs in acute myocardial infarction.* J Mol Cell Cardiol, 2012. **53**(5): p. 668-76.
51. Adachi, T., et al., *Plasma microRNA 499 as a biomarker of acute myocardial infarction.* Clin Chem, 2010. **56**(7): p. 1183-5.
52. Lv, P., et al., *Circulating miR-208b and miR-34a are associated with left ventricular remodeling after acute myocardial infarction.* Int J Mol Sci, 2014. **15**(4): p. 5774-88.
53. Wang, G.K., et al., *Circulating microRNA: a novel potential biomarker for early diagnosis of acute myocardial infarction in humans.* Eur Heart J, 2010. **31**(6): p. 659-66.
54. Eitel, I., et al., *Relation of circulating MicroRNA-133a concentrations with myocardial damage and clinical prognosis in ST-elevation myocardial infarction.* Am Heart J, 2012. **164**(5): p. 706-14.
55. Kuwabara, Y., et al., *Increased microRNA-1 and microRNA-133a levels in serum of patients with cardiovascular disease indicate myocardial damage.* Circ Cardiovasc Genet, 2011. **4**(4): p. 446-54.
56. Xiao, J., et al., *Serum microRNA-499 and microRNA-208a as biomarkers of acute myocardial infarction.* Int J Clin Exp Med, 2014. **7**(1): p. 136-41.
57. Yao, Y., et al., *Plasma Levels of MicroRNA-499 Provide an Early Indication of Perioperative Myocardial Infarction in Coronary Artery Bypass Graft Patients.* PLoS One, 2014. **9**(8): p. e104618.
58. Xin, Y., C. Yang, and Z. Han, *Circulating miR-499 as a potential biomarker for acute myocardial infarction.* Ann Transl Med, 2016. **4**(7): p. 135.
59. Widera, C., et al., *Diagnostic and prognostic impact of six circulating microRNAs in acute coronary syndrome.* J Mol Cell Cardiol, 2011. **51**(5): p. 872-5.
60. Condorelli, G., M.V. Latronico, and G.W. Dorn, 2nd, *microRNAs in heart disease: putative novel therapeutic targets?* Eur Heart J, 2010. **31**(6): p. 649-58.
61. Devaux, Y., et al., *Diagnostic and prognostic value of circulating microRNAs in patients with acute chest pain.* J Intern Med, 2013.
62. Suk, K.T. and D.J. Kim, *Drug-induced liver injury: present and future.* Clin Mol Hepatol, 2012. **18**(3): p. 249-57.
63. Giacomini, K.M., et al., *When good drugs go bad.* Nature, 2007. **446**(7139): p. 975-7.
64. Chalasani, N., et al., *Causes, clinical features, and outcomes from a prospective study of drug-induced liver injury in the United States.* Gastroenterology, 2008. **135**(6): p. 1924-34, 1934 e1-4.
65. Clarke, J.I., J.W. Dear, and D.J. Antoine, *Recent advances in biomarkers and therapeutic interventions for hepatic drug safety - false dawn or new horizon?* Expert Opin Drug Saf, 2016. **15**(5): p. 625-34.
66. Prescott, L.F., et al., *Treatment of paracetamol (acetaminophen) poisoning with N-acetylcysteine. .* Lancet, 1977. **2**: p. 432-434.
67. Vliegenthart, A.D., D.J. Antoine, and J.W. Dear, *Target biomarker profile for the clinical management of paracetamol overdose.* Br J Clin Pharmacol, 2015. **80**(3): p. 351-62.
68. Starkey Lewis, P.J., et al., *Circulating microRNAs as potential markers of human drug-induced liver injury.* Hepatology, 2011. **54**(5): p. 1767-76.
69. Chang, J., et al., *miR-122, a mammalian liver-specific microRNA, is processed from hcr mRNA and maydownregulate the high affinity cationic amino acid transporter CAT-1.* RNA biology, 2004. **1**(2): p. 106-113.

70. Hsu, S.-h., et al., *Essential metabolic, anti-inflammatory, and anti-tumorigenic functions of miR-122 in liver.* The Journal of clinical investigation, 2012. **122**(8): p. 2871-2883.
71. Vliegenthart, A.D., et al., *Retro-orbital blood acquisition facilitates circulating microRNA measurement in zebrafish with paracetamol hepatotoxicity.* Zebrafish, 2014. **11**(3): p. 219-226.
72. Tamai, S., et al., *A monkey model of acetaminophen-induced hepatotoxicity; phenotypic similarity to human.* The Journal of Toxicological Sciences, 2017. **42**(1): p. 73-84.
73. Rivkin, M., et al., *Inflammation-Induced Expression and Secretion of MicroRNA 122 Leads to Reduced Blood Levels of Kidney-Derived Erythropoietin and Anemia.* Gastroenterology, 2016. **151**(5): p. 999-1010. e3.
74. Antoine, D.J., et al., *Mechanistic biomarkers provide early and sensitive detection of acetaminophen‐induced acute liver injury at first presentation to hospital.* Hepatology, 2013. **58**(2): p. 777-787.
75. Dear, J.W., et al., *Risk stratification after paracetamol overdose using mechanistic biomarkers: results from two prospective cohort studies.* Lancet Gastroenterol Hepatol, 2018. **3**(2): p. 104-113.
76. Skog, J., et al., *Glioblastoma microvesicles transport RNA and proteins that promote tumour growth and provide diagnostic biomarkers.* Nat Cell Biol, 2008. **10**(12): p. 1470-6.
77. Pegtel, D.M., et al., *Functional delivery of viral miRNAs via exosomes.* Proc Natl Acad Sci U S A, 2010. **107**(14): p. 6328-33.
78. Mittelbrunn, M., et al., *Unidirectional transfer of microRNA-loaded exosomes from T cells to antigen-presenting cells.* Nat Commun, 2011. **2**: p. 282.
79. Thery, C., M. Ostrowski, and E. Segura, *Membrane vesicles as conveyors of immune responses.* Nat Rev Immunol, 2009. **9**(8): p. 581-93.
80. van der Pol, E., et al., *Classification, functions, and clinical relevance of extracellular vesicles.* Pharmacol Rev, 2012. **64**(3): p. 676-705.
81. Villarroya-Beltri, C., et al., *Sorting it out: regulation of exosome loading.* Semin Cancer Biol, 2014. **28**: p. 3-13.
82. Moreno-Gonzalo, O., C. Villarroya-Beltri, and F. Sanchez-Madrid, *Post-translational modifications of exosomal proteins.* Front Immunol, 2014. **5**: p. 383.
83. Huebner, A.R., et al., *Deubiquitylation of protein cargo is not an essential step in exosome formation.* Mol Cell Proteomics, 2016.
84. Agromayor, M. and J. Martin-Serrano, *Interaction of AMSH with ESCRT-III and deubiquitination of endosomal cargo.* J Biol Chem, 2006. **281**(32): p. 23083-91.
85. Villarroya-Beltri, C., et al., *Sumoylated hnRNPA2B1 controls the sorting of miRNAs into exosomes through binding to specific motifs.* Nat Commun, 2013. **4**: p. 2980.
86. Squadrito, M.L., et al., *Endogenous RNAs modulate microRNA sorting to exosomes and transfer to acceptor cells.* Cell Rep, 2014. **8**(5): p. 1432-46.
87. Sheldon, H., et al., *New mechanism for Notch signaling to endothelium at a distance by Delta-like 4 incorporation into exosomes.* Blood, 2010. **116**(13): p. 2385-94.
88. Cheng, L., et al., *Characterization and deep sequencing analysis of exosomal and non-exosomal miRNA in human urine.* Kidney Int, 2013.
89. Thery, C., et al., *Isolation and characterization of exosomes from cell culture supernatants and biological fluids.* Curr.Protoc.Cell Biol., 2006. **Chapter 3**: p. Unit.
90. Raposo, G. and W. Stoorvogel, *Extracellular vesicles: exosomes, microvesicles, and friends.* J Cell Biol, 2013. **200**(4): p. 373-83.
91. Keller, S., et al., *CD24 is a marker of exosomes secreted into urine and amniotic fluid.* Kidney Int, 2007. **72**(9): p. 1095-102.
92. Oosthuyzen, W., et al., *Quantification of human urinary exosomes by nanoparticle tracking analysis.* J Physiol, 2013. **591**(Pt 23): p. 5833-42.

93. Cocucci, E. and J. Meldolesi, *Ectosomes and exosomes: shedding the confusion between extracellular vesicles.* Trends Cell Biol, 2015. **25**(6): p. 364-72.
94. Yanez-Mo, M., et al., *Biological properties of extracellular vesicles and their physiological functions.* J Extracell Vesicles, 2015. **4**: p. 27066.
95. Cocucci, E., G. Racchetti, and J. Meldolesi, *Shedding microvesicles: artefacts no more.* Trends Cell Biol, 2009. **19**(2): p. 43-51.
96. Del Conde, I., et al., *Tissue-factor-bearing microvesicles arise from lipid rafts and fuse with activated platelets to initiate coagulation.* Blood, 2005. **106**(5): p. 1604-11.
97. Muralidharan-Chari, V., et al., *ARF6-regulated shedding of tumor cell-derived plasma membrane microvesicles.* Curr Biol, 2009. **19**(22): p. 1875-85.
98. Muralidharan-Chari, V., et al., *Microvesicles: mediators of extracellular communication during cancer progression.* J Cell Sci, 2010. **123**(Pt 10): p. 1603-11.
99. Akers, J.C., et al., *Biogenesis of extracellular vesicles (EV): exosomes, microvesicles, retrovirus-like vesicles, and apoptotic bodies.* J Neurooncol, 2013. **113**(1): p. 1-11.
100. van Engeland, M., et al., *Annexin V-affinity assay: a review on an apoptosis detection system based on phosphatidylserine exposure.* Cytometry, 1998. **31**(1): p. 1-9.
101. Rood, I.M., et al., *Comparison of three methods for isolation of urinary microvesicles to identify biomarkers of nephrotic syndrome.* Kidney Int, 2010. **78**(8): p. 810-6.
102. Gonzales, P.A., et al., *Large-scale proteomics and phosphoproteomics of urinary exosomes.* J Am Soc.Nephrol., 2009. **20**(2): p. 363-379.
103. Lotvall, J., et al., *Minimal experimental requirements for definition of extracellular vesicles and their functions: a position statement from the International Society for Extracellular Vesicles.* J Extracell Vesicles, 2014. **3**: p. 26913.
104. Witwer, K.W., et al., *Standardization of sample collection, isolation and analysis methods in extracellular vesicle research.* J Extracell Vesicles, 2013. **2**.
105. Zhou, H., et al., *Collection, storage, preservation, and normalization of human urinary exosomes for biomarker discovery.* Kidney Int, 2006. **69**(8): p. 1471-6.
106. Saetun, P., T. Semangoen, and V. Thongboonkerd, *Characterizations of urinary sediments precipitated after freezing and their effects on urinary protein and chemical analyses.* Am J Physiol Renal Physiol, 2009. **296**(6): p. F1346-54.
107. Harding, C. and P. Stahl, *Transferrin recycling in reticulocytes: pH and iron are important determinants of ligand binding and processing.* Biochem Biophys Res Commun, 1983. **113**(2): p. 650-8.
108. Johnstone, R.M., M. Adam, and B.T. Pan, *The fate of the transferrin receptor during maturation of sheep reticulocytes in vitro.* Can J Biochem Cell Biol, 1984. **62**(11): p. 1246-54.
109. Cvjetkovic, A., J. Lotvall, and C. Lasser, *The influence of rotor type and centrifugation time on the yield and purity of extracellular vesicles.* J Extracell Vesicles, 2014. **3**.
110. Musante, L., et al., *Biochemical and physical characterisation of urinary nanovesicles following CHAPS treatment.* PLoS One, 2012. **7**(7): p. e37279.
111. Boing, A.N., et al., *Single-step isolation of extracellular vesicles by size-exclusion chromatography.* J Extracell Vesicles, 2014. **3**.
112. Cheruvanky, A., et al., *Rapid isolation of urinary exosomal biomarkers using a nanomembrane ultrafiltration concentrator.* Am J Physiol Renal Physiol, 2007. **292**(5): p. F1657-61.
113. Hogan, M.C., et al., *Subfractionation, characterization, and in-depth proteomic analysis of glomerular membrane vesicles in human urine.* Kidney Int, 2014. **85**(5): p. 1225-37.
114. Willms, E., et al., *Cells release subpopulations of exosomes with distinct molecular and biological properties.* Sci Rep, 2016. **6**: p. 22519.
115. Schageman, J., et al., *The complete exosome workflow solution: from isolation to characterization of RNA cargo.* Biomed Res Int, 2013. **2013**: p. 253957.

116. Musante, L., D.E. Tataruch, and H. Holthofer, *Use and isolation of urinary exosomes as biomarkers for diabetic nephropathy.* Front Endocrinol (Lausanne), 2014. **5**: p. 149.
117. Alvarez, M.L., et al., *Comparison of protein, microRNA, and mRNA yields using different methods of urinary exosome isolation for the discovery of kidney disease biomarkers.* Kidney Int, 2012. **82**(9): p. 1024-32.
118. Wang, D. and W. Sun, *Urinary extracellular microvesicles: isolation methods and prospects for urinary proteome.* Proteomics, 2014. **14**(16): p. 1922-32.
119. Kalra, H., et al., *Comparative proteomics evaluation of plasma exosome isolation techniques and assessment of the stability of exosomes in normal human blood plasma.* Proteomics, 2013. **13**(22): p. 3354-64.
120. Ghosh, A., et al., *Rapid isolation of extracellular vesicles from cell culture and biological fluids using a synthetic peptide with specific affinity for heat shock proteins.* PLoS One, 2014. **9**(10): p. e110443.
121. Kowal, J., M. Tkach, and C. Thery, *Biogenesis and secretion of exosomes.* Curr Opin Cell Biol, 2014. **29**: p. 116-25.
122. Kanwar, S.S., et al., *Microfluidic device (ExoChip) for on-chip isolation, quantification and characterization of circulating exosomes.* Lab Chip, 2014. **14**(11): p. 1891-900.
123. Santana, S.M., et al., *Microfluidic isolation of cancer-cell-derived microvesicles from hetergeneous extracellular shed vesicle populations.* Biomed Microdevices, 2014. **16**(6): p. 869-77.
124. Liga, A., et al., *Exosome isolation: a microfluidic road-map.* Lab Chip, 2015. **15**(11): p. 2388-94.
125. Hogan, M.C., et al., *Identification of Biomarkers for PKD1 Using Urinary Exosomes.* J Am Soc Nephrol, 2014.
126. Mullier, F., et al., *More on: calibration for the measurement of microparticles: needs, interests, and limitations of calibrated polystyrene beads for flow cytometry-based quantification of biological microparticles.* J Thromb Haemost, 2011. **9**(8): p. 1679-81; author reply 1681-2.
127. Larson, M.C., et al., *Calcium-phosphate microprecipitates mimic microparticles when examined with flow cytometry.* Cytometry A, 2013. **83**(2): p. 242-50.
128. Salih, M., R. Zietse, and E.J. Hoorn, *Urinary extracellular vesicles and the kidney: biomarkers and beyond.* Am J Physiol Renal Physiol, 2014. **306**(11): p. F1251-9.
129. Street, J.M., et al., *Exosomal transmission of functional aquaporin 2 in kidney cortical collecting duct cells.* J Physiol, 2011. **589**(Pt 24): p. 6119-27.
130. Lee, C.G., et al., *Discovery of an integrative network of microRNAs and transcriptomics changes for acute kidney injury.* Kidney Int, 2014.
131. Wen, H., et al., *Urinary excretion of aquaporin-2 in rat is mediated by a vasopressin-dependent apical pathway.* J Am Soc Nephrol, 1999. **10**(7): p. 1416-29.
132. Ratajczak, J., et al., *Embryonic stem cell-derived microvesicles reprogram hematopoietic progenitors: evidence for horizontal transfer of mRNA and protein delivery.* Leukemia, 2006. **20**(5): p. 847-56.
133. Camussi, G., et al., *Exosomes/microvesicles as a mechanism of cell-to-cell communication.* Kidney Int, 2010. **78**(9): p. 838-48.
134. Dear, J.W., J.M. Street, and M.A. Bailey, *Urinary exosomes: a reservoir for biomarker discovery and potential mediators of intrarenal signalling.* Proteomics., 2013. **13**(10-11): p. 1572-1580.
135. van Balkom, B.W., et al., *Exosomes and the kidney: prospects for diagnosis and therapy of renal diseases.* Kidney Int, 2011. **80**(11): p. 1138-45.
136. Okada, H., *A new look at tubulointerstitial communication with exosomes.* J Am Soc Nephrol, 2013. **24**(3): p. 330-2.
137. Dimov, I., L. Jankovic Velickovic, and V. Stefanovic, *Urinary exosomes.* ScientificWorldJournal, 2009. **9**: p. 1107-18.

138. Higashijima, Y., et al., *Excretion of urinary exosomal AQP2 in rats is regulated by vasopressin and urinary pH.* Am J Physiol Renal Physiol, 2013. **305**(10): p. F1412-21.
139. Oosthuyzen, W., et al., *Vasopressin Regulates Extracellular Vesicle Uptake by Kidney Collecting Duct Cells.* J Am Soc Nephrol, 2016.
140. Hogan, M.C., et al., *Characterization of PKD protein-positive exosome-like vesicles.* J Am Soc Nephrol, 2009. **20**(2): p. 278-88.
141. Woollard, J.R., et al., *A mouse model of autosomal recessive polycystic kidney disease with biliary duct and proximal tubule dilatation.* Kidney Int, 2007. **72**(3): p. 328-36.
142. Masyuk, A.I., et al., *Biliary exosomes influence cholangiocyte regulatory mechanisms and proliferation through interaction with primary cilia.* Am J Physiol Gastrointest Liver Physiol, 2010. **299**(4): p. G990-9.
143. Borges, F.T., et al., *TGF-beta1-containing exosomes from injured epithelial cells activate fibroblasts to initiate tissue regenerative responses and fibrosis.* J Am Soc Nephrol, 2013. **24**(3): p. 385-92.
144. Reynolds, J.L., et al., *Human vascular smooth muscle cells undergo vesicle-mediated calcification in response to changes in extracellular calcium and phosphate concentrations: a potential mechanism for accelerated vascular calcification in ESRD.* J Am Soc Nephrol, 2004. **15**(11): p. 2857-67.
145. Herrera Sanchez, M.B., et al., *Human liver stem cells and derived extracellular vesicles improve recovery in a murine model of acute kidney injury.* Stem Cell Res Ther, 2014. **5**(6): p. 124.
146. Fleig, S.V. and B.D. Humphreys, *Rationale of mesenchymal stem cell therapy in kidney injury.* Nephron Clin Pract, 2014. **127**(1-4): p. 75-80.
147. Togel, F.E. and C. Westenfelder, *Kidney protection and regeneration following acute injury: progress through stem cell therapy.* Am J Kidney Dis, 2012. **60**(6): p. 1012-22.
148. Wise, A.F. and S.D. Ricardo, *Mesenchymal stem cells in kidney inflammation and repair.* Nephrology (Carlton), 2012. **17**(1): p. 1-10.
149. Reinders, M.E., W.E. Fibbe, and T.J. Rabelink, *Multipotent mesenchymal stromal cell therapy in renal disease and kidney transplantation.* Nephrol Dial Transplant, 2010. **25**(1): p. 17-24.
150. Asanuma, H., D.R. Meldrum, and K.K. Meldrum, *Therapeutic applications of mesenchymal stem cells to repair kidney injury.* J Urol, 2010. **184**(1): p. 26-33.
151. Bi, B., et al., *Stromal cells protect against acute tubular injury via an endocrine effect.* J Am Soc Nephrol, 2007. **18**(9): p. 2486-96.
152. Bruno, S., et al., *Microvesicles derived from mesenchymal stem cells enhance survival in a lethal model of acute kidney injury.* PLoS One, 2012. **7**(3): p. e33115.
153. Cantaluppi, V., et al., *Microvesicles derived from endothelial progenitor cells protect the kidney from ischemia-reperfusion injury by microRNA-dependent reprogramming of resident renal cells.* Kidney Int, 2012. **82**(4): p. 412-27.
154. Gatti, S., et al., *Microvesicles derived from human adult mesenchymal stem cells protect against ischaemia-reperfusion-induced acute and chronic kidney injury.* Nephrol Dial Transplant, 2011. **26**(5): p. 1474-83.
155. Zhou, Y., et al., *Exosomes released by human umbilical cord mesenchymal stem cells protect against cisplatin-induced renal oxidative stress and apoptosis in vivo and in vitro.* Stem Cell Res Ther, 2013. **4**(2): p. 34.
156. Biancone, L., et al., *Therapeutic potential of mesenchymal stem cell-derived microvesicles.* Nephrol Dial Transplant, 2012. **27**(8): p. 3037-42.
157. Collino, F., et al., *AKI Recovery Induced by Mesenchymal Stromal Cell-Derived Extracellular Vesicles Carrying MicroRNAs.* J Am Soc Nephrol, 2015.
158. Bitzer, M., I.Z. Ben-Dov, and T. Thum, *Microparticles and microRNAs of endothelial progenitor cells ameliorate acute kidney injury.* Kidney Int, 2012. **82**(4): p. 375-7.

159. Chen, H.H., et al., *Exosomal ATF3 RNA Attenuates Pro-inflammatory Gene MCP-1 Transcription in Renal Ischemia-Reperfusion.* J Cell Physiol, 2014.
160. Ho, J. and J.A. Kreidberg, *The long and short of microRNAs in the kidney.* J Am Soc Nephrol, 2012. **23**(3): p. 400-4.
161. Hiemstra, T.F., et al., *Human Urinary Exosomes as Innate Immune Effectors.* J Am Soc Nephrol, 2014.
162. Flores-Mireles, A.L., et al., *Urinary tract infections: epidemiology, mechanisms of infection and treatment options.* Nat Rev Microbiol, 2015. **13**(5): p. 269-84.
163. Khan, S.R., *Role of renal epithelial cells in the initiation of calcium oxalate stones.* Nephron Exp Nephrol, 2004. **98**(2): p. e55-60.
164. Zhuang, X., et al., *Treatment of brain inflammatory diseases by delivering exosome encapsulated anti-inflammatory drugs from the nasal region to the brain.* Mol Ther, 2011. **19**(10): p. 1769-79.
165. Sun, D., et al., *A novel nanoparticle drug delivery system: the anti-inflammatory activity of curcumin is enhanced when encapsulated in exosomes.* Mol Ther, 2010. **18**(9): p. 1606-14.
166. Tian, Y., et al., *A doxorubicin delivery platform using engineered natural membrane vesicle exosomes for targeted tumor therapy.* Biomaterials, 2014. **35**(7): p. 2383-90.
167. Hoshino, A., et al., *Tumour exosome integrins determine organotropic metastasis.* Nature, 2015.
168. Gildea, J.J., et al., *Exosomal transfer from human renal proximal tubule cells to distal tubule and collecting duct cells.* Clin Biochem, 2014.
169. Bryniarski, K., et al., *Antigen-specific, antibody-coated, exosome-like nanovesicles deliver suppressor T-cell microRNA-150 to effector T cells to inhibit contact sensitivity.* J Allergy Clin Immunol, 2013. **132**(1): p. 170-81.
170. Alvarez-Erviti, L., et al., *Delivery of siRNA to the mouse brain by systemic injection of targeted exosomes.* Nat.Biotechnol., 2011. **29**(4): p. 341-345.
171. Jang, S.C., et al., *Bioinspired exosome-mimetic nanovesicles for targeted delivery of chemotherapeutics to malignant tumors.* ACS Nano, 2013. **7**(9): p. 7698-710.
172. Chalmin, F., et al., *Membrane-associated Hsp72 from tumor-derived exosomes mediates STAT3-dependent immunosuppressive function of mouse and human myeloid-derived suppressor cells.* J Clin Invest, 2010. **120**(2): p. 457-71.
173. Ostrowski, M., et al., *Rab27a and Rab27b control different steps of the exosome secretion pathway.* Nat Cell Biol, 2010. **12**(1): p. 19-30; sup pp 1-13.
174. Bobrie, A., et al., *Rab27a supports exosome-dependent and -independent mechanisms that modify the tumor microenvironment and can promote tumor progression.* Cancer Res, 2012. **72**(19): p. 4920-30.
175. Peinado, H., et al., *Melanoma exosomes educate bone marrow progenitor cells toward a pro-metastatic phenotype through MET.* Nat Med, 2012. **18**(6): p. 883-91.
176. Savina, A., et al., *Rab11 promotes docking and fusion of multivesicular bodies in a calcium-dependent manner.* Traffic, 2005. **6**(2): p. 131-43.
177. Hsu, C., et al., *Regulation of exosome secretion by Rab35 and its GTPase-activating proteins TBC1D10A-C.* J Cell Biol, 2010. **189**(2): p. 223-32.
178. Pisitkun, T., et al., *Application of systems biology principles to protein biomarker discovery: urinary exosomal proteome in renal transplantation.* Proteomics Clin Appl, 2012. **6**(5-6): p. 268-78.
179. Granger, C.B., et al., *National Heart, Lung, And Blood Institute Clinical Proteomics Working Group report.* Circulation, 2004. **109**(14): p. 1697-703.
180. Zhou, H., et al., *Exosomal Fetuin-A identified by proteomics: a novel urinary biomarker for detecting acute kidney injury.* Kidney Int, 2006. **70**(10): p. 1847-57.
181. Alvarez, S., et al., *Urinary exosomes as a source of kidney dysfunction biomarker in renal transplantation.* Transplant Proc, 2013. **45**(10): p. 3719-23.
182. Mortality, G.B.D. and C. Causes of Death, *Global, regional, and national life expectancy, all-cause mortality, and cause-specific mortality for 249 causes of death,*

1980-2015: a systematic analysis for the Global Burden of Disease Study 2015. Lancet, 2016. **388**(10053): p. 1459-1544.
183. DALYs, G.B.D. and H. Collaborators, *Global, regional, and national disability-adjusted life-years (DALYs) for 315 diseases and injuries and healthy life expectancy (HALE), 1990-2015: a systematic analysis for the Global Burden of Disease Study 2015.* Lancet, 2016. **388**(10053): p. 1603-1658.
184. Shah, A.S., et al., *High-sensitivity cardiac troponin I at presentation in patients with suspected acute coronary syndrome: a cohort study.* Lancet, 2015. **386**(10012): p. 2481-8.
185. Care, A., et al., *MicroRNA-133 controls cardiac hypertrophy.* Nat Med, 2007. **13**(5): p. 613-8.
186. Bagnall, R.D., et al., *Global microRNA profiling of the mouse ventricles during development of severe hypertrophic cardiomyopathy and heart failure.* PLoS One, 2012. **7**(9): p. e44744.
187. Curcio, A., et al., *MicroRNA-1 downregulation increases connexin 43 displacement and induces ventricular tachyarrhythmias in rodent hypertrophic hearts.* PLoS One, 2013. **8**(7): p. e70158.
188. Ren, J., et al., *Signature of circulating microRNAs as potential biomarkers in vulnerable coronary artery disease.* PLoS One, 2013. **8**(12): p. e80738.
189. Bang, C., et al., *Cardiac fibroblast-derived microRNA passenger strand-enriched exosomes mediate cardiomyocyte hypertrophy.* J Clin Invest, 2014. **124**(5): p. 2136-46.
190. Barile, L., et al., *Extracellular vesicles from human cardiac progenitor cells inhibit cardiomyocyte apoptosis and improve cardiac function after myocardial infarction.* Cardiovasc Res, 2014. **103**(4): p. 530-41.
191. Hausenloy, D.J., et al., *Effect of remote ischaemic preconditioning on myocardial injury in patients undergoing coronary artery bypass graft surgery: a randomised controlled trial.* Lancet, 2007. **370**(9587): p. 575-9.
192. Friedlander, M.R., et al., *miRDeep2 accurately identifies known and hundreds of novel microRNA genes in seven animal clades.* Nucleic Acids Res, 2012. **40**(1): p. 37-52.
193. Ritchie, M.E., et al., *limma powers differential expression analyses for RNA-sequencing and microarray studies.* Nucleic Acids Res, 2015. **43**(7): p. e47.
194. Schmittgen, T.D. and K.J. Livak, *Analyzing real-time PCR data by the comparative C(T) method.* Nat Protoc, 2008. **3**(6): p. 1101-8.
195. Lai, C.T.M., et al., *Circulating MicroRNA in patients with repaired tetralogy of Fallot.* Eur J Clin Invest, 2017. **47**(8): p. 574-582.
196. Emanueli, C., et al., *Coronary Artery-Bypass-Graft Surgery Increases the Plasma Concentration of Exosomes Carrying a Cargo of Cardiac MicroRNAs: An Example of Exosome Trafficking Out of the Human Heart with Potential for Cardiac Biomarker Discovery.* PLoS One, 2016. **11**(4): p. e0154274.
197. Yang, W., et al., *Expression of Plasma microRNA-1/21/ 208a/499 in myocardial ischemic reperfusion injury.* Cardiology, 2015. **130**(4): p. 237-41.
198. Garmilla-Ezquerra, P., et al., *Analysis of the bone microRNome in osteoporotic fractures.* Calcif Tissue Int, 2015. **96**(1): p. 30-7.
199. Roberts, T.C., et al., *Extracellular microRNAs are dynamic non-vesicular biomarkers of muscle turnover.* Nucleic Acids Res, 2013. **41**(20): p. 9500-13.
200. Fang, Z. and X. Cui, *Design and validation issues in RNA-seq experiments.* Brief Bioinform, 2011. **12**(3): p. 280-7.
201. Camarena, L., et al., *Molecular mechanisms of ethanol-induced pathogenesis revealed by RNA-sequencing.* PLoS Pathog, 2010. **6**(4): p. e1000834.
202. Allison, D.B., et al., *Microarray data analysis: from disarray to consolidation and consensus.* Nat Rev Genet, 2006. **7**(1): p. 55-65.
203. Long, G., et al., *Circulating miR-30a, miR-195 and let-7b associated with acute myocardial infarction.* PLoS One, 2012. **7**(12): p. e50926.

204. van Rooij, E., et al., *A family of microRNAs encoded by myosin genes governs myosin expression and muscle performance.* Dev Cell, 2009. **17**(5): p. 662-73.
205. Tijsen, A.J., Y.M. Pinto, and E.E. Creemers, *Circulating microRNAs as diagnostic biomarkers for cardiovascular diseases.* Am J Physiol Heart Circ Physiol, 2012. **303**(9): p. H1085-95.
206. Chen, X., et al., *Kinetics of plasma microRNA-499 expression in acute myocardial infarction.* J Thorac Dis, 2015. **7**(5): p. 890-6.
207. Devaux, Y., et al., *Use of circulating microRNAs to diagnose acute myocardial infarction.* Clin Chem, 2012. **58**(3): p. 559-67.
208. Liu, N., et al., *An intragenic MEF2-dependent enhancer directs muscle-specific expression of microRNAs 1 and 133.* Proc Natl Acad Sci U S A, 2007. **104**(52): p. 20844-9.
209. Zhao, Y., E. Samal, and D. Srivastava, *Serum response factor regulates a muscle-specific microRNA that targets Hand2 during cardiogenesis.* Nature, 2005. **436**(7048): p. 214-20.
210. Salic, K. and L.J. De Windt, *MicroRNAs as biomarkers for myocardial infarction.* Curr Atheroscler Rep, 2012. **14**(3): p. 193-200.
211. Boeckel, J.N., et al., *Heparin selectively affects the quantification of microRNAs in human blood samples.* Clin Chem, 2013. **59**(7): p. 1125-7.
212. Kim, D.J., et al., *Plasma components affect accuracy of circulating cancer-related microRNA quantitation.* J Mol Diagn, 2012. **14**(1): p. 71-80.
213. Wu, C.S., et al., *Optimized Collection Protocol for Plasma MicroRNA Measurement in Patients with Cardiovascular Disease.* Biomed Res Int, 2016. **2016**: p. 2901938.
214. Rounge, T.B., et al., *microRNA Biomarker Discovery and High-Throughput DNA Sequencing Are Possible Using Long-term Archived Serum Samples.* Cancer Epidemiol Biomarkers Prev, 2015. **24**(9): p. 1381-7.
215. Grasedieck, S., et al., *Impact of serum storage conditions on microRNA stability.* Leukemia, 2012. **26**(11): p. 2414-6.
216. Farina, N.H., et al., *Standardizing analysis of circulating microRNA: clinical and biological relevance.* J Cell Biochem, 2014. **115**(5): p. 805-11.
217. Willeit, P., et al., *Circulating microRNAs as novel biomarkers for platelet activation.* Circ Res, 2013. **112**(4): p. 595-600.
218. Li, J., et al., *Effects of statin on circulating microRNAome and predicted function regulatory network in patients with unstable angina.* BMC Med Genomics, 2015. **8**: p. 12.
219. Goodsaid, F.M., F.W. Frueh, and W. Mattes, *The Predictive Safety Testing Consortium: A synthesis of the goals, challenges and accomplishments of the Critical Path.* Drug Discov Today Technol, 2007. **4**(2): p. 47-50.
220. Michael, L.H., et al., *Myocardial ischemia and reperfusion: a murine model.* Am J Physiol, 1995. **269**(6 Pt 2): p. H2147-54.
221. Looi, Y.H., et al., *Involvement of Nox2 NADPH oxidase in adverse cardiac remodeling after myocardial infarction.* Hypertension, 2008. **51**(2): p. 319-25.
222. Wong, N. and X. Wang, *miRDB: an online resource for microRNA target prediction and functional annotations.* Nucleic Acids Res, 2015. **43**(Database issue): p. D146-52.
223. Vlachos, I.S., et al., *DIANA-miRPath v3.0: deciphering microRNA function with experimental support.* Nucleic Acids Res, 2015. **43**(W1): p. W460-6.
224. Qin, H., et al., *The altered expression profile of microRNAs in cardiopulmonary bypass canine models and the effects of mir-499 on myocardial ischemic reperfusion injury.* J Transl Med, 2013. **11**: p. 154.
225. Wang, J.X., et al., *miR-499 regulates mitochondrial dynamics by targeting calcineurin and dynamin-related protein-1.* Nat Med, 2011. **17**(1): p. 71-8.

226. Zhu, J., et al., *Ischemic Postconditioning-Regulated miR-499 Protects the Rat Heart Against Ischemia/Reperfusion Injury by Inhibiting Apoptosis through PDCD4.* Cell Physiol Biochem, 2016. **39**(6): p. 2364-2380.
227. Li, Y., et al., *MiR-499-5p protects cardiomyocytes against ischaemic injury via anti-apoptosis by targeting PDCD4.* Oncotarget, 2016. **7**(24): p. 35607-35617.
228. Matkovich, S.J., et al., *Direct and indirect involvement of microRNA-499 in clinical and experimental cardiomyopathy.* Circ Res, 2012. **111**(5): p. 521-31.
229. Jayawardena, T.M., et al., *MicroRNA-mediated in vitro and in vivo direct reprogramming of cardiac fibroblasts to cardiomyocytes.* Circ Res, 2012. **110**(11): p. 1465-73.
230. Zhang, K., et al., *miR-499 Ameliorates Podocyte Injury by Targeting Calcineurin in Minimal Change Disease.* Am J Nephrol, 2018. **47**(2): p. 94-102.
231. Antman, E.M., et al., *Cardiac-specific troponin I levels to predict the risk of mortality in patients with acute coronary syndromes.* N Engl J Med, 1996. **335**(18): p. 1342-9.
232. Hallen, J., *Troponin for the estimation of infarct size: what have we learned?* Cardiology, 2012. **121**(3): p. 204-12.
233. Wu, A.H. and Y.J. Feng, *Biochemical differences between cTnT and cTnI and their significance for diagnosis of acute coronary syndromes.* Eur Heart J, 1998. **19 Suppl N**: p. N25-9.
234. Neumann, J.T., et al., *Diagnosis of Myocardial Infarction Using a High-Sensitivity Troponin I 1-Hour Algorithm.* JAMA Cardiol, 2016. **1**(4): p. 397-404.
235. Milani-Nejad, N. and P.M. Janssen, *Small and large animal models in cardiac contraction research: advantages and disadvantages.* Pharmacol Ther, 2014. **141**(3): p. 235-49.
236. Palomeque, J., et al., *Efficiency of eight different AAV serotypes in transducing rat myocardium in vivo.* Gene Ther, 2007. **14**(13): p. 989-97.
237. Zhou, H., et al., *Urinary exosomal transcription factors, a new class of biomarkers for renal disease.* Kidney Int, 2008. **74**(5): p. 613-21.
238. Bruno, S., et al., *Mesenchymal stem cell-derived microvesicles protect against acute tubular injury.* J Am Soc Nephrol, 2009. **20**(5): p. 1053-67.
239. Dominguez, J.H., et al., *Renal Tubular Cell-Derived Extracellular Vesicles Accelerate the Recovery of Established Renal Ischemia Reperfusion Injury.* J Am Soc Nephrol, 2017. **28**(12): p. 3533-3544.
240. Cheng, Y., et al., *A translational study of urine miRNAs in acute myocardial infarction.* J Mol.Cell Cardiol., 2012. **53**(5): p. 668-676.
241. Stahl, A.L., et al., *A novel mechanism of bacterial toxin transfer within host blood cell-derived microvesicles.* PLoS Pathog, 2015. **11**(2): p. e1004619.
242. Skokos, D., et al., *Mast cell-dependent B and T lymphocyte activation is mediated by the secretion of immunologically active exosomes.* J Immunol, 2001. **166**(2): p. 868-76.
243. Combes, V., et al., *In vitro generation of endothelial microparticles and possible prothrombotic activity in patients with lupus anticoagulant.* J Clin Invest, 1999. **104**(1): p. 93-102.
244. Sapet, C., et al., *Thrombin-induced endothelial microparticle generation: identification of a novel pathway involving ROCK-II activation by caspase-2.* Blood, 2006. **108**(6): p. 1868-76.
245. Faure, V., et al., *Elevation of circulating endothelial microparticles in patients with chronic renal failure.* J Thromb Haemost, 2006. **4**(3): p. 566-73.
246. Meckes, D.G., Jr. and N. Raab-Traub, *Microvesicles and viral infection.* J Virol, 2011. **85**(24): p. 12844-54.
247. Tati, R., et al., *Complement activation associated with ADAMTS13 deficiency in human and murine thrombotic microangiopathy.* J Immunol, 2013. **191**(5): p. 2184-93.

248. Park, J.E., et al., *Hypoxic tumor cell modulates its microenvironment to enhance angiogenic and metastatic potential by secretion of proteins and exosomes.* Mol Cell Proteomics, 2010. **9**(6): p. 1085-99.
249. Lehmann, B.D., et al., *Senescence-associated exosome release from human prostate cancer cells.* Cancer Res, 2008. **68**(19): p. 7864-71.
250. Pizzirani, C., et al., *Stimulation of P2 receptors causes release of IL-1beta-loaded microvesicles from human dendritic cells.* Blood, 2007. **109**(9): p. 3856-64.
251. Bianco, F., et al., *Astrocyte-derived ATP induces vesicle shedding and IL-1 beta release from microglia.* J Immunol, 2005. **174**(11): p. 7268-77.
252. Dear, J.W., J.M. Street, and M.A. Bailey, *Urinary exosomes: a reservoir for biomarker discovery and potential mediators of intrarenal signalling.* Proteomics, 2013. **13**(10-11): p. 1572-80.
253. Ryan, M.J., et al., *HK-2: an immortalized proximal tubule epithelial cell line from normal adult human kidney.* Kidney Int, 1994. **45**(1): p. 48-57.
254. Nielsen, R., et al., *Characterization of a kidney proximal tubule cell line, LLC-PK1, expressing endocytotic active megalin.* J Am Soc Nephrol, 1998. **9**(10): p. 1767-76.
255. Richardson, J.C., P. Waterson, and N.L. Simmons, *Isolation and culture of renal cortical tubules from neonate rabbit kidneys.* Q J Exp Physiol, 1982. **67**(2): p. 287-301.
256. Skelton, L.A. and W.F. Boron, *Effect of acute acid-base disturbances on ErbB1/2 tyrosine phosphorylation in rabbit renal proximal tubules.* Am J Physiol Renal Physiol, 2013. **305**(12): p. F1747-64.
257. Valencia, L., et al., *Nifedipine-activated Ca(2+) permeability in newborn rat cortical collecting duct cells in primary culture.* Am J Physiol Cell Physiol, 2001. **280**(5): p. C1193-203.
258. White, S. and H. Reeve, *Primary culture of collecting duct cell epithelium from neonate rabbit kidney in monolayer.* Exp Physiol, 1992. **77**(1): p. 129-39.
259. Ilatovskaya, D.V., et al., *Pharmacological characterization of the P2 receptors profile in the podocytes of the freshly isolated rat glomeruli.* Am J Physiol Cell Physiol, 2013. **305**(10): p. C1050-9.
260. Harris, P.J. and L.G. Navar, *Tubular transport responses to angiotensin.* Am J Physiol, 1985. **248**(5 Pt 2): p. F621-30.
261. Gildea, J.J., et al., *Differential D1 and D5 receptor regulation and degradation of the angiotensin type 1 receptor.* Hypertension, 2008. **51**(2): p. 360-6.
262. Hruska, K.A., et al., *Effects of parathyroid hormone on cytosolic calcium in renal proximal tubular primary cultures.* Am J Physiol, 1986. **251**(2 Pt 2): p. F188-98.
263. Amemiya, M., et al., *Expression of NHE-3 in the apical membrane of rat renal proximal tubule and thick ascending limb.* Kidney Int, 1995. **48**(4): p. 1206-15.
264. Ito, K., *ABCC2/Abcc2 transport property in different species and its modulation by heterogeneous factors.* Drug Metab Pharmacokinet, 2008. **23**(6): p. 394-405.
265. Gunness, P., et al., *Comparison of the novel HK-2 human renal proximal tubular cell line with the standard LLC-PK1 cell line in studying drug-induced nephrotoxicity.* Can J Physiol Pharmacol, 2010. **88**(4): p. 448-55.
266. Jenkinson, S.E., et al., *The limitations of renal epithelial cell line HK-2 as a model of drug transporter expression and function in the proximal tubule.* Pflugers Arch, 2012. **464**(6): p. 601-11.
267. Hull, R.N., W.R. Cherry, and G.W. Weaver, *The origin and characteristics of a pig kidney cell strain, LLC-PK.* In Vitro, 1976. **12**(10): p. 670-7.
268. Dudley, A.J., K. Bleasby, and C.D. Brown, *The organic cation transporter OCT2 mediates the uptake of beta-adrenoceptor antagonists across the apical membrane of renal LLC-PK(1) cell monolayers.* Br J Pharmacol, 2000. **131**(1): p. 71-9.
269. Nielsen, R., et al., *Transcellular transport of vitamin B(12) in LLC-PK1 renal proximal tubule cells.* J Am Soc Nephrol, 2001. **12**(6): p. 1099-106.

270. Unwin, R.J., M.A. Bailey, and G. Burnstock, *Purinergic signaling along the renal tubule: the current state of play.* News Physiol Sci, 2003. **18**: p. 237-41.
271. Bailey, M.A., et al., *Axial distribution and characterization of basolateral P2Y receptors along the rat renal tubule.* Kidney Int, 2000. **58**(5): p. 1893-901.
272. Menzies, R.I., et al., *Purinergic signaling in kidney disease.* Kidney Int, 2017. **91**(2): p. 315-323.
273. Bagorda, A., et al., *Extracellular adenine nucleotides regulate Na+/H+ exchanger NHE3 activity in A6-NHE3 transfectants by a cAMP/PKA-dependent mechanism.* J Membr Biol, 2002. **188**(3): p. 249-59.
274. Jin, W. and U. Hopfer, *Purinergic-mediated inhibition of Na+-K+-ATPase in proximal tubule cells: elevated cytosolic Ca2+ is not required.* Am J Physiol, 1997. **272**(4 Pt 1): p. C1169-77.
275. Waikar, S.S., et al., *Declining mortality in patients with acute renal failure, 1988 to 2002.* J Am Soc Nephrol, 2006. **17**(4): p. 1143-50.
276. Miller, R.P., et al., *Mechanisms of Cisplatin nephrotoxicity.* Toxins (Basel), 2010. **2**(11): p. 2490-518.
277. Pabla, N. and Z. Dong, *Cisplatin nephrotoxicity: mechanisms and renoprotective strategies.* Kidney Int, 2008. **73**(9): p. 994-1007.
278. Svensson, K.J., et al., *Exosome uptake depends on ERK1/2-heat shock protein 27 signaling and lipid Raft-mediated endocytosis negatively regulated by caveolin-1.* J Biol Chem, 2013. **288**(24): p. 17713-24.
279. Feng, D., et al., *Cellular internalization of exosomes occurs through phagocytosis.* Traffic., 2010. **11**(5): p. 675-687.
280. Tian, T., et al., *Exosome uptake through clathrin-mediated endocytosis and macropinocytosis and mediating miR-21 delivery.* J Biol Chem, 2014. **289**(32): p. 22258-67.
281. Mulcahy, L.A., R.C. Pink, and D.R. Carter, *Routes and mechanisms of extracellular vesicle uptake.* J Extracell Vesicles, 2014. **3**.
282. Bonventre, J.V., *Kidney injury molecule-1 (KIM-1): a urinary biomarker and much more.* Nephrol Dial Transplant, 2009. **24**(11): p. 3265-8.
283. Ichimura, T., et al., *Kidney injury molecule-1 is a phosphatidylserine receptor that confers a phagocytic phenotype on epithelial cells.* J Clin.Invest, 2008. **118**(5): p. 1657-1668.
284. Miyanishi, M., et al., *Identification of Tim4 as a phosphatidylserine receptor.* Nature, 2007. **450**(7168): p. 435-439.
285. Zhao, X., et al., *Kidney Injury Molecule-1 Enhances Endocytosis of Albumin in Renal Proximal Tubular Cells.* J Cell Physiol, 2015.
286. Wang, X., et al., *Unique molecular profile of exosomes derived from primary human proximal tubular epithelial cells under diseased conditions.* J Extracell Vesicles, 2017. **6**(1): p. 1314073.
287. Ichimura, T., et al., *Kidney injury molecule-1 is a phosphatidylserine receptor that confers a phagocytic phenotype on epithelial cells.* J Clin Invest, 2008. **118**(5): p. 1657-68.
288. Ichimura, T., et al., *Kidney injury molecule-1 (KIM-1), a putative epithelial cell adhesion molecule containing a novel immunoglobulin domain, is up-regulated in renal cells after injury.* J Biol.Chem., 1998. **273**(7): p. 4135-4142.
289. Han, W.K., et al., *Human kidney injury molecule-1 is a tissue and urinary tumor marker of renal cell carcinoma.* J Am Soc Nephrol, 2005. **16**(4): p. 1126-34.
290. Huang, J.X., et al., *Evaluation of biomarkers for in vitro prediction of drug-induced nephrotoxicity: comparison of HK-2, immortalized human proximal tubule epithelial, and primary cultures of human proximal tubular cells.* Pharmacol Res Perspect, 2015. **3**(3): p. e00148.
291. Fan, P.C., et al., *MicroRNAs in acute kidney injury.* Hum Genomics, 2016. **10**(1): p. 29.

292. Wei, Q., et al., *Targeted deletion of Dicer from proximal tubules protects against renal ischemia-reperfusion injury.* J Am Soc Nephrol, 2010. **21**(5): p. 756-61.
293. Tomasoni, S., et al., *Transfer of growth factor receptor mRNA via exosomes unravels the regenerative effect of mesenchymal stem cells.* Stem Cells Dev, 2013. **22**(5): p. 772-80.
294. Bhatt, K., et al., *MicroRNA-34a is induced via p53 during cisplatin nephrotoxicity and contributes to cell survival.* Mol Med, 2010. **16**(9-10): p. 409-16.
295. Joo, M.S., et al., *miR-125b transcriptionally increased by Nrf2 inhibits AhR repressor, which protects kidney from cisplatin-induced injury.* Cell Death Dis, 2013. **4**: p. e899.
296. Liang, Y., et al., *Characterization of microRNA expression profiles in normal human tissues.* BMC genomics, 2007. **8**(1): p. 1.
297. Rivoli, L., et al., *The effect of renal dysfunction and haemodialysis on circulating liver specific miR‐122.* British Journal of Clinical Pharmacology, 2016.
298. Brillant, N., et al., *Dynamic and accurate assessment of acetaminophen-induced hepatotoxicity by integrated photoacoustic imaging and mechanistic biomarkers in vivo.* Toxicol Appl Pharmacol, 2017. **332**: p. 64-74.
299. Vliegenthart, A.D., et al., *Retro-orbital blood acquisition facilitates circulating microRNA measurement in zebrafish with paracetamol hepatotoxicity.* Zebrafish, 2014. **11**(3): p. 219-26.
300. Chang, J., et al., *miR-122, a mammalian liver-specific microRNA, is processed from hcr mRNA and may downregulate the high affinity cationic amino acid transporter CAT-1.* RNA Biol, 2004. **1**(2): p. 106-13.
301. Cory, A.H., et al., *Use of an aqueous soluble tetrazolium/formazan assay for cell growth assays in culture.* Cancer Commun, 1991. **3**(7): p. 207-12.
302. Kanemura, Y., et al., *Evaluation of in vitro proliferative activity of human fetal neural stem/progenitor cells using indirect measurements of viable cells based on cellular metabolic activity.* J Neurosci Res, 2002. **69**(6): p. 869-79.
303. Wang, H.E., et al., *Acute kidney injury and mortality in hospitalized patients.* Am J Nephrol, 2012. **35**(4): p. 349-55.
304. Martin-Llahi, M., et al., *Prognostic importance of the cause of renal failure in patients with cirrhosis.* Gastroenterology, 2011. **140**(2): p. 488-496 e4.
305. Wong, F., *Acute kidney injury in liver cirrhosis: new definition and application.* Clin Mol Hepatol, 2016. **22**(4): p. 415-422.
306. O'Riordan, A., et al., *Acute kidney injury in patients admitted to a liver intensive therapy unit with paracetamol-induced hepatotoxicity.* Nephrol Dial Transplant, 2011. **26**(11): p. 3501-8.
307. Ozkaya, O., et al., *A case of acetaminophen (paracetamol) causing renal failure without liver damage in a child and review of literature.* Ren Fail, 2010. **32**(9): p. 1125-7.
308. Chen, J.F., et al., *Targeted deletion of Dicer in the heart leads to dilated cardiomyopathy and heart failure.* Proc Natl Acad Sci U S A, 2008. **105**(6): p. 2111-6.
309. Christianson, H.C., et al., *Cancer cell exosomes depend on cell-surface heparan sulfate proteoglycans for their internalization and functional activity.* Proc Natl Acad Sci U S A, 2013. **110**(43): p. 17380-5.
310. Mattis, A.N., et al., *A screen in mice uncovers repression of lipoprotein lipase by microRNA-29a as a mechanism for lipid distribution away from the liver.* Hepatology, 2015. **61**(1): p. 141-52.
311. Zhang, Z., et al., *Pretreatment of Cardiac Stem Cells With Exosomes Derived From Mesenchymal Stem Cells Enhances Myocardial Repair.* J Am Heart Assoc, 2016. **5**(1).
312. Chowdhary, V., et al., *miRNA-122 Protects Mice and Human Hepatocytes from Acetaminophen Toxicity by Regulating Cytochrome P450 Family 1 Subfamily A Member 2 and Family 2 Subfamily E Member 1 Expression.* Am J Pathol, 2017. **187**(12): p. 2758-2774.

Appendix

MiRNA of interest	Time point	log ΔCt		Comparison	Mean difference	95% CI of diff.	P-value
		Mean	SD				
miR-499a	T0	0.000003748	0.000004217				
	T2	0.000005434	0.000005798	T0 vs. T2	-0.000001687	-0.000005253 to 0.000001879	ns
	T6	0.000013840	0.000017080	T0 vs. T6	-0.000010100	-0.00002009 to -0.0000001037	*
	T24	0.000006560	0.000009445	T0 vs. T24	-0.000002813	-0.000008730 to 0.000003105	ns
miR-1	T0	0.000005461	0.000009607				
	T2	0.000016980	0.000027900	T0 vs. T2	-0.000011520	-0.00002441 to 0.000001373	ns
	T6	0.000032720	0.000037750	T0 vs. T6	-0.000027260	-0.00004787 to -0.000006645	*
	T24	0.000013140	0.000023170	T0 vs. T24	-0.000007678	-0.00002205 to 0.000006695	ns
miR-30a	T0	0.000156900	0.000153400				

	T2	0.000435300	0.000652400	T0 vs. T2	-0.000278400	-0.0006186 to 0.00006187	*
	T6	0.000447200	0.000474900	T0 vs. T6	-0.000290200	-0.0005644 to -0.00001610	*
	T24	0.000319500	0.000343700	T0 vs. T24	-0.000162600	-0.0003570 to 0.00003179	ns
miR-22	T0	0.000034830	0.000089100				
	T2	0.000244700	0.000487700	T0 vs. T2	-0.000209800	-0.0004588 to 0.00003912	ns
	T6	0.000104700	0.000183500	T0 vs. T6	-0.000069860	-0.0001883 to 0.00004861	ns
	T24	0.000047050	0.000063850	T0 vs. T24	-0.000012220	-0.00007263 to 0.00004820	ns
miR-378g	T0	0.000136600	0.000351500				
	T2	0.000070030	0.000091500	T0 vs. T2	0.000066600	-0.0001706 to 0.0003038	ns
	T6	0.000218500	0.000414800	T0 vs. T6	-0.000081840	-0.0004432 to 0.0002795	ns
	T24	0.000090730	0.000153100	T0 vs. T24	0.000045900	-0.0001508 to 0.0002426	ns
miR-23a	T0	0.000684600	0.000976500				
	T2	0.005804000	0.007533000	T0 vs. T2	-0.005119000	-0.01042 to 0.0001807	ns

	T6	0.002979000	0.003808000	T0 vs. T6	-0.002294000	-0.004823 to 0.0002345	ns
	T24	0.003334000	0.004531000	T0 vs. T24	-0.002649000	-0.005783 to 0.0004845	ns
miR-199a	T0	0.000806400	0.002988000				
	T2	0.000302000	0.000356200	T0 vs. T2	0.000504500	-0.001491 to 0.002500	ns
	T6	0.000192500	0.000225600	T0 vs. T6	0.000614000	-0.001370 to 0.002598	ns
	T24	0.000206300	0.000251000	T0 vs. T24	0.000600100	-0.001254 to 0.002454	ns
miR-125b	T0	0.000084900	0.000305900				
	T2	0.000042730	0.000079300	T0 vs. T2	0.000042170	-0.0001369 to 0.0002213	ns
	T6	0.000058090	0.000109800	T0 vs. T6	0.000026810	-0.0001626 to 0.0002163	ns
	T24	0.000064320	0.000188800	T0 vs. T24	0.000020580	-0.0001810 to 0.0002221	ns
miR-145	T0	0.000340400	0.001228000				
	T2	0.000112000	0.000103800	T0 vs. T2	0.000228400	-0.0004720 to 0.0009288	ns
	T6	0.000252600	0.000751700	T0 vs. T6	0.000087840	-0.0006929 to 0.0008686	ns
	T24	0.000080490	0.000165300	T0 vs. T24	0.000259900	-0.0004535 to 0.0009734	ns
miR-140	T0	0.000019760	0.000033540				
	T2	0.000045350	0.000075390	T0 vs. T2	-0.000025600	-0.00007339 to 0.00002220	ns

	T6	0.000039020	0.000036840	T0 vs. T6	-0.000019260	-0.00004577 to 0.000007243	ns
	T24	0.000050390	0.000126900	T0 vs. T24	-0.000030630	-0.0001044 to 0.00004311	ns
miR-208a	T0	0.000008664	0.000017020				
	T2	0.000008905	0.000014710	T0 vs. T2	-0.000000242	-0.000006832 to 0.000006349	ns
	T6	0.000034470	0.000054050	T0 vs. T6	-0.000025800	-0.00005769 to 0.000006088	ns
	T24	0.000039450	0.000128400	T0 vs. T24	-0.000030790	-0.0001018 to 0.00004027	ns
miR-99a	T0	0.000895900	0.001673000				
	T2	0.000709800	0.000913800	T0 vs. T2	0.000186100	-0.0008146 to 0.001187	ns
	T6	0.002601000	0.004492000	T0 vs. T6	-0.001705000	-0.004581 to 0.001170	ns
	T24	0.011800000	0.044200000	T0 vs. T24	-0.010910000	-0.03531 to 0.01350	ns
miR-769	T0	0.000385500	0.000915000				
	T2	0.000670200	0.001097000	T0 vs. T2	-0.000284700	-0.0007612 to 0.0001918	ns

	T6	0.001150000	0.002353000	T0 vs. T6	-0.000764900	-0.002184 to 0.0006539	ns
	T24	0.004240000	0.017840000	T0 vs. T24	-0.003855000	-0.01390 to 0.006190	ns
miR-133a	T0	0.000032370	0.000047510				
	T2	0.000046520	0.000082020	T0 vs. T2	-0.000014150	-0.00006569 to 0.00003738	ns
	T6	0.000261000	0.000746200	T0 vs. T6	-0.000228600	-0.0006540 to 0.0001967	ns
	T24	0.000491700	0.001799000	T0 vs. T24	-0.000459300	-0.001484 to 0.0005654	ns
Let-7e	T0	0.000134000	0.000267000				
	T2	0.000233000	0.000259800	T0 vs. T2	-0.000099070	-0.0002974 to 0.00009922	ns
	T6	0.000243800	0.000381800	T0 vs. T6	-0.000109800	-0.0003765 to 0.0001568	ns
	T24	0.000240700	0.000314400	T0 vs. T24	-0.000106800	-0.0003542 to 0.0001406	ns
miR-30d	T0	0.005874000	0.020540000				
	T2	0.000273800	0.000355800	T0 vs. T2	0.005600000	-0.006090 to 0.01729	ns
	T6	0.000639500	0.000836800	T0 vs. T6	0.005234000	-0.006538 to 0.01701	ns

	T24	0.001463000	0.004864000	T0 vs. T24	0.004411000	-0.007810 to 0.01663	ns
miR-99b	T0	0.001064000	0.004364000				
	T2	0.000139100	0.000233900	T0 vs. T2	0.000925100	-0.001587 to 0.003437	ns
	T6	0.000198000	0.000336600	T0 vs. T6	0.000866100	-0.001568 to 0.003300	ns
	T24	0.000810700	0.002416000	T0 vs. T24	0.000253400	-0.002552 to 0.003059	ns
miR-100	T0	0.000161100	0.000367200				
	T2	0.000401700	0.000870600	T0 vs. T2	-0.000240600	-0.0007900 to 0.0003088	ns
	T6	0.000564000	0.000543500	T0 vs. T6	-0.000402900	-0.0007796 to -0.00002621	ns
	T24	0.017370000	0.076110000	T0 vs. T6	-0.017210000	-0.0007796 to -0.00002621	ns

Appendix 1: rtPCR validation of plasma miRNA targets in human CABG cohort.

Mean expression of miRNAs of interest vary following CABG injury. Comparison to baseline levels was conducted using paired 1-way ANOVA and Dunnet's multiple comparison (significance 0.05, n=14). Plasma levels of miR-30a significantly increased at T2 in comparison to baseline. miR-499a, miR-1 and miR-30a significantly increased at 6 hours in comparison to baseline.

		log ΔCt					
MiRNA of interest	**Time point**	**Mean**	**SD**	**Comparison**	**Mean difference**	**95% CI of diff.**	**P-value**
miR-499a	T0	0.02232	0.07307				
	T2	0.02933	0.1105	T0 vs. T2	-0.007012	-0.09086 to 0.07684	ns
	T6	0.1215	0.3454	T0 vs. T6	-0.09917	-0.3192 to 0.1208	ns
miR-1	T0	0.005632	0.01355				
	T2	0.04779	0.1838	T0 vs. T2	-0.04216	-0.1555 to 0.07116	ns
	T6	0.2987	0.8501	T0 vs. T6	-0.293	-0.8128 to 0.2267	ns
miR-30a	T0	0.04277	0.06734				
	T2	1.317	5.087	T0 vs. T2	-1.274	-4.383 to 1.835	ns
	T6	4.755	13.5	T0 vs. T6	-4.713	-12.95 to 3.527	ns
miR-22	T0	0.008462	0.0141				
	T2	0.2229	0.8439	T0 vs. T2	-0.2145	-0.7304 to 0.3015	ns
	T6	1.259	4.58	T0 vs. T6	-1.251	-4.045 to 1.543	ns
miR-378g	T0	0.001104	0.003596				
	T2	0.003028	0.0108	T0 vs. T2	-0.001924	-0.009042 to 0.005193	ns
	T6	0.01057	0.03495	T0 vs. T6	-0.009466	-0.03110 to 0.01217	ns
miR-23a	T0	0.06895	0.163				
	T2	1.399	5.389	T0 vs. T2	-1.33	-4.628 to 1.968	ns
	T6	1.405	3.725	T0 vs. T6	-1.336	-3.625 to 0.9524	ns

miR-199a	T0	0.0004069	0.01074				
	T2	0.1557	0.3815	T0 vs. T2	-0.1553	-0.5295 to 0.2190	ns
	T6	0.04684	0.06786	T0 vs. T6	-0.04643	-0.1222 to 0.02938	ns
miR-125b	T0	0.000484	0.0009026				
	T2	0.0008554	0.002455	T0 vs. T2	-0.0003714	-0.002011 to 0.001268	ns
	T6	0.008451	0.02243	T0 vs. T6	-0.007967	-0.02170 to 0.005761	ns
miR-145	T0	0.001795	0.004365				
	T2	0.1601	0.5722	T0 vs. T2	-0.1583	-0.5075 to 0.1909	ns
	T6	0.2535	0.7037	T0 vs. T6	-0.2517	-0.6811 to 0.1778	ns
miR-140	T0	0.001789	0.005614				
	T2	0.0169	0.04407	T0 vs. T2	-0.01511	-0.04261 to 0.01240	ns
	T6	0.05663	0.1595	T0 vs. T6	-0.05484	-0.1491 to 0.03941	ns
miR-208a	T0	0.0000421 4	0.00007511				
	T2	0.0005938	0.002119	T0 vs. T2	-0.0005517	-0.001849 to 0.0007459	ns
	T6	0.001128	0.003147	T0 vs. T6	-0.001086	-0.003011 to 0.0008392	ns
miR-99a	T0	0.001445	0.00219				
	T2	0.06165	0.2359	T0 vs. T2	-0.0602	-0.2042 to 0.08382	ns
	T6	0.151	0.4108	T0 vs. T6	-0.1495	-0.4003 to 0.1012	ns
miR-769	T0	0.0007042	0.001452				
	T2	0.007904	0.02916	T0 vs. T2	-0.0072	-0.02508 to 0.01068	ns

	T6	0.02391	0.06403	T0 vs. T6	-0.0232	-0.06240 to 0.01600	ns
miR-133a	T0	0.004379	0.01074				
	T2	0.09958	0.3815	T0 vs. T2	-0.0952	-0.3285 to 0.1381	ns
	T6	0.01922	0.06786	T0 vs. T6	-0.01484	-0.05736 to 0.02768	ns
Let-7e	T0	0.0004526	0.0009721				
	T2	0.06011	0.2261	T0 vs. T2	-0.05965	-0.1976 to 0.07829	ns
	T6	0.01533	0.04892	T0 vs. T6	-0.01487	-0.04472 to 0.01497	ns
miR-30d	T0	0.006267	0.009753				
	T2	0.2184	0.8388	T0 vs. T2	-0.2122	-0.7246 to 0.3003	ns
	T6	0.3883	1.311	T0 vs. T6	-0.3821	-1.183 to 0.4184	ns
miR-99b	T0	0.000762	0.001324				
	T2	0.00805	0.02737	T0 vs. T2	-0.007288	-0.02406 to 0.009481	ns
	T6	0.05429	0.1564	T0 vs. T6	-0.05353	-0.1490 to 0.04198	ns
miR-100	T0	0.0004966	0.001007				
	T2	0.01504	0.05721	T0 vs. T2	-0.01454	-0.04950 to 0.02042	ns
	T6	0.1131	0.3097	T0 vs. T6	-0.1126	-0.3016 to 0.07642	ns

Appendix 2: rtPCR validation of plasma miRNA targets in human orthopaedic cohort

Mean expression of miRNAs of interest do not vary significantly following orthopaedic injury. Comparison to baseline expression was conducted using paired 1-way ANOVA and Dunnet's multiple comparison (significance level 0.05, n=6

Target Rank	Target Score	Gene Symbol	Gene Description
1	100	SOX6	SRY (sex determining region Y)-box 6
2	100	EPM2AIP1	EPM2A (laforin) interacting protein 1
3	99	VAV3	vav 3 guanine nucleotide exchange factor
4	99	EML4	echinoderm microtubule associated protein like 4
5	98	SOS2	son of sevenless homolog 2 (Drosophila)
6	97	DDX1	DEAD (Asp-Glu-Ala-Asp) box helicase 1
7	97	COL4A3BP	collagen, type IV, alpha 3 (Goodpasture antigen) binding protein
8	97	RCN2	reticulocalbin 2, EF-hand calcium binding domain
9	97	KPNA3	karyopherin alpha 3 (importin alpha 4)
10	96	ARGLU1	arginine and glutamate rich 1
11	96	SLC30A4	solute carrier family 30 (zinc transporter), member 4
12	96	REEP1	receptor accessory protein 1
13	96	OSBPL1A	oxysterol binding protein-like 1A
14	96	FOXP2	forkhead box P2
15	96	LRCH2	leucine-rich repeats and calponin homology (CH) domain containing 2
16	96	SKIL	SKI-like oncogene
17	96	CCRN4L	CCR4 carbon catabolite repression 4-like (S. cerevisiae)
18	95	SOX5	SRY (sex determining region Y)-box 5
19	95	RRAGB	Ras-related GTP binding B
20	95	C17orf75	chromosome 17 open reading frame 75
21	94	MYEF2	myelin expression factor 2
22	94	USP24	ubiquitin specific peptidase 24
23	94	SMIM15	small integral membrane protein 15
24	93	MAPK6	mitogen-activated protein kinase 6
25	93	H2AFZ	H2A histone family, member Z
26	93	PTBP3	polypyrimidine tract binding protein 3
27	93	HNRNPC	heterogeneous nuclear ribonucleoprotein C (C1/C2)
28	93	UBE2V2	ubiquitin-conjugating enzyme E2 variant 2
29	93	SLC12A2	solute carrier family 12 (sodium/potassium/chloride transporter), member 2
30	92	REST	RE1-silencing transcription factor
31	92	PTBP2	polypyrimidine tract binding protein 2
32	92	SDC2	syndecan 2
33	92	KIAA1468	KIAA1468
34	91	PHLDA2	pleckstrin homology-like domain, family A, member 2
35	91	MARS2	methionyl-tRNA synthetase 2, mitochondrial
36	90	SAMD8	sterile alpha motif domain containing 8
37	90	RSBN1	round spermatid basic protein 1
38	90	PCDHB11	protocadherin beta 11

39	89	RCAN3	RCAN family member 3
40	89	CNOT6L	CCR4-NOT transcription complex, subunit 6-like
41	88	GPC6	glypican 6
42	88	DCP2	decapping mRNA 2
43	88	TESK2	testis-specific kinase 2
44	88	SYBU	syntabulin (syntaxin-interacting)
45	87	RALYL	RALY RNA binding protein-like
46	87	NDUFA5	NADH dehydrogenase (ubiquinone) 1 alpha subcomplex, 5
47	87	INPP5E	inositol polyphosphate-5-phosphatase, 72 kDa
48	86	LIN28B	lin-28 homolog B (C. elegans)
49	86	LCOR	ligand dependent nuclear receptor corepressor
50	86	LPXN	leupaxin
51	85	ASPH	aspartate beta-hydroxylase
52	85	FAM168A	family with sequence similarity 168, member A
53	85	KLHL42	kelch-like family member 42
54	85	NOVA1	neuro-oncological ventral antigen 1
55	85	TMEM100	transmembrane protein 100
56	85	THBS2	thrombospondin 2
57	85	RCOR3	REST corepressor 3
58	84	RGS21	regulator of G-protein signaling 21
59	84	NCBP2	nuclear cap binding protein subunit 2, 20kDa
60	84	DNAJC25	DnaJ (Hsp40) homolog, subfamily C , member 25
61	84	LRRC8B	leucine rich repeat containing 8 family, member B
62	83	PAPOLA	poly(A) polymerase alpha
63	83	LAMP3	lysosomal-associated membrane protein 3
64	82	XRN1	5'-3' exoribonuclease 1
65	82	LRP8	low density lipoprotein receptor-related protein 8, apolipoprotein e receptor
66	81	TMBIM6	transmembrane BAX inhibitor motif containing 6
67	81	CHM	choroideremia (Rab escort protein 1)
68	81	ZNF711	zinc finger protein 711
69	81	SPTSSB	serine palmitoyltransferase, small subunit B
70	80	SEH1L	SEH1-like (S. cerevisiae)
71	80	ARID2	AT rich interactive domain 2 (ARID, RFX-like)
72	79	FAM60A	family with sequence similarity 60, member A
73	79	TRUB1	TruB pseudouridine (psi) synthase family member 1
74	78	RAB23	RAB23, member RAS oncogene family
75	78	EPHA5	EPH receptor A5
76	78	C3orf43	chromosome 3 open reading frame 43
77	78	SMC6	structural maintenance of chromosomes 6
78	78	COMT	catechol-O-methyltransferase
79	77	SRI	sorcin

80	77	NOL9	nucleolar protein 9
81	76	SLC9C1	solute carrier family 9, subfamily C (Na+-transporting carboxylic acid decarboxylase), member 1
82	75	FGF9	fibroblast growth factor 9
83	75	ATF2	activating transcription factor 2
84	75	PREPL	prolyl endopeptidase-like
85	75	JPH1	junctophilin 1
86	75	RICTOR	RPTOR independent companion of MTOR, complex 2
87	75	DSG2	desmoglein 2
88	75	JADE1	jade family PHD finger 1
89	74	PRKCE	protein kinase C, epsilon
90	74	RAB5C	RAB5C, member RAS oncogene family
91	74	DGCR8	DGCR8 microprocessor complex subunit
92	74	IRF2BPL	interferon regulatory factor 2 binding protein-like
93	74	PCDHB13	protocadherin beta 13
94	74	UBE2V1	ubiquitin-conjugating enzyme E2 variant 1
95	73	CPNE4	copine IV
96	73	RAD51	RAD51 recombinase
97	73	SEC11A	SEC11 homolog A (S. cerevisiae)
98	73	RTKN2	rhotekin 2
99	72	VPS13A	vacuolar protein sorting 13 homolog A (S. cerevisiae)
100	72	ZCCHC6	zinc finger, CCHC domain containing 6
101	72	C12orf29	chromosome 12 open reading frame 29
102	71	ZBTB10	zinc finger and BTB domain containing 10
103	71	TNFSF10	tumor necrosis factor (ligand) superfamily, member 10
104	71	P4HA1	prolyl 4-hydroxylase, alpha polypeptide I
105	71	RMDN3	regulator of microtubule dynamics 3
106	71	PNISR	PNN-interacting serine/arginine-rich protein
107	71	VCPIP1	valosin containing protein (p97)/p47 complex interacting protein 1
108	70	SECISBP2L	SECIS binding protein 2-like
109	70	SLC1A3	solute carrier family 1 (glial high affinity glutamate transporter), member 3
110	70	ANKRD40	ankyrin repeat domain 40
111	70	ZIC3	Zic family member 3
112	70	IKZF2	IKAROS family zinc finger 2 (Helios)
113	69	ZEB2	zinc finger E-box binding homeobox 2
114	68	ENPP2	ectonucleotide pyrophosphatase/phosphodiesterase 2
115	68	FAM199X	family with sequence similarity 199, X-linked
116	68	SHISA6	shisa family member 6
117	68	HEPHL1	hephaestin-like 1
118	68	KCNA4	potassium voltage-gated channel, shaker-related subfamily, member 4
119	68	IKZF5	IKAROS family zinc finger 5 (Pegasus)

120	68	CDC5L	cell division cycle 5-like
121	67	GTPBP4	GTP binding protein 4
122	67	SCRN1	secernin 1
123	67	DEPDC1B	DEP domain containing 1B
124	67	SIAH3	siah E3 ubiquitin protein ligase family member 3
125	67	TMTC3	transmembrane and tetratricopeptide repeat containing 3
126	67	PHLPP2	PH domain and leucine rich repeat protein phosphatase 2
127	67	CLDN11	claudin 11
128	66	RNF220	ring finger protein 220
129	66	FAM117B	family with sequence similarity 117, member B
130	66	EDAR	ectodysplasin A receptor
131	66	DNM1L	dynamin 1-like
132	66	FBN1	fibrillin 1
133	66	ZNF24	zinc finger protein 24
134	66	ZSWIM7	zinc finger, SWIM-type containing 7
135	66	UHRF1BP1	UHRF1 binding protein 1
136	66	TRAM1	translocation associated membrane protein 1
137	66	CDC27	cell division cycle 27
138	65	ADAM10	ADAM metallopeptidase domain 10
139	65	SMEK2	SMEK homolog 2, suppressor of mek1 (Dictyostelium)
140	65	FNBP4	formin binding protein 4
141	65	MEIS3	Meis homeobox 3
142	65	DUSP11	dual specificity phosphatase 11 (RNA/RNP complex 1-interacting)
143	65	NRARP	NOTCH-regulated ankyrin repeat protein
144	64	TGFA	transforming growth factor, alpha
145	64	ERCC4	excision repair cross-complementation group 4
146	64	FLRT2	fibronectin leucine rich transmembrane protein 2
147	64	NAV2	neuron navigator 2
148	64	ELMOD2	ELMO/CED-12 domain containing 2
149	63	CNOT7	CCR4-NOT transcription complex, subunit 7
150	63	GDF9	growth differentiation factor 9
151	63	ATRN	attractin
152	63	PTP4A1	protein tyrosine phosphatase type IVA, member 1
153	63	RALA	v-ral simian leukemia viral oncogene homolog A (ras related)
154	63	CHL1	cell adhesion molecule L1-like
155	63	PRKAA1	protein kinase, AMP-activated, alpha 1 catalytic subunit
156	63	LIMA1	LIM domain and actin binding 1
157	62	UBE2E1	ubiquitin-conjugating enzyme E2E 1
158	62	ATXN3	ataxin 3
159	62	LAMA4	laminin, alpha 4

160	62	TMEM64	transmembrane protein 64
161	62	SLC39A12	solute carrier family 39 (zinc transporter), member 12
162	61	STAU2	staufen double-stranded RNA binding protein 2
163	61	VPS13D	vacuolar protein sorting 13 homolog D (S. cerevisiae)
164	61	FAM172A	family with sequence similarity 172, member A
165	61	SKP1	S-phase kinase-associated protein 1
166	61	ARHGAP12	Rho GTPase activating protein 12
167	61	ZUFSP	zinc finger with UFM1-specific peptidase domain
168	60	C18orf54	chromosome 18 open reading frame 54
169	60	PRKAR1A	protein kinase, cAMP-dependent, regulatory, type I, alpha
170	60	AEBP2	AE binding protein 2
171	60	PLXNC1	plexin C1
172	60	STEAP2	STEAP family member 2, metalloreductase
173	60	YPEL1	yippee-like 1 (Drosophila)

Appendix 3: Predicted miR-499 targets in human tissue

Target Rank	Target Score	Gene Symbol	Gene Description
1	100	LPPR4	lipid phosphate phosphatase-related protein type 4
2	100	PTPLAD1	protein tyrosine phosphatase-like A domain containing 1
3	100	GLCCI1	glucocorticoid induced transcript 1
4	99	TPPP	tubulin polymerization promoting protein
5	99	ZMAT3	zinc finger, matrin-type 3
6	99	SLC44A1	solute carrier family 44 (choline transporter), member 1
7	99	CDK14	cyclin-dependent kinase 14
8	98	SNX2	sorting nexin 2
9	98	IP6K2	inositol hexakisphosphate kinase 2
10	98	NRP1	neuropilin 1
11	98	EIF4E	eukaryotic translation initiation factor 4E
12	98	FNDC3A	fibronectin type III domain containing 3A
13	98	EIF1AX	eukaryotic translation initiation factor 1A, X-linked
14	98	C2orf69	chromosome 2 open reading frame 69
15	98	VAMP2	vesicle-associated membrane protein 2 (synaptobrevin 2)
16	98	SOWAHC	sosondowah ankyrin repeat domain family member C
17	98	ANKIB1	ankyrin repeat and IBR domain containing 1
18	97	DDX5	DEAD (Asp-Glu-Ala-Asp) box helicase 5
19	97	KTN1	kinectin 1 (kinesin receptor)
20	97	HNRNPA3	heterogeneous nuclear ribonucleoprotein A3
21	97	ZNF280D	zinc finger protein 280D
22	97	RIT2	Ras-like without CAAX 2
23	97	CLCN3	chloride channel, voltage-sensitive 3
24	97	WDR48	WD repeat domain 48
25	97	AJUBA	ajuba LIM protein
26	97	HELZ2	helicase with zinc finger 2, transcriptional coactivator
27	97	ARCN1	archain 1
28	97	SMIM14	small integral membrane protein 14
29	96	HSP90B1	heat shock protein 90kDa beta (Grp94), member 1
30	96	C5orf51	chromosome 5 open reading frame 51
31	96	HNRNPU	heterogeneous nuclear ribonucleoprotein U (scaffold attachment factor A)
32	96	PHAX	phosphorylated adaptor for RNA export
33	96	NXT2	nuclear transport factor 2-like export factor 2
34	95	TMCC1	transmembrane and coiled-coil domain family 1
35	95	EDN1	endothelin 1
36	95	SRSF1	serine/arginine-rich splicing factor 1
37	95	CAAP1	caspase activity and apoptosis inhibitor 1
38	95	RAD54B	RAD54 homolog B (S. cerevisiae)
39	95	DGKH	diacylglycerol kinase, eta

40	95	CLTC	clathrin, heavy chain (Hc)
41	95	TAGLN2	transgelin 2
42	95	TMEM178A	transmembrane protein 178A
43	95	ETS1	v-ets avian erythroblastosis virus E26 oncogene homolog 1
44	94	TMOD2	tropomodulin 2 (neuronal)
45	94	GCH1	GTP cyclohydrolase 1
46	94	TMEM243	transmembrane protein 243, mitochondrial
47	94	SCAF11	SR-related CTD-associated factor 11
48	94	ANKRD29	ankyrin repeat domain 29
49	94	MAB21L1	mab-21-like 1 (C. elegans)
50	94	API5	apoptosis inhibitor 5
51	94	CNN3	calponin 3, acidic
52	94	RARB	retinoic acid receptor, beta
53	94	SPRED1	sprouty-related, EVH1 domain containing 1
54	94	CHSY1	chondroitin sulfate synthase 1
55	94	NCL	nucleolin
56	94	CPEB1	cytoplasmic polyadenylation element binding protein 1
57	93	THBS1	thrombospondin 1
58	93	SLC28A3	solute carrier family 28 (concentrative nucleoside transporter), member 3
59	93	TBC1D15	TBC1 domain family, member 15
60	93	CPED1	cadherin-like and PC-esterase domain containing 1
61	93	PDCD10	programmed cell death 10
62	93	CEBPZ	CCAAT/enhancer binding protein (C/EBP), zeta
63	93	SULF1	sulfatase 1
64	93	TNKS2	tankyrase, TRF1-interacting ankyrin-related ADP-ribose polymerase 2
65	93	CLOCK	clock circadian regulator
66	92	BDNF	brain-derived neurotrophic factor
67	92	HSPD1	heat shock 60kDa protein 1 (chaperonin)
68	92	C2CD5	C2 calcium-dependent domain containing 5
69	92	TRAPPC3	trafficking protein particle complex 3
70	92	HS3ST3B1	heparan sulfate (glucosamine) 3-O-sulfotransferase 3B1
71	92	MMD2	monocyte to macrophage differentiation-associated 2
72	92	PFDN1	prefoldin subunit 1
73	91	YWHAQ	tyrosine 3-monooxygenase/tryptophan 5-monooxygenase activation protein, theta
74	91	NEDD9	neural precursor cell expressed, developmentally down-regulated 9
75	91	PBX1	pre-B-cell leukemia homeobox 1
76	91	TSPAN4	tetraspanin 4
77	90	GPR137C	G protein-coupled receptor 137C
78	90	ZNF24	zinc finger protein 24
79	90	GJA1	gap junction protein, alpha 1, 43kDa

80	90	MXD1	MAX dimerization protein 1
81	90	PAX3	paired box 3
82	90	MEOX2	mesenchyme homeobox 2
83	90	IMPACT	impact RWD domain protein
84	90	GNPDA2	glucosamine-6-phosphate deaminase 2
85	90	ADPGK	ADP-dependent glucokinase
86	89	SRGAP2	SLIT-ROBO Rho GTPase activating protein 2
87	89	FAM91A1	family with sequence similarity 91, member A1
88	89	ATP6V1A	ATPase, H+ transporting, lysosomal 70kDa, V1 subunit A
89	89	USP33	ubiquitin specific peptidase 33
90	89	SLC25A22	solute carrier family 25 (mitochondrial carrier: glutamate), member 22
91	88	KIF2A	kinesin heavy chain member 2A
92	88	KANK4	KN motif and ankyrin repeat domains 4
93	88	E2F5	E2F transcription factor 5, p130-binding
94	88	UNC119B	unc-119 homolog B (C. elegans)
95	88	UST	uronyl-2-sulfotransferase
96	88	STEAP2	STEAP family member 2, metalloreductase
97	88	BCL11A	B-cell CLL/lymphoma 11A (zinc finger protein)
98	88	ADAMTSL3	ADAMTS-like 3
99	88	TRA2B	transformer 2 beta homolog (Drosophila)
100	88	UTRN	utrophin
101	88	KCNIP3	Kv channel interacting protein 3, calsenilin
102	88	SRSF9	serine/arginine-rich splicing factor 9
103	88	NDRG3	NDRG family member 3
104	88	OSBPL7	oxysterol binding protein-like 7
105	87	SFRP1	secreted frizzled-related protein 1
106	87	PDIK1L	PDLIM1 interacting kinase 1 like
107	87	AP1G1	adaptor-related protein complex 1, gamma 1 subunit
108	87	SLC10A7	solute carrier family 10, member 7
109	87	ARFIP1	ADP-ribosylation factor interacting protein 1
110	86	FAM63B	family with sequence similarity 63, member B
111	86	TKT	transketolase
112	86	NET1	neuroepithelial cell transforming 1
113	86	MON2	MON2 homolog (S. cerevisiae)
114	86	TRIM2	tripartite motif containing 2
115	86	NBEA	neurobeachin
116	86	DGKE	diacylglycerol kinase, epsilon 64kDa
117	86	SLC8A1	solute carrier family 8 (sodium/calcium exchanger), member 1
118	86	WWC1	WW and C2 domain containing 1
119	85	MAP3K1	mitogen-activated protein kinase kinase kinase 1, E3 ubiquitin protein ligase

120	85	FAM84A	family with sequence similarity 84, member A
121	85	PCDHB13	protocadherin beta 13
122	85	Septin 6	septin 6
123	85	SAMD8	sterile alpha motif domain containing 8
124	85	GPD2	glycerol-3-phosphate dehydrogenase 2 (mitochondrial)
125	85	FN1	fibronectin 1
126	85	HMBOX1	homeobox containing 1
127	85	IGF1	insulin-like growth factor 1 (somatomedin C)
128	85	STC2	stanniocalcin 2
129	85	AP3D1	adaptor-related protein complex 3, delta 1 subunit
130	84	WBP1L	WW domain binding protein 1-like
131	84	PGM2	phosphoglucomutase 2
132	84	AZIN1	antizyme inhibitor 1
133	84	CBL	Cbl proto-oncogene, E3 ubiquitin protein ligase
134	84	MAL2	mal, T-cell differentiation protein 2 (gene/pseudogene)
135	83	SLC25A36	solute carrier family 25 (pyrimidine nucleotide carrier), member 36
136	83	MGAT4A	mannosyl (alpha-1,3-)-glycoprotein beta-1,4-N-acetylglucosaminyltransferase, isozyme A
137	83	NFATC3	nuclear factor of activated T-cells, cytoplasmic, calcineurin-dependent 3
138	83	FBP1	fructose-1,6-bisphosphatase 1
139	82	DRD1	dopamine receptor D1
140	82	SDPR	serum deprivation response
141	82	MCHR1	melanin-concentrating hormone receptor 1
142	82	PRKRIR	protein-kinase, interferon-inducible double stranded RNA dependent inhibitor, repressor of (P58 repressor)
143	82	LRRC8A	leucine rich repeat containing 8 family, member A
144	82	CREM	cAMP responsive element modulator
145	82	TBP	TATA box binding protein
146	81	METTL21A	methyltransferase like 21A
147	81	RICTOR	RPTOR independent companion of MTOR, complex 2
148	81	CTTNBP2NL	CTTNBP2 N-terminal like
149	81	SPATS2L	spermatogenesis associated, serine-rich 2-like
150	81	BHLHE22	basic helix-loop-helix family, member e22
151	81	ATRNL1	attractin-like 1
152	81	MMD	monocyte to macrophage differentiation-associated
153	81	FRS2	fibroblast growth factor receptor substrate 2
154	80	CORO1C	coronin, actin binding protein, 1C
155	80	SEC22C	SEC22 vesicle trafficking protein homolog C (S. cerevisiae)
156	80	RNF165	ring finger protein 165
157	80	PPIB	peptidylprolyl isomerase B (cyclophilin B)
158	80	RASA1	RAS p21 protein activator (GTPase activating protein) 1

159	80	LRCH1	leucine-rich repeats and calponin homology (CH) domain containing 1
160	80	ANXA2	annexin A2
161	79	CD2AP	CD2-associated protein
162	79	G6PD	glucose-6-phosphate dehydrogenase
163	79	BACH2	BTB and CNC homology 1, basic leucine zipper transcription factor 2
164	79	PABPC1L2B	poly(A) binding protein, cytoplasmic 1-like 2B
165	79	ZNF800	zinc finger protein 800
166	79	POGK	pogo transposable element with KRAB domain
167	78	JOSD1	Josephin domain containing 1
168	78	HIAT1	hippocampus abundant transcript 1
169	78	CXorf23	chromosome X open reading frame 23
170	78	UBE4A	ubiquitination factor E4A
171	78	ARID2	AT rich interactive domain 2 (ARID, RFX-like)
172	77	MIPOL1	mirror-image polydactyly 1
173	77	C20orf112	chromosome 20 open reading frame 112
174	77	C15orf57	chromosome 15 open reading frame 57
175	76	VAMP4	vesicle-associated membrane protein 4
176	76	KIAA2022	KIAA2022
177	76	ABCB7	ATP-binding cassette, sub-family B (MDR/TAP), member 7
178	76	ADAR	adenosine deaminase, RNA-specific
179	76	FBXL14	F-box and leucine-rich repeat protein 14
180	76	RTN4IP1	reticulon 4 interacting protein 1
181	76	C12orf49	chromosome 12 open reading frame 49
182	76	CAV2	caveolin 2
183	76	HOOK1	hook microtubule-tethering protein 1
184	76	AKAP11	A kinase (PRKA) anchor protein 11
185	75	ARF3	ADP-ribosylation factor 3
186	75	BAG4	BCL2-associated athanogene 4
187	75	EYA4	eyes absent homolog 4 (Drosophila)
188	75	RSBN1	round spermatid basic protein 1
189	75	EBPL	emopamil binding protein-like
190	75	KCTD10	potassium channel tetramerization domain containing 10
191	75	UHMK1	U2AF homology motif (UHM) kinase 1
192	75	JARID2	jumonji, AT rich interactive domain 2
193	75	PRKCE	protein kinase C, epsilon
194	75	ASH2L	ash2 (absent, small, or homeotic)-like (Drosophila)
195	75	ABHD6	abhydrolase domain containing 6
196	75	PAFAH1B1	platelet-activating factor acetylhydrolase 1b, regulatory subunit 1 (45kDa)
197	75	HACE1	HECT domain and ankyrin repeat containing E3 ubiquitin protein ligase 1
198	74	TNPO2	transportin 2

199	74	BET1	Bet1 golgi vesicular membrane trafficking protein
200	74	SH3BGRL	SH3 domain binding glutamate-rich protein like
201	74	ZFP36L1	ZFP36 ring finger protein-like 1
202	74	PPP1R3B	protein phosphatase 1, regulatory subunit 3B
203	74	SMEK2	SMEK homolog 2, suppressor of mek1 (Dictyostelium)
204	74	WDR61	WD repeat domain 61
205	73	CREBL2	cAMP responsive element binding protein-like 2
206	73	EML3	echinoderm microtubule associated protein like 3
207	73	ATF2	activating transcription factor 2
208	73	ABI2	abl-interactor 2
209	73	TWF1	twinfilin actin-binding protein 1
210	73	MSANTD2	Myb/SANT-like DNA-binding domain containing 2
211	73	RFWD3	ring finger and WD repeat domain 3
212	73	TSPAN9	tetraspanin 9
213	73	RAB5A	RAB5A, member RAS oncogene family
214	73	SNAP25	synaptosomal-associated protein, 25kDa
215	73	SLC35F1	solute carrier family 35, member F1
216	73	SUV420H1	suppressor of variegation 4-20 homolog 1 (Drosophila)
217	73	PDE7A	phosphodiesterase 7A
218	73	SPATA13	spermatogenesis associated 13
219	72	DDX55	DEAD (Asp-Glu-Ala-Asp) box polypeptide 55
220	72	HIPK3	homeodomain interacting protein kinase 3
221	72	TMSB4X	thymosin beta 4, X-linked
222	72	BPNT1	3'(2'), 5'-bisphosphate nucleotidase 1
223	72	RNF145	ring finger protein 145
224	72	LARP4	La ribonucleoprotein domain family, member 4
225	72	ZDHHC21	zinc finger, DHHC-type containing 21
226	71	PUM2	pumilio RNA-binding family member 2
227	71	GPR125	G protein-coupled receptor 125
228	71	SRI	sorcin
229	71	ZNF609	zinc finger protein 609
230	71	MAP1A	microtubule-associated protein 1A
231	71	LASP1	LIM and SH3 protein 1
232	71	PEAK1	pseudopodium-enriched atypical kinase 1
233	71	SYN3	synapsin III
234	70	RNF138	ring finger protein 138, E3 ubiquitin protein ligase
235	70	MRO	maestro
236	70	TTC7B	tetratricopeptide repeat domain 7B
237	70	PTPRG	protein tyrosine phosphatase, receptor type, G
238	70	MATR3	matrin 3
239	70	PTPN1	protein tyrosine phosphatase, non-receptor type 1

240	70	RAPH1	Ras association (RalGDS/AF-6) and pleckstrin homology domains 1
241	70	EPHB1	EPH receptor B1
242	69	PHF6	PHD finger protein 6
243	69	MYOCD	myocardin
244	69	WEE1	WEE1 G2 checkpoint kinase
245	69	SEC63	SEC63 homolog (S. cerevisiae)
246	69	ZNF547	zinc finger protein 547
247	69	PABPC4L	poly(A) binding protein, cytoplasmic 4-like
248	69	ARHGEF18	Rho/Rac guanine nucleotide exchange factor (GEF) 18
249	68	ABHD2	abhydrolase domain containing 2
250	68	DHX15	DEAH (Asp-Glu-Ala-His) box helicase 15
251	68	HNRNPK	heterogeneous nuclear ribonucleoprotein K
252	68	FBXO33	F-box protein 33
253	68	C2orf71	chromosome 2 open reading frame 71
254	67	NETO2	neuropilin (NRP) and tolloid (TLL)-like 2
255	67	IFI44L	interferon-induced protein 44-like
256	67	ACER2	alkaline ceramidase 2
257	67	CDC42SE1	CDC42 small effector 1
258	67	OTX2	orthodenticle homeobox 2
259	66	NAP1L5	nucleosome assembly protein 1-like 5
260	66	ZBTB4	zinc finger and BTB domain containing 4
261	66	YWHAZ	tyrosine 3-monooxygenase/tryptophan 5-monooxygenase activation protein, zeta
262	66	SLC25A17	solute carrier family 25 (mitochondrial carrier; peroxisomal membrane protein, 34kDa), member 17
263	65	C3orf80	chromosome 3 open reading frame 80
264	65	POLA1	polymerase (DNA directed), alpha 1, catalytic subunit
265	65	CASK	calcium/calmodulin-dependent serine protein kinase (MAGUK family)
266	65	TMEM68	transmembrane protein 68
267	65	AMOT	angiomotin
268	65	GRK6	G protein-coupled receptor kinase 6
269	65	TBC1D9	TBC1 domain family, member 9 (with GRAM domain)
270	65	BSCL2	Berardinelli-Seip congenital lipodystrophy 2 (seipin)
271	64	NDFIP1	Nedd4 family interacting protein 1
272	64	LOC102723422	uncharacterized LOC102723422
273	64	HIGD1A	HIG1 hypoxia inducible domain family, member 1A
274	64	ZNF281	zinc finger protein 281
275	64	COIL	coilin
276	64	TMEM232	transmembrane protein 232
277	63	ZEB2	zinc finger E-box binding homeobox 2
278	63	KMT2E	lysine (K)-specific methyltransferase 2E
279	63	RNF111	ring finger protein 111

280	63	HMGCR	3-hydroxy-3-methylglutaryl-CoA reductase
281	63	NFATC2	nuclear factor of activated T-cells, cytoplasmic, calcineurin-dependent 2
282	63	DLG4	discs, large homolog 4 (Drosophila)
283	63	BCKDHB	branched chain keto acid dehydrogenase E1, beta polypeptide
284	63	WNT3	wingless-type MMTV integration site family, member 3
285	62	PRR14L	proline rich 14-like
286	62	FUBP1	far upstream element (FUSE) binding protein 1
287	62	SUSD1	sushi domain containing 1
288	62	NUP50	nucleoporin 50kDa
289	62	FAM72B	family with sequence similarity 72, member B
290	62	FAM72D	family with sequence similarity 72, member D
291	62	TCF7L2	transcription factor 7-like 2 (T-cell specific, HMG-box)
292	62	SEMA6D	sema domain, transmembrane domain (TM), and cytoplasmic domain, (semaphorin) 6D
293	62	ARHGAP20	Rho GTPase activating protein 20
294	62	PSIP1	PC4 and SFRS1 interacting protein 1
295	62	FAM72A	family with sequence similarity 72, member A
296	62	FAM72C	family with sequence similarity 72, member C
297	62	TEX35	testis expressed 35
298	61	TMED5	transmembrane emp24 protein transport domain containing 5
299	61	CPLX2	complexin 2
300	61	ANXA4	annexin A4
301	61	TMEM55B	transmembrane protein 55B
302	61	CELF2	CUGBP, Elav-like family member 2
303	61	FNDC3B	fibronectin type III domain containing 3B
304	61	STXBP4	syntaxin binding protein 4
305	61	UNC50	unc-50 homolog (C. elegans)
306	61	SLC38A3	solute carrier family 38, member 3
307	61	RAB43	RAB43, member RAS oncogene family
308	61	PI15	peptidase inhibitor 15
309	61	ZNF148	zinc finger protein 148
310	60	RYBP	RING1 and YY1 binding protein
311	60	CCL2	chemokine (C-C motif) ligand 2
312	60	NOTCH2	notch 2
313	60	ZNF516	zinc finger protein 516
314	60	THAP5	THAP domain containing 5
315	60	NADK	NAD kinase
316	60	TNPO1	transportin 1
317	60	VSIG1	V-set and immunoglobulin domain containing 1
318	60	SP2	Sp2 transcription factor

Appendix 4: Predicted miR-1 targets in human tissue

Target Rank	Target Score	Gene Symbol	Gene Description
1	100	TNRC6A	trinucleotide repeat containing 6A
2	100	CELSR3	cadherin, EGF LAG seven-pass G-type receptor 3
3	100	LHX8	LIM homeobox 8
4	100	EED	embryonic ectoderm development
5	100	SCN2A	sodium channel, voltage-gated, type II, alpha subunit
6	100	ANKRA2	ankyrin repeat, family A (RFXANK-like), 2
7	100	BRWD3	bromodomain and WD repeat domain containing 3
8	100	PLEKHM3	pleckstrin homology domain containing, family M, member 3
9	100	NT5E	5'-nucleotidase, ecto (CD73)
10	100	PHTF2	putative homeodomain transcription factor 2
11	100	YAF2	YY1 associated factor 2
12	100	WDR7	WD repeat domain 7
13	100	RFX7	regulatory factor X, 7
14	100	EEA1	early endosome antigen 1
15	100	POLR3E	polymerase (RNA) III (DNA directed) polypeptide E (80kD)
16	100	KLHL20	kelch-like family member 20
17	99	PPARGC1B	peroxisome proliferator-activated receptor gamma, coactivator 1 beta
18	99	ANKRD17	ankyrin repeat domain 17
19	99	PCGF5	polycomb group ring finger 5
20	99	STK39	serine threonine kinase 39
21	99	STAC	SH3 and cysteine rich domain
22	99	PDE7A	phosphodiesterase 7A
23	99	PTP4A1	protein tyrosine phosphatase type IVA, member 1
24	99	GMNC	geminin coiled-coil domain containing
25	99	SCN9A	sodium channel, voltage-gated, type IX, alpha subunit
26	99	CCDC43	coiled-coil domain containing 43
27	99	EML4	echinoderm microtubule associated protein like 4
28	99	RTKN2	rhotekin 2
29	99	PIP4K2A	phosphatidylinositol-5-phosphate 4-kinase, type II, alpha
30	99	KLF10	Kruppel-like factor 10
31	99	DDAH1	dimethylarginine dimethylaminohydrolase 1
32	99	RRAD	Ras-related associated with diabetes
33	99	LRRC40	leucine rich repeat containing 40
34	99	MBNL3	muscleblind-like splicing regulator 3
35	98	PIK3CD	phosphatidylinositol-4,5-bisphosphate 3-kinase, catalytic subunit delta
36	98	EXTL2	exostosin-like glycosyltransferase 2
37	98	CCNE2	cyclin E2
38	98	ATG12	autophagy related 12
39	98	ZBTB41	zinc finger and BTB domain containing 41

40	98	COL13A1	collagen, type XIII, alpha 1
41	98	LRRC17	leucine rich repeat containing 17
42	98	SNX18	sorting nexin 18
43	98	USP37	ubiquitin specific peptidase 37
44	98	REEP3	receptor accessory protein 3
45	98	CAMK2D	calcium/calmodulin-dependent protein kinase II delta
46	98	TMEM181	transmembrane protein 181
47	98	UBE2V2	ubiquitin-conjugating enzyme E2 variant 2
48	98	KIAA2026	KIAA2026
49	98	ZMYND8	zinc finger, MYND-type containing 8
50	98	STOX2	storkhead box 2
51	98	FOXG1	forkhead box G1
52	98	ALG10	ALG10, alpha-1,2-glucosyltransferase
53	98	FAM160B1	family with sequence similarity 160, member B1
54	98	LCLAT1	lysocardiolipin acyltransferase 1
55	98	PTGFRN	prostaglandin F2 receptor inhibitor
56	98	ADAMTS9	ADAM metallopeptidase with thrombospondin type 1 motif, 9
57	98	NRIP1	nuclear receptor interacting protein 1
58	98	PTPN13	protein tyrosine phosphatase, non-receptor type 13 (APO-1/CD95 (Fas)-associated phosphatase)
59	98	CCDC97	coiled-coil domain containing 97
60	98	PRDM1	PR domain containing 1, with ZNF domain
61	98	FRZB	frizzled-related protein
62	98	PPP3R1	protein phosphatase 3, regulatory subunit B, alpha
63	98	BRD1	bromodomain containing 1
64	97	GRIA2	glutamate receptor, ionotropic, AMPA 2
65	97	ZNRF1	zinc and ring finger 1, E3 ubiquitin protein ligase
66	97	KLHL28	kelch-like family member 28
67	97	TTLL7	tubulin tyrosine ligase-like family, member 7
68	97	PPP4R4	protein phosphatase 4, regulatory subunit 4
69	97	OTUD6B	OTU domain containing 6B
70	97	LRRK2	leucine-rich repeat kinase 2
71	97	SLC12A6	solute carrier family 12 (potassium/chloride transporter), member 6
72	97	ZNF608	zinc finger protein 608
73	97	YTHDF3	YTH domain family, member 3
74	97	SCN1A	sodium channel, voltage-gated, type I, alpha subunit
75	97	ITGA6	integrin, alpha 6
76	97	ABCC9	ATP-binding cassette, sub-family C (CFTR/MRP), member 9
77	97	SETD5	SET domain containing 5
78	96	STX16	syntaxin 16
79	96	RAP1B	RAP1B, member of RAS oncogene family

80	96	BNIP3L	BCL2/adenovirus E1B 19kDa interacting protein 3-like
81	96	DESI2	desumoylating isopeptidase 2
82	96	CLOCK	clock circadian regulator
83	96	GSKIP	GSK3B interacting protein
84	96	FLVCR2	feline leukemia virus subgroup C cellular receptor family, member 2
85	96	SLC35A3	solute carrier family 35 (UDP-N-acetylglucosamine (UDP-GlcNAc) transporter), member A3
86	96	BDP1	B double prime 1, subunit of RNA polymerase III transcription initiation factor IIIB
87	96	LPPR4	lipid phosphate phosphatase-related protein type 4
88	96	CALU	calumenin
89	96	PCDH17	protocadherin 17
90	96	ANKHD1	ankyrin repeat and KH domain containing 1
91	96	RIMBP2	RIMS binding protein 2
92	96	DNMT3A	DNA (cytosine-5-)-methyltransferase 3 alpha
93	96	RAPGEF2	Rap guanine nucleotide exchange factor (GEF) 2
94	96	CAPZA1	capping protein (actin filament) muscle Z-line, alpha 1
95	96	LIN28B	lin-28 homolog B (C. elegans)
96	96	PAPD4	PAP associated domain containing 4
97	96	EDEM3	ER degradation enhancer, mannosidase alpha-like 3
98	95	FAP	fibroblast activation protein, alpha
99	95	RARG	retinoic acid receptor, gamma
100	95	PAPOLA	poly(A) polymerase alpha
101	95	MAN1A2	mannosidase, alpha, class 1A, member 2
102	95	MEX3B	mex-3 RNA binding family member B
103	95	CHL1	cell adhesion molecule L1-like
104	95	CADPS	Ca++-dependent secretion activator
105	95	SRSF7	serine/arginine-rich splicing factor 7
106	95	FYCO1	FYVE and coiled-coil domain containing 1
107	95	MAML1	mastermind-like 1 (Drosophila)
108	95	CBX2	chromobox homolog 2
109	95	CARS	cysteinyl-tRNA synthetase
110	95	GRM3	glutamate receptor, metabotropic 3
111	95	EML1	echinoderm microtubule associated protein like 1
112	95	KDM3A	lysine (K)-specific demethylase 3A
113	95	CHST2	carbohydrate (N-acetylglucosamine-6-O) sulfotransferase 2
114	95	ZBTB39	zinc finger and BTB domain containing 39
115	95	ARID4A	AT rich interactive domain 4A (RBP1-like)
116	95	FNDC3A	fibronectin type III domain containing 3A
117	95	MIER3	mesoderm induction early response 1, family member 3
118	95	PNKD	paroxysmal nonkinesigenic dyskinesia
119	95	TMEM87A	transmembrane protein 87A

120	95	B3GNT5	UDP-GlcNAc:betaGal beta-1,3-N-acetylglucosaminyltransferase 5
121	95	CBLB	Cbl proto-oncogene B, E3 ubiquitin protein ligase
122	94	BCOR	BCL6 corepressor
123	94	NAALADL2	N-acetylated alpha-linked acidic dipeptidase-like 2
124	94	CALCR	calcitonin receptor
125	94	ADAM19	ADAM metallopeptidase domain 19
126	94	ARF4	ADP-ribosylation factor 4
127	94	MARF6	membrane-associated ring finger (C3HC4) 6, E3 ubiquitin protein ligase
128	94	DSG2	desmoglein 2
129	94	PPAPDC2	phosphatidic acid phosphatase type 2 domain containing 2
130	94	FAM210B	family with sequence similarity 210, member B
131	94	PIGA	phosphatidylinositol glycan anchor biosynthesis, class A
132	94	B4GALT6	UDP-Gal:betaGlcNAc beta 1,4- galactosyltransferase, polypeptide 6
133	94	MMD	monocyte to macrophage differentiation-associated
134	94	DLL4	delta-like 4 (Drosophila)
135	94	MBNL2	muscleblind-like splicing regulator 2
136	94	PDSS1	prenyl (decaprenyl) diphosphate synthase, subunit 1
137	94	FBXO45	F-box protein 45
138	94	WIPF1	WAS/WASL interacting protein family, member 1
139	94	KCNMB2	potassium large conductance calcium-activated channel, subfamily M, beta member 2
140	94	SLC38A2	solute carrier family 38, member 2
141	94	MAST4	microtubule associated serine/threonine kinase family member 4
142	94	PCMTD2	protein-L-isoaspartate (D-aspartate) O-methyltransferase domain containing 2
143	94	RQCD1	RCD1 required for cell differentiation1 homolog (S. pombe)
144	94	PHACTR2	phosphatase and actin regulator 2
145	94	RAPGEF4	Rap guanine nucleotide exchange factor (GEF) 4
146	94	LIMCH1	LIM and calponin homology domains 1
147	94	SCN3A	sodium channel, voltage-gated, type III, alpha subunit
148	94	WDR44	WD repeat domain 44
149	93	RUNX2	runt-related transcription factor 2
150	93	NF1	neurofibromin 1
151	93	UBE2J1	ubiquitin-conjugating enzyme E2, J1
152	93	SHOC2	soc-2 suppressor of clear homolog (C. elegans)
153	93	ACTR1A	ARP1 actin-related protein 1 homolog A, centractin alpha (yeast)
154	93	AFF4	AF4/FMR2 family, member 4
155	93	RFX6	regulatory factor X, 6
156	93	KIAA1804	mixed lineage kinase 4
157	93	ZBTB44	zinc finger and BTB domain containing 44

158	93	HCFC2	host cell factor C2
159	93	ENOX2	ecto-NOX disulfide-thiol exchanger 2
160	93	P4HA2	prolyl 4-hydroxylase, alpha polypeptide II
161	93	GOLGA4	golgin A4
162	93	SH3RF1	SH3 domain containing ring finger 1
163	93	TAOK1	TAO kinase 1
164	93	ACTC1	actin, alpha, cardiac muscle 1
165	93	CHD1	chromodomain helicase DNA binding protein 1
166	93	SH2B3	SH2B adaptor protein 3
167	93	PICALM	phosphatidylinositol binding clathrin assembly protein
168	93	PRKAA2	protein kinase, AMP-activated, alpha 2 catalytic subunit
169	93	RAD23B	RAD23 homolog B (S. cerevisiae)
170	93	ZDHHC17	zinc finger, DHHC-type containing 17
171	92	R3HDM1	R3H domain containing 1
172	92	NDEL1	nudE neurodevelopment protein 1-like 1
173	92	CCNT2	cyclin T2
174	92	ABI3BP	ABI family, member 3 (NESH) binding protein
175	92	SAMD4A	sterile alpha motif domain containing 4A
176	92	CCDC117	coiled-coil domain containing 117
177	92	RAB23	RAB23, member RAS oncogene family
178	92	GATM	glycine amidinotransferase (L-arginine:glycine amidinotransferase)
179	92	ZNF280B	zinc finger protein 280B
180	92	SEC24A	SEC24 family member A
181	92	PSMD7	proteasome (prosome, macropain) 26S subunit, non-ATPase, 7
182	92	FNIP2	folliculin interacting protein 2
183	92	FRMD6	FERM domain containing 6
184	92	ARAF	v-raf murine sarcoma 3611 viral oncogene homolog
185	92	TRPM7	transient receptor potential cation channel, subfamily M, member 7
186	92	NFAT5	nuclear factor of activated T-cells 5, tonicity-responsive
187	92	STIM2	stromal interaction molecule 2
188	92	ABL1	c-abl oncogene 1, non-receptor tyrosine kinase
189	92	MFSD6	major facilitator superfamily domain containing 6
190	92	KSR1	kinase suppressor of ras 1
191	91	NECAP1	NECAP endocytosis associated 1
192	91	CDK12	cyclin-dependent kinase 12
193	91	HIVEP1	human immunodeficiency virus type I enhancer binding protein 1
194	91	PPID	peptidylprolyl isomerase D
195	91	ZNF521	zinc finger protein 521
196	91	SCML1	sex comb on midleg-like 1 (Drosophila)
197	91	CACNB2	calcium channel, voltage-dependent, beta 2 subunit

198	91	ELL2	elongation factor, RNA polymerase II, 2
199	91	FAM43A	family with sequence similarity 43, member A
200	91	FAM91A1	family with sequence similarity 91, member A1
201	91	SORCS3	sortilin-related VPS10 domain containing receptor 3
202	91	FZD3	frizzled class receptor 3
203	91	PPP1R14C	protein phosphatase 1, regulatory (inhibitor) subunit 14C
204	91	CSNK1A1	casein kinase 1, alpha 1
205	91	NEDD4	neural precursor cell expressed, developmentally down-regulated 4, E3 ubiquitin protein ligase
206	90	FAHD1	fumarylacetoacetate hydrolase domain containing 1
207	90	TWF1	twinfilin actin-binding protein 1
208	90	ZBTB11	zinc finger and BTB domain containing 11
209	90	FAM214A	family with sequence similarity 214, member A
210	90	DPY19L1	dpy-19-like 1 (C. elegans)
211	90	DCTN4	dynactin 4 (p62)
212	90	ENTHD2	ENTH domain containing 2
213	90	MAP3K13	mitogen-activated protein kinase kinase kinase 13
214	90	BNC1	basonuclin 1
215	90	HOXA1	homeobox A1
216	90	ZFAND5	zinc finger, AN1-type domain 5
217	90	MROH9	maestro heat-like repeat family member 9
218	90	YPEL5	yippee-like 5 (Drosophila)
219	90	SLC4A7	solute carrier family 4, sodium bicarbonate cotransporter, member 7
220	90	PDXDC1	pyridoxal-dependent decarboxylase domain containing 1
221	90	FKBP3	FK506 binding protein 3, 25kDa
222	90	LCORL	ligand dependent nuclear receptor corepressor-like
223	89	KMT2A	lysine (K)-specific methyltransferase 2A
224	89	DNAJC13	DnaJ (Hsp40) homolog, subfamily C, member 13
225	89	CSNK1G1	casein kinase 1, gamma 1
226	89	PON2	paraoxonase 2
227	89	UBE2I	ubiquitin-conjugating enzyme E2I
228	89	CCNK	cyclin K
229	89	NFATC2	nuclear factor of activated T-cells, cytoplasmic, calcineurin-dependent 2
230	89	SON	SON DNA binding protein
231	89	SEC22C	SEC22 vesicle trafficking protein homolog C (S. cerevisiae)
232	88	CPSF6	cleavage and polyadenylation specific factor 6, 68kDa
233	88	MCF2L	MCF.2 cell line derived transforming sequence-like
234	88	MKRN3	makorin ring finger protein 3
235	88	UBN1	ubinuclein 1
236	88	BECN1	beclin 1, autophagy related
237	88	UNC5C	unc-5 homolog C (C. elegans)

238	88	CHKA	choline kinase alpha
239	88	RUNDC3B	RUN domain containing 3B
240	88	LRRC8D	leucine rich repeat containing 8 family, member D
241	88	ELMOD2	ELMO/CED-12 domain containing 2
242	88	ACAP2	ArfGAP with coiled-coil, ankyrin repeat and PH domains 2
243	88	SOX9	SRY (sex determining region Y)-box 9
244	88	TBC1D15	TBC1 domain family, member 15
245	88	ATG5	autophagy related 5
246	88	PPP1R12A	protein phosphatase 1, regulatory subunit 12A
247	88	DPYSL2	dihydropyrimidinase-like 2
248	88	XPO1	exportin 1
249	88	OXR1	oxidation resistance 1
250	87	KMT2C	lysine (K)-specific methyltransferase 2C
251	87	ARID1A	AT rich interactive domain 1A (SWI-like)
252	87	AMOTL2	angiomotin like 2
253	87	AVL9	AVL9 homolog (S. cerevisiase)
254	87	HIC2	hypermethylated in cancer 2
255	87	PAFAH1B2	platelet-activating factor acetylhydrolase 1b, catalytic subunit 2 (30kDa)
256	87	CPNE8	copine VIII
257	87	CNOT6	CCR4-NOT transcription complex, subunit 6
258	87	RORA	RAR-related orphan receptor A
259	87	AFAP1L2	actin filament associated protein 1-like 2
260	87	SP4	Sp4 transcription factor
261	87	SH3PXD2A	SH3 and PX domains 2A
262	87	LRP6	low density lipoprotein receptor-related protein 6
263	86	KIF11	kinesin family member 11
264	86	PAXBP1	PAX3 and PAX7 binding protein 1
265	86	EXOC6	exocyst complex component 6
266	86	BRAP	BRCA1 associated protein
267	86	PPFIA2	protein tyrosine phosphatase, receptor type, f polypeptide (PTPRF), interacting protein (liprin), alpha 2
268	86	KIAA0226L	KIAA0226-like
269	86	RASA1	RAS p21 protein activator (GTPase activating protein) 1
270	86	FAM110B	family with sequence similarity 110, member B
271	86	PTPN2	protein tyrosine phosphatase, non-receptor type 2
272	86	GLCE	glucuronic acid epimerase
273	86	GALNT7	polypeptide N-acetylgalactosaminyltransferase 7
274	86	RPRD1A	regulation of nuclear pre-mRNA domain containing 1A
275	86	LYPLAL1	lysophospholipase-like 1
276	86	SNX10	sorting nexin 10
277	86	LARGE	like-glycosyltransferase
278	86	SPEN	spen family transcriptional repressor

279	86	SRSF10	serine/arginine-rich splicing factor 10
280	86	GOLGA1	golgin A1
281	85	ZBTB18	zinc finger and BTB domain containing 18
282	85	NADK	NAD kinase
283	85	NUS1	nuclear undecaprenyl pyrophosphate synthase 1 homolog (S. cerevisiae)
284	85	SOCS3	suppressor of cytokine signaling 3
285	85	DET1	de-etiolated homolog 1 (Arabidopsis)
286	85	GALNT1	polypeptide N-acetylgalactosaminyltransferase 1
287	85	RAB38	RAB38, member RAS oncogene family
288	85	ADAMTS6	ADAM metallopeptidase with thrombospondin type 1 motif, 6
289	85	MTDH	metadherin
290	85	HNRNPUL2	heterogeneous nuclear ribonucleoprotein U-like 2
291	85	USP2	ubiquitin specific peptidase 2
292	84	KPNA6	karyopherin alpha 6 (importin alpha 7)
293	84	BCL10	B-cell CLL/lymphoma 10
294	84	ME1	malic enzyme 1, NADP(+)-dependent, cytosolic
295	84	RAB4B	RAB4B, member RAS oncogene family
296	84	KLF9	Kruppel-like factor 9
297	84	SEC23A	Sec23 homolog A (S. cerevisiae)
298	84	DOLPP1	dolichyldiphosphatase 1
299	84	PNN	pinin, desmosome associated protein
300	84	C9orf72	chromosome 9 open reading frame 72
301	84	ATAD2B	ATPase family, AAA domain containing 2B
302	84	SDAD1	SDA1 domain containing 1
303	83	MAPK8	mitogen-activated protein kinase 8
304	83	ABCD2	ATP-binding cassette, sub-family D (ALD), member 2
305	83	CSAD	cysteine sulfinic acid decarboxylase
306	83	EBF2	early B-cell factor 2
307	83	NEURL1B	neuralized E3 ubiquitin protein ligase 1B
308	83	IL1RAPL2	interleukin 1 receptor accessory protein-like 2
309	83	GFPT2	glutamine-fructose-6-phosphate transaminase 2
310	83	NEDD4L	neural precursor cell expressed, developmentally down-regulated 4-like, E3 ubiquitin protein ligase
311	83	NRG3	neuregulin 3
312	83	CTNND2	catenin (cadherin-associated protein), delta 2
313	83	LMBR1	limb development membrane protein 1
314	83	CARF	calcium responsive transcription factor
315	83	DACT1	dishevelled-binding antagonist of beta-catenin 1
316	83	ESCO1	establishment of sister chromatid cohesion N-acetyltransferase 1
317	83	MBTPS2	membrane-bound transcription factor peptidase, site 2
318	83	SKP2	S-phase kinase-associated protein 2, E3 ubiquitin protein ligase

319	83	YWHAZ	tyrosine 3-monooxygenase/tryptophan 5-monooxygenase activation protein, zeta
320	83	MEIOB	meiosis specific with OB domains
321	83	SCN8A	sodium channel, voltage gated, type VIII, alpha subunit
322	82	RPS6KA2	ribosomal protein S6 kinase, 90kDa, polypeptide 2
323	82	JAK1	Janus kinase 1
324	82	USP45	ubiquitin specific peptidase 45
325	82	NHLH2	nescient helix loop helix 2
326	82	SLC35D3	solute carrier family 35, member D3
327	82	ACTR3C	ARP3 actin-related protein 3 homolog C (yeast)
328	82	PRLR	prolactin receptor
329	82	ZCCHC6	zinc finger, CCHC domain containing 6
330	82	SNX33	sorting nexin 33
331	82	CCDC6	coiled-coil domain containing 6
332	82	ANO4	anoctamin 4
333	82	NCAM1	neural cell adhesion molecule 1
334	81	WDR64	WD repeat domain 64
335	81	PIP4K2B	phosphatidylinositol-5-phosphate 4-kinase, type II, beta
336	81	SAMD8	sterile alpha motif domain containing 8
337	81	PGP	phosphoglycolate phosphatase
338	81	UBE2D3	ubiquitin-conjugating enzyme E2D 3
339	81	KIAA0408	KIAA0408
340	81	USO1	USO1 vesicle transport factor
341	81	OTUD4	OTU deubiquitinase 4
342	81	SEMA6B	sema domain, transmembrane domain (TM), and cytoplasmic domain, (semaphorin) 6B
343	81	SLC5A3	solute carrier family 5 (sodium/myo-inositol cotransporter), member 3
344	81	HDAC9	histone deacetylase 9
345	81	PLXNC1	plexin C1
346	80	FBXO32	F-box protein 32
347	80	TULP4	tubby like protein 4
348	80	VKORC1L1	vitamin K epoxide reductase complex, subunit 1-like 1
349	80	LPGAT1	lysophosphatidylglycerol acyltransferase 1
350	80	RMND5A	required for meiotic nuclear division 5 homolog A (S. cerevisiae)
351	80	PRUNE2	prune homolog 2 (Drosophila)
352	80	DOK5	docking protein 5
353	80	PGM1	phosphoglucomutase 1
354	80	PAWR	PRKC, apoptosis, WT1, regulator
355	80	MYO1H	myosin IH
356	80	RAP2C	RAP2C, member of RAS oncogene family
357	80	NEUROD6	neuronal differentiation 6
358	80	SHISA3	shisa family member 3

359	79	CDK19	cyclin-dependent kinase 19
360	79	ADRA1D	adrenoceptor alpha 1D
361	79	GABRB1	gamma-aminobutyric acid (GABA) A receptor, beta 1
362	79	SLC6A9	solute carrier family 6 (neurotransmitter transporter, glycine), member 9
363	79	TXNDC5	thioredoxin domain containing 5 (endoplasmic reticulum)
364	79	PHIP	pleckstrin homology domain interacting protein
365	79	PLXNA2	plexin A2
366	79	PPTC7	PTC7 protein phosphatase homolog (S. cerevisiae)
367	79	KIF16B	kinesin family member 16B
368	79	FAM83F	family with sequence similarity 83, member F
369	78	ZNF518A	zinc finger protein 518A
370	78	DLGAP4	discs, large (Drosophila) homolog-associated protein 4
371	78	SGCB	sarcoglycan, beta (43kDa dystrophin-associated glycoprotein)
372	78	VAT1L	vesicle amine transport 1-like
373	78	IP6K3	inositol hexakisphosphate kinase 3
374	78	NEFL	neurofilament, light polypeptide
375	78	CBFB	core-binding factor, beta subunit
376	78	SLC35B4	solute carrier family 35 (UDP-xylose/UDP-N-acetylglucosamine transporter), member B4
377	78	SLC25A36	solute carrier family 25 (pyrimidine nucleotide carrier), member 36
378	78	SIX4	SIX homeobox 4
379	78	VAT1	vesicle amine transport 1
380	78	SOCS1	suppressor of cytokine signaling 1
381	77	LGI1	leucine-rich, glioma inactivated 1
382	77	CFL2	cofilin 2 (muscle)
383	77	CCNA1	cyclin A1
384	77	FGD6	FYVE, RhoGEF and PH domain containing 6
385	77	LRCH2	leucine-rich repeats and calponin homology (CH) domain containing 2
386	77	GRHL1	grainyhead-like 1 (Drosophila)
387	77	CUL2	cullin 2
388	77	ZCCHC24	zinc finger, CCHC domain containing 24
389	77	CDC37L1	cell division cycle 37-like 1
390	77	GNG10	guanine nucleotide binding protein (G protein), gamma 10
391	77	ACTBL2	actin, beta-like 2
392	77	TMEM229A	transmembrane protein 229A
393	77	STRIP1	striatin interacting protein 1
394	77	COL8A1	collagen, type VIII, alpha 1
395	77	SPG20	spastic paraplegia 20 (Troyer syndrome)
396	77	PPARGC1A	peroxisome proliferator-activated receptor gamma, coactivator 1 alpha
397	77	RP11-16E12.2	uncharacterized LOC283710

398	76	SYPL1	synaptophysin-like 1
399	76	ATP2B2	ATPase, Ca++ transporting, plasma membrane 2
400	76	NRBP1	nuclear receptor binding protein 1
401	76	AGO3	argonaute RISC catalytic component 3
402	76	NAPG	N-ethylmaleimide-sensitive factor attachment protein, gamma
403	76	DTWD1	DTW domain containing 1
404	76	ERLIN1	ER lipid raft associated 1
405	76	RHD	Rh blood group, D antigen
406	76	YY2	YY2 transcription factor
407	76	TBC1D10B	TBC1 domain family, member 10B
408	76	ZBTB6	zinc finger and BTB domain containing 6
409	76	MSI2	musashi RNA-binding protein 2
410	76	KIAA0355	KIAA0355
411	76	PRICKLE1	prickle homolog 1 (Drosophila)
412	76	ELOVL7	ELOVL fatty acid elongase 7
413	76	LIN7C	lin-7 homolog C (C. elegans)
414	76	KLF12	Kruppel-like factor 12
415	76	STK35	serine/threonine kinase 35
416	76	RAB10	RAB10, member RAS oncogene family
417	76	UBE2F	ubiquitin-conjugating enzyme E2F (putative)
418	76	ADO	2-aminoethanethiol (cysteamine) dioxygenase
419	76	YIPF6	Yip1 domain family, member 6
420	76	TMEM56	transmembrane protein 56
421	75	NUP93	nucleoporin 93kDa
422	75	XPR1	xenotropic and polytropic retrovirus receptor 1
423	75	EPC2	enhancer of polycomb homolog 2 (Drosophila)
424	75	TMEM121	transmembrane protein 121
425	75	KIAA1715	KIAA1715
426	75	SIX1	SIX homeobox 1
427	75	COL4A3BP	collagen, type IV, alpha 3 (Goodpasture antigen) binding protein
428	75	FAM69A	family with sequence similarity 69, member A
429	75	SLC35F1	solute carrier family 35, member F1
430	75	SAMHD1	SAM domain and HD domain 1
431	75	RASD1	RAS, dexamethasone-induced 1
432	75	FLVCR1	feline leukemia virus subgroup C cellular receptor 1
433	75	CEP350	centrosomal protein 350kDa
434	75	NARG2	NMDA receptor regulated 2
435	75	DDHD2	DDHD domain containing 2
436	75	PFN2	profilin 2
437	74	GLDC	glycine dehydrogenase (decarboxylating)
438	74	DSTYK	dual serine/threonine and tyrosine protein kinase

439	74	CAMKK2	calcium/calmodulin-dependent protein kinase kinase 2, beta
440	74	ARL4A	ADP-ribosylation factor-like 4A
441	74	JAKMIP2	janus kinase and microtubule interacting protein 2
442	74	RNF169	ring finger protein 169
443	74	GNAI2	guanine nucleotide binding protein (G protein), alpha inhibiting activity polypeptide 2
444	74	TMEM47	transmembrane protein 47
445	74	REV1	REV1, polymerase (DNA directed)
446	74	FAM196A	family with sequence similarity 196, member A
447	74	CHST1	carbohydrate (keratan sulfate Gal-6) sulfotransferase 1
448	74	VPS26B	vacuolar protein sorting 26 homolog B (S. pombe)
449	74	ARHGEF6	Rac/Cdc42 guanine nucleotide exchange factor (GEF) 6
450	74	TMEM170B	transmembrane protein 170B
451	74	NKX2-2	NK2 homeobox 2
452	74	NSG1	neuron specific gene family member 1
453	73	ADAM22	ADAM metallopeptidase domain 22
454	73	CYP3A5	cytochrome P450, family 3, subfamily A, polypeptide 5
455	73	RAB32	RAB32, member RAS oncogene family
456	73	CSMD3	CUB and Sushi multiple domains 3
457	73	SCARA5	scavenger receptor class A, member 5 (putative)
458	73	PDS5B	PDS5, regulator of cohesion maintenance, homolog B (S. cerevisiae)
459	73	EPDR1	ependymin related 1
460	73	FRMPD1	FERM and PDZ domain containing 1
461	73	GPCPD1	glycerophosphocholine phosphodiesterase GDE1 homolog (S. cerevisiae)
462	73	IRS1	insulin receptor substrate 1
463	73	SETD3	SET domain containing 3
464	73	TP53INP1	tumor protein p53 inducible nuclear protein 1
465	73	EIF5A2	eukaryotic translation initiation factor 5A2
466	73	S100PBP	S100P binding protein
467	73	TTLL2	tubulin tyrosine ligase-like family, member 2
468	73	NFATC3	nuclear factor of activated T-cells, cytoplasmic, calcineurin-dependent 3
469	73	ATG2B	autophagy related 2B
470	73	LRRC8C	leucine rich repeat containing 8 family, member C
471	73	FAM13A	family with sequence similarity 13, member A
472	73	LYN	v-yes-1 Yamaguchi sarcoma viral related oncogene homolog
473	72	DDIT4	DNA-damage-inducible transcript 4
474	72	SLC30A4	solute carrier family 30 (zinc transporter), member 4
475	72	MAGI2	membrane associated guanylate kinase, WW and PDZ domain containing 2
476	72	GCSAM	germinal center-associated, signaling and motility
477	72	CACHD1	cache domain containing 1

478	72	MZT1	mitotic spindle organizing protein 1
479	72	GMEB2	glucocorticoid modulatory element binding protein 2
480	72	MEIS2	Meis homeobox 2
481	72	UBE2V1	ubiquitin-conjugating enzyme E2 variant 1
482	72	PCDH20	protocadherin 20
483	72	SLC36A4	solute carrier family 36 (proton/amino acid symporter), member 4
484	71	TNKS	tankyrase, TRF1-interacting ankyrin-related ADP-ribose polymerase
485	71	TENM3	teneurin transmembrane protein 3
486	71	CCDC120	coiled-coil domain containing 120
487	71	OCRL	oculocerebrorenal syndrome of Lowe
488	71	KCTD9	potassium channel tetramerization domain containing 9
489	71	KPNA3	karyopherin alpha 3 (importin alpha 4)
490	71	SLC35C1	solute carrier family 35 (GDP-fucose transporter), member C1
491	71	SYNGR3	synaptogyrin 3
492	71	UBAC1	UBA domain containing 1
493	71	REEP1	receptor accessory protein 1
494	71	AKIRIN1	akirin 1
495	71	IL1A	interleukin 1, alpha
496	71	GLI2	GLI family zinc finger 2
497	71	JOSD1	Josephin domain containing 1
498	71	CAPN5	calpain 5
499	71	PPIL4	peptidylprolyl isomerase (cyclophilin)-like 4
500	71	RAB11A	RAB11A, member RAS oncogene family
501	71	IFNAR2	interferon (alpha, beta and omega) receptor 2
502	71	PAK7	p21 protein (Cdc42/Rac)-activated kinase 7
503	71	FBXO34	F-box protein 34
504	71	KXD1	KxDL motif containing 1
505	71	MARK1	MAP/microtubule affinity-regulating kinase 1
506	71	SSX2IP	synovial sarcoma, X breakpoint 2 interacting protein
507	71	BAHD1	bromo adjacent homology domain containing 1
508	71	ARPC5	actin related protein 2/3 complex, subunit 5, 16kDa
509	70	CEP41	centrosomal protein 41kDa
510	70	SPAST	spastin
511	70	LIN28A	lin-28 homolog A (C. elegans)
512	70	VPS13C	vacuolar protein sorting 13 homolog C (S. cerevisiae)
513	70	JPH4	junctophilin 4
514	70	MAN1B1	mannosidase, alpha, class 1B, member 1
515	70	MAP3K12	mitogen-activated protein kinase kinase kinase 12
516	70	PITPNM2	phosphatidylinositol transfer protein, membrane-associated 2
517	70	GIGYF2	GRB10 interacting GYF protein 2

518	70	STC1	stanniocalcin 1
519	70	WDR82	WD repeat domain 82
520	70	NR5A2	nuclear receptor subfamily 5, group A, member 2
521	70	OMG	oligodendrocyte myelin glycoprotein
522	70	C10orf25	chromosome 10 open reading frame 25
523	70	RAB22A	RAB22A, member RAS oncogene family
524	70	CHMP2B	charged multivesicular body protein 2B
525	70	STX12	syntaxin 12
526	70	MATR3	matrin 3
527	70	SLC25A34	solute carrier family 25, member 34
528	69	PTPRK	protein tyrosine phosphatase, receptor type, K
529	69	ACVR1	activin A receptor, type I
530	69	TAF4B	TAF4b RNA polymerase II, TATA box binding protein (TBP)-associated factor, 105kDa
531	69	HNRNPA3	heterogeneous nuclear ribonucleoprotein A3
532	69	SLCO6A1	solute carrier organic anion transporter family, member 6A1
533	69	PPIP5K2	diphosphoinositol pentakisphosphate kinase 2
534	69	TFDP1	transcription factor Dp-1
535	69	CELF3	CUGBP, Elav-like family member 3
536	69	RNF165	ring finger protein 165
537	69	LHFPL2	lipoma HMGIC fusion partner-like 2
538	69	TDG	thymine-DNA glycosylase
539	69	IRF4	interferon regulatory factor 4
540	69	MIB1	mindbomb E3 ubiquitin protein ligase 1
541	69	ESPN	espin
542	69	TM4SF1	transmembrane 4 L six family member 1
543	69	ZNF382	zinc finger protein 382
544	69	SCYL3	SCY1-like 3 (S. cerevisiae)
545	68	YPEL2	yippee-like 2 (Drosophila)
546	68	LMBR1L	limb development membrane protein 1-like
547	68	NFIB	nuclear factor I/B
548	68	MICAL1	microtubule associated monooxygenase, calponin and LIM domain containing 1
549	68	RAB8A	RAB8A, member RAS oncogene family
550	68	TM4SF20	transmembrane 4 L six family member 20
551	68	UGT2A3	UDP glucuronosyltransferase 2 family, polypeptide A3
552	68	FAM46A	family with sequence similarity 46, member A
553	68	FAM49A	family with sequence similarity 49, member A
554	68	NAGPA	N-acetylglucosamine-1-phosphodiester alpha-N-acetylglucosaminidase
555	68	SNX30	sorting nexin family member 30
556	67	EAF1	ELL associated factor 1
557	67	ARID4B	AT rich interactive domain 4B (RBP1-like)

558	67	TMCC1	transmembrane and coiled-coil domain family 1
559	67	CCDC178	coiled-coil domain containing 178
560	67	ADAMTS3	ADAM metallopeptidase with thrombospondin type 1 motif, 3
561	67	ERCC4	excision repair cross-complementation group 4
562	67	HNRNPC	heterogeneous nuclear ribonucleoprotein C (C1/C2)
563	67	IL36RN	interleukin 36 receptor antagonist
564	67	A1CF	APOBEC1 complementation factor
565	67	ABHD10	abhydrolase domain containing 10
566	67	ATP2B1	ATPase, Ca++ transporting, plasma membrane 1
567	66	NECAB1	N-terminal EF-hand calcium binding protein 1
568	66	C4orf19	chromosome 4 open reading frame 19
569	66	GJA1	gap junction protein, alpha 1, 43kDa
570	66	ADRA2A	adrenoceptor alpha 2A
571	66	GPR125	G protein-coupled receptor 125
572	66	LYRM7	LYR motif containing 7
573	66	AP3S1	adaptor-related protein complex 3, sigma 1 subunit
574	66	CHD7	chromodomain helicase DNA binding protein 7
575	66	PITPNC1	phosphatidylinositol transfer protein, cytoplasmic 1
576	66	LOC101060521	DNA-directed RNA polymerase III subunit RPC5-like
577	66	MCC	mutated in colorectal cancers
578	66	ASCC3	activating signal cointegrator 1 complex subunit 3
579	66	ICK	intestinal cell (MAK-like) kinase
580	66	JARID2	jumonji, AT rich interactive domain 2
581	66	SSH2	slingshot protein phosphatase 2
582	66	SPTSSB	serine palmitoyltransferase, small subunit B
583	66	NDUFC2	NADH dehydrogenase (ubiquinone) 1, subcomplex unknown, 2, 14.5kDa
584	66	GALNT13	polypeptide N-acetylgalactosaminyltransferase 13
585	66	TSEN15	TSEN15 tRNA splicing endonuclease subunit
586	66	CECR6	cat eye syndrome chromosome region, candidate 6
587	65	TASP1	taspase, threonine aspartase, 1
588	65	FBXL17	F-box and leucine-rich repeat protein 17
589	65	GZF1	GDNF-inducible zinc finger protein 1
590	65	UBE3C	ubiquitin protein ligase E3C
591	65	SPOCK3	sparc/osteonectin, cwcv and kazal-like domains proteoglycan (testican) 3
592	65	PAPOLB	poly(A) polymerase beta (testis specific)
593	65	CA10	carbonic anhydrase X
594	65	CHIC1	cysteine-rich hydrophobic domain 1
595	65	HERC2	HECT and RLD domain containing E3 ubiquitin protein ligase 2
596	65	CMTM4	CKLF-like MARVEL transmembrane domain containing 4
597	65	UFM1	ubiquitin-fold modifier 1

598	65	KIAA1211	KIAA1211
599	65	ZDHHC20	zinc finger, DHHC-type containing 20
600	65	EMB	embigin
601	65	CAMK4	calcium/calmodulin-dependent protein kinase IV
602	65	CCNY	cyclin Y
603	65	GNPDA1	glucosamine-6-phosphate deaminase 1
604	65	PRDM13	PR domain containing 13
605	65	MYBL2	v-myb avian myeloblastosis viral oncogene homolog-like 2
606	64	NAP1L2	nucleosome assembly protein 1-like 2
607	64	TRIM13	tripartite motif containing 13
608	64	PPP1R1C	protein phosphatase 1, regulatory (inhibitor) subunit 1C
609	64	ERCC6	excision repair cross-complementation group 6
610	64	STAG2	stromal antigen 2
611	64	MESDC2	mesoderm development candidate 2
612	64	UQCRB	ubiquinol-cytochrome c reductase binding protein
613	64	SALL4	spalt-like transcription factor 4
614	64	BTBD10	BTB (POZ) domain containing 10
615	64	DIP2B	DIP2 disco-interacting protein 2 homolog B (Drosophila)
616	64	PPP1R2	protein phosphatase 1, regulatory (inhibitor) subunit 2
617	64	SMIM11	small integral membrane protein 11
618	64	MAST3	microtubule associated serine/threonine kinase 3
619	64	FOXD1	forkhead box D1
620	63	DGKD	diacylglycerol kinase, delta 130kDa
621	63	USP48	ubiquitin specific peptidase 48
622	63	TMOD2	tropomodulin 2 (neuronal)
623	63	PDE4D	phosphodiesterase 4D, cAMP-specific
624	63	PLA2G12A	phospholipase A2, group XIIA
625	63	ZPBP2	zona pellucida binding protein 2
626	63	KCTD20	potassium channel tetramerization domain containing 20
627	63	MBOAT1	membrane bound O-acyltransferase domain containing 1
628	63	UCP3	uncoupling protein 3 (mitochondrial, proton carrier)
629	63	PER2	period circadian clock 2
630	63	CEP76	centrosomal protein 76kDa
631	63	HLF	hepatic leukemia factor
632	63	GALNT3	UDP-N-acetyl-alpha-D-galactosamine:polypeptide N-acetylgalactosaminyltransferase 3 (GalNAc-T3)
633	63	SGMS2	sphingomyelin synthase 2
634	63	PLEKHO2	pleckstrin homology domain containing, family O member 2
635	62	C10orf76	chromosome 10 open reading frame 76
636	62	TRMT10C	tRNA methyltransferase 10 homolog C (S. cerevisiae)
637	62	CAMTA1	calmodulin binding transcription activator 1

638	62	CRKL	v-crk avian sarcoma virus CT10 oncogene homolog-like
639	62	ALS2	amyotrophic lateral sclerosis 2 (juvenile)
640	62	ZDBF2	zinc finger, DBF-type containing 2
641	62	SEMA6D	sema domain, transmembrane domain (TM), and cytoplasmic domain, (semaphorin) 6D
642	62	RSF1	remodeling and spacing factor 1
643	62	GRIN2A	glutamate receptor, ionotropic, N-methyl D-aspartate 2A
644	62	KCTD8	potassium channel tetramerization domain containing 8
645	62	ADAM12	ADAM metallopeptidase domain 12
646	62	STXBP5	syntaxin binding protein 5 (tomosyn)
647	62	DPY19L3	dpy-19-like 3 (C. elegans)
648	62	NEFM	neurofilament, medium polypeptide
649	62	OR11A1	olfactory receptor, family 11, subfamily A, member 1
650	62	PAPOLG	poly(A) polymerase gamma
651	62	TMEM35	transmembrane protein 35
652	62	IKBIP	IKBKB interacting protein
653	62	HELZ	helicase with zinc finger
654	62	CREB1	cAMP responsive element binding protein 1
655	61	STOML1	stomatin (EPB72)-like 1
656	61	PROSER1	proline and serine rich 1
657	61	DGKZ	diacylglycerol kinase, zeta
658	61	SLC7A5	solute carrier family 7 (amino acid transporter light chain, L system), member 5
659	61	DLGAP1	discs, large (Drosophila) homolog-associated protein 1
660	61	SLC1A2	solute carrier family 1 (glial high affinity glutamate transporter), member 2
661	61	RBM12	RNA binding motif protein 12
662	61	FAM208A	family with sequence similarity 208, member A
663	61	CTDSPL2	CTD (carboxy-terminal domain, RNA polymerase II, polypeptide A) small phosphatase like 2
664	61	ZNF644	zinc finger protein 644
665	61	RAI14	retinoic acid induced 14
666	61	SMIM14	small integral membrane protein 14
667	61	ZNF148	zinc finger protein 148
668	61	CTHRC1	collagen triple helix repeat containing 1
669	61	SMAP1	small ArfGAP 1
670	61	TSPYL5	TSPY-like 5
671	61	AIDA	axin interactor, dorsalization associated
672	61	DGKH	diacylglycerol kinase, eta
673	61	ZFP36L2	ZFP36 ring finger protein-like 2
674	61	SEC62	SEC62 homolog (S. cerevisiae)
675	61	MGEA5	meningioma expressed antigen 5 (hyaluronidase)
676	61	MTA1	metastasis associated 1
677	61	TRPS1	trichorhinophalangeal syndrome I

678	60	EPB41	erythrocyte membrane protein band 4.1 (elliptocytosis 1, RH-linked)
679	60	GAREM	GRB2 associated, regulator of MAPK1
680	60	RAPH1	Ras association (RalGDS/AF-6) and pleckstrin homology domains 1
681	60	Septin 6	septin 6
682	60	ARL13B	ADP-ribosylation factor-like 13B
683	60	ZNF746	zinc finger protein 746
684	60	VOPP1	vesicular, overexpressed in cancer, prosurvival protein 1
685	60	GTF2H1	general transcription factor IIH, polypeptide 1, 62kDa
686	60	CLDND1	claudin domain containing 1
687	60	GALR1	galanin receptor 1
688	60	Septin 8	septin 8
689	60	GALNT2	polypeptide N-acetylgalactosaminyltransferase 2
690	60	SIKE1	suppressor of IKBKE 1
691	60	CD2AP	CD2-associated protein
692	60	H6PD	hexose-6-phosphate dehydrogenase (glucose 1-dehydrogenase)
693	60	CDCA7	cell division cycle associated 7
694	60	NFYB	nuclear transcription factor Y, beta
695	60	NOV	nephroblastoma overexpressed

Appendix 5: Predicted miR-1 targets in human tissue